

Research Reports from the Communications Research Laboratory
at Ilmenau University of Technology

Jianhui Li

**Signal Processing for High Data Rate
Wireless Communications**



ILMENAU UNIVERSITY OF TECHNOLOGY



Fakultät für Elektrotechnik und Informationstechnik
der Technischen Universität Ilmenau

SIGNAL PROCESSING
FOR HIGH DATA RATE WIRELESS COMMUNICATIONS

September 16, 2014

Jianhui Li
geboren am 26.03.1982 in Shandong, China

Dissertation zur Erlangung des
akademischen Grades Doktor-Ingenieur (Dr.-Ing)

Anfertigung im: Fachgebiet Nachrichtentechnik
Institut für Informationstechnik
Fakultät für Elektrotechnik und Informationstechnik

Gutachter: Prof. Dr.-Ing. Martin Haardt
Prof. Dr.-Ing. Eduard Jorswieck
Prof. Dr.-Ing. Aydin Sezgin

Vorgelegt am: 01.04.2014

Verteidigt am: 08.09.2014

Verf.-Nr.: EI

urn:nbn:de:gbv:ilm1-2014000236

Abstract

In this thesis, we deal with advanced signal processing for wireless communications at very high data rates and consider two application areas in the radio frequency range and the infrared range.

In the first part of this thesis, the concept of sharing the radio spectrum and the infrastructure between multiple operators is illustrated, which is within the vision of the European's seventh framework research project SAPHYRE. We introduce the SAPHYRE concept, which defines two topologies including the spectrum sharing as well as both spectrum and infrastructure (relay) sharing scenarios.

In the first topology, the spectrum is shared between multiple operators. The downlink of this spectrum sharing scenario is considered, where the base stations (BSs) of different operators transmit over the same channel, each dedicated to its own user terminal (UTs). Two closed-form transmit beamformers are first developed for this model. Based on that, an iterative transmit beamforming technique, named as flexible coordinated beamforming (FlexCoBF) for spectrum sharing is designed to exploit the inter-operator interference in a more effective manner so as to further enhance the system sum rate performance.

Concerning the second topology, both the spectrum and infrastructure sharing are taken into account. To be more specific, the relay assisted communications are investigated for this topology, where the relay as well as the spectrum are shared between multiple operators. We employ a multiple-input multiple output (MIMO) amplify and forward (AF) relay to assist the transmission between multiple pairs of BSs and UTs, where two cases are studied. In the first case, the direct link between the BSs and the UTs is too weak and can be neglected. We propose several algorithms for the relay precoder design to further improve the system performance. First a set of algorithms named efficient relay sharing rate maximization (EReSh-RM) are designed to improve the system sum rate under the relay transmit power constraint. After that, the relay precoder design is systematically studied for power efficient transmission. When the BSs and UTs are equipped with single antennas, a global optimum solution is firstly derived, which uses a convex optimization tool to exploit the structure of the relay precoder. Taking this as a benchmark, several suboptimal beamforming algorithms are proposed to find a compromise between the achievable power efficiency and the computational complexity, including a closed-form algorithm named Efficient Resource Sharing Power Minimization (EReSh-PM) and block diagonalization (BD) based solutions. Further, a novel robust relay precoder design is proposed by considering imperfect channel state information at the relay. At last, we extend our work to a general study where each pair of BSs and UTs are equipped with multiple antennas and a novel relay matrix design is derived for multiple

stream transmission between multiple pairs of BSs and UTs. Furthermore, another relay application case study is discussed, when the direct link is not negligible. We consider the linear precoding design for the AF relaying strategy, assuming multiple antennas employed at all BSs, UTs, and the AF relay. The single stream and multiple stream transmission are studied. Moreover, the SAPHYRE sharing gain is exploited, showing the advantage of spectrum and relay sharing in comparison with the exclusive access of the resources.

In the second part of this thesis, the physical layer design for a high speed infrared (IR) system in indoor environment is developed, which is within the scope the European Union's seventh framework research project OMEGA. The recent developments in an indoor infrared (IR) systems prove that IR has emerged as a strong candidate for high speed indoor communications, which is expected to play an important role in the future wireless networks. The infrared transmission operating at one Gigabit per second (Gbps) in the indoor environment is quite challenging, with a requirement to provide coverage as well as high data rate. The physical layer design for a high speed IR system is considered, which is focused on the line-of-sight (LOS) data transmission using IR wavelengths.

The system model of the high speed IR transmission is first introduced, where individual components suitable for Gbps IR systems are analyzed and specified. In particular, the modulation scheme that is appropriate for the Gbps IR transmission is briefly discussed. Thereafter, the baseline wander effect is considered, which is induced by the alternating current (AC) coupling inherent in the receiver's preamplifier. In order to overcome this, a novel line coding named concatenated flipped bit insertion (CFBI) code is elaborately addressed. Following that, the implementation of an analog Bessel low-pass filter is specified for noise rejection. A high-pass filter for the Gbps IR system is carefully selected, which is applied to block the direct current (DC) photocurrent generated by the received ambient light as well as to reduce the harmonics caused by the fluorescent lighting. Then the photodiode detectors for high speed IR transmission are discussed, including positive-intrinsic-negative (PIN) photodiodes and the Avalanche photodiodes. It is important to notice various noise sources generated in the IR system, including the shot noise and the thermal noise with constant power spectrum density (PSD), as well as the so called f^2 noise whose PSD increases with the square of the frequency. All these types of noise are analyzed in this thesis. Based on this analysis and the specification of the individual components, the link budget for a LOS Gbps IR transmission with a narrow angle field of view (FOV) is given. Finally, the transmit and receive angle diversity are discussed in order to further extend the system FOV.

Zusammenfassung

Die vorliegende Arbeit behandelt Signalverarbeitungsverfahren für drahtlose Kommunikationssysteme mit sehr hohen Datenraten. Dabei werden zum einen Funkssysteme und zum anderen Infrarot-basierte optische Übertragungssysteme als Anwendungsgebiete betrachtet.

Im ersten Teil der Arbeit wird das Konzept des “resource sharing” beleuchtet, was die willentliche und koordinierte gemeinsame Nutzung von Ressourcen zwischen mehreren Betreibern beschreibt. Dieses Ziel wurde im Rahmen des europäischen Forschungsprojektes SAPHYRE eingehend untersucht. Die Arbeit beschreibt die Vision des SAPHYRE-Projektes und geht auf zwei konkrete Topologien näher ein: die gemeinsame Nutzung der Spektren (“spectrum sharing”) sowie die gemeinsame Nutzung der Spektren und der Infrastruktur wie etwa der Relay-Stationen (“spectrum and infrastructure sharing”).

In der ersten Topologie teilen sich mehrere Betreiber Teile des Spektrums. Hierfür wird die Abwärtsstrecke betrachtet, in welcher die Basisstationen (BS) der verschiedenen Betreiber jeweils zu einem eigenen User-Terminal (UT) senden und sich dafür denselben Kanal teilen. Zuerst werden für dieses Modell geschlossene Lösungen für die Antennengewichte der Sender entwickelt. Basierend auf diesem Ansatz wird dann ein iteratives Verfahren namens “Flexible Coordinated Beamforming (FlexCoBF)” für den Spectrum-Sharing-Fall entwickelt, welches es erlaubt, die Interferenz zwischen den Betreibern effektiv auszunutzen, um so die Summenrate des Systems zu steigern.

Im Anschluss wird die zweite Topologie betrachtet, in der sowohl das Spektrum als auch Teile der Infrastruktur gemeinsam genutzt werden. Insbesondere wird dabei ein Relay-basiertes Kommunikationssystem untersucht, für welches mehrere Betreiber sowohl das Spektrum als auch die Relay-Station gemeinsam nutzen. Das Relay wird im “Amplify and Forward” (AF)-Betrieb verwendet und ist mit mehreren Sende- und Empfangsantennen ausgestattet. Zunächst wird der Fall betrachtet, dass die direkte Verbindung zwischen BS und UT zu schwach ist und daher vernachlässigt werden kann. Für diesen Fall werden Sendestrategien für die Relay-Station untersucht. Dabei wird zuerst eine Gruppe von Verfahren namens “efficient relay sharing rate maximization (EReSh-RM)” entwickelt, welche die Summenrate des Systems, unter Berücksichtigung einer Sendeleistungsbeschränkung des Relays, steigern. Im Anschluss wird der systematische Entwurf der Sendestrategien für energieeffiziente Übertragungen beleuchtet. Für den Spezialfall, in dem alle Basisstationen und alle User-Terminals nur eine Antenne besitzen, wird zunächst die global optimale Lösung unter Verwendung von konvexer Optimierung hergeleitet. Diese Lösung dient als Benchmark zur Bewertung einfacher suboptimaler Lösungen, die im Anschluss vorgeschlagen werden. Diese stellen einen Kompromiss zwischen der erreichbaren Energieeffizienz und dem nötigen Rechenaufwand dar, beispielsweise die geschlossene Lösung namens “Efficient Resource Sharing Power Minimization (EReSh-PM)” sowie Ansätze die auf dem “Block Diagonalization (BD)“-Verfahren basieren. Darüber hinaus wird eine neuartige robuste Sendestrategie

für das Relay vorgeschlagen, die die Unsicherheiten über den genauen Kanalzustand am Relay berücksichtigt. Schließlich werden die Konzepte auf den allgemeinen Fall erweitert, in dem jede Basisstation und jedes User-Terminal mehrere Antennen besitzen können. Für dieses Szenario wird ebenfalls eine Sendestrategie am Relay hergeleitet, die die Übertragung mehrerer Datenströme zwischen jedem Paar von BS und UT erlaubt. Für den Fall, dass die direkte Verbindung zwischen BS und UT nicht vernachlässigbar schwach ist, werden im Anschluss ebenfalls Übertragungsverfahren beleuchtet, wobei BS, UT und das Relay mehrere Antennen besitzen können. Hierbei wird unterschieden zwischen der Übertragung von jeweils einem Datenstrom und mehreren Datenströmen von jeder BS zu dem zugehörigen UT. Um den Vorteil des Resource-Sharings zu quantifizieren wird der "SAPHYRE sharing gain" verwendet welcher die erreichbare Summenrate mit und ohne Sharing ins Verhältnis setzt.

Im zweiten Teil der Arbeit wird das Design der physikalischen Übertragungsschicht für schnelle Infrarot (IR)-basierte Indoor-Übertragungssysteme untersucht. Dies geschah im Rahmen des europäischen Forschungsprojektes OMEGA. Die jüngsten Entwicklungen in Indoor-IR-Übertragungssystemen haben gezeigt, dass IR hochratige Datenübertragung unterstützt und im Indoor-Bereich entscheidende Vorteile besitzt. Deshalb wird erwartet, dass IR Technologien für zukünftige drahtlose Netzwerke eine wichtige Rolle spielen werden. Das Ziel des OMEGA-Projektes war die IR-Übertragung bei einem Gigabit pro Sekunde (Gbps), welches im Hinblick auf Ausleuchtung und Datenrate eine große Herausforderung darstellt. In der Arbeit wird der Entwurf der physikalischen Übertragungsschicht für den Fall der Infrarot-Übertragung mit direkter Sichtverbindung ("Line of Sight") untersucht.

Zunächst wird das Systemmodell für schnelle IR-Übertragung eingeführt und die für Gbps in Frage kommenden Komponenten spezifiziert und analysiert. Insbesondere werden für Gbps-IR geeignete Modulationsverfahren diskutiert. Danach wird der "Baseline Wander"-Effekt betrachtet, der durch die Einkopplung des Wechselstroms im Empfangs-Vorverstärker entsteht. Um diesem Effekt zu entgehen wird ein neues Leitungs-Kodierverfahren namens "Concatenated Flipped Bit Insertion (CFBI)" ausführlich beschrieben. Im Anschluss wird die Implementierung eines analogen Bessel-Tiefpassfilters zur Rauschunterdrückung betrachtet. Ein Hochpassfilter für das Gbps-IR-System zur Unterdrückung des Gleichanteils des Photodioden-Stroms, welcher durch das empfangene Umgebungslicht entsteht, wird sorgfältig ausgewählt. Dieser Filter kann gleichzeitig die harmonischen Komponenten abschwächen, die durch Leuchtstoffröhren entstehen. Die Photodioden für schnelle IR-Systeme werden in der Folge diskutiert, wobei sowohl auf PIN-Dioden als auch auf "Avalanche"-Photodioden eingegangen wird. Dabei ist es entscheidend, die unterschiedlichen Rauschquellen in IR-Systemen zu betrachten, insbesondere das Schrot-Rauschen und das thermische Rauschen mit konstanter spektraler Leistungsdichte, sowie das sogenannte f^2 -Rauschen, dessen spektrale Leistungsdichte mit dem Quadrat der Frequenz ansteigt. Diese Rauschquellen werden in der Arbeit eingehend analysiert. Darauf basierend, sowie unter Berücksichtigung der Spezifikationen der einzelnen Komponenten, wird das Link-Budget für Gbps-IR-Übertragung mit Sichtverbindung und einem entsprechend schmalen Sichtfeld (Field of View) hergeleitet. Abschließend wird noch die Nutzung von Raumdiversität am Sender und am Empfänger untersucht mit dem Ziel, das Sichtfeld des Systems zu vergrößern.

Contents

Abstract	i
Zusammenfassung	iii
Contents	v
List of Figures	ix
List of Tables	xiii
1. Introduction	1
1.1. Part I: Sharing Physical Resources (SAPHYRE)	3
1.2. Part II: hOME Gigabit Access (OMEGA)	7
I. Sharing Physical Resources (SAPHYRE)	11
2. SAPHYRE Concept	13
Spectrum Sharing Scenario	14
Relay Assisted Spectrum and Infrastructure Sharing Scenario	14
Fractional sharing gain	15
3. Spectrum Sharing	19
3.1. System Model	20
3.2. Block-Diagonalization (BD) and Regularized Block-Diagonalization (RBD) for the Interference Channel	21
3.3. Flexible Coordinated Beamforming for the Interference Channel	24
4. Multiple Operator One-Way Relaying without Direct Link	29
4.1. System Model	31
4.2. System Sum Rate Maximization	32
4.3. Relay Power Minimization for Single Stream Transmission	38
4.3.1. Optimum Solution of Relay Power Minimization for Single Stream . . .	39
4.3.2. Efficient Resource Sharing Power Minimization (EReSh-PM)	41
4.3.3. BD based solution	44
4.3.4. Conclusion	51
4.4. Robust Relay Precoder Design with Imperfect Channel State Information (CSI)	52

4.5. Relay Power Minimization for Multiple Stream Transmission	57
5. Multiple Operator One-Way Relaying with Direct Link	65
5.1. System Sum Rate Maximization for Single Stream Transmission	66
5.1.1. Relay Amplification Matrix Design	68
5.1.2. Precoder Design at the BSs	69
5.2. System Sum Rate Maximization for Multiple Stream Transmission	75
5.2.1. Relay Amplification Matrix Design	77
5.2.2. Precoder Design at the BSs	78
II. Home Gigabit Access (OMEGA)	85
6. OMEGA Concept	87
7. System Model	89
7.1. Modulation	90
7.2. Line Coding	90
7.2.1. Desirable Line Code Properties	91
7.2.2. 8B10B Codes	93
7.2.3. Simulation Results	99
7.3. Bessel filter	102
7.4. High-pass filter	106
7.5. Photodiode for Gbps system	107
7.5.1. PIN photodiode	108
7.5.2. Avalanche photodiode (APD)	111
7.6. Noise	111
7.6.1. Shot noise	112
7.6.2. Preamplifier frontend noise	114
7.6.3. Artificial light	114
8. Link Budget	117
8.1. Receiver sensitivity limit with PIN and APD for Gbps transmission	117
8.2. Link budget for Gbps transmission	119
9. Angle Diversity	123
9.1. Multi-element configuration	123
9.2. Establishment of a link	125
9.3. Preliminary analysis on the required radiant intensity per transmitter element	128
9.4. Demonstrator	131

10. Conclusions and future work	133
10.1. Part I: Sharing Physical Resources (SAPHYRE)	133
10.2. Part II: hOME Gigabit Access (OMEGA)	135
Acronyms	137
Notations	139
Erklärung	151

List of Figures

1.1. Expected data rates in fixed and wireless communication systems [Haa08] . . .	2
1.2. Infrared spectrum bandwidth	3
1.3. SAPHYRE vision (www.SAPHYRE.eu)	4
1.4. Home area network in OMEGA definition (www.ict-omega.eu)	7
2.1. relay enhanced communications	16
3.1. Spectrum sharing scenario, BS _{<i>i</i>} has $M_{T,i}$ antennas and UT _{<i>i</i>} has $M_{U,i}$ antennas	21
3.2. Sum rate vs SNR for the non-orthogonal spectrum sharing scenario	26
3.3. Sharing gain for the non-orthogonal spectrum sharing scenario	27
4.1. System Model for relay sharing between multiple operators	31
4.2. System sum rate versus SNR with $M_{T,k} = M_{U,k} = 1 \forall k$, $M_R = 4$	36
4.3. System sum rate versus SNR with $M_{T,k} = M_{U,k} = 1 \forall k$, $M_R = 4$	36
4.4. System sum rate versus SNR with $M_{T,k} = M_{U,k} = 2 \forall k$, $M_R = 6$	37
4.5. System sum rate versus SNR with $M_{T,k} = M_{U,k} = 2 \forall k$, $M_R = 6$	38
4.6. P_R versus P_T with target SINR = 0 dB	47
4.7. Elapsed time versus P_T with target SINR = 0 dB	48
4.8. P_R versus M_R with target SINR = 0 dB, $P_T = 10$ dBW	49
4.9. Failure probability of the feasibility check versus M_R with target SINR = 0 dB, $P_T = 10$ dBW	49
4.10. SAPHYRE gain in terms of power for multiple operator one-way relaying . . .	52
4.11. P_R versus SINR threshold γ at SNR = 20 dB	56
4.12. Outage probability of SINR versus SINR threshold γ at SNR = 20 dB	57
4.13. SAPHYRE gain in terms of power for the robust design	58
4.14. P_R versus SNR with target SINR = 0 dB, $K = 2$, $r_k = 2$, $M_R = 8$	63
4.15. histogram of SINR at $P_T = 25$ dB with target SINR = 0 dB, $K = 2$, $M_{T,k} = 3$, $M_{U,k} = 3$, $M_R = 8$, $r_k = 3$	64
5.1. Block Diagram of the Interference Relay Channel where the relay R (infras- tructure) and spectrum are shared between two operators	66
5.2. Sum rate vs SNR for the interference relay channel, the DFT matrix is applied at the relay, $M_{T,i} = M_{U,i} = M_R = 4$	70
5.3. Sum rate of the interference relay channel for different relaying strategies, IRC FlexCoBF RBD is applied at BSs, $M_{T,i} = M_{U,i} = M_R = 4$	71

5.4. Path loss model of the interference relay channel, d_1 denotes the distance between the BSs and their desired UTs and d_2 is the distance between the two interfering links	71
5.5. Sum rate for interference relay channel path loss model at SNR = 0 dB, the DFT matrix is applied at the relay, $M_{T,i} = M_{U,i} = M_R = 4$	73
5.6. Sum rate for interference relay channel path loss model at SNR = 20 dB, the DFT matrix is applied at the relay, $M_{T,i} = M_{U,i} = M_R = 4$	74
5.7. Sharing gain of the IRC over the RC, the DFT matrix is used at the relay, IRC FlexCoBF and eigen-beamforming are used for IRC and RC, respectively . . .	75
5.8. Sum rate for different relay strategies, $M_{T,i} = M_{U,i} = M_R = 4$	79
5.9. Sum rate vs SNR for $M_{T,i} = M_{U,i} = M_R = 4$, DFT matrix is applied at the relay	80
5.10. Path loss model for IRC	80
5.11. Sum rate for the path loss model at SNR = 20 dB for $M_{T,i} = M_{U,i} = M_R = 4$.	81
5.12. Histogram of the number of streams at different d_2/d_1 values for $M_{T,i} = M_{U,i} = M_R = 4$	82
5.13. sharing gain due to the use of the shared relay instead of accessing the relay in a TDMA mode	83
7.1. Gbps LOS infrared system concept	89
7.2. Block diagram of the Gbps wireless IR system	90
7.3. Flowchart of CFBI 5B6B encoder	95
7.4. BIM 5B6B encoder flowchart	97
7.5. Flowchart of CFBI 5B6B decoder	98
7.6. Histogram of HPF output using IBM 8B10B	100
7.7. Baseline wander reduction using line coding	101
7.8. BER comparison of IBM 8B10B and CFBI 8B10B	102
7.9. 5th order Bessel filter configuration for $R_s \geq R_l$	103
7.10. 5th order Bessel filter configuration for $R_s < R_l$	103
7.11. 5th Order Bessel Filter transfer function	105
7.12. First order high-pass filter	106
7.13. Impulse response of the high-pass filter combined with the 5th order Bessel filter, $f_{3dB} = R_{line}/2 = 625$ MHz, $f_c = 0.004 \cdot R_{line} = 5$ MHz	107
7.14. PIN photodiode	108
7.15. Maximum transit time and diode capacitance per area versus the intrinsic layer thickness for Si PIN at reasonable biased voltages	110
7.16. Illustration of the solid angle	112
8.1. Required receiver irradiance with the photodiode area	118
8.2. Required radiant intensity with the photodiode area to obtain a 1 m LOS link, $C_D/A_D = 60\text{pF}/(\text{mm}^2)$ for InGaAs diodes	120
8.3. Receiver sensitivity to obtain a 1 m LOS link,	121

9.1. Visualization of the transmit and receive beam pattern with 7 elements	124
9.2. Illustration of the seven element configuration. The central element points straight up and the six neighboring elements are uniformly placed around the central element with 30° elevation. It can be calculated that the angle between these two elements is less than 30° (marked in green) to ensure that the radiant intensity is always larger than half of the peak value even at the edge between any two elements.	125
9.3. Radiant intensity distribution with the proposed seven elements configuration. The colorbar provides the normalized radiant intensity to the peak value of a single transmitter element. It can be larger than one in the middle area due to the overlap between the seven elements. It clearly verifies that the obtained radiance intensity is never less than half of the peak, even between the element edges.	126
9.4. Transmit power gain	127
9.5. Required transmit radiant intensity for a 1m LOS link	128
9.6. Transmitter and receiver block diagram	129
9.7. Link establishment process	130
9.8. Rice factor distribution in a typical room	131
9.9. The best case configuration, where the transmitter is located in the ceiling center and the receiver is 3 m away straightly under the transmitter. The transmitter and the receiver are aligned to each other.	132
9.10. Required radiant intensity for the transmission distance of 3 m	132

List of Tables

2.1. Comparison of analog AF, digital AF and DF	15
5.1. Precoding design at the BSs for IRC FlexCoBF [LRH11b]	72
7.1. Rule of Running Disparity for IBM Code	94
7.2. Precoding Table of CFBI 5B6B	96
7.3. Precoding Table of CFBI 3B4B	99
7.4. Comparison of IBM code and CFBI code	100
7.5. normalized RLC-Values for $R_s = R_l$	103
7.6. normalized RLC-Values for $R_s < R_l$	103
7.7. denormalized RLC-Values for $R_s = R_l$ assumed $R_l = 50 \Omega$	104
7.8. denormalized RLC-Values for $R_s = 1/8 \cdot R_l$ assumed $R_l = 50 \Omega$	104
7.9. Theoretical parameters of Si photodiodes with transit times of less than 1 ns.	111
7.10. Parameters used for link budget analysis	115

1. Introduction

The urgent demands for high data rate transmission lead to continued technology evolution in wireless communications. In the past decade, the third generation (3G) mobile communication systems have already been developed to fulfill the high speed requirements. However, the recent booming growth in wireless applications, such as Voice over Internet Protocol (VoIP), video conferences, network gaming, etc., demands much higher data rates compared to the evolving 3G systems. A new standard has been introduced by the International Telecommunication Union (ITU), which is entitled International Mobile Telecommunications (IMT)-Advanced or the fourth generation (4G) mobile systems [Rec03]. According to the performance and technical requirements defined in [Rec08], future IMT-Advanced systems can support very high peak data rates for mobile users, up to 1 Gb/s in static and pedestrian environments, and up to 100 Mb/s in high-speed mobile environments. As shown in Fig. 1.1 [Haa08], the data rates of wireless system will experience an exponential growth with a time offset of less than five years with respect to the wireline systems, which is in line with the vision of the Wireless World Research Forum (WWRF) that up to seven trillion wireless devices will serve up to seven billion people by the year 2017. That means we are currently faced with the situation of running out of the available spectrum. Therefore an increased spectrum efficiency is required and it has become indispensable for future wireless systems to incorporate advanced signal processing techniques on the physical layer.

To fulfill the high data rate requirements in the IMT-Advanced system, it becomes more and more important for the operators to possess the limited and precious radio spectrum. Based on the analysis of spectrum demands of IMT-Advanced, the World Radio Communication Conference (WRC) 2007 identified new spectrum to fulfil the growing spectrum requirements. However, the identified bands per operator required for high data rate services will not result in a sufficient number of operators to support competition. Moreover, it costs a huge amount to purchase 360 MHz Long Term Evolution (LTE) bandwidth for 4 operators in the German segment. To alleviate the pressure of spectrum management as well as to find a more cost effective approach, the concept of spectrum sharing is often considered as a medium-to-long-term solution and some general pioneering ideas [US 07], [US 05] have been patented revealing its potential to further enhance the spectrum efficiency. Another finding in a recent report is that the site construction costs impose a strict constraint on developing the IMT-Advanced system and different levels of sharing (site, antenna, backbone, radio network controller (RNC), etc.) are possible to further reduce the infrastructure costs. Based on the aforementioned analysis, the concept of sharing the radio spectrum and the infrastructure between multiple operators has been introduced in the European FP7 (framework programme

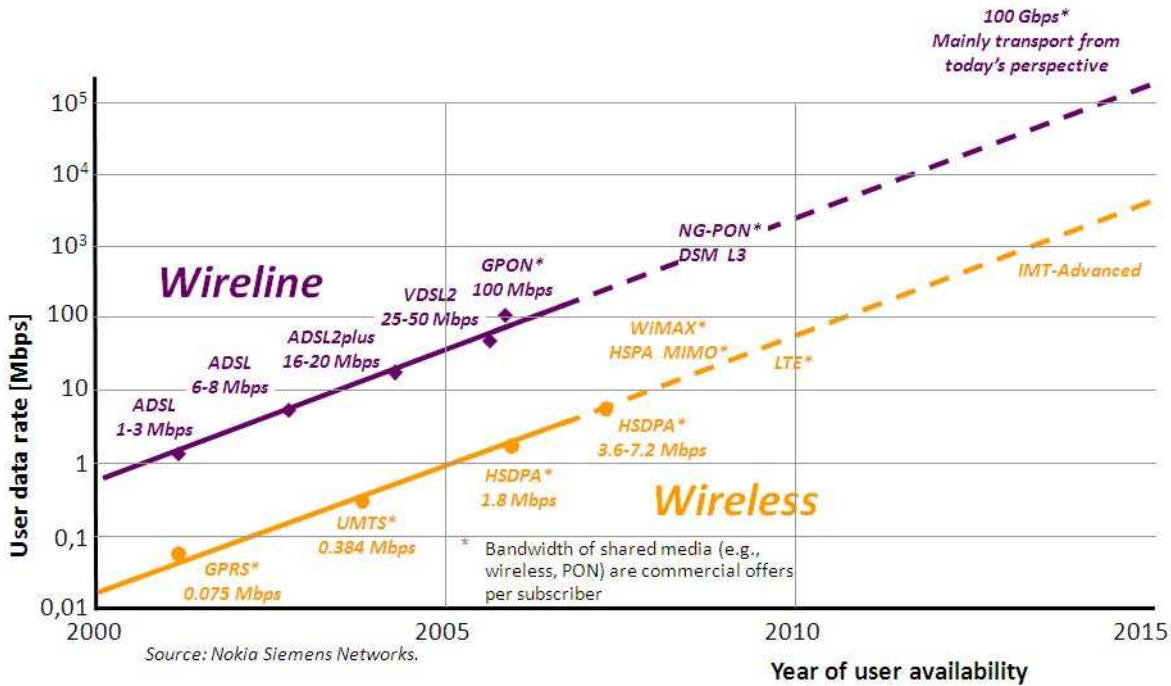


Figure 1.1.: Expected data rates in fixed and wireless communication systems [Haa08]

seven) research project ShAring PHYsical REsources (SAPHYRE) (www.SAPHYRE.eu) to make more effective use of the limited physical resources. This paves the way for a paradigm change from the traditional exclusive resource allocation to voluntary physical resource sharing. More advanced signal processing techniques, including multiple-input multiple-output (MIMO), multi-hop relaying cooperative transmission and so on, are developed to deal with the created interference caused by sharing as well as to further enhance the system spectral efficiency and power efficiency.

Furthermore, the next generation wireless communications system or the 4G mobile system will not be based on a single access technique but it will encompass a number of different technologies [BDHM01, OKW⁺05]. As a complementary access technique to RF to provide high speed connectivity, especially for short range communications within the home network area, infrared (IR) transmission will play an important role. Compared to the more and more intense competition over the limited spectrum in RF, the THz of bandwidth offers IR a big advantage as shown in Fig. 1.2, which qualifies it a competitive candidate for indoor short-range transmission. Moreover, the infrared emitters and detectors capable of high speed operation are available at low costs [KB97], which is another persuasive support for the IR technique. Currently, the deployment of fibre to the home area networks offers the potential to deliver the data at a speed of more than 100 Mbit/s. However, the rapidly increasing demand for high data rate transmission prompts the future vision of home area networks operating at the speed which is a factor of ten faster. All of this mentioned above precipitates the further development on high speed IR technology deployed in Gigabit home area networks, which

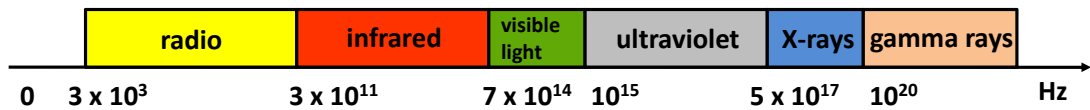


Figure 1.2.: Infrared spectrum bandwidth

is within the scope of the European Union’s seventh framework R&D programme project, entitled hOME Gigabit Access (OMEGA) (www.ict-omega.eu). The OMEGA project aims at bridging the gap between mobile broadband terminals and the wired backbone at home. As a part of it, we focus on the physical layer design and the integration of an IR system operating at one Gigabit per second (Gbps).

In this thesis, we consider advanced signal processing for wireless communications at very high data rates. The overall structure of this thesis consists of two parts, which demonstrate two application areas in the radio frequency range and the IR areas and can be read independently. The following sections provide a brief motivation for these two parts, outlining the possible applications, the state-of-the-art, the open problems of the existing solutions, and summarizing the major contributions.

1.1. Part I: Sharing Physical Resources (SAPHYRE)

In the first part of this thesis, the concept of sharing the radio spectrum and the infrastructure between multiple operators is illustrated, which is within the vision of the European’s seventh framework research project SAPHYRE (www.SAPHYRE.eu).

In current wireless communications, the spectrum and the infrastructure are usually allocated exclusively by each operator so that the interference is avoided, which is called orthogonal resource sharing. However, to alleviate the pressure of spectrum management as well as to further reduce the infrastructure costs, more and more people reach consensus on the concept of non-orthogonal resource sharing. This trend requires more flexible use of the physical resources, which is supported by novel developments in radio technology. Taking the spectrum sharing for instance, there are several steps to realize the flexible spectrum usage, as explained in [JBF⁺12], [JBF⁺11]. The first step is intra-operator spectrum sharing, which includes the dynamic allocation within the spectrum blocks of a single operator. A further step moves to that the spectrum bands of more than one operators are allocated to users belonging to them but one spectrum band is still exclusively assigned to one operator so that no additional interference is created. The most flexible way of spectrum sharing is non-orthogonal inter-operator spectrum sharing, which is proposed in SAPHYRE. This type of sharing creates interference on the physical layer. However, by clever transceiver optimization, user selection, etc., gains in terms of spectral efficiency are reported in [JBF⁺10].

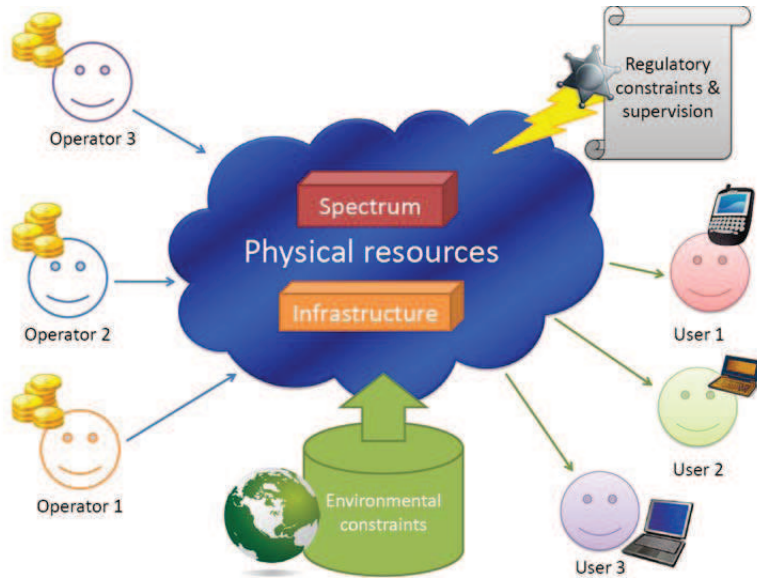


Figure 1.3.: SAPHYRE vision (www.SAPHYRE.eu)

The differentiation of the resource sharing concept in SAPHYRE to other common and important types of sharing, including cooperative multi-point (CoMP), fractional frequency reuse (FFR), and cognitive radio (CR) will be clarified in the following, and a brief state-of-the-art overview is provided. The main idea behind CoMP is to exploit the inter-cell interference in order to increase the spectral efficiency [MF04] [IDM⁺11] [SKM⁺10] [GHH⁺10]. In contrast to inter-operator orthogonal and non-orthogonal sharing, the cooperation is performed between sectors or different sites of the same operator. In addition to the exchange of channel state information (CSI), it also requires the exchange of user data via high-data backbone connections for joint precoding and transmit optimization. Comparing the SAPHYRE approach to FFR, the difference lies in that FFR is applied within one operator and the decision on the frequency band assignment is usually based on the average received power, i.e., a signal-to-interference-plus-noise (SINR) threshold [GML08]. It is also important to note the difference between the SAPHYRE approach and cognitive radio (CR) [MM99, Hay05]. Cognitive radios operate in the way that a secondary system is allowed to access the licensed spectrum owned by a primary (legacy) operator as long as it does not disturb the primary system operation. In order to guarantee the absence of disturbance, the secondary users must operate on the basis of sensing so-called spectrum holes, which basically are chunks of spectrum left vacant by the primary system and over which interference is sensed as weak. In contrast, SAPHYRE puts an emphasis on the efficient and simultaneous use of the same physical resources by two (or more) equal-priority wireless systems placed on an equal footing.

As shown in Fig. 1.3, there is generally a set of common physical resources, which are categorized into two classes, namely spectrum and infrastructure. Based on these limited resources, the future wireless network development is mainly faced with two challenges. Firstly, the identified bands for IMT-Advanced operating at high data rate do not result in a suffi-

cient number of operators to support competition. Secondly, to make more efficient use of the resources, SAPHYRE has developed a framework where the spectrum and infrastructure are simultaneously shared between equal-priority players consisting of a set operators and users. SAPHYRE has demonstrated how equal-priority resource sharing in wireless networks improves the spectral efficiency, enhances coverage, increases user satisfaction, leads to an increased revenue for operators, and decreases capital and operating expenditures [JBF⁺10]. Within the framework of SAPHYRE, the resource of each operator is voluntarily shared so as to achieve a common efficient operating mode. Furthermore, the environmental and regulatory constraints have to be taken into account, e.g., to balance the fairness, social welfare, etc.

Chapter 2 gives more a detailed motivation for the SAPHYRE concept. Two topologies are discussed throughout this thesis, which are defined within the scope of SAPHYRE. In Chapter 2, we first give an overview for the spectrum sharing only scenario. Following that, the model for spectrum and infrastructure (relay) sharing is introduced. To be more specific, we consider the relay assisted communication between multiple operators and various relaying operation modes are compared and discussed. Finally, to clearly illustrate the advantage of the sharing schemes compared to the traditional exclusive use of the physical resources, the SAPHYRE sharing gain is defined in terms of both spectral efficiency as well as power efficiency, which are used as a main performance metric from Chapter 3 to Chapter 5.

An introduction to the data model is given in Chapter 3, where only the spectrum is shared between multiple operators. The downlink of the spectrum sharing scenario is considered, where the base stations (BSs) of different operators transmit over the same channel, each dedicated to its own user terminal (UT). This scenario is modeled as the interference channel with several concurrent point-to-point transmissions interfering each other, which is one of the fundamental building blocks from the spectrum sharing point of view. The interference channel has been intensely studied over last few decades starting from [Car78]. We view this scenario as a special case of voluntary spectrum sharing in SAPHYRE. Two closed-form transmit beamformers are first developed for this model. Based on that, an iterative transmit beamforming technique, named as flexible coordinated beamforming (FlexCoBF) for spectrum sharing is designed to exploit the inter-operator interference in a more effective manner so as to further enhance the system sum rate performance [KGH⁺11, LKK⁺11].

Both the spectrum and infrastructure sharing are taken into account in Chapter 4 and Chapter 5. To be more specific, the relay assisted communications are investigated for this topology, where the relay as well as the spectrum are shared between multiple operators. In recent years, the use of relays has drawn enormous attention due to its promising capability in achieving reliable communications and coverage extension in wireless networks. In these scenarios, where the link quality cannot be guaranteed due to large path loss, shadowing effect, multipath fading, etc., relays can be employed between the source and the destination to assist the communication [LWT01], [LW00], [SEA03a], [SEA03b]. Various relaying schemes have been presented in the literature, including the amplify-and-forward (AF) [MMVA07],

[TH07], [RW04], decode-and-forward (DF) [LW00] and compress-and-forward (CF) [KGG05] schemes. Among several cooperative schemes, the AF is more attractive since it does not do decoding but simply amplifies the received signal from the source and forward it to the destination. Throughout this thesis, we focus on the AF relaying scheme.

Moreover, considering the fact that the MIMO technique [Tel99] enhances the system capacity by combating fading and interference, it makes sense to exploit the advantages of the combination MIMO and relay. Several works on capacity bounds of MIMO relay channels have been firstly addressed in [WZ03], [WZHM05], [HMZ05], and [LVRWH05]. The optimal design of AF MIMO relay in point-to-point communication is investigated in [MMVA07] and [TH07]. In addition to that, the MIMO relay is also deployed on the multi-user downlink to improve the system performance [CTHC08] [ZCL09]. More recently, the MIMO AF relay is applied for multi-point to multi-point communication, which is the scenario discussed in Chapter 4. In this chapter, we employ an MIMO AF relay to assist the transmission between multiple pairs of BSs and UTs, where the direct link between the source and destination is neglected. We propose several algorithms for the relay precoder design to further improve the system performance. First a set of algorithms named efficient relay sharing rate maximization (EReSh-RM) are designed to improve the system sum rate under the relay transmit power constraint. After that, the relay precoder design is systematically studied for power efficient transmission. In the previous work [CVL07] and [CV09], the relay precoder is designed with respect to the worst case of the relay transmit power, considering perfect and imperfect channel state information at the relay separately. Our work is focused on minimizing the average relay transmit power under the SINR constraint to be satisfied for each transceiver pair. For the case where the BSs and UTs are equipped with single antennas, a global optimum solution is firstly derived, which uses a convex optimization tool to exploit the structure of the relay precoder. Taking this as a benchmark, several suboptimal beamforming algorithms are proposed to find a compromise between the achievable power efficiency and the computational complexity, including a closed-form algorithm named Efficient Resource Sharing Power Minimization (EReSh-PM) and block diagonalization (BD) [SSH04] based solutions. Further, a novel robust relay precoder design is proposed by considering imperfect CSI at the relay. At last, we extend our study to the case where each pair of BSs and UTs are equipped with multiple antennas and a novel relay matrix design is derived for multiple stream transmission between multiple pairs of BSs and UTs.

Furthermore, when the direct link is not negligible, we discuss another relay application scheme in Chapter 5, where the relay is used to assist the pairwise concurrent point to point transmission. This scenario is called interference relay channel as firstly defined in [SE07], which is another fundamental building block including both spectrum and infrastructure sharing. Some pioneering works [SSE09], [SES09], [TY09] have studied the impact of a full duplex DF relay with a single antenna in such a scheme, considering in-band and out-of-band transmission or reception modes, the relay transmit power, etc. In contrast to this, we consider the linear precoding design for the AF relaying strategy in Chapter 5, assuming multiple antennas employed at all BSs, UTs, and the AF relay. Two cases are studied, categorized

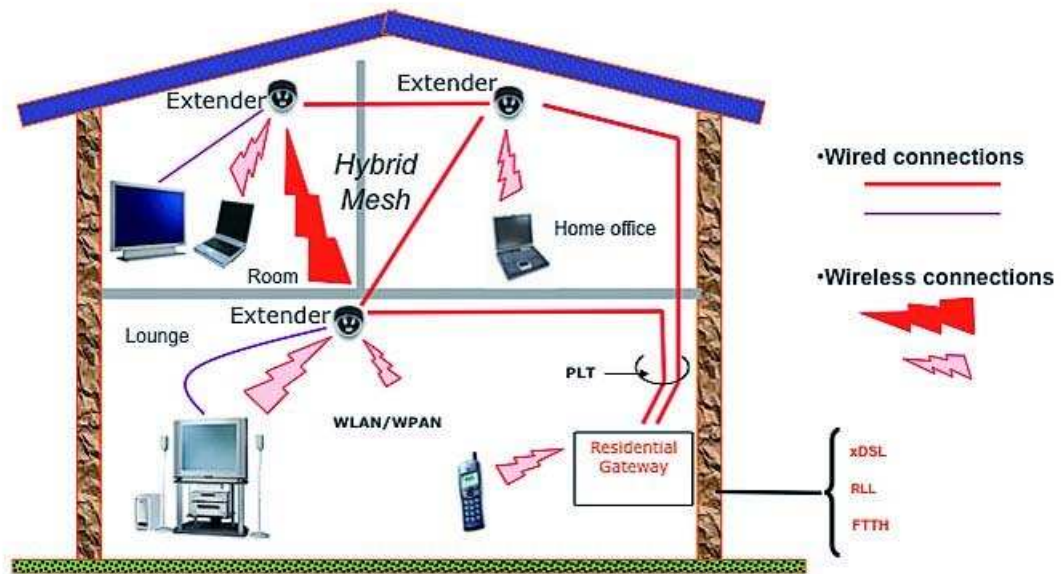


Figure 1.4.: Home area network in OMEGA definition (www.ict-omega.eu)

into single stream and multiple stream transmission. In both cases, the SAPHYRE sharing gain is exploited, showing the advantage of spectrum and relay sharing in comparison with the exclusive access of the resources.

1.2. Part II: hOME Gigabit Access (OMEGA)

In the second part of this thesis, the physical layer design for a high speed infrared (IR) system in indoor environment is developed, which is within the scope the European Union's FP7 project OMEGA (www.ict-omega.eu).

As stated in the white paper [OKW⁺05], future systems will not only connect users and their personal equipment but also access to independent equipment will be provided. Ultimately one would expect that everybody and everything will be seamlessly connected. This vision places the short range communications in a position of preponderance, which is envisaged in OMEGA shown in Figure 1.4. To provide high speed connectivity within the home area network, a large number of different complementary access techniques are considered. In addition to the wired power line communications, the wireless links will use radio frequency, infrared as well as the visible light transmission to fulfill the vision of broadband home networking without adding new wires. In this part, we focus on the infrared communication in the home area.

In the past few decades, infrared communication has been widely applied in point to point transmission. For example, infrared remote controls and devices that communicate according to the Infrared Data Association (IrDA) are in widespread use. Recently there have been a number of high-speed point to point link demonstrations and products. One example is the

link by JVC which provides a 1.5Gbit/s for uncompressed High Definition TV. Beyond that, OMEGA aims at a substantial improvement in the state of the art as it demonstrates an infrared network rather than simple point to point connections. Further, this project provides novel optical-wireless solutions for home applications using IR at up to one gigabit per second (Gbps).

The recent developments in indoor IR systems [GJHL08] prove that IR has emerged as a strong candidate for high speed indoor communications [LG07, JBVS08, KJ03], which is expected to play a role in the future wireless networks. In the contrary to the limited available spectrum in RF as stated in Part I, the infrared channel has THz of unregulated bandwidth, and is free from electromagnetic interference. The multipath fading suffered by RF transmission is also avoidable in IR by selecting a proper modulation and detection scheme. Furthermore, IR communications are highly secured, which is attributed to the natural confinement of the optical signals that is to their disability to penetrate walls. Therefore, it becomes easier to construct cell-based secure networks via wavelength reuse in different rooms.

The Gbps infrared transmission in indoor wireless systems is quite challenging, with a requirement to provide coverage as well as high data rate. The field of view (FOV) required in a typical home environment is around 90 degrees at both transmitter and receiver. This wide FOV for robust indoor coverage makes the system considerably more challenging. Thus multiple links will be required to cover the target FOV, and the control and management of these is thought to be where most of the innovation in OMEGA lies, as the state of the art is relatively undeveloped.

In particular, the basic IR system topology is categorized into diffuse and line of sight (LOS) systems [KB97]. The diffuse system creates a large number of paths from the transmitter to the receiver, which makes the system robust and prevents it from getting blocked. However, it suffers from multipath dispersion, which causes pulse spread and significant inter-symbol interference, in addition to higher path losses compared to direct LOS links. To fulfill the Gbps data transmission requirement, OMEGA adopts a LOS system topology. Direct LOS links improve the power efficiency and reduce the multipath dispersion, but require an inherent alignment between the transmitter and the receiver in order to establish a reliable communication. The path loss combined with the narrow transmitter and receiver FOV determine the link budget and the available data rate of the system. In general, the narrower the FOV, the higher is the data rate that is achievable. However, such narrow links do not provide coverage, and thus cellular systems using a number of LOS links are employed in order to increase the coverage and achieve high data rates. Generally speaking, there are two approaches to implement multiple element transmitters and receivers. One is to use imaging transmitters and receivers, where light beams are transmitted at different angles within the desired coverage area while the receiver uses a detector array so that radiations from different angles reach particular elements within the range of the detector [PFOE01, WN97, OFJ⁺03]. An alternative is to build an angle diversity system where individual transmitters and receivers are arranged to point at different angles to provide the desired coverage [CK00]. In

OMEGA, the latter choice is made since there are not sufficient resources within the project to fabricate the necessary custom devices for the imaging solution.

In this part, the physical layer design for a high speed IR system is considered, which is focused on LOS data transmission using IR wavelengths. The physical layer analysis on integration and feasibility investigation of Gbps IR system is presented. The system consists of a base station located at the ceiling and terminals that move around at the ground. Both transmitters and receivers are build with seven elements in the demonstrator [MOF⁺10, OMF⁺10], where each element covers a relatively narrow FOV and together a data link with a wide FOV is created.

The contributions of this part are summarized as follows. In Chapter 7, the system model of the high speed IR transmission is introduced, where individual components suitable for Gbps IR system are analyzed and specified. In particular, the modulation scheme that is appropriate for the Gbps IR transmission is first briefly discussed. The baseline wander effect is considered, which is induced by the alternating current (AC) coupling inherent in the receiver's preamplifier. In order to overcome this, a novel line coding named as concatenated flipped bit insertion (CFBI) code is elaborately addressed [LWH09]. Compared to the classic IBM code [WF83], the CFBI code offers a comparable susceptibility to the transient baseline wander effect while it is much easier to implement due to a very simple logic. Following that, the implementation of an analog Bessel low-pass filter is specified for noise rejection. A high-pass filter for the Gbps IR system is carefully selected, which is applied to block the direct current (DC) photocurrent generated by the received ambient light as well as to reduce the harmonics caused by the fluorescent lighting. Then the photodiode detectors for high speed IR transmission are discussed, including PIN photodiodes and the Avalanche types. It is important to notice various noise sources generated in the IR system, including shot noise and thermal noise with constant power spectrum density (PSD), as well as the so called f^2 noise whose PSD increases with the square of the frequency. All the types of the noise are analyzed in this thesis. Based on this analysis and the specification of the individual components, the link budget for a LOS Gbps IR transmission with narrow angle FOV is given in Chapter 8. At last, the transmit and receive angle diversity are discussed in Chapter 9, in order to further extend the system FOV.

Part I.

Sharing Physical Resources (SAPHYRE)

2. SAPHYRE Concept

In current wireless communication systems, the radio spectrum and the infrastructure are typically used such that the interference is avoided by exclusive allocation of frequency bands and employment of base stations. Various types of techniques applying orthogonality in frequency, time and coding have been used for resource allocation. For example, time division multiple access (TDMA) combined with frequency division multiple access (FDMA) used in GSM systems or code division multiple access (CDMA) in 3G systems is applied to mitigate the intra-cell interference among users that belong to a single operator within a cell. For different cells, the inter-cell interference is controlled by applying different frequency reuse factors with fractional and adaptive frequency reuse.

Very recently, techniques for separating transmissions from different operators (inter-operator interference) without orthogonal resource allocation have been developed. The first flexible resource sharing approaches [BL06, HPI08] indicate that the overall system spectrum efficiency can be improved between several operators by sharing their resources, which can be divided into two classes, namely spectrum and infrastructure. Sharing of spectrum or infrastructure ends up in creating interference on the physical layer. To mitigate the resulting inter-operator interference as well as to further enhance the system performance (sum rate, required power, rate region, etc.), advanced signal processing techniques (for multiple antennas and multiple hops) have received more and more interest. Furthermore, SAPHYRE (www.SAPHYRE.eu) has demonstrated how equal-priority resource sharing in wireless networks improves the spectral efficiency, enhances the coverage, increases the user satisfaction, leads to an increased revenue for operators, and decreases the capital and operating expenditures [JBF⁺10]. In this work, we focus on the advanced signal processing techniques, such as MIMO precoding algorithms with inter-cell interference coordination algorithms based on resource sharing. They are developed both for the spectrum and the infrastructure (here relay) sharing scenario, which are defined in the framework of SAPHYRE.

In this chapter, we first provide an overview of the spectrum sharing scenario. Following that, the relay assisted communications between multiple operators is introduced and various relaying operation modes are compared and discussed. Finally, to clearly illustrate the advantage of sharing schemes, the SAPHYRE sharing gain is defined in terms of both spectral efficiency as well as power efficiency compared to the traditional exclusive use of the physical resources.

Spectrum Sharing Scenario

SAPHYRE envisions that future cellular networks will achieve higher spectral efficiency if the operators decide to share parts of the spectrum that has been exclusively licensed to them. As discussed at the beginning of this chapter, inter-operator spectrum can be used in an orthogonal manner by applying a time division multiple TDMA scheme. However, the utmost gain is expected when the operators share the spectrum non-orthogonally, i.e., they use the same frequency bands simultaneously. In this case, the major impairment received by each operator is the interference caused by co-channel transmissions. The simplest setup for the downlink of the non-orthogonal spectrum sharing scenario is that two neighboring base stations (BSs) belonging to different operators transmit towards their user terminals (UTs), respectively, and the UTs receive the desired transmission as well as the inter-operator interference. SAPHYRE advocates that reliable communication can be achieved in both links by applying advanced signal processing techniques to mitigate the interference caused by sharing. A detailed description of this scenario will be addressed in Chapter 3, where we will introduce several transmit beamforming techniques to further enhance the system spectral efficiency.

Relay Assisted Spectrum and Infrastructure Sharing Scenario

Various relaying concepts have been widely studied in wireless networks since [CA79] due to their potential gains in terms of spectral efficiency compared to a point-to-point transmission. Recently, relays have been studied as wireless backhaul to provide efficient coverage extension and a capacity increase. They can be employed with little or no incremental backhaul expense and applied in various scenarios where a fixed line backhaul is difficult to deploy. For example, relays expand the coverage to mountainous regions or sparsely populated areas and enhance the throughput for cell edge users [ITN10].

The relay technology has experienced many years' development. The traditional relay is an analog amplify-and-forward (AF) relay. The radio signals received on the downlink from the BSs or that on the uplink from the UTs are simply amplified without further processing. Thereby, it is also called repeater or booster. The advantage of this kind of relay is that it is quite simple and no processing delay is caused. However, the interference as well as noise at the relay are amplified simultaneously together with the desired signal. In contrast to the analog AF, the present AF relay usually down converts the radio frequency signal into the baseband and incorporates additional baseband processing such as sampling, spatial filtering, etc. After processing in the digital domain, the signal will be amplified and up converted for forward transmission. To distinguish these two types of AF relays, we call the latter the digital AF. Unlike analog AF, the digital storage facilitates processing in digital domain and operation in half duplex mode. Furthermore, the digital AF does not require decoding and re-encoding of the data as required for the decode-and-forward (DF) relay, where more

Relay technology	Analog AF	Digital AF	DF
latency	no	low	high
possible processing	real-valued scalar amplification	multiplication with a complex matrix (beamforming)	decoding re-encoding
noise forwarding	yes	yes	no
baseband processing	no	simple	complex

Table 2.1.: Comparison of analog AF, digital AF and DF

complicated baseband processing causes a much higher latency. Furthermore, the capacity of DF might be lower than AF when the channel between the source and the relay is statistically worse than the other channels in relay assisted cooperative communication [NBK04], [YL05]. Thereby, it can be concluded that the digital AF is a good trade-off between performance and complexity. The comparison of these three types of relays is shown in Table 2.1.

By incorporating the digital AF into the wireless network, the relay is employed to assist the BS in addition to a direct transmission between the BSs and UTs, which might be quite weak to be negligible. We can extend this model to multiple transceiver pairs that belong to multiple operators, which exploits the benefit of the relay sharing for further system throughput improvement and expenditure saving. The spectrum and relay sharing model for two operators is shown in Figure 2.1, which has been investigated under the scope of SAPHYRE. In this case, the relay is shared and accessed by both the BSs at the same time instead of an exclusive use of the relay for each operator. A more detailed discussion about this scenario can be found in Chapter 4 and Chapter 5, without and with consideration of the direct link between the BSs and UTs, respectively.

Fractional sharing gain

In order to evaluate the benefits of advanced signal processing algorithms to exploit the additional degrees of freedom brought by sharing the spectrum and relays in multi-operator environments, it is important to:

- define a performance metric,
- show the gain (loss) with respect to the chosen performance metric as compared to a non-sharing scenario,
- point out conditions when a significant gain can be achieved for the chosen scenario (topology), and
- illustrate the order of magnitude of this gain.

We define this sharing gain as the SAPHYRE gain. In this part, two types of SAPHYRE gains are defined in terms of the system rate and the relay transmit power. These gains are obtained for the sharing scenario compared to the exclusive use of the spectrum and the

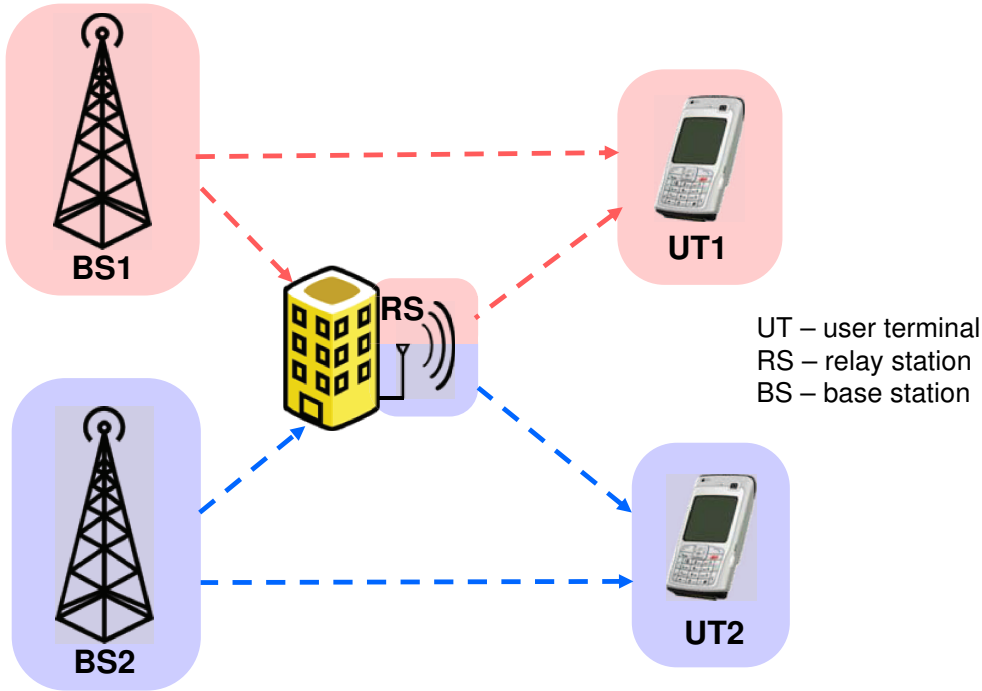


Figure 2.1.: relay enhanced communications

infrastructure (i.e., the relay) by a single operator (time division case, in this case, the users are multiplexed via TDMA).

The fractional SAPHYRE gain in terms of system sum rate is defined as

$$\Xi_{F,\text{rate}} = \frac{\sum_{k=1}^K U_k}{\frac{1}{K} \sum_{k=1}^K U_k^{\text{SU}}}, \quad (2.1)$$

where $k \in \{1, 2, \dots, K\}$ is the user index. The sum rate of the k th user in the sharing scenario and the time division case are denoted by U_k and U_k^{SU} , respectively [LRH11b] [LZR⁺11] [LRH11a] [LSH11].

In addition to that, we could also interpret the SAPHYRE sharing gain in terms of the relay transmit power, i.e., the required relay transmit power consumed in the sharing scenario is compared to that consumed by the exclusive use of the spectrum and infrastructure for a single operator (TDMA access).

The fractional SAPHYRE gain in terms of relay transmit power is defined as

$$\bar{\Xi}_{\text{F,power}} = \frac{K \sum_{k=1}^K P_k^{\text{SU}}}{\sum_{k=1}^K P_k}, \quad (2.2)$$

where the relay transmit power of the k -th user in the sharing scenario and the time division case are denoted by P_k and P_k^{SU} [LRH11a].

Part I of this dissertation is organized as follows. The non-orthogonal spectrum sharing scheme is first introduced and several efficient algorithms designed for sum rate maximization of the system are addressed in Chapter 3. Following that, the schemes including both spectrum and infrastructure sharing are addressed in Chapter 4 and Chapter 5. In particular, the relay assisted resource sharing scenario is considered in Chapter 4 by neglecting the direct link between the BSs and UTs. In particular, the system model for the AF relay sharing scenario is introduced in Section 4.1. Then the relay precoders designed to enhance the system sum rate are addressed in Section 4.2. To make more efficient use of the relay transmit power, several algorithms are proposed in Section 4.3 - Section 4.5 concerning different transmission schemes. Section 4.3 starts with the single stream transmission scheme, where each BS and UT are equipped with a single antenna. After that, Section 4.4 describes a robust relay precoder design assuming that an erroneous channel state information (CSI) is available. Section 4.5 extends the work to multiple stream transmission for the more general case, where both BSs and UTs have multiple antennas. A novel algorithm is proposed to minimize the relay transmit power subject to the signal to noise plus interference ratio (SINR) constraint for each data stream. In contrast to Chapter 4, Chapter 5 considers the case where the direct link between the BSs and UTs is not negligible. The precoder design for system sum rate maximization is discussed for this scenario, which consists of two case studies, including the single stream transmission as addressed in Section 5.1 as well as the multiple stream case in Section 5.2. As an important metric in SAPHYRE, the sharing gain compared to the exclusive use of the spectrum and the relay is discussed throughout this part, i.e., from Chapter 3 to Chapter 5, in terms of sum rate as well as in terms of relay transmit power.

3. Spectrum Sharing

In recent years, the increasing demand for high data rate transmission makes the radio frequency (RF) spectrum more and more scarce. It is thus getting much more expensive to acquire a spectrum licence and the cost of operation is even higher for the operators. To make more effective use of the spectrum, spectrum sharing would be a reasonable solution.

There are various types of spectrum sharing [JBF⁺12], [JBF⁺11]. Intra-operator spectrum sharing is realized by dynamic allocation within the spectrum bands of a single operator. A further step moves to inter-operator orthogonal sharing, i.e., the spectrum bands of more than one operator are allocated to users belonging to them but one spectrum band is still exclusively assigned to one operator so that no additional interference is created. The highest gain is expected when the operators share the spectrum non-orthogonally, i.e., they concurrently use the same frequency bands in the same geographical location, which is proposed in SAPHYRE. This type of sharing creates interference on the physical layer. However, by applying advanced beamforming techniques, gains in terms of spectral efficiency are reported in [JBF⁺10].

In this chapter, we introduce the non-orthogonal spectrum sharing scenario, where the complete spectrum is shared between different operators. It consists of two base stations (BSs) belonging to different operators and their respective user terminals (UTs). Each base station transmits over the same frequency band to its target user while interference is caused by the other operator, which is modeled as the interference channel. It can be seen as one of the fundamental building blocks of wireless networks from the spectrum sharing point of view. It has been intensely studied over last few decades starting from [Car78]. We view this scenario as a special case of voluntary spectrum sharing, which has been investigated in SAPHYRE [KGH⁺11].

There is a huge amount of literature about the transmit beamforming design for the interference channel from the theoretical point of view [SCP11, PSP10, DY10], which use convex optimization methods. However, the computational complexity is too high for practical implementation since this optimization has to be done on each subcarrier of the orthogonal frequency division multiplexing (OFDM) system. For a practical implementation, the complexity has to be reduced. In this chapter, we introduce three efficient transmit beamforming techniques with a reduced computational complexity. The original block diagonalization (BD) scheme [SSH04] has been designed to suppress the inter-user interference as well as to maximize the system throughput on the downlink of a multi-user MIMO system. The key idea is to zero force the inter-user interferences, which appear as the off-block-diagonal elements of the effective channel of the multi-user MIMO system. Later on the work [SH08] devel-

oped a regularized block diagonalization (RBD) algorithm to further improve the system rate performance. Both precoding algorithms BD and RBD have been widely accepted especially due to their extremely low implementation simplicity. Based on that, we modify the original BD and RBD to adapt them to the interference channel (IC), namely BD and RBD for the IC. To verify the effectiveness of these techniques in real RF signal transmission, they were implemented on a flexible hardware-in-the-loop (HIL) testbed [LKK⁺11]. Both BD and RBD can be applied when multiple antennas are used at BSs and UTs. As a special case, when the BSs employ multiple antennas while the UTs only have single antennas, i.e., multiple-input single-output (MISO) channels, BD and RBD for the IC are simplified to the zero-forcing (ZF) and the minimum mean square error (MMSE) methods, respectively, as shown in [LLL⁺12] and have a low computational complexity.

Although efficient, the biggest shortage of BD and RBD is that they are limited by the transmit and receive antenna configuration, i.e., the number of transmit antennas at BSs must be greater than or equal to the number of receive antennas at UTs. Furthermore, a recent efficient technique named coordinated ZF beamforming (CoZF) [CHHT12] has the dimensionality constraint in the other way. In order to break the antenna configuration constraint and enhance the system spectrum efficiency, the work in [SRH10] developed an iterative beamforming algorithm using BD and RBD at the BSs combined with maximum ratio combining (MRC) at the UTs, which is called flexible coordinated beamforming (FlexCoBF). In contrast to BD, RBD and CoZF, FlexCoBF can be applied for any transmit and receive antenna configuration. We also modify this algorithm for the interference channel, called IC FlexCoBF. In the simulation, the sum rate performance of IC FlexCoBF will be illustrated, taking the work in [CHHT12] as a reference.

The structure of this chapter is arranged as follows. The system model of the non-orthogonal spectrum sharing scenario is introduced in Section 3.1. Following that, two closed-form transmit beamforming techniques BD and RBD for the IC are developed in Section 3.2. The FlexCoBF algorithm for the IC is addressed in Section 3.3.

3.1. System Model

Fig. 3.1 shows the spectrum sharing scenario considered in this chapter, which is modeled as a two-user interference channel (IC). Two base stations (BSs) belonging to two different operators transmit signals in the same spectrum and each BS has one dedicated user terminal (UT). We assume that the BSs and UTs are equipped with $M_{T,i}$ and $M_{U,i}$ transmit and receive antennas respectively, where $i = 1, 2$ denotes the index of each operator. A general case is considered, where several data streams per UT are transmitted.

The easiest way for implementation is to apply linear precoding and decoding at BSs and

UTs, respectively [LLL⁺12]. The received signal $\mathbf{y}_i \in \mathbb{C}^{r_i}$, $i \in \{1, 2\}$ at the UTs are written as

$$\begin{bmatrix} \mathbf{y}_1 \\ \mathbf{y}_2 \end{bmatrix} = \underbrace{\begin{bmatrix} \mathbf{W}_1^H \mathbf{H}_1 \mathbf{F}_1 & \mathbf{W}_1^H \mathbf{G}_1 \mathbf{F}_2 \\ \mathbf{W}_2^H \mathbf{G}_2 \mathbf{F}_1 & \mathbf{W}_2^H \mathbf{H}_2 \mathbf{F}_2 \end{bmatrix}}_{\mathbf{H}_e} \begin{bmatrix} \mathbf{s}_1 \\ \mathbf{s}_2 \end{bmatrix} + \begin{bmatrix} \mathbf{W}_1^H \mathbf{e}_1 \\ \mathbf{W}_2^H \mathbf{e}_2 \end{bmatrix}, \quad (3.1)$$

where r_i is the the number of data streams to be transmitted and $r_i \leq \min\{M_{T,i}, M_{U,i}\}$. The matrices $\mathbf{F}_i \in \mathbb{C}^{M_{T,i} \times r_i}$ and $\mathbf{W}_i \in \mathbb{C}^{M_{U,i} \times r_i}$ denote the precoding and decoding matrices at the BSs and the UTs, respectively. The matrices $\mathbf{H}_i \in \mathbb{C}^{M_{U,i} \times M_{T,i}}$ denote the channel between the BS_{*i*} and the dedicated UT_{*i*} while $\mathbf{G}_i \in \mathbb{C}^{M_{U,i} \times M_{T,j}}$ is the interference channel from the BS_{*j*} to the undesired UT_{*i*}, $i, j \in \{1, 2\}, i \neq j$, as illustrated in Fig. 3.1. The matrix $\mathbf{H}_e \in \mathbb{C}^{2r_i \times 2r_i}$ represents the effective channel. The data vector \mathbf{s}_i has zero mean and $\mathbb{E}\{\mathbf{s}_i \mathbf{s}_i^H\} = \mathbf{I}_{r_i}$. The noise received at the UTs $\mathbf{e}_i \in \mathbb{C}^{M_{U,i}}$ contain independent, identically distributed (i.i.d.) complex additive white Gaussian samples with zero mean and variance σ_n^2 . Based on this model, two closed-form transmit beamforming algorithms are first introduced in Section 3.2, followed by a more flexible iterative algorithm addressed in Section 3.3.

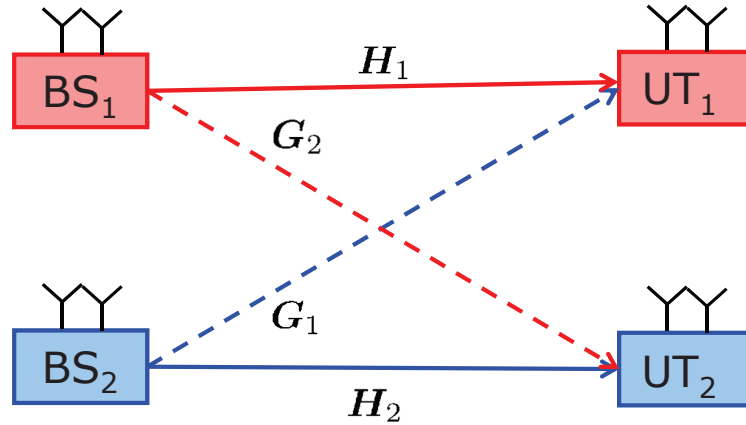


Figure 3.1.: Spectrum sharing scenario, BS_{*i*} has $M_{T,i}$ antennas and UT_{*i*} has $M_{U,i}$ antennas

3.2. Block-Diagonalization (BD) and Regularized Block-Diagonalization (RBD) for the Interference Channel

The original block diagonalization (BD) [SSH04] and regularized block diagonalization (RBD) [SH08] algorithms have been designed to suppress the inter-user interference as well as to maximize the system throughput on the downlink of multi-user MIMO systems. The key idea is to zero force the inter-user interference and to minimize the power of the inter-user interference plus noise, respectively. Both solutions are closed-form and have a low computational complexity from the implementation point of view. Based on these concepts, we modify the BD

and RBD algorithm to be adapted for the inter-operator non-orthogonal spectrum sharing scenario.

We first address the BD algorithm for the IC. The goal is to remove the off-block-diagonal elements in the effective channel \mathbf{H}_e , as defined in equation (3.1), which represent the inter-operator interference. To do that, the null space of the interference channel \mathbf{G}_j , is first extracted. The singular value decomposition (SVD) \mathbf{G}_j is computed as

$$\mathbf{G}_j = \mathbf{U}_j \cdot \boldsymbol{\Sigma}_j \cdot \mathbf{V}_j^H = \mathbf{U}_j \cdot \boldsymbol{\Sigma}_j \cdot \begin{bmatrix} \mathbf{V}_j^{(1)} & \mathbf{V}_j^{(0)} \end{bmatrix}^H \in \mathbb{C}^{M_{U,j} \times M_{T,i}}, \quad (3.2)$$

$j \in \{1, 2\}$. The row space and the null space of \mathbf{G}_j are obtained as the space spanned by the columns of $\mathbf{V}_j^{(1)} \in \mathbb{C}^{M_{T,i} \times l_j}$ and $\mathbf{V}_j^{(0)} \in \mathbb{C}^{M_{T,i} \times (M_{T,i} - l_j)}$, respectively, where l_i denotes the rank of \mathbf{G}_j . After zero-forcing the inter-operator interference, the system is decoupled into parallel single-user MIMO systems and the precoding matrix is designed to maximize the system rate for each operator. The SVD of the effective channel for operator i is written as

$$\mathbf{H}_i \mathbf{V}_j^{(0)} = \mathbf{U}_i \cdot \boldsymbol{\Sigma}_i \cdot \mathbf{V}_i^H = \mathbf{U}_i \cdot \begin{bmatrix} \boldsymbol{\Sigma}_i & \mathbf{0} \\ \mathbf{0} & \mathbf{0} \end{bmatrix} \begin{bmatrix} \mathbf{V}_i^{(1)} & \mathbf{V}_i^{(0)} \end{bmatrix}^H \quad (3.3)$$

for $i, j \in \{1, 2\}$, $i \neq j$, where the columns of $\mathbf{V}_i^{(1)} \in \mathbb{C}^{(M_{T,i} - l_j) \times l_i}$ span the row space of \mathbf{H}_i projected into the null space of \mathbf{G}_j with l_i denoting the rank of $\mathbf{H}_i \mathbf{V}_j^{(0)}$. In order to maximize the sum rate of the operator i , the precoding matrix at BS $_i$ is obtained as

$$\mathbf{F}_i = \mathbf{V}_j^{(0)} \mathbf{V}_i^{(1)} \boldsymbol{\Lambda}^{\frac{1}{2}}, \quad (3.4)$$

where $\boldsymbol{\Lambda} \in \mathbb{C}^{l_i \times l_i}$ is a diagonal power loading matrix using water-filling based on the singular values $\boldsymbol{\Sigma}_i \in \mathbb{C}^{l_i \times l_i}$ as for the single user MIMO system [PNG03]. The decoding matrix at UT $_i$ is

$$\mathbf{W}_i = \mathbf{U}_i^{(1)}, \quad (3.5)$$

where columns of $\mathbf{U}_i^{(1)}$ span the column space of $\mathbf{H}_i \mathbf{V}_j^{(0)}$. In the case of single stream transmission, the precoding vector is simplified to $\mathbf{f}_i = \mathbf{V}_j^{(0)} \mathbf{v}_i^{(1)}$, where $\mathbf{v}_i^{(1)}$ is the first column of $\mathbf{V}_i^{(1)}$. The decoding vector at the UTs is obtained as $\mathbf{w}_i = \mathbf{u}_i^{(1)}$ with $\mathbf{u}_i^{(1)}$ denoting the left dominant singular vector of $\mathbf{H}_i \mathbf{V}_j^{(0)}$.

Instead of zero-forcing the inter-operator interference, RBD for the IC is designed to maximize the system sum rate under the constraint that the Frobenius norm of the inter-operator interference plus noise is minimized. The precoding matrix at BS $_i$ is designed as $\mathbf{F}_i = \beta \mathbf{F}_{i,a} \mathbf{F}_{i,b}$, where $\mathbf{F}_{i,a}$ is used to suppress the inter-operator interference while $\mathbf{F}_{i,b}$ facilitates the rate optimization for operator i . Additionally, we have a scalar β to fulfill the transmit power constraint at the BSs. Assuming that $\|\mathbf{F}_{i,b}\|_F = 1$ and full-power transmission, we have $\beta^2 \|\mathbf{F}_{i,a} \mathbf{F}_{i,b}\|_F^2 = \beta^2 \|\mathbf{F}_{i,a}\|_F^2 = P_T$. Therefore, we choose $\beta = \sqrt{P_T} / \|\mathbf{F}_{i,a}\|_F$. The matrix $\mathbf{F}_{i,a}$ is

designed to minimize the Frobenius norm of the inter-operator interference plus noise, i.e.,

$$\mathbf{F}_{i,a} = \min_{\mathbf{F}_{i,a}} \mathbb{E} \left\{ \left\| \mathbf{G}_j \mathbf{F}_{i,a} \right\|_F^2 + \frac{\left\| \mathbf{n}_j \right\|_2^2}{\beta^2} \right\}, \quad (3.6)$$

where $i, j \in \{1, 2\}$, $i \neq j$. After similar derivations as in [SH08] and in combination with (3.2), we get

$$\mathbf{F}_{i,a} = \mathbf{M}_{i,a} \mathbf{D}_{i,a}, \quad (3.7)$$

where

$$\mathbf{M}_{i,a} = \mathbf{V}_j \in \mathbb{C}^{M_{T,i} \times M_{T,i}} \quad (3.8)$$

and

$$\mathbf{D}_{i,a} = \left(\boldsymbol{\Sigma}_j^T \boldsymbol{\Sigma}_j + \frac{M_{U,j} \cdot \sigma_n^2}{P_{T,i}} \right)^{-\frac{1}{2}} \in \mathbb{C}^{M_{T,i} \times M_{T,i}} \quad (3.9)$$

is a diagonal power loading matrix. Using similar steps as in BD for the IC, the effective channel after interference suppression is written as

$$\mathbf{H}_i \mathbf{F}_{i,a} = \mathbf{U}_i \cdot \boldsymbol{\Sigma}_i \cdot \mathbf{V}_i^H = \mathbf{U}_i \cdot \boldsymbol{\Sigma}_i \cdot \begin{bmatrix} \mathbf{V}_i^{(1)} & \mathbf{V}_i^{(0)} \end{bmatrix}^H. \quad (3.10)$$

The matrix $\mathbf{F}_{i,b}$ is obtained as $\mathbf{F}_{i,b} = \mathbf{V}_i^{(1)} \boldsymbol{\Lambda}^{\frac{1}{2}}$ to enhance the sum rate for operator i , where the columns of $\mathbf{V}_i^{(1)} \in \mathbb{C}^{M_{T,i} \times l_i}$ span the row space of $\mathbf{H}_i \mathbf{F}_{i,a}$ with l_i denoting the rank of $\mathbf{H}_i \mathbf{F}_{i,a}$. The matrix $\boldsymbol{\Lambda}$ is the diagonal power loading matrix using water-filling. The decoding matrix is obtained as $\mathbf{W}_i = \mathbf{U}_i^{(1)}$, where the columns of $\mathbf{U}_i^{(1)}$ span the row space of $\mathbf{H}_i \mathbf{F}_{i,a}$. Considering the special case of single stream transmission, the precoding vector is obtained as $\mathbf{f}_{i,b} = \mathbf{v}_i^{(1)}$ to enhance the signal to interference plus noise (SINR), where $\mathbf{v}_i^{(1)}$ is the right dominant singular vector of $\mathbf{H}_i \mathbf{F}_{i,a}$. The decoding vector is $\mathbf{w}_i = \mathbf{u}_i^{(1)}$, which is the left dominant singular vector of $\mathbf{H}_i \mathbf{F}_{i,a}$.

Both BD and RBD for the IC are closed-form solutions and no iterations are required, which keeps the implementation complexity extremely low. Furthermore, RBD for the IC improves the system sum rate performance at low SNRs compared to BD due to that it balances the inter-operator interference with the noise enhancement. At high SNRs, the sum rate performance obtained by BD for the IC and RBD for the IC converge. The drawback of BD for the IC is that the system has an antenna configuration constraint to assure the existence of the null space, i.e., $M_{T,i} > M_{U,j}$ for $i, j \in \{1, 2\}$, $i \neq j$. The RBD algorithm for the IC could be applied to any antenna configuration, but the sum rate performance degrades dramatically as the SNR increases when $M_{T,i} \leq M_{U,j}$ due to the fact that RBD for the IC turns out to extract the null space at high SNRs as BD for the IC does [LLL⁺12].

3.3. Flexible Coordinated Beamforming for the Interference Channel

On the basis of BD and RBD for the IC, we introduce a low-complexity suboptimal transceiver design named flexible coordinated beamforming for the interference channel (IC FlexCoBF) [KGH⁺11]. This algorithm is designed for any antenna configuration in order to relax the dimensionality constraint in BD and RBD for the IC. Furthermore, it maximizes the sum rate by suppressing the interference iteratively and strengthening the desired signal.

The original FlexCoBF algorithm [SRH10] has been designed to iteratively suppress the inter-user interference on the downlink of multi-user MIMO systems, utilizing either BD [SSH04] or RBD [SH08] at the BSs, combined with maximum ratio combining (MRC) at the receiver. Inspired by this idea, we derive an algorithm suitable for the non-orthogonal spectrum sharing scenario.

To start, the decoding matrices \mathbf{W}_1 , \mathbf{W}_2 are randomly initialized. In the following, we sketch the design of \mathbf{F}_i at the BS $_i$, $i = 1, 2$, which uses either BD for the IC or RBD for the IC. If BD for the IC is applied, we first calculate the SVD of the equivalent interference channel which operator i causes to operator j with $j \neq i$ as

$$\tilde{\mathbf{G}}_j = \mathbf{W}_j^H \mathbf{G}_j = \tilde{\mathbf{U}}_j \cdot \tilde{\Sigma}_j \cdot \begin{bmatrix} \tilde{\mathbf{V}}_j^{(1)} & \tilde{\mathbf{V}}_j^{(0)} \end{bmatrix}^H. \quad (3.11)$$

The row space and the null subspace of $\tilde{\mathbf{G}}_j$ is spanned by the columns of $\tilde{\mathbf{V}}_j^{(1)} \in \mathbb{C}^{M_{T,i} \times \tilde{l}_j}$ and $\tilde{\mathbf{V}}_j^{(0)} \in \mathbb{C}^{M_{T,i} \times (M_{T,i} - \tilde{l}_j)}$, respectively, where \tilde{l}_j is rank of $\tilde{\mathbf{G}}_j$. In order to maximize the sum rate of operator i under the zero-interference constraint to operator j , we calculate the SVD of the equivalent desired channel of operator i

$$\mathbf{W}_i^H \mathbf{H}_i \tilde{\mathbf{V}}_j^{(0)} = \mathbf{U}'_i \cdot \begin{bmatrix} \Sigma'_i & \mathbf{0} \\ \mathbf{0} & \mathbf{0} \end{bmatrix} \cdot \begin{bmatrix} \mathbf{V}'_i^{(1)} & \mathbf{V}'_i^{(0)} \end{bmatrix}^H, \quad (3.12)$$

where $\Sigma'_i \in \mathbb{C}^{l'_i \times l'_i}$, $\mathbf{V}'_i^{(1)} \in \mathbb{C}^{(M_{T,i} - \tilde{l}_j) \times l'_i}$ and l'_i denotes the rank of $\mathbf{W}_i^H \mathbf{H}_i \tilde{\mathbf{V}}_j^{(0)}$. The precoder \mathbf{F}_i is thus obtained as

$$\mathbf{F}_i = \tilde{\mathbf{V}}_j^{(0)} \tilde{\mathbf{V}}_i'^{(1)} \tilde{\mathbf{A}}_i^{\frac{1}{2}} \in \mathbb{C}^{M_{T,i} \times l'_i}, \quad (3.13)$$

where $\tilde{\mathbf{A}}_i \in \mathbb{C}^{l'_i \times l'_i}$ is a diagonal power loading matrix using water-filling on the basis of the singular values $\tilde{\Sigma}_i$.

When RBD for the IC is used, the precoder is designed in two steps. Let $\mathbf{F}_i = \alpha \mathbf{F}_{i,a} \mathbf{F}_{i,b}$, where $\mathbf{F}_{i,a}$ is used to suppress the interference that the operator i causes to operator j and $\mathbf{F}_{i,b}$ facilitates the sum rate optimization of the operator i . The scalar α is used to fulfill the transmit power constraint. Assuming that $\|\mathbf{F}_{i,b}\| = 1$ and that the transmit signal \mathbf{s}_i are temporally uncorrelated with zero mean and unit variance $\mathbb{E}\{\mathbf{s}_i \mathbf{s}_i^H\} = \mathbf{I}_{r_i}$, we have

$\alpha^2 \|\mathbf{F}_{i,a} \mathbf{F}_{i,b} \mathbf{s}_i\|_2^2 = \alpha^2 \|\mathbf{F}_{i,a}\|_F^2 \leq P_{T,i}$. Therefore, we choose

$$\alpha = P_{T,i} / \text{tr}\{\mathbf{F}_{i,a} \mathbf{F}_{i,a}^H\} \quad (3.14)$$

with $P_{T,i}$ denoting the transmit power of BS_{*i*}. After computing the SVD of the effective interference channel

$$\tilde{\mathbf{G}}_j = \mathbf{W}_j^H \mathbf{G}_j = \tilde{\mathbf{U}}_j \cdot \tilde{\Sigma}_j \cdot \tilde{\mathbf{V}}_j^H, \quad (3.15)$$

we get

$$\mathbf{F}_{i,a} = \mathbf{M}_{i,a} \mathbf{D}_{i,a} \quad (3.16)$$

similarly as in (3.7), where

$$\mathbf{M}_{i,a} = \tilde{\mathbf{V}}_j \in \mathbb{C}^{M_{T,i} \times M_{T,i}} \quad (3.17)$$

and

$$\mathbf{D}_{i,a} = \left(\tilde{\Sigma}_j^T \tilde{\Sigma}_j + \frac{M_{U,j} \sigma_n^2}{P_{T,i}} \mathbf{I}_{M_{T,i}} \right)^{-1/2} \in \mathbb{C}^{M_{T,i} \times M_{T,i}} \quad (3.18)$$

is a diagonal power loading matrix. By computing the SVD of the equivalent desired channel

$$\mathbf{W}_i^H \mathbf{H}_i \mathbf{F}_{i,a} = \mathbf{U}'_i \cdot \begin{bmatrix} \Sigma'_i & \mathbf{0} \\ \mathbf{0} & \mathbf{0} \end{bmatrix} \cdot \left[\mathbf{V}'_i^{(1)} \quad \mathbf{V}'_i^{(0)} \right]^H, \quad (3.19)$$

the matrix $\mathbf{F}_{i,b}$ is obtained as

$$\mathbf{F}_{i,b} = \mathbf{V}'_i^{(1)} \mathbf{\Lambda}'_i^{\frac{1}{2}}, \quad (3.20)$$

where $\mathbf{V}'_i^{(1)} \in \mathbb{C}^{M_{T,i} \times l'_i}$ with l'_i denoting the rank of $\mathbf{W}_i^H \mathbf{H}_i \mathbf{F}_{i,a}$ and $\mathbf{\Lambda}'_i \in \mathbb{C}^{l'_i \times l'_i}$ is the diagonal power loading matrix using water filling based on Σ'_i . The precoding matrix is finally obtained as

$$\mathbf{F}_i = \alpha \mathbf{F}_{i,a} \mathbf{F}_{i,b}, \quad (3.21)$$

where α , $\mathbf{F}_{i,a}$ and $\mathbf{F}_{i,b}$ are specified in (3.14), (3.16) and (3.20).

After the precoding matrix is obtained from either BD for the IC using (3.13) or RBD for the IC using (3.21), the decoding matrix at UT_{*i*} is updated as $\mathbf{W}_i = \mathbf{H}_i \mathbf{F}_i$ for the next iteration. The procedure continues until the stopping criterion is fulfilled, i.e., the interference power is below a predefined threshold.

Simulations

Without loss of generality, we consider the single-stream transmission in the non-orthogonal

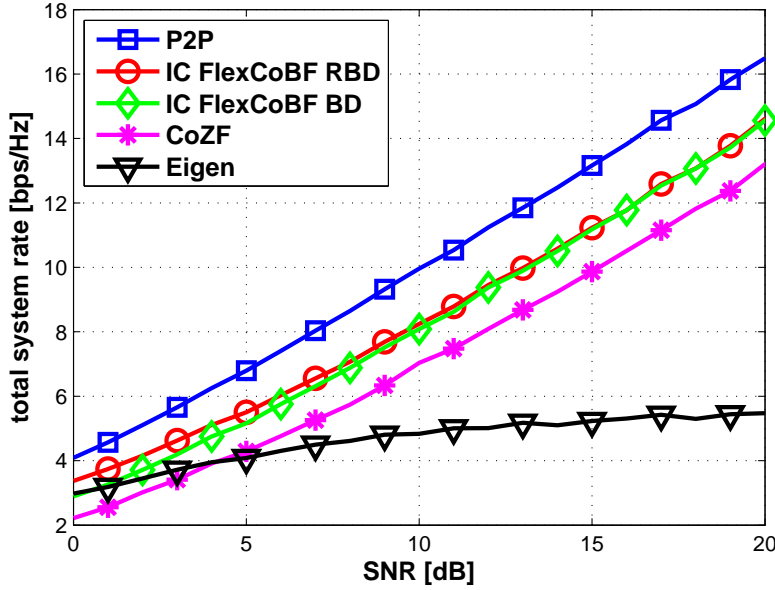


Figure 3.2.: Sum rate vs SNR for the non-orthogonal spectrum sharing scenario

spectrum sharing scenario. A recent technique named ZF coordinated beamforming (CoZF) [CHHT12] is used as a benchmark. The basic principle is that assuming MRC at UTs, the precoder is chosen as a generalized eigenvector of $\mathbf{G}_i^H \mathbf{H}_i$ and $\mathbf{H}_j^H \mathbf{G}_j$ for $i \neq j$ so as to zero-forcing the inter-operator interference. Although simple, this method has the dimensionality constraint that $M_{T,i} \leq M_{U,j}$ due to the full-rank requirement of these equivalent channel matrices.

The sum rate performance in the non-orthogonal spectrum sharing scenario is given in Fig. 3.2, by applying precoding at BSs using IC FlexCoBF as well as CoZF. We assume that perfect link adaptation and perfect synchronization can be achieved. Each element of the channels \mathbf{H}_i and \mathbf{G}_i is a zero mean circularly symmetric complex Gaussian random variable with unit variance $\mathcal{CN}(0,1)$. The transmit power of the BSs is P_T and the SNR is defined as P_T/σ_n^2 . Both the BSs and UTs are equipped with 2 antennas. Single stream transmission is assumed here as [CHHT12] did. As a reference, we also include an ideal point-to-point (P2P) transmission as the upper bound, where eigen-beamforming is performed at the BSs and no inter-operator interference is taken into account. Another reference scheme named Eigen is also plotted, where eigen-beamforming is performed at both BSs while treating the inter-operator interference as noise. It is observed that IC FlexCoBF combined with either RBD or BD for the IC performs much better than CoZF within all SNR ranges. At low SNRs, IC FlexCoBF with RBD for the IC gives a better performance than that of IC FlexCoBF with BD for the IC due to a better balance of the interference suppression and the noise enhancement. In this regime, Eigen is also an alternative which improves the system sum rate compared to the benchmark CoZF.

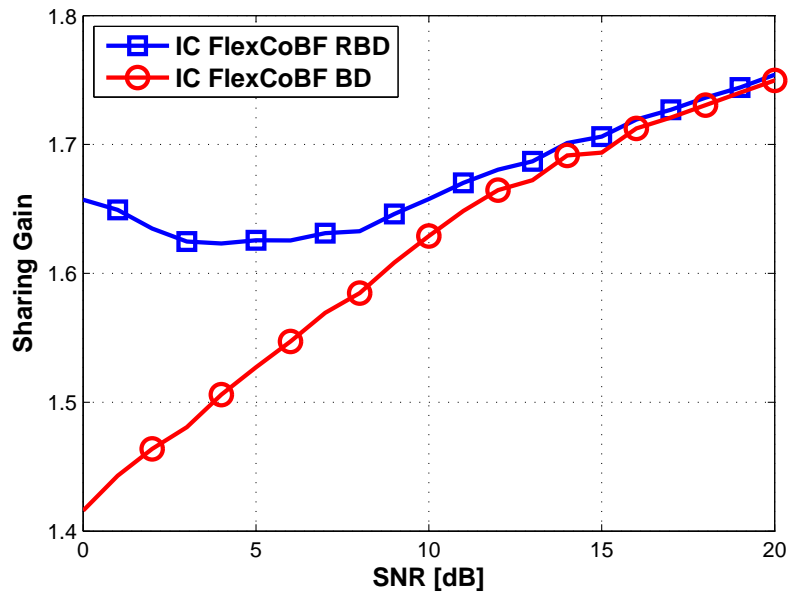


Figure 3.3.: Sharing gain for the non-orthogonal spectrum sharing scenario

We refer to the ratio of throughput (TP) of the non-orthogonal spectrum sharing over that of orthogonal spectrum sharing, written as $TP_{\text{non-orthogonal}} / TP_{\text{orthogonal}}$, as the *sharing gain* due to the use of the shared spectrum instead of accessing the spectrum by each operator in a time division multiple access (TDMA) manner. This sharing gain is shown in Fig. 3.3, where IC FlexCoBF and eigen beamforming are applied at the BS for the non-orthogonal sharing and orthogonal sharing case, respectively. It can be seen that non-orthogonal spectrum sharing scenario utilizing either IC FlexCoBF with RBD for the IC or IC FlexCoBF with BD for the IC provides a significant sharing gain over the orthogonal sharing scheme which uses the spectrum exclusively. For IC FlexCoBF with BD for the IC, the non-orthogonal sharing gain becomes larger as the SNR increases. When IC FlexCoBF with RBD for the IC is applied, there is even an improvement at low SNRs due to the regularization of RBD for the IC. This shows that non-orthogonal spectrum sharing is more advantageous compared to the exclusive use of the spectrum.

To summarize, the precoding design for the non-orthogonal spectrum sharing scenario is introduced in this chapter, where two BSs belonging to different operators transmit simultaneously over the same spectrum. Two closed-form transmit beamforming schemes, i.e., BD for the IC and RBD for the IC are first developed for this scenario. On as basis of that, a more flexible beamforming algorithm named IC FlexCoBF is designed to further enhance the system spectrum efficiency, which can be applied for any transmit and receive antenna configuration. Simulation results reveal that the proposed IC FlexCoBF improves the spectral efficiency dramatically compared to the state of the art work and a large sharing gain is observed by non-orthogonal spectrum sharing instead of exclusive use of the spectrum. The precoding algorithms introduced in this chapter can be easily extended to more than

two operators. In the case of BD for the IC, the precoder of each BS is designed to extract the common null space of the interference channels, which are induced by each BS to the undesired users. Similarly as for the two-user case, RBD for the IC turns out to minimize the power of the noise plus the interference caused by a specified BS to all the undesired users. Based on that, IC FlexCoBF can be also applied in the multiple operator scheme.

4. Multiple Operator One-Way Relaying without Direct Link

In addition to non-orthogonal spectrum sharing introduced in Chapter 3, SAPHYRE also investigates a scheme that includes both spectrum and infrastructure sharing in order to make more effective use of the physical resources, i.e., to alleviate the pressure of spectrum management as well as to further reduce the infrastructure cost. Infrastructure can be shared in various ways, including base station, antenna, relay, radio network controller, etc. In particular, we discuss relay sharing between multiple operators throughout Part I of this dissertation. To be more specific, the relay assisted communications are investigated in Chapter 4 and Chapter 5, where the relay as well as the spectrum are shared between multiple operators.

In recent years, the use of relays has drawn enormous attention due to its promising capability in achieving reliable communications and coverage extension in wireless networks. In these scenarios, where the link quality cannot be guaranteed due to large path loss, shadowing effect, multipath fading, etc., relays can be employed between the source and the destination to assist the communication [LWT01], [LW00], [SEA03a], [SEA03b]. Various relaying schemes have been presented in the literature, including the amplify-and-forward (AF) [MMVA07], [TH07], [RW04], and decode-and-forward (DF) [LW00]. The comparison between analog AF, digital AF, and DF can be found in Table 2.1. Among several cooperative schemes, the digital AF is more attractive since it does not do decoding but simply amplifies the received signal from the source and forwards it to the destination. Moreover, the digital AF does not require decoding and re-encoding of the data as required for the DF relay, where more complicated baseband processing causes a much higher latency. Throughout this thesis, we focus on the design of the digital AF relaying.

Moreover, considering the fact that the MIMO technique [Tel99] enhances the system capacity by combating fading and interference, it makes sense to exploit the advantages of the combination of MIMO and relays. Several works on capacity bounds of MIMO relay channels have been firstly addressed in [WZ03], [WZHM05], [HMZ05], and [LVRWH05]. The optimal design of the AF MIMO relay in a point-to-point communication is investigated in [MMVA07] and [TH07]. In addition to that, the MIMO relay is also deployed on the multi-user downlink to improve the system performance [CTHC08], [ZCL09]. More recently, the MIMO AF relay is applied for multi-point to multi-point communication, which is the scenario discussed in this chapter.

In this scenario, a MIMO AF relay is employed to assist the transmission between multiple

pairs of BSs and UTs, where the direct link between the source and the destination is neglected. There are many relay operation modes, including one-way relaying, two-way relaying, etc. Two-way relaying transmission is not always advantageous over one-way relaying. As pointed out in [SY12], two-way relaying is not always more energy efficient than one-way relaying if the number of bits to be transmitted in the two directions are unequal, or the circuit power consumptions at each node are different. Moreover, one-way relaying attracts more interest from the implementation point of view because of the difficult synchronization between the BSs and the UTs to transmit simultaneously [FLZS12]. In this thesis, we focus on one-way relaying transmission. We propose several algorithms for the relay precoder design to further improve the system performance. First a set of algorithms named efficient relay sharing rate maximization (EReSh-RM) is designed to improve the system sum rate under the relay transmit power constraint. After that, the relay precoder design is systematically studied for power efficient transmission. In the previous work [CVL07], the relay precoder is designed with respect to relay transmit power, considering perfect channel state information at the relay. Later on the work in [CV09] designs a relay precoder in order to minimize the relay transmit power in the worst case subject to the worst case SINR, assuming imperfect channel state information at the relay. The worst case of the relay transmit power and SINR refer to the maximum relay power and the minimum SINR for the largest possible channel errors, respectively. Our work is focused on minimizing the average relay transmit power under the SINR constraint to be satisfied for each transceiver pair. For the case where the BSs and UTs are equipped with single antennas, a global optimum solution is firstly derived, which uses a convex optimization tool to exploit the structure of the relay precoder. Taking this as a benchmark, several suboptimal beamforming algorithms are proposed to find a compromise between the achievable power efficiency and the computational complexity, including a closed-form algorithm named Efficient Resource Sharing Power Minimization (EReSh-PM) and block diagonalization (BD) [SSH04] based solutions. Further, a novel robust relay precoder design is proposed by considering imperfect CSI at the relay. At last, we extend our study to the case where each pair of BSs and UTs are equipped with multiple antennas and a novel relay matrix design is derived for multiple stream transmission between multiple pairs of BSs and UTs.

The structure of this chapter is arranged as follows. The system model for the AF relay sharing scenario is introduced in Section 4.1. Then the EReSh-RM algorithms are addressed in Section 4.2. To make more efficient use of the relay power, several algorithms are proposed for the single stream transmission scheme in Section 4.3, where each BS and UT are equipped with a single antenna. After that, Section 4.4 describes a robust relay precoder design assuming that only an erroneous channel estimation is available. Section 4.5 extends the work to multiple stream transmission for the more general case and a novel algorithm is proposed to minimize the relay transmit power subject to the SINR constraints for each data stream.

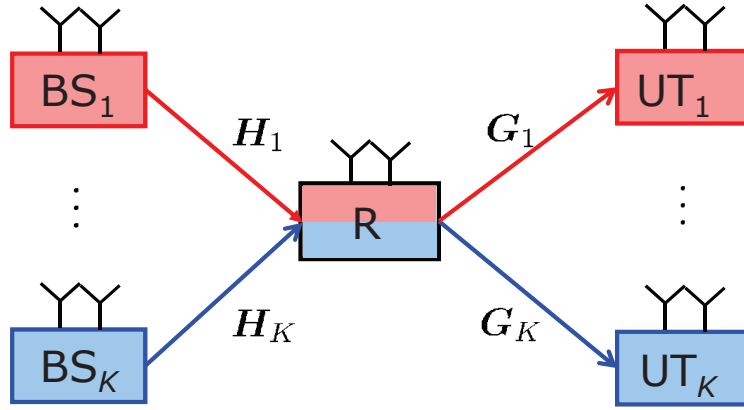


Figure 4.1.: System Model for relay sharing between multiple operators

4.1. System Model

A multi-user amplify and forward (AF) relay sharing system is considered as shown in Fig. 4.1, where K BSs transmit data to their respective target UTs with the assistance of a shared AF relay which operates in half-duplex mode. Each BS and UT is equipped with $M_{T,k}$ and $M_{U,k}$ antennas, where $k = 1, \dots, K$. The total number of antennas at the BSs and the UTs are denoted as $M_T = \sum_{k=1}^K M_{T,k}$ and $M_U = \sum_{k=1}^K M_{U,k}$, respectively. The relay has M_R antennas. In this chapter, the direct links between BSs and UTs are not used since we assume that they are weak due to large path loss or shadowing. Later in Chapter 5, the direct link is assumed to be not negligible.

The transmission process consists of two phases. During the multiple access channel (MAC) phase, the received signal vector at the relay from multiple BSs is

$$\mathbf{y}_R = \mathbf{H}\bar{\mathbf{s}} + \mathbf{n}_R,$$

where $\mathbf{H} = [\mathbf{H}_1, \dots, \mathbf{H}_K] \in \mathbb{C}^{M_R \times M_T}$. The matrices $\mathbf{H}_k \in \mathbb{C}^{M_R \times M_{T,k}}$ denote the channels between each BS and the relay. The transmit signal at each BS is $\bar{\mathbf{s}}_k = \mathbf{F}_k \mathbf{s}_k \in \mathbb{C}^{M_{T,k}}$, where \mathbf{F}_k are the precoding matrices at the BSs. In compact form, the transmit signal is written as $\bar{\mathbf{s}} = [\bar{\mathbf{s}}_1^T, \dots, \bar{\mathbf{s}}_K^T]^T \in \mathbb{C}^{M_T}$. The transmit power at each BS is constrained by P_T , i.e., $\mathbb{E}\{\text{tr}(\bar{\mathbf{s}}_k \bar{\mathbf{s}}_k^H)\} \leq P_T$. In the broadcast channel (BC) phase, the relay amplifies the received signal \mathbf{y}_R and forwards it to the UTs. The transmitted signal of the shared relay is

$$\mathbf{x}_R = \mathbf{F}_R \mathbf{y}_R = \mathbf{F}_R \mathbf{H} \bar{\mathbf{s}} + \mathbf{F}_R \mathbf{n}_R = \sum_{k=1}^K \mathbf{F}_R \mathbf{H}_k \bar{\mathbf{s}}_k + \mathbf{F}_R \mathbf{n}_R,$$

where $\mathbf{F}_R \in \mathbb{C}^{M_R \times M_R}$ denotes the relay amplification matrix. The signals received at the UTs

are given by

$$\mathbf{y}_k = \mathbf{G}_k \mathbf{F}_R \mathbf{H}_k \bar{\mathbf{s}}_k + \left(\sum_{j=1, j \neq k}^K \mathbf{G}_k \mathbf{F}_R \mathbf{H}_j \bar{\mathbf{s}}_j \right) + \mathbf{G}_k \mathbf{F}_R \mathbf{n}_R + \mathbf{n}_k \in \mathbb{C}^{M_{U,k}}, k = 1, 2, \dots, K$$

where $\mathbf{G} = \left[\mathbf{G}_1^T, \dots, \mathbf{G}_K^T \right]^T \in \mathbb{C}^{M_U \times M_R}$ and $\mathbf{G}_k \in \mathbb{C}^{M_{U,k} \times M_R}$ denotes the channel between the relay and each UT. The first term denotes the desired signal while the second term stands for the interference that needs to be mitigated. All the remaining terms are the effective noise. The noise at the relay \mathbf{n}_R and that at the UTs \mathbf{n}_k for $k = 1, 2, \dots, K$ contain independent, identically distributed complex additive white Gaussian noise samples with variance σ_n^2 , i.e., $\mathbb{E}\{\mathbf{n}_R \mathbf{n}_R^H\} = \sigma_n^2 \mathbf{I}_{M_R}$ and $\mathbb{E}\{|n_k|^2\} = \sigma_n^2$. In Section 4.3 and Section 4.5 it is assumed that the relay has perfect knowledge of all the channel state information (CSI), i.e., it knows all \mathbf{H}_k and \mathbf{G}_k perfectly, while in Section 4.4 an erroneous CSI is available at the relay.

4.2. System Sum Rate Maximization

In this section, a set of algorithms is developed for system sum rate maximization under the relay transmit power constraint. We name it as efficient relay sharing rate maximization (EReSh-RM). The main contribution of this section has been published in reference [LRH11a].

The relay amplification matrix is designed as $\mathbf{F}_R = \gamma \tilde{\mathbf{F}}_R$, where

$$\tilde{\mathbf{F}}_R = \mathbf{F}_{BC} \boldsymbol{\Phi} \mathbf{F}_{MAC} \in \mathbb{C}^{M_R \times M_R} \quad (4.1)$$

and γ is a real scaling factor to fulfill the relay transmit power constraint. The matrices \mathbf{F}_{MAC} and \mathbf{F}_{BC} are applied for interference suppression during the MAC and the BC phase, respectively. The block diagonal matrix $\boldsymbol{\Phi} = \text{blockdiag}\{\boldsymbol{\Phi}_1, \boldsymbol{\Phi}_2, \dots, \boldsymbol{\Phi}_K\}$ is used to strengthen the desired signal of each operator, where $\text{blockdiag}\{\cdot\}$ means that the matrices $\boldsymbol{\Phi}_k$ are arranged in a block diagonal manner.

The first method belonging to the EReSh-RM family is called regularized block diagonalization / single channel algebraic norm maximization (RBD/SC-ANOMAX). To design \mathbf{F}_{MAC} and \mathbf{F}_{BC} , the regularized block diagonalization (RBD) [SH08] algorithm is adopted due to the fact that RBD offers a good sum rate performance by balancing the interference suppression and noise power enhancement. Take the design of \mathbf{F}_{MAC} as an example. The matrix \mathbf{F}_{MAC} is used to minimize the induced interference and noise power during the MAC phase. An additional constraint is imposed on $\mathbf{F}_{MAC,k}$ so that a non-trivial solution is obtained. The problem is formulated as follows,

$$\begin{aligned} \mathbf{F}_{MAC} &= \arg \min_{\mathbf{F}_{MAC}} \left\| \sum_{k=1}^K \mathbf{F}_{MAC,k} \tilde{\mathbf{H}}_k \tilde{\mathbf{s}}_k \right\|_2^2 + \left\| \sum_{k=1}^K \mathbf{F}_{MAC,k} \mathbf{n}_R \right\|_2^2, \\ \text{s.t. } \mathbb{E} \left\| \mathbf{F}_{MAC,k} \right\|_2 &= 1 \end{aligned} \quad (4.2)$$

The first term denotes the block off-diagonal elements that form the interference, where

$\tilde{\mathbf{H}}_k = \left[\mathbf{H}_1, \dots, \mathbf{H}_{k-1}, \mathbf{H}_{k+1}, \dots, \mathbf{H}_K \right]$ and $\tilde{\mathbf{s}}_k = \left[\mathbf{s}_1^T, \dots, \mathbf{s}_{k-1}^T, \mathbf{s}_{k+1}^T, \dots, \mathbf{s}_K^T \right]^T$. Furthermore, the cost function of (4.2) can be further written as

$$\mathbf{F}_{\text{MAC}} = \arg \min_{\mathbf{F}_{\text{MAC},k}} \sum_{k=1}^K \text{tr} \left(\mathbf{F}_{\text{MAC},k} \left(\frac{P_{\text{T}}}{M_{\text{T},k}} \tilde{\mathbf{H}}_k \tilde{\mathbf{H}}_k^H + \sigma_{\text{R}}^2 \mathbf{I}_{M_{\text{R}}} \right) \mathbf{F}_{\text{MAC},k}^H \right). \quad (4.3)$$

By computing the singular value decomposition (SVD) of $\tilde{\mathbf{H}}_k = \tilde{\mathbf{U}}_{\tilde{\mathbf{H}}_k} \tilde{\Sigma}_{\tilde{\mathbf{H}}_k} \tilde{\mathbf{V}}_{\tilde{\mathbf{H}}_k}^H$ and inserting it into (4.3), the matrix \mathbf{F}_{MAC} is obtained as

$$\mathbf{F}_{\text{MAC}} = \arg \min_{\mathbf{F}_{\text{MAC},k}} \sum_{k=1}^K \text{tr} \left(\mathbf{F}_{\text{MAC},k} \tilde{\mathbf{U}}_{\tilde{\mathbf{H}}_k} \left(\frac{P_{\text{T}}}{M_{\text{T},k}} \tilde{\Sigma}_{\tilde{\mathbf{H}}_k} \tilde{\Sigma}_{\tilde{\mathbf{H}}_k}^T + \sigma_{\text{R}}^2 \mathbf{I}_{M_{\text{R}}} \right) \tilde{\mathbf{U}}_{\tilde{\mathbf{H}}_k}^H \mathbf{F}_{\text{MAC},k}^H \right). \quad (4.4)$$

A solution to (4.4) is derived in a similar procedure as in the appendix of [SH08], which gives a non-scaled solution as $\tilde{\mathbf{F}}_{\text{MAC},k}$ as follows,

$$\tilde{\mathbf{F}}_{\text{MAC},k} = \left(\frac{P_{\text{T}}}{M_{\text{T},k}} \tilde{\Sigma}_{\tilde{\mathbf{H}}_k} \tilde{\Sigma}_{\tilde{\mathbf{H}}_k}^T + \sigma_{\text{R}}^2 \mathbf{I}_{M_{\text{R}}} \right)^{-1/2} \mathbf{U}_{\tilde{\mathbf{H}}_k}^H \in \mathbb{C}^{M_{\text{R}} \times M_{\text{R}}}. \quad (4.5)$$

The matrix obtained in (4.5) is further normalized as $\mathbf{F}_{\text{MAC},k} = \tilde{\mathbf{F}}_{\text{MAC},k} / \|\tilde{\mathbf{F}}_{\text{MAC},k}\|$ so that the constraint in (4.2) is satisfied. Finally, the matrix \mathbf{F}_{MAC} is formed as

$$\mathbf{F}_{\text{MAC}} = \left[\mathbf{F}_{\text{MAC},1}^H, \dots, \mathbf{F}_{\text{MAC},K}^H \right]^H. \quad (4.6)$$

Similarly, the matrix \mathbf{F}_{BC} is designed to minimize the power of the generated interference plus noise during the BC phase, i.e.,

$$\begin{aligned} \mathbf{F}_{\text{BC}} &= \arg \min_{\mathbf{F}_{\text{BC}}} \left\| \sum_{k=1}^K \tilde{\mathbf{G}}_k \mathbf{F}_{\text{BC},k} \tilde{\mathbf{s}}_k \right\|_2^2 + \frac{\|\mathbf{n}\|_2^2}{\beta^2}, \\ \text{s.t. } \mathbb{E} \|\mathbf{F}_{\text{BC},k}\|_2 &= 1 \end{aligned} \quad (4.7)$$

where $\tilde{\mathbf{G}}_k = \left[\mathbf{G}_1^H, \dots, \mathbf{G}_{k-1}^H, \mathbf{G}_{k+1}^H, \dots, \mathbf{G}_K^H \right]^H$ and $\mathbf{n} = \left[\mathbf{n}_1^T, \dots, \mathbf{n}_K^T \right]^T$ is the noise vector. The parameter β is a real scaling factor that is used to fulfill the relay transmit power constraint, which is a function of \mathbf{F}_{BC} . A similar derivation procedure is applied as in the MAC phase and a non-scaled solution $\tilde{\mathbf{F}}_{\text{BC},k}$ is obtained as follows,

$$\tilde{\mathbf{F}}_{\text{BC},k} = \mathbf{V}_{\tilde{\mathbf{G}}_k} \left(\frac{P_{\text{T}}}{M_{\text{T},k}} \left(\tilde{\Sigma}_{\tilde{\mathbf{G}}_k} \tilde{\Sigma}_{\tilde{\mathbf{G}}_k} + \frac{M_{\text{U}} \sigma_{\text{n}}^2}{P_{\text{R}}} \mathbf{I}_{M_{\text{R}}} \right) \right)^{-1/2} \in \mathbb{C}^{M_{\text{R}} \times M_{\text{R}}} \quad (4.8)$$

The matrix $\mathbf{V}_{\tilde{\mathbf{G}}_k}$ and $\tilde{\Sigma}_{\tilde{\mathbf{G}}_k}$ comes from the SVD of $\tilde{\mathbf{G}}_k$, which is given by $\tilde{\mathbf{G}}_k = \tilde{\mathbf{U}}_{\tilde{\mathbf{G}}_k} \tilde{\Sigma}_{\tilde{\mathbf{G}}_k} \tilde{\mathbf{V}}_{\tilde{\mathbf{G}}_k}^H$. The matrix obtained in (4.8) is further normalized as $\mathbf{F}_{\text{BC},k} = \tilde{\mathbf{F}}_{\text{BC},k} / \|\tilde{\mathbf{F}}_{\text{BC},k}\|$ so that the constraint in (4.7) is satisfied.

The matrix \mathbf{F}_{BC} is obtained as

$$\mathbf{F}_{\text{BC}} = \left[\mathbf{F}_{\text{BC},1}, \dots, \mathbf{F}_{\text{BC},K} \right] \quad (4.9)$$

After applying \mathbf{F}_{MAC} and \mathbf{F}_{BC} , the system is decoupled into multiple parallel one-way relaying sub-systems and the received signal vector at each UT is given by

$$\mathbf{y}_k = \mathbf{G}_k \mathbf{F}_{\text{BC},k} \boldsymbol{\Phi}_k \mathbf{F}_{\text{MAC},k} \mathbf{H}_k \mathbf{s}_k + \mathbf{G}_k \mathbf{F}_{\text{BC},k} \boldsymbol{\Phi}_k \mathbf{F}_{\text{MAC},k} \mathbf{n}_R + \tilde{\mathbf{n}}_k. \quad (4.10)$$

The term $\tilde{\mathbf{n}}_k$ represents the additive white Gaussian noise plus the residual interference at each UT. In order to further strengthen the desired signal for each operator, an algorithm inspired by the algebraic norm maximization (ANOMAX) scheme [RH09] is utilized for single-stream transmission for the design of $\boldsymbol{\Phi}_k$. The original ANOMAX algorithm has been designed for the two-way relaying scheme. We modify it here to use it for the one-way relaying channel and call it single-channel ANOMAX (SC-ANOMAX). Instead of maximizing the Frobenius norm of the forward and backward channel as in ANOMAX, SC-ANOMAX maximizes the Frobenius norm of the equivalent forward channel $\mathbf{G}_k \mathbf{F}_{\text{BC},k} \boldsymbol{\Phi}_k \mathbf{F}_{\text{MAC},k} \mathbf{H}_k$, i.e.,

$$\begin{aligned} \boldsymbol{\Phi}_k &= \arg \max_{\boldsymbol{\Phi}_k, \|\boldsymbol{\Phi}_k\|_F=1} \left\| \mathbf{G}_k \mathbf{F}_{\text{BC},k} \boldsymbol{\Phi}_k \mathbf{F}_{\text{MAC},k} \mathbf{H}_k \right\|_F^2 \\ &= \arg \max_{\boldsymbol{\Phi}_k, \|\boldsymbol{\Phi}_k\|_F=1} \left\| \underbrace{(\mathbf{F}_{\text{MAC},k} \mathbf{H}_k)^T \otimes (\mathbf{G}_k \mathbf{F}_{\text{BC},k})}_{\mathbf{K}} \cdot \underbrace{\text{vec}\{\boldsymbol{\Phi}_k\}}_{\boldsymbol{\phi}_k} \right\|_2^2 \\ &= \arg \max_{\boldsymbol{\phi}_k, \|\boldsymbol{\phi}_k\|_2=1} \frac{\boldsymbol{\phi}_k^H \mathbf{K}^H \mathbf{K} \boldsymbol{\phi}_k}{\boldsymbol{\phi}_k^H \boldsymbol{\phi}_k}. \end{aligned} \quad (4.11)$$

The maximum value of (4.11) is obtained by $\lambda_{\max}(\mathbf{K}^H \mathbf{K})$, where $\lambda_{\max}(\mathbf{K}^H \mathbf{K})$ denotes the largest eigenvalue of $\mathbf{K}^H \mathbf{K}$. By computing the SVD of $\mathbf{K} = \mathbf{U} \boldsymbol{\Sigma} \mathbf{V}^H$, $\boldsymbol{\phi}_k$ is obtained as $\boldsymbol{\phi}_k = \mathbf{v}_1$, where \mathbf{v}_1 denotes the first column of \mathbf{V} . Then $\boldsymbol{\Phi}_k \in \mathbb{C}^{M_R \times M_R}$ is formed by the rearrangement of elements of \mathbf{v}_1 . Finally, $\boldsymbol{\Phi}$ is obtained as $\boldsymbol{\Phi} = \text{blockdiag}\{ \boldsymbol{\Phi}_1 \dots \boldsymbol{\Phi}_K \}$.

The matrix $\tilde{\mathbf{F}}_R$ is designed by combing (4.1) - (4.11). Due to the relay transmit power constraint, the relay amplification matrix is finally obtained as $\mathbf{F}_R = \gamma \tilde{\mathbf{F}}_R$, where γ is a scalar to fulfill the power constraint with

$$\gamma = \sqrt{\frac{P_R}{\text{tr}\{\tilde{\mathbf{F}}_R (\frac{P_T}{M_T} \mathbf{H} \mathbf{H}^H + \sigma_n^2 \mathbf{I}_{M_R}) \tilde{\mathbf{F}}_R^H\}}}. \quad (4.12)$$

RBD/SC-ANOMAX gives a better sum rate performance compared to the state of the art work [JKHL09] for single stream transmission, which will be shown in the simulation results. Moreover, this closed-form algorithm does not require any iterations as [JKHL09].

Moreover, concerning multiple stream transmission, a rank restored (RR) modification of RBD/SC-ANOMAX named RBD/RR SC-ANOMAX restores the rank while preserving the same subspace, which achieves more spatial multiplexing gain and improves the sum rate

performance further. The original RR ANOMAX [RH10] has been designed for two-way relaying and the method RBD/RR SC-ANOMAX is an extension for relay sharing between multiple operators.

The basic principle behind it is to adjust the singular values of the relay amplification matrix for each operator in an exhaustive manner so that the spatial multiplexing gain is fully exploited. To be more specific, the SVD of the relay amplification matrix for each operator $\mathbf{F}_{R,k}$ obtained from SC-ANOMAX is first calculated as $\mathbf{F}_{R,k} = \mathbf{F}_{BC,k} \mathbf{\Phi}_k \mathbf{F}_{MAC,k} = \mathbf{U}_k \cdot \mathbf{\Sigma}_k \cdot \mathbf{V}_k^H$. Then we preserve the singular vectors \mathbf{U}_k and \mathbf{V}_k and the singular value profiles need to be adjusted via the vector $\boldsymbol{\sigma}_k = [\sigma_{k,1}, \sigma_{k,2}, \dots, \sigma_{k,M_R}]$. On a basis of $\boldsymbol{\sigma}_k$, the relay amplification matrix for RBD/RR SC-ANOMAX is defined as $\mathbf{F}_{R,k}(\boldsymbol{\sigma}_k) = \mathbf{U}_k \cdot \text{diag}\{\boldsymbol{\sigma}_k\} \cdot \mathbf{V}_k^H$, where $\text{diag}\{\boldsymbol{\sigma}_k\}$ is a diagonal matrix containing elements of $\boldsymbol{\sigma}_k$ on its main diagonal. The optimization problem is formulated as

$$\begin{aligned} \max_{\boldsymbol{\sigma}_k} \quad & \frac{1}{2} \left| \mathbf{I}_{M_{U,k}} + \frac{P_T}{M_{T,k}} \mathbf{R}_k^{-1} \mathbf{H}_{\text{eff},k} \mathbf{H}_{\text{eff},k}^H \right|, \\ \text{s.t.} \quad & \|\boldsymbol{\sigma}_k\| = 1, \sigma_1 \geq \sigma_2 \geq \dots \geq 0 \end{aligned} \quad (4.13)$$

where $\mathbf{H}_{\text{eff},k} = \mathbf{G}_k \mathbf{F}_{R,k} \mathbf{H}_k$ denotes the effective channel of the k -th operator with the amplification matrix $\mathbf{F}_{R,k}$ and $\mathbf{R}_k = \sigma_n^2 \mathbf{G}_k \mathbf{F}_{R,k} \mathbf{F}_{R,k}^H \mathbf{G}_k^H + \sigma_n^2 \mathbf{I}_{M_{U,k}}$ is the noise covariance matrix. The optimization problem using an exhaustive search can be simplified by considering the properties of the parameters. Firstly, the norm constraint on $\boldsymbol{\sigma}_k$ can be used to reduce the search space to $M_R - 1$ dimensions by optimizing over $\bar{\boldsymbol{\sigma}}_k = [\sigma_{k,2}/\sigma_{k,1}, \dots, \sigma_{k,M_R}/\sigma_{k,1}]$, where each element of $\bar{\boldsymbol{\sigma}}_k$ is in $[0, 1]$. Secondly, the search space for $\bar{\boldsymbol{\sigma}}_k$ can be further reduced by taking into account that the singular values are ordered, i.e., the i -th element of $\bar{\boldsymbol{\sigma}}_k$ is optimized in the interval between 0 and the current value of the $(i - 1)$ -th element of $\bar{\boldsymbol{\sigma}}_k$.

Simulation results

A two operator system with a shared AF relay is considered. Each element of all channel matrices is a zero mean circularly symmetric complex Gaussian random variable with unit variance $\mathcal{CN}(0, 1)$. Each figure is based on simulations over 1000 channel realizations.

Fig. 4.2 gives the system sum rate for the antenna configurations of $M_{T,k} = M_{U,k} = 1$ and $M_R = 4$. The SNR is defined as P_T/σ_n^2 . Compared to the recent MMSE BD method [JKHL09], the proposed EReSh-RM using RBD/SC-ANOMAX offers a further rate improvement while no iterations are required through a closed-form solution. In [JKHL09], it uses Lagrangian multipliers with a bisection search to find the optimum operating point, where iterations are unavoidable. We also include the results obtained from the orthogonal use of the spectrum and relay between multiple operators as a benchmark. In this case, the relay is designed using SC-ANOMAX and it is accessed by different operators in a time-division-multiple-access (TDMA) manner. The method labeled as TDMA $M_R = 4$ corresponds to the case of orthogonal use of the spectrum with a shared relay. The TDMA method with half of the relay antennas $M_R = 2$ means that both the spectrum and the relay are non-shared. Fig. 4.2 clearly shows that a significant sharing gain can be obtained compared to the orthogonal use of the

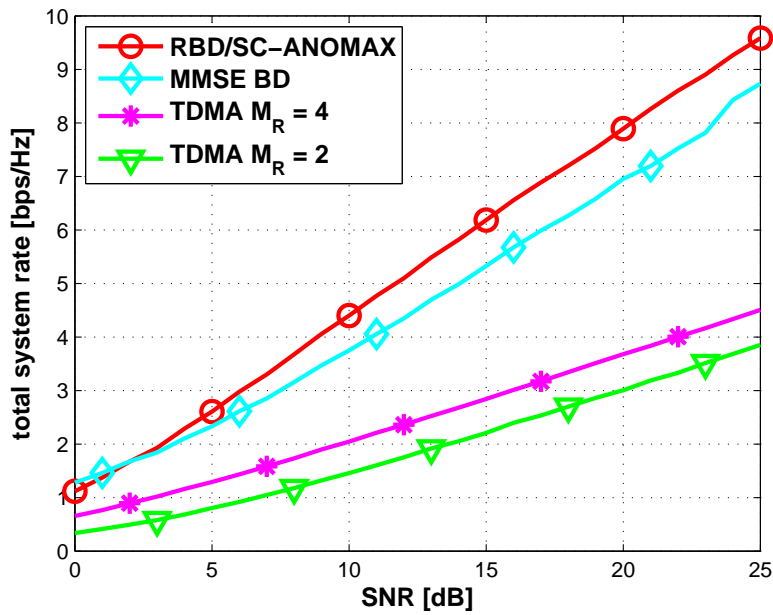


Figure 4.2.: System sum rate versus SNR with $M_{T,k} = M_{U,k} = 1 \forall k$, $M_R = 4$

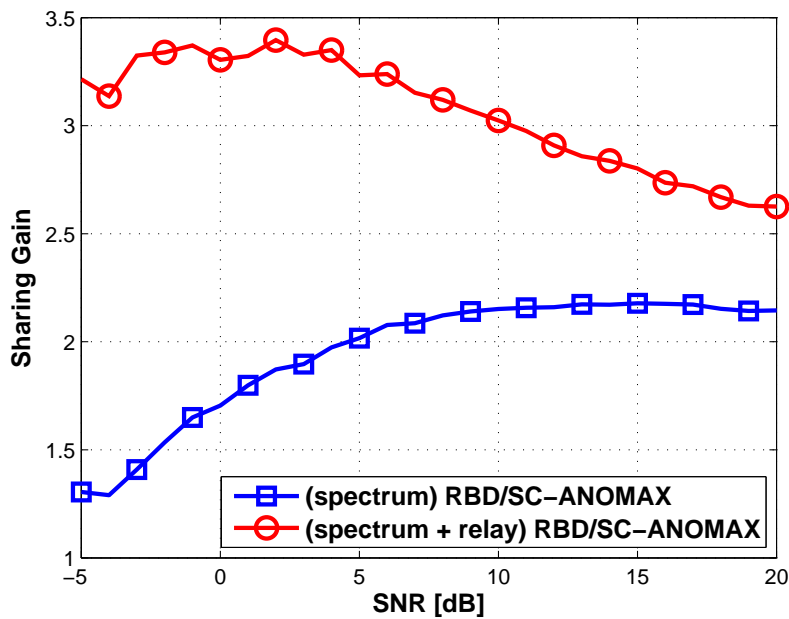


Figure 4.3.: System sum rate versus SNR with $M_{T,k} = M_{U,k} = 1 \forall k$, $M_R = 4$

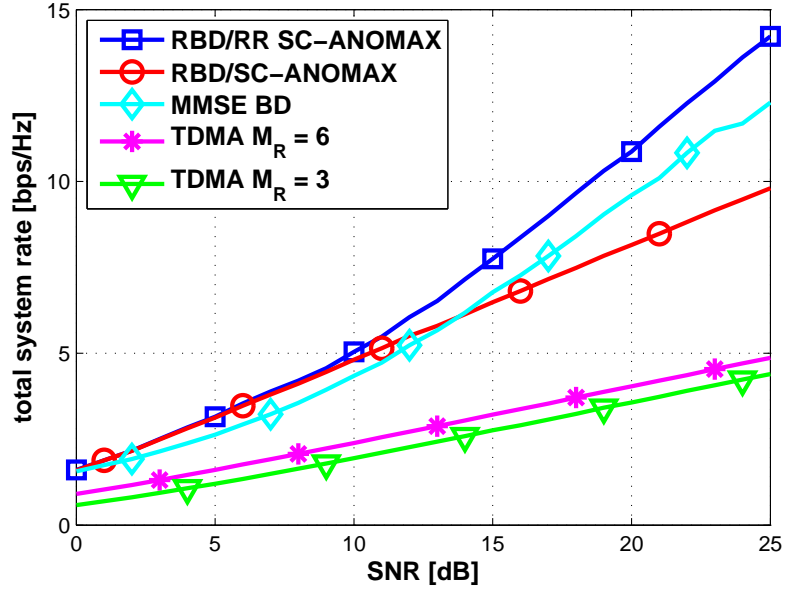


Figure 4.4.: System sum rate versus SNR with $M_{T,k} = M_{U,k} = 2 \forall k$, $M_R = 6$

physical resources, i.e., spectrum as well as the infrastructure (relay).

As defined in equation (2.1), the fractional SAPHYRE gain in terms of system sum rate is

$$\Xi_F = \frac{\sum_{k=1}^K U_k}{\frac{1}{K} \sum_{k=1}^K U_k^{\text{SU}}},$$

where $k \in \{1, 2, \dots, K\}$ is the index of the users. The utility function of the k th user in the sharing scenario and the time division case are denoted by U_k and U_k^{SU} , respectively. To be more specific, Fig. 4.3 depicts the SAPHYRE spectrum sharing gain in the blue curve, which is defined as the system sum rate obtained by the SAPHYRE scenario divided by that obtained by the TDMA use of the spectrum by different operators ($M_R = 4$ for each operator). In addition to that, an infrastructure (relay) sharing gain is obtained compared to the case where the relay is equipped with half of the number of antennas $M_R = 2$. The sharing gain with respect to both the spectrum and the relay sharing case is depicted by the red curve.

However, when multiple stream transmission is considered, EReSh-RM using RBD/SC-ANOMAX performs worse than MMSE BD at high SNRs as shown in Fig. 4.4, where $M_{T,k} = M_{U,k} = 2$ and $M_R = 6$. This is because RBD/SC-ANOMAX is a low-rank solution, which does not explore the full spatial multiplexing gain and thereby degrades the sum rate performance dramatically at high SNRs. By replacing EReSh-RM using RBD/SC-ANOMAX with EReSh-RM using RBD/RR SC-ANOMAX, the spatial multiplexing gain is fully exploited and thereby a higher sum rate performance is achieved in the high SNR regime. The sharing gain for this configuration is depicted in Fig. 4.5. A huge spectrum sharing gain is observed by using

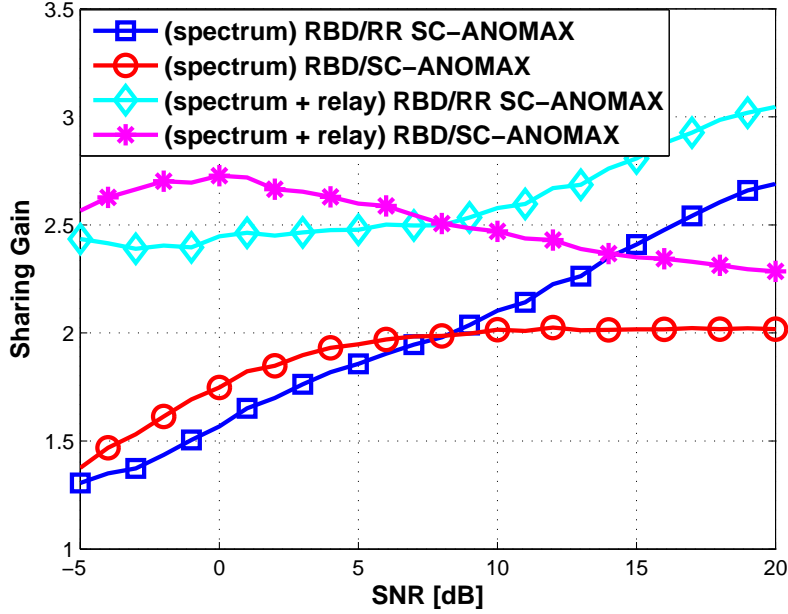


Figure 4.5.: System sum rate versus SNR with $M_{T,k} = M_{U,k} = 2 \forall k$, $M_R = 6$

EReSh-RM either with RBD/SC-ANOMAX or RBD/RR SC-ANOMAX compared to the TDMA case with $M_R = 6$ and an additional infrastructure (relay) sharing gain compared to the TDMA case with half of the number of antennas $M_R = 3$.

4.3. Relay Power Minimization for Single Stream Transmission

In this section, a power efficient transmission is considered for the multiple operator AF relay sharing system, which is described in Section 4.1. We study the special case that the BSs and the UTs are equipped with single antennas, where only single stream transmission is possible. Further, it is assumed that the transmit signals of all BSs are zero mean and statistically independent with transmit covariance matrix equal to $\mathbb{E}\{\bar{\mathbf{s}}\bar{\mathbf{s}}^H\} = \mathbb{E}\{\mathbf{s}\mathbf{s}^H\} = P_T \mathbf{I}_{M_T}$. Our objective is to design the relay precoder so as to minimize the relay transmit power $P_R = \mathbb{E}\{\text{tr}(\mathbf{x}_R \mathbf{x}_R^H)\}$ while meeting the signal to interference plus noise ratio (SINR) requirements at each user terminal.

Recently, a method named zero-forcing beamforming (ZFBF) [LP10] has been designed for relay transmit power minimization subject to an SINR constraint per user, which achieves the local optimum due to the use of the convex optimization tool. It first applies zero-forcing to cancel the interferences between the multiple operators completely. By doing this, the SINR constraint is degraded to an SNR requirement per user, which is easy for the relay precoder design. However, some degrees of freedom are lost, which makes ZFBF a suboptimal solution. Another drawback is that the implementation of ZFBF is not efficient enough due to the use of the convex optimization tool. Therefore, we propose several methods for further

improvements in terms of two aspects. Either a global optimum solution is obtained for performance enhancement or the computational complexity is reduced without degrading the power efficiency compared to ZFBF.

This section is structured as follows. A global optimum solution is firstly derived in Subsection 4.3.1, which uses a convex optimization tool to exploit the structure of the relay precoder. Taking this as a benchmark, several suboptimal beamforming algorithms are proposed in Subsection 4.3.2 and Subsection 4.3.3 to find a compromise between the achievable power efficiency and the computational complexity, which are based on zero-forcing and block diagonalization [SSH04] techniques for interference mitigation. The power efficiency performance and the complexity of all the schemes will be compared in the simulation results including the state-of-the-art work in [LP10]. Following that, the SAPHYRE sharing gain is investigated in terms of the required relay transmit power and the conclusions are drawn in Subsection 4.3.4.

4.3.1. Optimum Solution of Relay Power Minimization for Single Stream

We first consider an optimum solution of the relay precoder design in the multiple operator AF relay sharing system, where the total relay transmit power is to be minimized while guaranteeing a prescribed SINR constraint at each UT.

As described in Section 4.1, the relay transmit power is expressed as

$$\begin{aligned} P_R &= \mathbb{E}\{\text{tr}(\mathbf{x}_R \mathbf{x}_R^H)\} \\ &= \text{tr}(\mathbf{F}_R \mathbf{H} \mathbf{R}_{\bar{\mathbf{s}}} \mathbf{H}^H \mathbf{F}_R^H) + \sigma_n^2 \text{tr}(\mathbf{F}_R \mathbf{F}_R^H), \end{aligned} \quad (4.14)$$

where $\mathbf{H} \in \mathbb{C}^{M_R \times K}$. The transmit covariance matrix is $\mathbf{R}_{\bar{\mathbf{s}}} = \mathbb{E}\{\bar{\mathbf{s}} \bar{\mathbf{s}}^H\} = \mathbb{E}\{\mathbf{s} \mathbf{s}^H\} = P_T \mathbf{I}_{M_T}$. By inserting this into (4.14) and making use of the property of vec-operator [HJ85], i.e.,

$$\text{vec}(\mathbf{A} \mathbf{X} \mathbf{B}) = (\mathbf{B}^T \otimes \mathbf{A}) \text{vec}(\mathbf{X}), \quad (4.15)$$

the relay transmit power P_R can be further written as

$$\begin{aligned} P_R &= P_T \text{tr}(\mathbf{F}_R \mathbf{H} \mathbf{H}^H \mathbf{F}_R^H) + \sigma_n^2 \text{tr}(\mathbf{F}_R \mathbf{F}_R^H) \\ &= P_T \text{tr} \left\{ \underbrace{(\mathbf{H}^T \otimes \mathbf{I}_{M_R})}_P \underbrace{\text{vec}(\mathbf{F}_R)}_{\mathbf{f}_R} \text{vec}(\mathbf{F}_R)^H (\mathbf{H}^T \otimes \mathbf{I}_{M_R})^H \right\} \\ &= P_T \mathbf{f}_R^H \mathbf{P}^H \mathbf{P} \mathbf{f}_R, \end{aligned} \quad (4.16)$$

which is a function of the vectorized relay amplification matrix $\mathbf{f}_R = \text{vec}(\mathbf{F}_R)$.

At the receiver side, the received signal at UT_k is obtained as

$$y_k = \mathbf{g}_k^T \mathbf{F}_R \mathbf{h}_k s_k + \sum_{j \neq k} \mathbf{g}_k^T \mathbf{F}_R \mathbf{h}_j s_j + \mathbf{g}_k^T \mathbf{F}_R \mathbf{n}_R + n_k, \quad (4.17)$$

where the first term on the right hand side (RHS) denotes the desired signal while the second

term represents the inter-operator interference received at user UT_k . The effective noise is given by the remaining RHS terms. Based on (4.17), we express the SINR constraint at UT_k in terms of \mathbf{f}_R in the following.

Firstly, the power of the desired signal is calculated as

$$\mathbb{E}\left\{\left|\mathbf{g}_k^T \mathbf{F}_R \mathbf{h}_k s_k\right|^2\right\} = P_{\text{T}} \text{tr}\left\{\mathbf{g}_k^T \mathbf{F}_R \mathbf{h}_k \mathbf{h}_k^H \mathbf{F}_R^H \mathbf{g}_k^*\right\} \quad (4.18)$$

with $\mathbb{E}\{|s_k|^2\} = P_{\text{T}}$. Then by use of (4.15), (4.18) is further written as

$$\begin{aligned} P_{\text{T}} \text{tr}\left\{\mathbf{g}_k^T \mathbf{F}_R \mathbf{h}_k \mathbf{h}_k^H \mathbf{F}_R^H \mathbf{g}_k^*\right\} &= P_{\text{T}} \text{tr}\left\{\underbrace{(\mathbf{h}_k^T \otimes \mathbf{g}_k^T)}_{\mathbf{a}^T} \underbrace{\text{vec}(\mathbf{F}_R)}_{\mathbf{f}_R} \text{vec}(\mathbf{F}_R)^H (\mathbf{h}_k^T \otimes \mathbf{g}_k^T)^H\right\} \\ &= P_{\text{T}} \mathbf{f}_R^H \mathbf{a}^* \mathbf{a}^T \mathbf{f}_R \end{aligned} \quad (4.19)$$

The power of the inter-operator interference is obtained as

$$\mathbb{E}\left\{\left|\sum_{j \neq k} \mathbf{g}_k^T \mathbf{F}_R \mathbf{h}_j s_j\right|^2\right\} = P_{\text{T}} \text{tr}\left\{\mathbf{g}_k^T \mathbf{F}_R \tilde{\mathbf{H}}_k \tilde{\mathbf{H}}_k^H \mathbf{F}_R^H \mathbf{g}_k^*\right\}, \quad (4.20)$$

where the interference matrix for UT_k is defined as $\tilde{\mathbf{H}}_k = [\mathbf{h}_1, \dots, \mathbf{h}_{k-1}, \mathbf{h}_{k+1}, \dots, \mathbf{h}_K] \in \mathbb{C}^{M_R \times (K-1)}$. Similarly as (4.19), equation (4.20) is transformed to

$$\begin{aligned} P_{\text{T}} \text{tr}\left\{\mathbf{g}_k^T \mathbf{F}_R \tilde{\mathbf{H}}_k \tilde{\mathbf{H}}_k^H \mathbf{F}_R^H \mathbf{g}_k^*\right\} &= P_{\text{T}} \text{tr}\left\{\underbrace{(\tilde{\mathbf{H}}_k^T \otimes \mathbf{g}_k^T)}_{\mathbf{A}} \underbrace{\text{vec}(\mathbf{F}_R)}_{\mathbf{f}_R} \text{vec}(\mathbf{F}_R)^H (\tilde{\mathbf{H}}_k^T \otimes \mathbf{g}_k^T)^H\right\} \\ &= P_{\text{T}} \mathbf{f}_R^H \mathbf{A}^H \mathbf{A} \mathbf{f}_R. \end{aligned} \quad (4.21)$$

Assuming that the noise at the relay \mathbf{n}_R and the noise at the single antenna UT n_k are independent, the power of the effective noise is calculated as

$$\mathbb{E}\left\{\left|\mathbf{g}_k^T \mathbf{F}_R \mathbf{n}_R + n_k\right|^2\right\} = \sigma_n^2 \text{tr}\left\{\mathbf{g}_k^T \mathbf{F}_R \mathbf{F}_R^H \mathbf{g}_k^*\right\} + \sigma_n^2, \quad (4.22)$$

where the noise at the relay and the UTs contain the zero-mean circularly symmetric complex Gaussian (ZMCSCG) noise samples with $\mathbb{E}\{\mathbf{n}_R \mathbf{n}_R^H\} = \sigma_n^2 \mathbf{I}_{M_R}$ and $\mathbb{E}\{|n_k|^2\} = \sigma_n^2$. Equation (4.22) is further written as

$$\begin{aligned} \sigma_n^2 \text{tr}\left\{\mathbf{g}_k^T \mathbf{F}_R \mathbf{F}_R^H \mathbf{g}_k^*\right\} + \sigma_n^2 &= \sigma_n^2 \text{tr}\left\{\underbrace{(\mathbf{I}_{M_R} \otimes \mathbf{g}_k^T)}_{\mathbf{B}} \underbrace{\text{vec}(\mathbf{F}_R)}_{\mathbf{f}_R} \text{vec}(\mathbf{F}_R)^H (\mathbf{I}_{M_R} \otimes \mathbf{g}_k^T)^H\right\} + \sigma_n^2 \\ &= \sigma_n^2 \mathbf{f}_R^H \mathbf{B}^H \mathbf{B} \mathbf{f}_R + \sigma_n^2. \end{aligned} \quad (4.23)$$

Combining (4.19), (4.21) and (4.23), the SINR constraint for UT_k is expressed by

$$\frac{P_T \mathbf{f}_R^H \mathbf{a}^* \mathbf{a}^T \mathbf{f}_R}{P_T \mathbf{f}_R^H \mathbf{A}^H \mathbf{A} \mathbf{f}_R + \sigma_n^2 \mathbf{f}_R^H \mathbf{B}^H \mathbf{B} \mathbf{f}_R + \sigma_n^2} \geq \gamma_k, \quad (4.24)$$

which can be written as

$$\mathbf{f}_R^H \left(P_T \mathbf{a}^* \mathbf{a}^T - \gamma_k P_T \mathbf{A}^H \mathbf{A} - \gamma_k \sigma_n^2 \mathbf{B}^H \mathbf{B} \right) \mathbf{f}_R \geq \gamma_k \sigma_n^2. \quad (4.25)$$

By defining $\mathbf{W} = \mathbf{f}_R \mathbf{f}_R^H \in \mathbb{C}^{M_R^2}$, the problem of minimizing the relay transmit power defined in (4.16) under SINR constraint in (4.25) is formulated as

$$\begin{aligned} \min_{\mathbf{W}} \quad & \text{tr}\{P_T \mathbf{P}^H \mathbf{P} \mathbf{W}\} \\ \text{s.t.} \quad & \text{tr}\left\{ \left(P_T \mathbf{a}^* \mathbf{a}^T - \gamma_k P_T \mathbf{A}^H \mathbf{A} - \gamma_k \sigma_n^2 \mathbf{B}^H \mathbf{B} \right) \mathbf{W} \right\} \geq \gamma_k \sigma_n^2, k = 1, 2, \dots, K \\ & \text{rank}(\mathbf{W}) = 1, \end{aligned} \quad (4.26)$$

where

$$\begin{aligned} \mathbf{P} &= \mathbf{H}^T \otimes \mathbf{I}_{M_R}, \\ \mathbf{a} &= (\mathbf{h}_k^T \otimes \mathbf{g}_k^T)^T, \\ \mathbf{A} &= \tilde{\mathbf{H}}_k^T \otimes \mathbf{g}_k^T, \\ \mathbf{B} &= \mathbf{I}_{M_R} \otimes \mathbf{g}_k^T. \end{aligned}$$

The original problem in (4.26) is a non-convex quadratically constrained quadratic program (QCQP). By relaxing the non-convex constraint $\text{rank}(\mathbf{W}) = 1$ in (4.26), the original problem turns out to be convex in \mathbf{W} and can be solved effectively by semi-definite relaxation (SDR) [HP10, LMS⁺10] using the convex optimization toolbox *cvx* [BV04, GBY09]. However, the rank of \mathbf{W} is usually more than one since we discarded the rank-1 constraint. Therefore, we need to extract a rank-1 solution \mathbf{f}_R from \mathbf{W} by a tight rank-1 decomposition method. In [AHZ11], a rank-1 decomposition theorem has been proved and it is shown that the SDRs of complex-valued QCQPs with not more than 4 constraints are tight. In our case, if the number of operators is less or equal than 4, an optimum \mathbf{f}_R can be reconstructed from \mathbf{W} based on the theorem and the algorithm of rank-1 decomposition [AHZ11].

4.3.2. Efficient Resource Sharing Power Minimization (EReSh-PM)

In [LP10], a zero-forcing beamforming (ZFBF) algorithm is designed for relay transmit power minimization subject to the SINR constraint per user, which achieves a local optimum. This ZFBF first applies zero-forcing to cancel the inter-operator interferences completely, simplifying the SINR constraint for each user in (4.24) to SNR requirement per user. Then the problem turns out to minimize the total relay transmit power with multiple SNR constraints.

However, this method needs to be implemented by using a convex optimization tool and iterative procedures are unavoidable. In order to overcome this, we seek a closed-form solution named efficient relay sharing power minimization (EReSh-PM) algorithm. Meanwhile, we will show that the proposed EReSh-PM scheme approaches the same performance as the ZFBF method and no iterations are required. The main contribution of this section has been published in reference [LRH11a].

In order to simplify the design of \mathbf{F}_R , the following structure of \mathbf{F}_R is used,

$$\mathbf{F}_R = \mathbf{F}_{BC} \Phi \mathbf{F}_{MAC}^H. \quad (4.27)$$

The matrices \mathbf{F}_{MAC} and \mathbf{F}_{BC} suppress the interferences generated in the multiple access (MAC) phase from the BSs to the relay and the broadcasting (BC) phase from the relay to UTs, respectively. The diagonal matrix

$$\Phi = \text{diag}\{ \sqrt{\Phi_1}, \dots, \sqrt{\Phi_K} \} \in \mathbb{C}^{K \times K} \quad (4.28)$$

is used to allocate the power to each UT.

As the first step, the interference is mitigated during the MAC phase and the BC phase using the ZF method. To design \mathbf{F}_{MAC} , the pseudo inverse of the channel \mathbf{H} is first calculated as

$$\mathbf{H}^+ = (\mathbf{H}^H \mathbf{H})^{-1} \mathbf{H}^H = \left[\bar{\mathbf{h}}_1, \dots, \bar{\mathbf{h}}_K \right]^T \in \mathbb{C}^{K \times M_R}$$

with $\bar{\mathbf{h}}_k \in \mathbb{C}^{M_R}$. Then \mathbf{F}_{MAC} is formed as

$$\mathbf{F}_{MAC} = \left[\mathbf{f}_{MAC,1}, \dots, \mathbf{f}_{MAC,K} \right] \in \mathbb{C}^{M_R \times K}, \quad (4.29)$$

where $\mathbf{f}_{MAC,k}$ is a unit norm vector and $\mathbf{f}_{MAC,k} = \bar{\mathbf{h}}_k / \|\bar{\mathbf{h}}_k\|_2 \in \mathbb{C}^{M_R}$.

Similarly in the BC phase, the pseudo inverse of \mathbf{G} is

$$\mathbf{G}^+ = \mathbf{G}^H (\mathbf{G} \mathbf{G}^H)^{-1} = \left[\bar{\mathbf{g}}_1, \dots, \bar{\mathbf{g}}_K \right] \in \mathbb{C}^{M_R \times K}$$

with $\bar{\mathbf{g}}_k \in \mathbb{C}^{M_R}$. Then the matrix \mathbf{F}_{BC} is obtained as

$$\mathbf{F}_{BC} = \left[\mathbf{f}_{BC,1}, \dots, \mathbf{f}_{BC,K} \right] \in \mathbb{C}^{M_R \times K}, \quad (4.30)$$

where $\mathbf{f}_{BC,k} = \bar{\mathbf{g}}_k / \|\bar{\mathbf{g}}_k\|_2 \in \mathbb{C}^{M_R}$.

Inserting (4.29) and (4.30) into (4.27), \mathbf{F}_R is written as

$$\begin{aligned} \mathbf{F}_R &= \mathbf{F}_{BC} \Phi \mathbf{F}_{MAC}^H \\ &= \underbrace{\mathbf{f}_{BC,1} \sqrt{\Phi_1} \mathbf{f}_{MAC,1}^H}_{\mathbf{F}_{R,1}} + \dots + \underbrace{\mathbf{f}_{BC,K} \sqrt{\Phi_K} \mathbf{f}_{MAC,K}^H}_{\mathbf{F}_{R,K}} \end{aligned} \quad (4.31)$$

with

$$\mathbf{F}_{R,k} = \mathbf{f}_{BC,K} \sqrt{\Phi_K} \mathbf{f}_{MAC,K}^H. \quad (4.32)$$

After applying \mathbf{F}_{MAC} and \mathbf{F}_{BC} , the inter-operator interferences generated during the MAC phase and the BC phase are completely removed. Thus the received signal at the UT_k is obtained as

$$y_k = \mathbf{g}_k^T \mathbf{f}_{BC,k} \sqrt{\Phi_k} \mathbf{f}_{MAC,k}^H \mathbf{h}_k s_k + \mathbf{g}_k^T \mathbf{f}_{BC,k} \sqrt{\Phi_k} \mathbf{f}_{MAC,k}^H \mathbf{n}_R + n_k,$$

where the first term on the RHS is the desired signal for UT_k while all the others represent the effective noise. By defining $\widehat{\mathbf{g}}_k = \mathbf{g}_k^T \mathbf{f}_{BC,k}$ and $\widehat{\mathbf{h}}_k = \mathbf{f}_{MAC,k}^H \mathbf{h}_k$, the SINR constraint at each UT is written as

$$\text{SINR}_k = \frac{P_T |\widehat{\mathbf{g}}_k|^2 |\widehat{\mathbf{h}}_k|^2 \Phi_k}{\sigma_n^2 |\widehat{\mathbf{g}}_k|^2 \Phi_k + \sigma_n^2} \geq \gamma_k, \quad (4.33)$$

where γ_k is a predefined constant.

Since the system is decoupled into K independent parallel transceiver pairs, the total relay transmit power $P_R = \sum_{k=1}^K P_{R,k}$, where $P_{R,k}$ denotes the relay transmit power for the k -th operator. Instead of minimizing the total relay transmit power $P_R = \|\mathbf{F}_R \mathbf{H} \mathbf{s} + \mathbf{F}_R \mathbf{n}_R\|_2^2$ proposed in [LP10], we design Φ_k to minimize the relay transmit power for each operator, i.e., $P_{R,k} = \mathbb{E} \left\{ \|\mathbf{F}_{R,k} \mathbf{h}_k s_k + \mathbf{F}_{R,k} \mathbf{n}_R\|_2^2 \right\}$. Combining (4.32) and the definition of $\widehat{\mathbf{h}}_k = \mathbf{f}_{MAC,k}^H \mathbf{h}_k$, $P_{R,k}$ can be further written as

$$\begin{aligned} P_{R,k} &= \mathbb{E} \left\{ \|\mathbf{F}_{R,k} \mathbf{h}_k s_k + \mathbf{F}_{R,k} \mathbf{n}_R\|_2^2 \right\} \\ &= \mathbb{E} \left\{ \|\mathbf{f}_{BC,k} \sqrt{\Phi_k} \mathbf{f}_{MAC,k}^H \mathbf{h}_k s_k + \mathbf{f}_{BC,k} \sqrt{\Phi_k} \mathbf{f}_{MAC,k}^H \mathbf{n}_R\|_2^2 \right\} \\ &= \text{tr} \left\{ \mathbf{f}_{BC,k} (P_T |\widehat{\mathbf{h}}_k|^2 \Phi_k + \sigma_n^2 \Phi_k) \mathbf{f}_{BC,k}^H \right\} \\ &= (P_T |\widehat{\mathbf{h}}_k|^2 + \sigma_n^2) \Phi_k. \end{aligned} \quad (4.34)$$

The last step comes from the fact that $\mathbf{f}_{BC,k}^H \mathbf{f}_{BC,k} = \widehat{\mathbf{g}}_k^H \widehat{\mathbf{g}}_k / \|\widehat{\mathbf{g}}_k\|_2^2 = 1$ since $\mathbf{f}_{BC,k}$ is a unit norm vector.

Our objective turns out to find the diagonal elements $\sqrt{\Phi_k}$ in equation (4.28) for each user to minimize the individual relay transmit power $P_{R,k}$ in (4.34) under the individual constraint $\text{SINR}_k \geq \gamma_k$ as described in (4.33). Therefore, the problem is formulated as

$$\begin{aligned} \min_{\Phi_k \geq 0} \quad & (P_T |\widehat{\mathbf{h}}_k|^2 + \sigma_n^2) \Phi_k, \\ \text{s.t.} \quad & \frac{P_T |\widehat{\mathbf{g}}_k|^2 |\widehat{\mathbf{h}}_k|^2 \Phi_k}{\sigma_n^2 |\widehat{\mathbf{g}}_k|^2 \Phi_k + \sigma_n^2} \geq \gamma_k. \end{aligned} \quad (4.35)$$

It is obvious that $(P_T|\widehat{h}_k|^2 + 1)\Phi_k$ increases monotonically with Φ_k and thereby Φ_k is obtained in a closed-form,

$$\Phi_k = \frac{\gamma_k \sigma_n^2}{|\widehat{g}_k|^2 (P_T|\widehat{h}_k|^2 - \gamma_k \sigma_n^2)}. \quad (4.36)$$

In order to guarantee that Φ_k is non-negative, the feasibility check has to be passed, i.e.,

$$P_T|\widehat{h}_k|^2 - \gamma_k \sigma_n^2 > 0. \quad (4.37)$$

Using equations (4.27) - (4.30) and (4.36) - (4.37), the relay amplification matrix is finally constructed as $\mathbf{F}_R = \mathbf{F}_{BC}\Phi\mathbf{F}_{MAC}^H$. The relay transmit power is calculated as $P_R = \mathbb{E}\left\{\|\mathbf{F}_R\mathbf{H}\mathbf{s} + \mathbf{F}_R\mathbf{n}_R\|_2^2\right\} = \text{tr}\left\{\mathbf{F}_R(P_T\mathbf{H}\mathbf{H}^H + \sigma_n^2\mathbf{I}_{M_R})\mathbf{F}_R^H\right\}$.

4.3.3. BD based solution

In this section, an alternative solution is presented for relay power minimization with SINR constraints, which is based on the block diagonalization (BD) algorithm [SSH04]. The algorithm is named as block diagonalization single channel algebraic norm maximization (BD/SC-ANOMAX), which is a closed-form solution to minimize the relay transmit power under the SINR constraints. The original BD is used to suppress the interferences between users in the multi-user MIMO downlink. Here we use BD to eliminate the inter-operator interference. Unlike the zero-forcing method used in EReSh-PM as introduced in Section 4.3.2 and the ZFBF algorithm [LP10], we apply the classical BD method to mitigate the interference generated in the MAC phase and BC phase.

The relay amplification matrix is still designed as

$$\mathbf{F}_R = \mathbf{F}_{BC}\Phi\mathbf{F}_{MAC} \in \mathbb{C}^{M_R \times M_R}, \quad (4.38)$$

where \mathbf{F}_{MAC} and \mathbf{F}_{BC} are the precoding matrices in the MAC phase and BC phase for interference cancelation while Φ is a block diagonal matrix used for relay transmit power minimization. In the MAC phase, we define $\tilde{\mathbf{H}}_k = \begin{bmatrix} \mathbf{h}_1, & \dots, & \mathbf{h}_{k-1}, & \mathbf{h}_{k+1}, & \dots, & \mathbf{h}_K \end{bmatrix} \in \mathbb{C}^{M_R \times (K-1)}$ to represent the channel between all the BSs and the relay excluding the k -th BS, where $\mathbf{h}_i \in \mathbb{C}^{M_R}$ with $i = 1, \dots, K, i \neq k$ denote the channel vector from BS $_i$ to the relay. To completely cancel the inter-operator interference generated in the MAC phase for user k , we assign the precoding matrix $\mathbf{F}_{MAC,k}$ at BS $_k$ to lie in the null space of the interference channel $\tilde{\mathbf{H}}_k$ from all the other users. In order to extract this null space, the singular value decomposition (SVD) of $\tilde{\mathbf{H}}_k$ is first computed,

$$\tilde{\mathbf{H}}_k = \tilde{\mathbf{U}}_{\tilde{\mathbf{H}}_k} \cdot \tilde{\Sigma}_{\tilde{\mathbf{H}}_k} \cdot \tilde{\mathbf{V}}_{\tilde{\mathbf{H}}_k}^H = \begin{bmatrix} \tilde{\mathbf{U}}_{\tilde{\mathbf{H}}_k}^{(1)}, & \tilde{\mathbf{U}}_{\tilde{\mathbf{H}}_k}^{(0)} \end{bmatrix} \cdot \tilde{\Sigma}_{\tilde{\mathbf{H}}_k} \cdot \tilde{\mathbf{V}}_{\tilde{\mathbf{H}}_k}^H.$$

The matrices $\tilde{\mathbf{U}}_{\tilde{\mathbf{H}}_k}^{(1)}$ and $\tilde{\mathbf{U}}_{\tilde{\mathbf{H}}_k}^{(0)}$ are acquired from the left $K-1$ columns and the right $M_R - K + 1$

columns of $\tilde{\mathbf{U}}_{\tilde{\mathbf{H}}_k}$, which span the signal space and the null space of $\tilde{\mathbf{H}}_k$, respectively. To mitigate the inter-operator interference received from others, the precoding matrix for user k in the MAC phase is obtained as

$$\mathbf{F}_{\text{MAC},k} = \tilde{\mathbf{U}}_{\tilde{\mathbf{H}}_k}^{(0)} \tilde{\mathbf{U}}_{\tilde{\mathbf{H}}_k}^{(0)\text{H}} \quad (4.39)$$

To completely cancel the inter-operator interferences between all interfering pairs, the relay precoding matrix in the MAC phase is designed as

$$\mathbf{F}_{\text{MAC}} = \begin{bmatrix} \mathbf{F}_{\text{MAC},1} \\ \vdots \\ \mathbf{F}_{\text{MAC},K} \end{bmatrix} = \begin{bmatrix} \tilde{\mathbf{U}}_{\tilde{\mathbf{H}}_1}^{(0)} \tilde{\mathbf{U}}_{\tilde{\mathbf{H}}_1}^{(0)\text{H}} \\ \vdots \\ \tilde{\mathbf{U}}_{\tilde{\mathbf{H}}_K}^{(0)} \tilde{\mathbf{U}}_{\tilde{\mathbf{H}}_K}^{(0)\text{H}} \end{bmatrix} \in \mathbb{C}^{KM_{\text{R}} \times M_{\text{R}}}.$$

Similarly in the BC phase, we define $\tilde{\mathbf{G}}_k = [\mathbf{g}_1, \dots, \mathbf{g}_{k-1}, \mathbf{g}_{k+1}, \dots, \mathbf{g}_K]^{\text{T}} \in \mathbb{C}^{(K-1) \times M_{\text{R}}}$ with $\mathbf{g}_i \in \mathbb{C}^{M_{\text{R}}}$ denoting the channel vector from the relay to the UT $_i$. Thereby, the precoding matrix for user k at the BC phase is designed as

$$\mathbf{F}_{\text{BC},k} = \tilde{\mathbf{V}}_{\tilde{\mathbf{G}}_k}^{(0)} \tilde{\mathbf{V}}_{\tilde{\mathbf{G}}_k}^{(0)\text{H}} \quad (4.40)$$

and thus the precoding matrix \mathbf{F}_{BC} at the BC phase is obtained as

$$\mathbf{F}_{\text{BC}} = [\mathbf{F}_{\text{BC},1}, \dots, \mathbf{F}_{\text{BC},K}] = [\tilde{\mathbf{V}}_{\tilde{\mathbf{G}}_1}^{(0)} \tilde{\mathbf{V}}_{\tilde{\mathbf{G}}_1}^{(0)\text{H}}, \dots, \tilde{\mathbf{V}}_{\tilde{\mathbf{G}}_K}^{(0)} \tilde{\mathbf{V}}_{\tilde{\mathbf{G}}_K}^{(0)\text{H}}] \in \mathbb{C}^{M_{\text{R}} \times KM_{\text{R}}},$$

where the columns of $\tilde{\mathbf{V}}_{\tilde{\mathbf{G}}_k}^{(0)}$ span the null space of $\tilde{\mathbf{G}}_k$, which is obtained from computing the SVD of $\tilde{\mathbf{G}}_k$, i.e.,

$$\tilde{\mathbf{G}}_k = \tilde{\mathbf{U}}_{\tilde{\mathbf{G}}_k} \cdot \tilde{\Sigma}_{\tilde{\mathbf{G}}_k} \cdot \tilde{\mathbf{V}}_{\tilde{\mathbf{G}}_k}^{\text{H}} = \tilde{\mathbf{U}}_{\tilde{\mathbf{G}}_k} \cdot \tilde{\Sigma}_{\tilde{\mathbf{G}}_k} \cdot [\tilde{\mathbf{V}}_{\tilde{\mathbf{G}}_k}^{(1)}, \tilde{\mathbf{V}}_{\tilde{\mathbf{G}}_k}^{(0)}]^{\text{H}}.$$

After applying BD in both the MAC phase and the BC phase, the received signal vector excluding the noise is obtained as follows,

$$\begin{aligned} \mathbf{G}\mathbf{F}_{\text{R}}\mathbf{H}\mathbf{s} &= \begin{bmatrix} \mathbf{g}_1^{\text{T}} \\ \vdots \\ \mathbf{g}_K^{\text{T}} \end{bmatrix} \begin{bmatrix} \mathbf{F}_{\text{BC},1}, & \dots, & \mathbf{F}_{\text{BC},K} \end{bmatrix} \underbrace{\begin{bmatrix} \Phi_1 & & \\ & \ddots & \\ & & \Phi_K \end{bmatrix}}_{\Phi} \begin{bmatrix} \mathbf{F}_{\text{MAC},1} \\ \vdots \\ \mathbf{F}_{\text{MAC},K} \end{bmatrix} \begin{bmatrix} \mathbf{h}_1, & \dots, & \mathbf{h}_K \end{bmatrix} \begin{bmatrix} s_1 \\ \vdots \\ s_K \end{bmatrix} \\ &= \begin{bmatrix} \mathbf{g}_1^{\text{T}} \mathbf{F}_{\text{BC},1} & & \\ & \ddots & \\ & & \mathbf{g}_K^{\text{T}} \mathbf{F}_{\text{BC},K} \end{bmatrix} \begin{bmatrix} \Phi_1 & & \\ & \ddots & \\ & & \Phi_K \end{bmatrix} \begin{bmatrix} \mathbf{F}_{\text{MAC},1} \mathbf{h}_1 & & \\ & \ddots & \\ & & \mathbf{F}_{\text{MAC},K} \mathbf{h}_K \end{bmatrix} \begin{bmatrix} s_1 \\ \vdots \\ s_K \end{bmatrix} \\ &= \begin{bmatrix} \mathbf{g}_1^{\text{T}} \mathbf{F}_{\text{BC},1} \Phi_1 \mathbf{F}_{\text{MAC},1} \mathbf{h}_1 & & \\ & \ddots & \\ & & \mathbf{g}_K^{\text{T}} \mathbf{F}_{\text{BC},K} \Phi_K \mathbf{F}_{\text{MAC},K} \mathbf{h}_K \end{bmatrix} \begin{bmatrix} s_1 \\ \vdots \\ s_K \end{bmatrix}. \end{aligned}$$

All the off-diagonal elements become zero since all the interferences are removed. The matrix Φ is block diagonal, written as $\Phi = \text{blockdiag}\{ \Phi_1, \dots, \Phi_K \} \in \mathbb{C}^{KM_R \times KM_R}$. It can be seen that the system is now decoupled into K independent transceiver pairs and more degrees of freedom are achieved for the design of $\Phi \in \mathbb{C}^{KM_R \times KM_R}$ after applying BD instead of $\Phi \in \mathbb{C}^{K \times K}$ by utilizing ZF.

The received signal for user k is written as

$$y_k = \mathbf{g}_k^T \mathbf{F}_{\text{BC},k} \Phi_k \mathbf{F}_{\text{MAC},k} \mathbf{h}_k s_k + \mathbf{g}_k^T \mathbf{F}_{\text{BC},k} \Phi_k \mathbf{F}_{\text{MAC},k} \mathbf{n}_R + n_k. \quad (4.41)$$

where the first term is the desired signal whereas the remaining terms represent the effective noise vectors.

Since the system is decoupled into K independent transceiver pairs after applying BD for interference mitigation, (4.38) can be further written as

$$\begin{aligned} \mathbf{F}_R &= \mathbf{F}_{\text{BC}} \Phi \mathbf{F}_{\text{MAC}} \\ &= \sum_{k=1}^K \mathbf{F}_{\text{BC},k} \Phi_k \mathbf{F}_{\text{MAC},k} \\ &= \sum_{k=1}^K \mathbf{F}_k \in \mathbb{C}^{M_R \times M_R} \end{aligned} \quad (4.42)$$

and $\mathbf{F}_{\text{MAC},k}$ and $\mathbf{F}_{\text{BC},k}$ are obtained from (4.39) and (4.40). Then the algorithm SC-ANOMAX is to design the diagonal matrix Φ_k , which is similar to that introduced in Section 4.2.

$$\begin{aligned} \Phi_k &= \arg \max_{\Phi_k, \|\Phi_k\|_F=1} \left\| \mathbf{g}_k^T \mathbf{F}_{\text{BC},k} \Phi_k \mathbf{F}_{\text{MAC},k} \mathbf{h}_k \right\|_F^2 \\ &= \arg \max_{\Phi_k, \|\Phi_k\|_F=1} \left\| \underbrace{(\mathbf{F}_{\text{MAC},k} \mathbf{h}_k)^T \otimes (\mathbf{g}_k^T \mathbf{F}_{\text{BC},k})}_K \cdot \underbrace{\text{vec}\{\Phi_k\}}_{\phi_k} \right\|_2^2 \\ &= \arg \max_{\phi_k, \|\phi_k\|_2=1} \frac{\phi_k^H \mathbf{K}^H \mathbf{K} \phi_k}{\phi_k^H \phi_k} \\ &= \lambda_{\max}(\mathbf{K}^H \mathbf{K}). \end{aligned} \quad (4.43)$$

By computing the SVD of $\mathbf{K} = \mathbf{U} \Sigma \mathbf{V}^H$, ϕ_k is obtained as $\phi_k = \mathbf{v}_1$, where \mathbf{v}_1 denotes the first column of \mathbf{V} . Then $\Phi_k \in \mathbb{C}^{M_R \times M_R}$ is formed by the rearrangement of elements of \mathbf{v}_1 .

In order to fulfill the SINR constraint for each user, we define $\tilde{\mathbf{F}}_{R,k} = \beta_k \mathbf{F}_{R,k}$, where β is a scalar. Then the SINR constraint is written as

$$\begin{aligned} \text{SINR}_k &= \frac{P_T |\mathbf{g}_k^T \tilde{\mathbf{F}}_{R,k} \mathbf{h}_k|^2}{\sigma_n^2 \left\| \mathbf{g}_k^T \tilde{\mathbf{F}}_{R,k} \right\|_2^2 + \sigma_n^2} \\ &= \frac{P_T \beta^2 |\mathbf{g}_k^T \mathbf{F}_{\text{BC},k} \Phi_k \mathbf{F}_{\text{MAC},k} \mathbf{h}_k|^2}{\sigma_n^2 \beta^2 \left\| \mathbf{g}_k^T \mathbf{F}_{\text{BC},k} \Phi_k \mathbf{F}_{\text{MAC},k} \right\|_2^2 + \sigma_n^2} \geq \gamma_k. \end{aligned}$$

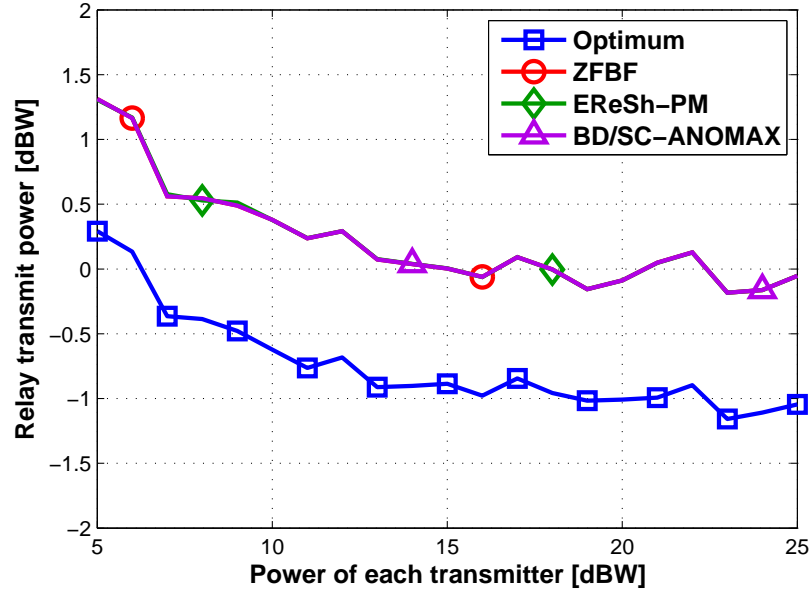


Figure 4.6.: P_R versus P_T with target SINR = 0 dB

Thereby, the scaling factor β_k for each transceiver pair is obtained as

$$\beta_k = \sqrt{\frac{\gamma_k \sigma_n^2}{P_T |\mathbf{g}_k^T \mathbf{F}_{BC,k} \Phi_k \mathbf{F}_{MAC,k} \mathbf{h}_k|^2 - \gamma_k \sigma_n^2 \|\mathbf{g}_k^T \mathbf{F}_{BC,k} \Phi_k \mathbf{F}_{MAC,k}\|_2^2}}. \quad (4.44)$$

It is obvious that the feasible set for the BD/SC-ANOMAX solution is that $\beta \geq 0$.

Combing (4.42)-(4.44) and (4.39)-(4.40), the relay amplification matrix is finally designed as

$$\mathbf{F}_R = \sum_{k=1}^K \tilde{\mathbf{F}}_{R,k} = \sum_{k=1}^K \beta_k \mathbf{F}_{BC,k} \Phi_k \mathbf{F}_{MAC,k} \quad (4.45)$$

with the feasibility check $\beta \geq 0$.

Simulation results

A two operator system with a shared AF relay is considered. Each element of all channel matrices is a zero mean circularly symmetric complex Gaussian random variable with unit norm $\mathcal{CN}(0,1)$. Each figure is based on simulation over 1000 channel realizations. Fig. 4.6 gives the consumed relay transmit power versus P_T using $M_R = 4$. The SINR constraint at each UT is set to be 0 dB and unit noise variance is assumed. The proposed closed-form solutions EReSh-PM as well as BD/SC-ANOMAX algorithms provide the same relay transmit power which achieves the local optimum as ZFBF. Moreover, instead of using the convex optimization tool in [LP10], the EReSh-PM and the BD/SC-ANOMAX method gives the solution directly and no iteration is required. Compared to the optimum solution which is depicted by the

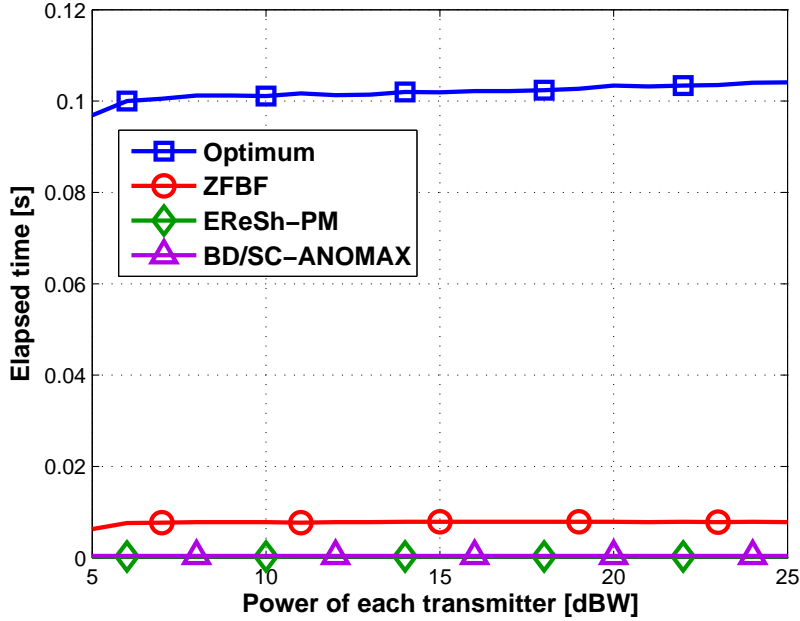


Figure 4.7.: Elapsed time versus P_T with target SINR = 0 dB

blue curve, all the suboptimal solutions have 1 dB degradation, of which EReSh-PM and BD/SC-ANOMAX methods are proposed due to its extremely low computational complexity.

To verify that, the average elapsed time of CPU over one channel realization for all the methods is plotted in Fig. 4.7 based on 1000 channel realizations. The SINR constraint at each UT is still set to 0 dB and $M_R = 4$. It is observed that the optimum solution is more time consuming than other methods due to the use of the convex optimization tool as well as the rank-1 decomposition. Furthermore, although ZFBF can be efficiently performed with the convex optimization tool, it is apparent to see that the closed-form solutions EReSh-PM and BD/SC-ANOMAX consume even much less time, of which EReSh-PM performs slightly better than BD/SC-ANOMAX.

The impact of the number of relay antennas on the relay transmit power is shown in Fig. 4.8. Here P_T is 10 dBW and the target SINR at each UT is set to 0 dB. All the suboptimal solutions give almost the same performance, which is slightly worse than the optimum method.

The feasibility check is investigated for all the schemes. For the optimum solution, the convex feasible region is checked in (4.26). Concerning the benchmark work ZFBF [LP10], the condition $P_T \widehat{h}_k^2 - \gamma_k > 0$ and $P_T - \gamma_k \|\mathbf{f}_{\text{MAC},k}\|^2 \geq 0$ must be fulfilled for the implementation of this method. Furthermore, EReSh-PM and BD/SC-ANOMAX are restricted by (4.37) (4.44), respectively. The probability that the feasibility test fails is depicted in Fig. 4.9. The transmit power at each BS P_T and the target SINR are the same as in Fig. 4.8. It is observed that all the suboptimal methods ZFBF, EReSh-PM, and BD/SC-ANOMAX have lower infeasible probability than the optimum solution when $M_R = 3$. When the number of relay antennas

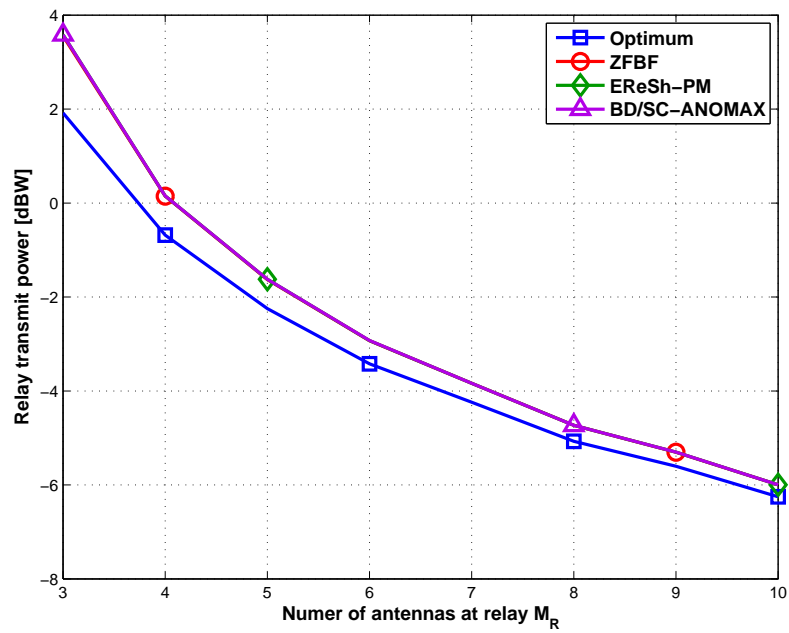


Figure 4.8.: P_R versus M_R with target SINR = 0 dB, $P_T = 10$ dBW

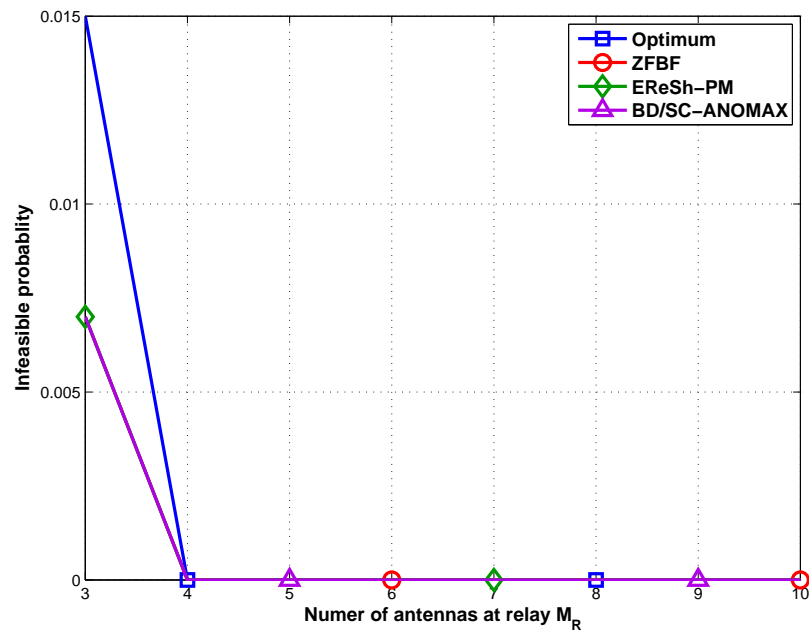


Figure 4.9.: Failure probability of the feasibility check versus M_R with target SINR = 0 dB, $P_T = 10$ dBW

increases, there exist no difference. Therefore, EReSh-PM and BD/SC-ANOMAX provide a good compromise between the performance and complexity since iterations are avoidable.

In addition to the SAPHYRE gain with respect to the system rate, we can also interpret the SAPHYRE sharing gain in terms of the consumed transmit power. That is, the transmit power consumed in the sharing scenario is compared to the that by the exclusive use of the spectrum and infrastructure for a single operator (TDMA access). The fractional SAPHYRE gain in terms of power is defined in equation (2.2). The numerator denotes the average required transmit power for achieving certain QoS metrics (e.g., minimum required SINR for each user, minimum required total data rate of the network, minimum required SNR per user, etc.) in the non-sharing case and the factor K is due to the use of resources in subsequent K time slots. The denominator denotes the required transmit power for achieving the same performance metrics in the sharing case.

For the SAPHYRE scenario, we use the EReSh-PM [LRH11a] described in Section 4.3.2 compromising between the performance and the computational complexity. The TDMA scenario is used as a benchmark. At each time slot, the relay amplification matrix is designed for each operator to minimize the relay transmit power subject to the SINR constraint at a single user. The optimum solution for the TDMA access is derived as follows.

In the case that the relay is accessed by each operator, the received signal at the UT is

$$y_k = \mathbf{g}_k^T \mathbf{F}_R \mathbf{h}_k s_k + \mathbf{g}_k^T \mathbf{F}_R \mathbf{n}_R + n_k.$$

The relay transmit power is calculated as

$$\begin{aligned} & \mathbb{E} \left\{ \left\| \mathbf{F}_R \mathbf{h}_k s_k + \mathbf{F}_R \mathbf{n}_R \right\|^2 \right\} \\ &= \text{tr} \left\{ P_T \mathbf{F}_R \mathbf{h}_k \mathbf{h}_k^H \mathbf{F}_R^H \right\} + \text{tr} \left\{ \sigma_n^2 \mathbf{F}_R \mathbf{F}_R^H \right\} \\ &= P_T \left\| \mathbf{F}_R \mathbf{h}_k \right\|_2^2 + \sigma_n^2 \left\| \mathbf{F}_R \right\|_F^2 \\ &= P_T \left\| \underbrace{(\mathbf{h}_k^T \otimes \mathbf{I}_{M_R})}_{\mathbf{B}} \underbrace{\text{vec}(\mathbf{F}_R)}_{\mathbf{w}} \right\|_2^2 + \sigma_n^2 \left\| \underbrace{\text{vec}(\mathbf{F}_R)}_{\mathbf{w}} \right\|_2^2 \\ &= \mathbf{w}^H \underbrace{(P_T \mathbf{B}^H \mathbf{B} + \sigma_n^2 \mathbf{I}_{M_R})}_{\mathbf{D}} \mathbf{w} \\ &= \text{tr} \{ \mathbf{D} \mathbf{W}_k \}. \end{aligned} \tag{4.46}$$

The SINR constraint for each UT is

$$\text{SINR}_k = \frac{P_T |\mathbf{g}_k^T \mathbf{F}_R \mathbf{h}_k|^2}{\sigma_n^2 \left\| \mathbf{g}_k^T \mathbf{F}_R \right\|_2^2 + \sigma_n^2}. \tag{4.47}$$

(4.47) could be further simplified using the following equations,

$$\mathbf{g}_k^T \mathbf{F}_R \mathbf{h}_k = \text{vec}(\mathbf{g}_k^T \mathbf{F}_R \mathbf{h}_k) = \underbrace{(\mathbf{h}_k^T \otimes \mathbf{g}_k^T)}_{\mathbf{c}^T} \underbrace{\text{vec}(\mathbf{F}_R)}_{\mathbf{w}}, \quad (4.48)$$

$$\|\mathbf{g}_k^T \mathbf{F}_R\|_2^2 = \|\mathbf{g}_k^T \mathbf{F}_R \mathbf{I}_{M_R}\|_2^2 = \left\| \underbrace{(\mathbf{I}_{M_R} \otimes \mathbf{g}_k^T)}_{\mathbf{A}} \underbrace{\text{vec}(\mathbf{F}_R)}_{\mathbf{w}} \right\|_2^2. \quad (4.49)$$

By inserting (4.48) and (4.49) into (4.47), we have

$$\text{SINR}_k = \frac{P_T \text{tr} \{ \mathbf{w}^H \mathbf{c}^* \mathbf{c}^T \mathbf{w} \}}{\sigma_n^2 \text{tr} \{ \mathbf{w}^H \mathbf{A}^H \mathbf{A} \mathbf{w} \} + \sigma_n^2} \geq \gamma_k,$$

which is finally transformed to

$$\text{tr} \{ (P_T \mathbf{c}^* \mathbf{c}^T - \gamma_k \sigma_n^2 \mathbf{A}^H \mathbf{A}) \mathbf{W}_k \} \geq \gamma_k \sigma_n^2.$$

Thereby, the problem is formulated as

$$\begin{aligned} \min_{\mathbf{W}_k} \quad & \text{tr} \{ \mathbf{D} \mathbf{W}_k \}, \\ \text{s.t.} \quad & \text{tr} \{ (P_T \mathbf{c}^* \mathbf{c}^T - \gamma_k \sigma_n^2 \mathbf{A}^H \mathbf{A}) \mathbf{W}_k \} \geq \gamma_k \sigma_n^2, \\ & \text{rank}(\mathbf{W}_k) = 1. \end{aligned} \quad (4.50)$$

Without considering the constraint $\text{rank}(\mathbf{W}_k) = 1$, \mathbf{W}_k could be obtained through convex optimization tools. To retrieve \mathbf{w}_k from \mathbf{W}_k , the rank-1 decomposition is performed using the theorem [AHZ11], which is similar as introduced in Section 4.3.1.

The required relay transmit power using EReSh-PM for the SAPHYRE scenario and the TDMA solution for the non-sharing case is plotted in Fig. 4.10. The SINR constraint is set to 0 dB at each UT. As seen from the figure, the gap between the blue curve obtained by EReSh-PM and the red one for TDMA scenario with $M_R = 8$ denote the spectrum sharing gain. There is around 2 dB loss by making exclusive use of the spectrum with 2 operators. Moreover, the gap between the EReSh-PM method and TDMA access with $M_R = 4$ give the spectrum and the infrastructure sharing gain of 6 dB in the case that half number of the relay antennas are accessed by each operator subsequently.

4.3.4. Conclusion

In this section, an optimum algorithm and several suboptimal solutions are proposed to achieve a power efficient transmission for the multiple operator AF relay sharing system. We study the special case that the BSs and the UTs are equipped with single antennas, where only single stream transmission is possible. A global optimum solution is firstly derived in Subsection 4.3.1, which uses a convex optimization tool to exploit the structure of the relay

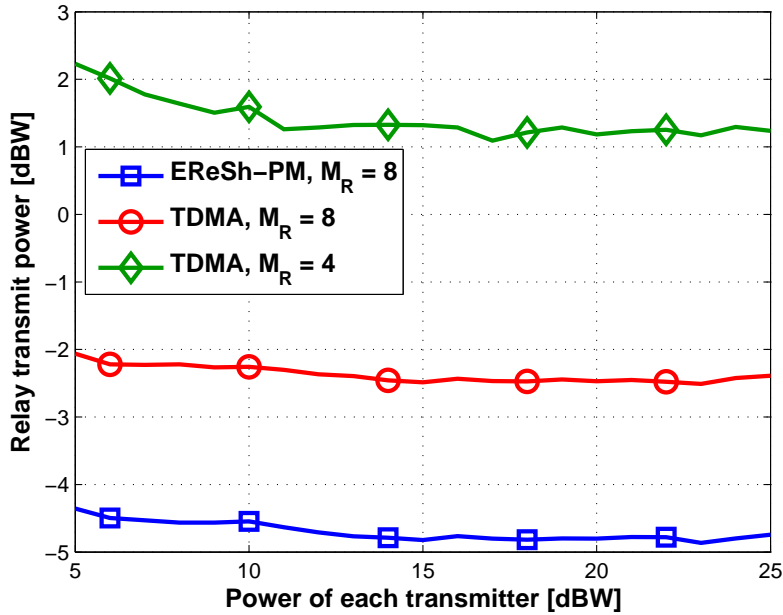


Figure 4.10.: SAPHYRE gain in terms of power for multiple operator one-way relaying

precoder. Taking this as a benchmark, two suboptimal algorithms named EReSh-PM and BD/SC-ANOMAX are proposed in Subsection 4.3.2 and Subsection 4.3.3 to find a compromise between the achievable power efficiency and the computational complexity, which are based on zero-forcing and block diagonalization techniques for interference mitigation. Both of them are closed-form solutions and no iteration is required. Compared to the optimum solution, both the suboptimal algorithms achieve almost the same good performance and have only 1 dB degradation. Hence, EReSh-PM and BD/SC-ANOMAX methods are strongly proposed due to their extremely low computational complexity. Following that, the SAPHYRE sharing gain is investigated in terms of the required relay transmit power. There is 2 dB gain by sharing the spectrum and a 6 dB gain is observed by both the spectrum and relay sharing compared to the exclusive use of these physical resources.

4.4. Robust Relay Precoder Design with Imperfect Channel State Information (CSI)

In the previous sections, the power efficient algorithms are investigated based on the assumption that the channel state information (CSI) at the BSs and the relay is perfect. This is an ideal assumption due to the fact that the relay has to obtain the CSI of the BSs to the relay as well as that of the UTs to relay link via feedback channels. More practically, we have the channel estimation error due to the quantization error, feedback delay, etc.. In this section, we consider a robust design of the relay precoder in the multiple operator AF relay sharing system, where the CSI at the relay is assumed to be imperfect. The same scenario is

studied as in Section 4.3, where each BS and UT is equipped with a single antenna while the relay employs multiple antennas. The main contribution of this section has been published in reference [LH13].

In the state-of-the-art work [CV09], the authors design a relay precoder to minimize the relay transmit power in the worst case subject to the worst case signal-to-interference-plus-noise ratio (SINR). The worst case of the relay transmit power and SINR refer to the maximum relay power and the minimum SINR for the largest possible channel errors, respectively. In contrast to that reference, our work is focused on a novel robust relay precoder design in order to minimize the average relay transmit power under the SINR constraints for each operator. Monte-Carlo simulation results show that the proposed robust method outperforms the non-robust solution significantly in terms of the outage probability of the SINR. Furthermore, we demonstrate the sharing gain achieved by this robust method via spectrum and relay sharing between multiple operators compared to the case where the spectrum and the relay are accessed exclusively by each operator.

As stated in [UC11], the CSI errors can be modeled in two ways. One is named stochastic error (SE) model, where the probability distribution of the CSI error is Gaussian. This model is applicable when the channel estimation error dominates compared to the quantization errors. The other is the norm-bounded error (NBE) model, where the CSI error is specified by an uncertainty set. This model is used when the CSI error is mainly due to the quantization errors. We apply the SE error model in this work. The channel uncertainties is modeled as follows [UC11],

$$\begin{aligned} \mathbf{h}_k &= \widehat{\mathbf{h}}_k + \mathbf{e}_k, \\ \mathbf{g}_k^T &= \widehat{\mathbf{g}}_k^T + \mathbf{f}_k^T, \quad k = 1, 2, \dots, K. \end{aligned} \quad (4.51)$$

The vectors \mathbf{h}_k and \mathbf{g}_k^T represent the true CSI between the BS_{*k*} and the relay and that between the relay and the UT_{*k*}. The imperfect CSI available at the relay are denoted by $\widehat{\mathbf{h}}_k$ and $\widehat{\mathbf{g}}_k^T$. The corresponding CSI error are \mathbf{e}_k and \mathbf{f}_k^T , respectively. Equivalently, we write the equation (4.51) in a compact form,

$$\begin{aligned} \mathbf{H} &= \widehat{\mathbf{H}} + \mathbf{E}, \\ \mathbf{G} &= \widehat{\mathbf{G}} + \mathbf{F}, \end{aligned} \quad (4.52)$$

where $\mathbf{H} = [\mathbf{h}_1, \dots, \mathbf{h}_K]$ and $\mathbf{G} = [\mathbf{g}_1, \dots, \mathbf{g}_K]^T$. The channel estimation error matrices \mathbf{E} and \mathbf{F} are assumed Gaussian distributed with zero mean and $\mathbb{E}\{\text{vec}(\mathbf{E})\text{vec}(\mathbf{E}^H)\} = \sigma_E^2 \mathbf{I}_{KM_R}$, $\mathbb{E}\{\text{vec}(\mathbf{F})\text{vec}(\mathbf{F}^H)\} = \sigma_F^2 \mathbf{I}_{KM_R}$. Hence, it is obtained that

$$\begin{aligned} \mathbb{E}\{\mathbf{E}\mathbf{E}^H\} &= K\sigma_E^2 \mathbf{I}_{M_R}, \\ \mathbb{E}\{\mathbf{F}\mathbf{F}^H\} &= M_R\sigma_F^2 \mathbf{I}_K. \end{aligned} \quad (4.53)$$

Furthermore, we assume that \mathbf{E} and \mathbf{F} are uncorrelated with $\widehat{\mathbf{H}}$ and $\widehat{\mathbf{G}}$, respectively.

As described in Section 4.1, the relay transmit power is expressed as

$$\begin{aligned} P_R &= \mathbb{E}\left\{\text{tr}(\mathbf{x}_R \mathbf{x}_R^H)\right\} \\ &= P_T \mathbb{E}\left\{\text{tr}(\mathbf{F}_R \mathbf{H} \mathbf{H}^H \mathbf{F}_R^H)\right\} + \sigma_n^2 \text{tr}(\mathbf{F}_R \mathbf{F}_R^H). \end{aligned} \quad (4.54)$$

By inserting (4.52) and (4.53) into (4.54), P_R is further written as

$$\begin{aligned} P_R &= P_T \mathbb{E}\left\{\text{tr}\left(\mathbf{F}_R (\widehat{\mathbf{H}} + \mathbf{E}) (\widehat{\mathbf{H}} + \mathbf{E})^H \mathbf{F}_R^H\right)\right\} + \sigma_n^2 \text{tr}(\mathbf{F}_R \mathbf{F}_R^H) \\ &= P_T \text{tr}(\mathbf{F}_R \widehat{\mathbf{H}} \widehat{\mathbf{H}}^H \mathbf{F}_R^H) + P_T \mathbb{E}\left\{\text{tr}(\mathbf{F}_R \mathbf{E} \mathbf{E}^H \mathbf{F}_R^H)\right\} + \sigma_n^2 \text{tr}(\mathbf{F}_R \mathbf{F}_R^H) \\ &= P_T \text{tr}(\mathbf{F}_R \widehat{\mathbf{H}} \widehat{\mathbf{H}}^H \mathbf{F}_R^H) + (P_T K \sigma_E^2 + \sigma_n^2) \text{tr}(\mathbf{F}_R \mathbf{F}_R^H) \\ &= P_T \text{tr}\left(\underbrace{(\widehat{\mathbf{H}}^T \otimes \mathbf{I}_{M_R})}_{\mathbf{P}} \underbrace{\text{vec}(\mathbf{F}_R)}_{\mathbf{f}_R} \text{vec}(\mathbf{F}_R)^H (\widehat{\mathbf{H}}^T \otimes \mathbf{I}_{M_R})^H\right) \\ &\quad + (P_T K \sigma_E^2 + \sigma_n^2) \text{tr}\left(\text{vec}(\mathbf{F}_R) \text{vec}(\mathbf{F}_R)^H\right) \\ &= P_T \text{tr}(\mathbf{f}_R^H \mathbf{P}^H \mathbf{P} \mathbf{f}_R) + (P_T K \sigma_E^2 + \sigma_n^2) \text{tr}(\mathbf{f}_R^H \mathbf{f}_R) \\ &= \mathbf{f}_R^H \left(P_T \mathbf{P}^H \mathbf{P} + (P_T K \sigma_E^2 + \sigma_n^2) \mathbf{I}_{M_R}^2\right) \mathbf{f}_R. \end{aligned} \quad (4.55)$$

With respect to the SINR constraint at the UTs, we first derive the received signal at UT $_k$ as

$$y_k = \mathbf{g}_k^T \mathbf{F}_R \mathbf{h}_k s_k + \sum_{j \neq k} \mathbf{g}_k^T \mathbf{F}_R \mathbf{h}_j s_j + \mathbf{g}_k^T \mathbf{F}_R \mathbf{n}_R + n_k, \quad (4.56)$$

where the first term is the desired signal and the second term represents the inter-operator interference caused to user k . The effective noise is given by the remaining terms on the right hand side. In the following, we express the SINR of UT $_k$ as a function of \mathbf{f}_R .

The power of the desired signal in (4.56) is calculated as

$$\mathbb{E}\left\{|\mathbf{g}_k^T \mathbf{F}_R \mathbf{h}_k s_k|^2\right\} = P_T \mathbb{E}\left\{\text{tr}\left(\left(\widehat{\mathbf{g}}_k^T + \mathbf{f}_k^T\right) \mathbf{F}_R (\widehat{\mathbf{h}}_k + \mathbf{e}_k) (\widehat{\mathbf{h}}_k^H + \mathbf{e}_k^H) \mathbf{F}_R^H (\widehat{\mathbf{g}}_k^* + \mathbf{f}_k^*)\right)\right\}. \quad (4.57)$$

Due to the assumption that $\widehat{\mathbf{g}}_k^T$ and $\widehat{\mathbf{f}}_k$ are uncorrelated with $\widehat{\mathbf{f}}_k^T$ and $\widehat{\mathbf{e}}_k$, we could further write (4.57) as follows

$$\begin{aligned} &P_T \mathbb{E}\left\{\text{tr}\left(\left(\widehat{\mathbf{g}}_k^T + \mathbf{f}_k^T\right) \mathbf{F}_R (\widehat{\mathbf{h}}_k + \mathbf{e}_k) (\widehat{\mathbf{h}}_k^H + \mathbf{e}_k^H) \mathbf{F}_R^H (\widehat{\mathbf{g}}_k^* + \mathbf{f}_k^*)\right)\right\} \\ &= P_T \text{tr}(\widehat{\mathbf{g}}_k^T \mathbf{F}_R \widehat{\mathbf{h}}_k \widehat{\mathbf{h}}_k^H \mathbf{F}_R^H \widehat{\mathbf{g}}_k^* + \sigma_E^2 \widehat{\mathbf{g}}_k^T \mathbf{F}_R \mathbf{F}_R^H \widehat{\mathbf{g}}_k^* + \sigma_F^2 \mathbf{F}_R \widehat{\mathbf{h}}_k \widehat{\mathbf{h}}_k^H \mathbf{F}_R^H + \sigma_E^2 \sigma_F^2 \mathbf{F}_R \mathbf{F}_R^H) \\ &= P_T \text{tr}\left(\underbrace{(\widehat{\mathbf{h}}_k^T \otimes \widehat{\mathbf{g}}_k^T)}_{\mathbf{a}^T} \underbrace{\text{vec}(\mathbf{F}_R)}_{\mathbf{f}_R} \text{vec}(\mathbf{F}_R)^H (\widehat{\mathbf{h}}_k^T \otimes \widehat{\mathbf{g}}_k^T)^H + \sigma_E^2 \underbrace{(\mathbf{I}_{M_R} \otimes \widehat{\mathbf{g}}_k^T)}_{\mathbf{B}} \text{vec}(\mathbf{F}_R) \text{vec}(\mathbf{F}_R)^H (\mathbf{I}_{M_R} \otimes \widehat{\mathbf{g}}_k^T)^H\right) \\ &\quad + \sigma_F^2 \underbrace{(\widehat{\mathbf{h}}_k^T \otimes \mathbf{I}_{M_R})}_{\mathbf{C}} \text{vec}(\mathbf{F}_R) \text{vec}(\mathbf{F}_R)^H (\widehat{\mathbf{h}}_k^T \otimes \mathbf{I}_{M_R})^H + \sigma_E^2 \sigma_F^2 \text{vec}(\mathbf{F}_R) \text{vec}(\mathbf{F}_R)^H \\ &= P_T \mathbf{f}_R^H (\mathbf{a}^* \mathbf{a}^T + \sigma_E^2 \mathbf{B}^H \mathbf{B} + \sigma_F^2 \mathbf{C}^H \mathbf{C} + \sigma_E^2 \sigma_F^2 \mathbf{I}_{M_R}^2) \mathbf{f}_R. \end{aligned} \quad (4.58)$$

Based on (4.56), the power of the inter-operator interference is obtained as

$$\mathbb{E}\left\{\left|\sum_{j \neq k} \mathbf{g}_k^T \mathbf{F}_R \mathbf{h}_j s_j\right|^2\right\} = P_T \mathbb{E}\left\{\text{tr}(\mathbf{g}_k^T \mathbf{F}_R \tilde{\mathbf{H}}_k \tilde{\mathbf{H}}_k^H \mathbf{F}_R^H \mathbf{g}_k^*)\right\}, \quad (4.59)$$

where $\tilde{\mathbf{H}}_k$ is defined as $\tilde{\mathbf{H}}_k = [\mathbf{h}_1, \dots, \mathbf{h}_{k-1}, \mathbf{h}_{k+1}, \dots, \mathbf{h}_K]$ and $\tilde{\mathbf{H}}_k = \widehat{\mathbf{H}}_k + \tilde{\mathbf{E}}_k$. The matrix $\tilde{\mathbf{E}}_k$ is the channel estimation error matrix excluding user k . Similarly as in (4.57) and (4.58), (4.59) is further calculated as

$$\begin{aligned} & P_T \mathbb{E}\left\{\text{tr}(\mathbf{g}_k^T \mathbf{F}_R \tilde{\mathbf{H}}_k \tilde{\mathbf{H}}_k^H \mathbf{F}_R^H \mathbf{g}_k^*)\right\} \\ &= P_T \text{tr}(\widehat{\mathbf{g}}_k^T \mathbf{F}_R \widehat{\mathbf{H}}_k \widehat{\mathbf{H}}_k^H \mathbf{F}_R^H \widehat{\mathbf{g}}_k^* + \sigma_E^2 \widehat{\mathbf{g}}_k^T \mathbf{F}_R \mathbf{F}_R^H \widehat{\mathbf{g}}_k^* + \sigma_F^2 \mathbf{F}_R \widehat{\mathbf{H}}_k \widehat{\mathbf{H}}_k^H \mathbf{F}_R^H + \sigma_E^2 \sigma_F^2 \mathbf{F}_R \mathbf{F}_R^H) \\ &= P_T \text{tr}\left(\underbrace{(\widehat{\mathbf{H}}_k^T \otimes \widehat{\mathbf{g}}_k^T)}_A \underbrace{\text{vec}(\mathbf{F}_R)}_{\mathbf{f}_R} \text{vec}(\mathbf{F}_R) (\widehat{\mathbf{H}}_k^T \otimes \widehat{\mathbf{g}}_k^T)^H + \sigma_E^2 \underbrace{(\mathbf{I}_{M_R} \otimes \widehat{\mathbf{g}}_k^T)}_B \text{vec}(\mathbf{F}_R) \text{vec}(\mathbf{F}_R)^H (\mathbf{I}_{M_R} \otimes \widehat{\mathbf{g}}_k^T)^H\right. \\ &\quad \left.+ \sigma_F^2 \underbrace{(\widehat{\mathbf{H}}_k^T \otimes \mathbf{I}_{M_R})}_D \text{vec}(\mathbf{F}_R) \text{vec}(\mathbf{F}_R)^H (\widehat{\mathbf{H}}_k^T \otimes \mathbf{I}_{M_R})^H + \sigma_E^2 \sigma_F^2 \text{vec}(\mathbf{F}_R) \text{vec}(\mathbf{F}_R)^H\right) \\ &= P_T \mathbf{f}_R^H (\mathbf{A}^H \mathbf{A} + \sigma_E^2 \mathbf{B}^H \mathbf{B} + \sigma_F^2 \mathbf{D}^H \mathbf{D} + \sigma_E^2 \sigma_F^2 \mathbf{I}_{M_R^2}) \mathbf{f}_R. \end{aligned} \quad (4.60)$$

Concerning the power of the effective noise,

$$\begin{aligned} & \mathbb{E}\left\{\left|\mathbf{g}_k^T \mathbf{F}_R \mathbf{n}_R + n_k\right|^2\right\} \\ &= \sigma_n^2 \mathbb{E}\left\{\text{tr}(\mathbf{g}_k^T \mathbf{F}_R \mathbf{F}_R^H \mathbf{g}_k^*)\right\} + \sigma_n^2 \\ &= \sigma_n^2 \mathbb{E}\left\{\text{tr}\left((\widehat{\mathbf{g}}_k^T + \mathbf{f}_k^T) \mathbf{F}_R \mathbf{F}_R^H (\widehat{\mathbf{g}}_k^* + \mathbf{f}_k^*)\right)\right\} + \sigma_n^2 \\ &= \sigma_n^2 \text{tr}(\widehat{\mathbf{g}}_k^T \mathbf{F}_R \mathbf{F}_R^H \widehat{\mathbf{g}}_k^* + \sigma_F^2 \mathbf{F}_R \mathbf{F}_R^H) + \sigma_n^2 \\ &= \sigma_n^2 \text{tr}\left(\underbrace{(\mathbf{I}_{M_R} \otimes \widehat{\mathbf{g}}_k^T)}_B \underbrace{\text{vec}(\mathbf{F}_R)}_{\mathbf{f}_R} \text{vec}(\mathbf{F}_R) (\mathbf{I}_{M_R} \otimes \widehat{\mathbf{g}}_k^T)^H + \sigma_F^2 \text{vec}(\mathbf{F}_R) \text{vec}(\mathbf{F}_R)^H\right) + \sigma_n^2 \\ &= \sigma_n^2 \mathbf{f}_R^H (\mathbf{B}^H \mathbf{B} + \sigma_F^2 \mathbf{I}_{M_R^2}) \mathbf{f}_R + \sigma_n^2. \end{aligned} \quad (4.61)$$

Combing (4.58), (4.60) and (4.61), the SINR constraint for the k -th user is expressed as

$$\frac{P_T \mathbf{f}_R^H (\mathbf{a}^* \mathbf{a}^T + \sigma_E^2 \mathbf{B}^H \mathbf{B} + \sigma_F^2 \mathbf{C}^H \mathbf{C} + \sigma_E^2 \sigma_F^2 \mathbf{I}_{M_R^2}) \mathbf{f}_R}{P_T \mathbf{f}_R^H (\mathbf{A}^H \mathbf{A} + \sigma_E^2 \mathbf{B}^H \mathbf{B} + \sigma_F^2 \mathbf{D}^H \mathbf{D} + \sigma_E^2 \sigma_F^2 \mathbf{I}_{M_R^2}) \mathbf{f}_R + \sigma_n^2 \mathbf{f}_R^H (\mathbf{B}^H \mathbf{B} + \sigma_F^2 \mathbf{I}_{M_R^2}) \mathbf{f}_R + \sigma_n^2} \geq \gamma_k. \quad (4.62)$$

The equation (4.62) can be written as

$$\begin{aligned} & \mathbf{f}_R^H \left(P_T \mathbf{a}^* \mathbf{a}^T + (P_T \sigma_E^2 - \gamma_k P_T \sigma_E^2 - \gamma_k \sigma_n^2) \mathbf{B}^H \mathbf{B} + P_T \sigma_F^2 \mathbf{C}^H \mathbf{C} \right. \\ & \left. + (P_T \sigma_E^2 \sigma_F^2 - \gamma_k P_T \sigma_E^2 \sigma_F^2 - \gamma_k \sigma_n^2 \sigma_F^2) \mathbf{I}_{M_R^2} - \gamma_k P_T \mathbf{A}^H \mathbf{A} - \gamma_k P_T \sigma_F^2 \mathbf{D}^H \mathbf{D} \right) \mathbf{f}_R \geq \gamma_k \sigma_n^2. \end{aligned} \quad (4.63)$$

By defining $\mathbf{W} = \mathbf{f}_R \mathbf{f}_R^H$, the problem of minimizing the relay transmit power under SINR

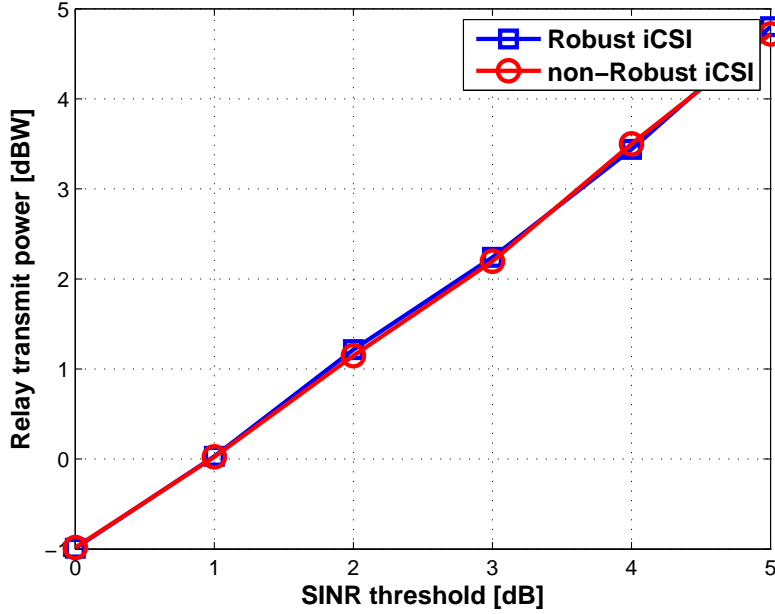


Figure 4.11.: P_R versus SINR threshold γ at SNR = 20 dB

constraint is formulated as

$$\begin{aligned}
\min_{\mathbf{W}} \quad & \text{tr}\left((P_T \mathbf{P}^H \mathbf{P} + (P_T K \sigma_E^2 + \sigma_n^2) \mathbf{I}_{M_R^2}) \mathbf{W}\right) \\
\text{s.t.} \quad & \text{tr}\left(\left(P_T \mathbf{a}^* \mathbf{a}^T + (P_T \sigma_E^2 - \gamma_k P_T \sigma_E^2 - \gamma_k \sigma_n^2) \mathbf{B}^H \mathbf{B} + P_T \sigma_F^2 \mathbf{C}^H \mathbf{C}\right.\right. \\
& \left.\left.+ (P_T \sigma_E^2 \sigma_F^2 - \gamma_k P_T \sigma_E^2 \sigma_F^2 - \gamma_k \sigma_n^2 \sigma_F^2) \mathbf{I}_{M_R^2} - \gamma_k P_T \mathbf{A}^H \mathbf{A} - \gamma_k P_T \sigma_F^2 \mathbf{D}^H \mathbf{D}\right) \mathbf{W}\right) \geq \gamma_k \sigma_n^2, \\
& k = 1, 2, \dots, K \\
& \text{rank}(\mathbf{W}) = 1.
\end{aligned} \tag{4.64}$$

Without considering the constraint $\text{rank}(\mathbf{W}) = 1$, \mathbf{W} can be solved effectively by semi-definite relaxation (SDR) [HP10, LMS⁺10] using the convex optimization toolbox cvx [BV04, GBY09]. Following that, a rank-1 solution is extracted from \mathbf{W} by a tight rank-1 decomposition method [AHZ11]. In our case, if the number of operators is less or equal than 4, an optimum \mathbf{w} can be reconstructed from \mathbf{W} .

Simulation results

A two operator AF relay sharing system is considered. Each element of all channel matrices is a zero mean circularly symmetric complex Gaussian random variable with unit variance $\mathcal{CN}(0, 1)$. The simulation results are obtained over 1000 channel realizations.

Fig. 4.11 gives the consumed relay transmit power versus the SINR threshold γ for the robust and non-robust methods. The relay employs $M_R = 4$ antennas. The simulation runs for SNR = 20 dB and unit noise variance is assumed. The CSI error variance is set to

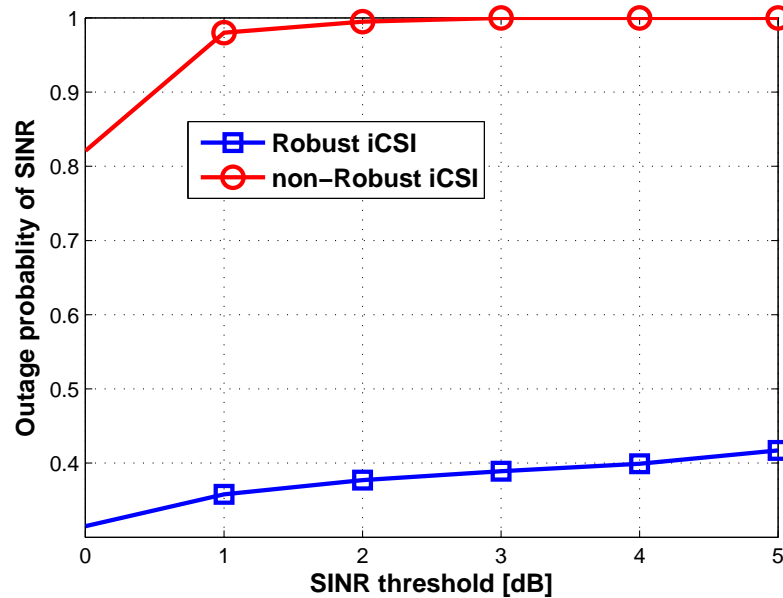


Figure 4.12.: Outage probability of SINR versus SINR threshold γ at SNR = 20 dB

$\sigma_E = \sigma_F = 0.1$. It is observed that the relay transmit power for both cases increases with an increasing SINR threshold. This is because more power has to be paid in order to meet higher QoS requirement. Both robust and non-robust methods consume almost the same relay power. However, the robust solution outperforms the non-robust method significantly in terms of the outage probability of SINR, as can be seen from Fig. 4.12. By using the robust method, the SINR requirements are much more often satisfied compared to the non-robust method.

The required relay transmit power using the robust method for the SAPHYRE scenario and that for the TDMA access in the non-sharing case is plotted in Fig. 4.13. The gap between the blue curve obtained by robust method and the red one for TDMA scenario with $M_R = 8$ denote the spectrum sharing gain. There is a gain of around 5 dB by the shared use of the spectrum between the two operators at high SNRs. An additional 2 dB gain is obtained by an additional sharing of the relay compared to the exclusive access of the relay with half of the number of relay antennas $M_R = 4$ for each operator.

4.5. Relay Power Minimization for Multiple Stream Transmission

More practically, each BS and UT are equipped with multiple antennas, denoted by $M_{T,k}$ and $M_{U,k}$. In this section, we extend the relay matrix design for multiple stream transmission in the multiple operator AF relaying system. Perfect channel state information is assumed at the relay.

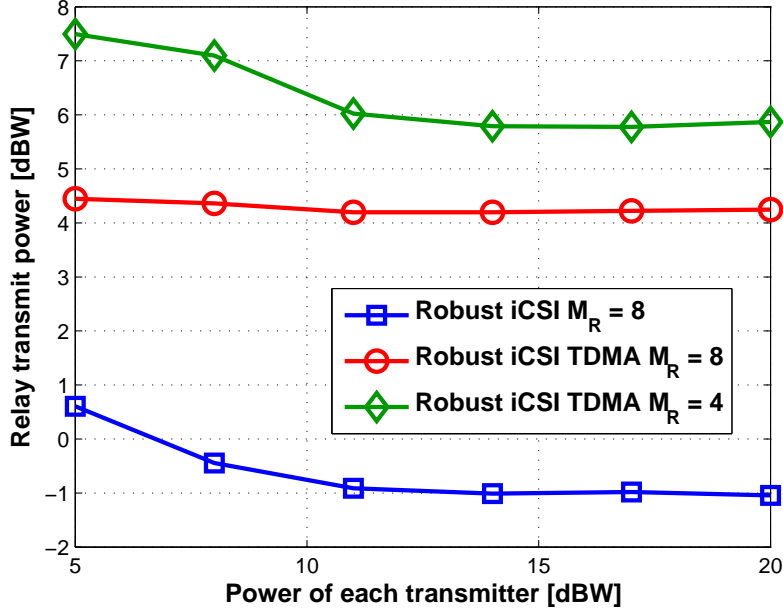


Figure 4.13.: SAPHYRE gain in terms of power for the robust design

Due to different modulation and coding schemes, we may have different SINR constraints for different data streams. Therefore, we investigate the relay amplification matrix design to minimize the relay transmit power under the SINR constraint per stream of each user.

The relay amplification matrix is designed as $\mathbf{F}_R = \mathbf{F}_{BC}\mathbf{F}_S\mathbf{F}_{MAC} \in \mathbb{C}^{M_R \times M_R}$, where \mathbf{F}_{MAC} and \mathbf{F}_{BC} are used for zero-forcing the interference generated in the MAC and BC phases while \mathbf{F}_S is designed for relay transmit power minimization.

To design \mathbf{F}_{MAC} , the pseudo inverse of the channel $\mathbf{H} \in \mathbb{C}^{M_R \times M_T}$ with $M_R > M_T$ between the BSs and the relay is obtained as

$$\mathbf{H}^+ = (\mathbf{H}^H \mathbf{H})^{-1} \mathbf{H}^H = \left[\bar{\mathbf{H}}_1^H, \dots, \bar{\mathbf{H}}_K^H \right]^H \in \mathbb{C}^{M_T \times M_R},$$

where $\bar{\mathbf{H}}_k \in \mathbb{C}^{M_T, k \times M_R}$. After that, the QR decomposition is performed on $\bar{\mathbf{H}}_k^H$ to retrieve its orthonormal basis $\mathbf{Q}_{\bar{\mathbf{H}}_k^H}$ multiplied by an upper triangular matrix $\mathbf{R}_{\bar{\mathbf{H}}_k^H} \in \mathbb{C}^{M_T, k \times M_T, k}$, which is expressed as

$$\bar{\mathbf{H}}_k^H = \mathbf{Q}_{\bar{\mathbf{H}}_k^H} \mathbf{R}_{\bar{\mathbf{H}}_k^H} \in \mathbb{C}^{M_R \times M_T, k}. \quad (4.65)$$

The matrix \mathbf{F}_{MAC} is obtained as

$$\mathbf{F}_{MAC} = \left[\mathbf{F}_{MAC,1}^T, \dots, \mathbf{F}_{MAC,K}^T \right]^T \in \mathbb{C}^{M_T \times M_R} \quad (4.66)$$

with $\mathbf{F}_{MAC,k} = \mathbf{Q}_{\bar{\mathbf{H}}_k^H} \in \mathbb{C}^{M_T, k \times M_R}$. In the BC phase, the pseudo inverse of the channel $\mathbf{G} \in$

$\mathbb{C}^{M_U \times M_R}$ with $M_R > M_U$ between the relay and the UTs is obtained as

$$\mathbf{G}^+ = \mathbf{G}^H (\mathbf{G} \mathbf{G}^H)^{-1} = \left[\bar{\mathbf{G}}_1, \dots, \bar{\mathbf{G}}_K \right] \in \mathbb{C}^{M_R \times M_U},$$

where $\bar{\mathbf{G}}_k \in \mathbb{C}^{M_R \times M_U, k}$. Similarly as in the MAC phase, the QR decomposition is performed on $\bar{\mathbf{G}}_k$ as

$$\bar{\mathbf{G}}_k = \mathbf{Q}_{\bar{\mathbf{G}}_k} \mathbf{R}_{\bar{\mathbf{G}}_k} \quad (4.67)$$

and the matrix \mathbf{F}_{BC} is obtained as

$$\mathbf{F}_{\text{BC}} = \left[\mathbf{F}_{\text{BC},1}, \dots, \mathbf{F}_{\text{BC},K} \right] \in \mathbb{C}^{M_R \times M_U} \quad (4.68)$$

with $\mathbf{F}_{\text{BC},k} = \mathbf{Q}_{\bar{\mathbf{G}}_k} \in \mathbb{C}^{M_R \times M_U, k}$.

After applying \mathbf{F}_{MAC} and \mathbf{F}_{BC} , all the inter-operator interferences are removed and the received signals at UTs are given as

$$\mathbf{y}_k = \underbrace{\mathbf{G}_k \mathbf{F}_{\text{BC},k}}_{\hat{\mathbf{G}}_k} \mathbf{F}_{\text{S},k} \underbrace{\mathbf{F}_{\text{MAC},k} \mathbf{H}_k}_{\hat{\mathbf{H}}_k} \bar{\mathbf{s}}_k + \mathbf{G}_k \mathbf{F}_{\text{BC},k} \mathbf{F}_{\text{S},k} \mathbf{F}_{\text{MAC},k} \mathbf{n}_R + \mathbf{n}_k, k = 1, 2, \dots, K \quad (4.69)$$

where $\bar{\mathbf{s}}_k = \mathbf{F}_k \mathbf{s}_k$ represents the precoded signal with \mathbf{F}_k denoting the precoding matrix at the BSs.

Next we want to design $\mathbf{F}_S = \text{diag}\{\mathbf{F}_{S,1}, \dots, \mathbf{F}_{S,K}\}$. We first compute the singular value decomposition (SVD) of $\widehat{\mathbf{H}}_k$ and $\widehat{\mathbf{G}}_k$ as $\widehat{\mathbf{H}}_k = \mathbf{U}_{\widehat{\mathbf{H}}_k} \boldsymbol{\Sigma}_{\widehat{\mathbf{H}}_k} \mathbf{V}_{\widehat{\mathbf{H}}_k}^H \in \mathbb{C}^{M_T, k \times M_T, k}$ and $\widehat{\mathbf{G}}_k = \mathbf{U}_{\widehat{\mathbf{G}}_k} \boldsymbol{\Sigma}_{\widehat{\mathbf{G}}_k} \mathbf{V}_{\widehat{\mathbf{G}}_k}^H \in \mathbb{C}^{M_U, k \times M_U, k}$. Then the matrix $\mathbf{F}_{S,k}$ is designed as

$$\mathbf{F}_{S,k} = \mathbf{V}_{\widehat{\mathbf{G}}_k} \boldsymbol{\Phi}_k \mathbf{U}_{\widehat{\mathbf{H}}_k}^H \in \mathbb{C}^{M_U, k \times M_T, k} \quad (4.70)$$

so that the effective channel can be written in a generalized SVD form

$$\mathbf{H}_{\text{eff}} = \widehat{\mathbf{G}}_k \mathbf{F}_{S,k} \widehat{\mathbf{H}}_k = \mathbf{U}_{\widehat{\mathbf{G}}_k} \boldsymbol{\Sigma}_{\widehat{\mathbf{G}}_k} \boldsymbol{\Phi}_k \boldsymbol{\Sigma}_{\widehat{\mathbf{H}}_k} \mathbf{V}_{\widehat{\mathbf{H}}_k}^H = \mathbf{U}_{\text{eff}} \boldsymbol{\Sigma}_{\text{eff}} \mathbf{V}_{\text{eff}}^H \in \mathbb{C}^{M_U, k \times M_T, k} \quad (4.71)$$

With respect to the effective diagonal matrix, $\boldsymbol{\Sigma}_{\widehat{\mathbf{H}}_k} = \text{diag}\{\alpha_{k,1}, \dots, \alpha_{k, M_T, k}\}$ and $\boldsymbol{\Sigma}_{\widehat{\mathbf{G}}_k} = \text{diag}\{\alpha_{k,1}, \dots, \alpha_{k, M_U, k}\}$. The diagonal matrix $\boldsymbol{\Phi}_k \in \mathbb{C}^{M_U, k \times M_T, k}$ with $\{\boldsymbol{\Phi}_{k,1}, \dots, \boldsymbol{\Phi}_{k, r_k}\}$ on its main diagonal has to be determined.

By inserting equation (4.70) into equation (4.69), the received signal is rewritten as

$$\mathbf{y}_k = \mathbf{U}_{\widehat{\mathbf{G}}_k} \boldsymbol{\Sigma}_{\widehat{\mathbf{G}}_k} \boldsymbol{\Phi}_k \boldsymbol{\Sigma}_{\widehat{\mathbf{H}}_k} \mathbf{V}_{\widehat{\mathbf{H}}_k}^H \mathbf{F}_k \mathbf{s}_k + \mathbf{U}_{\widehat{\mathbf{G}}_k} \boldsymbol{\Sigma}_{\widehat{\mathbf{G}}_k} \boldsymbol{\Phi}_k \mathbf{U}_{\widehat{\mathbf{H}}_k}^H \mathbf{Q}_{\widehat{\mathbf{H}}_k}^H \mathbf{n}_R + \mathbf{n}_k \in \mathbb{C}^{M_U, k}. \quad (4.72)$$

After that a transmit filter \mathbf{F}_k and a receive filter \mathbf{W}_k are applied at the BSs and UTs,

$$\begin{aligned}\mathbf{W}_k &= \underbrace{\begin{bmatrix} \mathbf{I}_{r_k} & \mathbf{0}_{r_k \times (M_{U,k} - r_k)} \end{bmatrix}}_{\mathbf{A}} \cdot \mathbf{U}_{\widehat{\mathbf{G}}_k}^H = \mathbf{A} \mathbf{U}_{\widehat{\mathbf{G}}_k}^H, \\ \mathbf{F}_k &= \mathbf{V}_{\widehat{\mathbf{H}}_k}^H \cdot \underbrace{\begin{bmatrix} \mathbf{I}_{r_k} & \mathbf{0}_{r_k \times (M_{T,k} - r_k)} \end{bmatrix}}_{\mathbf{B}}^T = \mathbf{V}_{\widehat{\mathbf{H}}_k}^H \mathbf{B},\end{aligned}\quad (4.73)$$

where $r_k = \min(M_{T,k}, M_{U,k})$ denotes the number of transmitted data streams for user k . Then the received signal is obtained as

$$\tilde{\mathbf{y}}_k = \mathbf{W}_k \mathbf{y}_k = \mathbf{A} \Sigma_{\widehat{\mathbf{G}}_k} \Phi_k \Sigma_{\widehat{\mathbf{H}}_k} \mathbf{B} \mathbf{s}_k + \mathbf{A} \Sigma_{\widehat{\mathbf{G}}_k} \Phi_k \mathbf{U}_{\widehat{\mathbf{H}}_k}^H \mathbf{Q}_{\widehat{\mathbf{H}}_k}^H \mathbf{n}_R + \mathbf{A} \Sigma_{\widehat{\mathbf{G}}_k} \mathbf{n}_k \in \mathbb{C}^{r_k} \quad (4.74)$$

such that the r_k data streams are extracted. By defining a diagonal matrix

$$\tilde{\Phi}_k = \mathbf{A} \Phi_k \mathbf{B} = \text{diag}\{\Phi_{k,1}, \dots, \Phi_{k,r_k}\} \in \mathbb{C}^{r_k \times r_k} \quad (4.75)$$

the matrix Φ_k is written as

$$\Phi_k = \mathbf{A}^+ \tilde{\Phi}_k \mathbf{B}^+,$$

where $\mathbf{A}^+ = \begin{bmatrix} \mathbf{I}_{r_k} & \mathbf{0}_{r_k \times (M_{U,k} - r_k)} \end{bmatrix}^T$ and $\mathbf{B}^+ = \begin{bmatrix} \mathbf{I}_{r_k} & \mathbf{0}_{r_k \times (M_{T,k} - r_k)} \end{bmatrix}$ denote the pseudo inverse of \mathbf{A} and \mathbf{B} , respectively. Then the received signal is reformulated as

$$\begin{aligned}\tilde{\mathbf{y}}_k &= \underbrace{\mathbf{A} \Sigma_{\widehat{\mathbf{G}}_k} \mathbf{A}^+}_{\tilde{\Sigma}_{\widehat{\mathbf{G}}_k}} \underbrace{\tilde{\Phi}_k \mathbf{B}^+ \Sigma_{\widehat{\mathbf{H}}_k} \mathbf{B}}_{\tilde{\Sigma}_{\widehat{\mathbf{H}}_k}} \mathbf{s}_k + \underbrace{\mathbf{A} \Sigma_{\widehat{\mathbf{G}}_k} \mathbf{A}^+}_{\tilde{\Sigma}_{\widehat{\mathbf{G}}_k}} \underbrace{\tilde{\Phi}_k \mathbf{B}^+ \mathbf{U}_{\widehat{\mathbf{H}}_k}^H \mathbf{Q}_{\widehat{\mathbf{H}}_k}^H}_{\tilde{\mathbf{C}}_k} \mathbf{n}_R + \underbrace{\mathbf{A} \Sigma_{\widehat{\mathbf{G}}_k} \mathbf{n}_k}_{\tilde{\mathbf{n}}_k} \in \mathbb{C}^{r_k}. \\ &= \tilde{\Sigma}_{\widehat{\mathbf{G}}_k} \tilde{\Phi}_k \tilde{\Sigma}_{\widehat{\mathbf{H}}_k} \mathbf{s}_k + \tilde{\Sigma}_{\widehat{\mathbf{G}}_k} \tilde{\Phi}_k \tilde{\mathbf{C}}_k \mathbf{n}_R + \tilde{\mathbf{n}}_k\end{aligned}\quad (4.76)$$

The first term on the right hand side is the effective signal while the other two terms denote the effective noise vector of user k . Due to the fact that the SINR constraint is imposed on each data stream per user, we need to analyze the received signal (4.76) for each stream such as to derive its SINR constraint. Let us first take a look at the signal component, which is denoted by

$$\mathbf{x}_k = \underbrace{\tilde{\Sigma}_{\widehat{\mathbf{G}}_k} \tilde{\Phi}_k \tilde{\Sigma}_{\widehat{\mathbf{H}}_k}}_{\mathbf{A}_k \in \mathbb{C}^{r_k \times r_k}} \mathbf{s}_k = \mathbf{A}_k \mathbf{s}_k.$$

The signal component of the m -th stream of user k is expressed by

$$\begin{aligned}x_{k,m} &= \lambda_m s_{k,m}, m = 1, 2, \dots, r_k, \\ \text{where } \lambda_m &= \alpha_{k,m} \beta_{k,m} \Phi_{k,m}, \tilde{\Sigma}_{\widehat{\mathbf{H}}_k} = \text{diag}\{\alpha_{k,1}, \dots, \alpha_{k,r_k}\}, \\ \tilde{\Sigma}_{\widehat{\mathbf{G}}_k} &= \text{diag}\{\beta_{k,1}, \dots, \beta_{k,r_k}\}, \tilde{\Phi}_k = \text{diag}\{\Phi_{k,1}, \dots, \Phi_{k,r_k}\}.\end{aligned}\quad (4.77)$$

Thereby, the signal power of $r_{k,m}$ is

$$\mathbb{E}|r_{k,m}|^2 = \mathbb{E}|\lambda_m s_{k,m}|^2 = \frac{P_T}{r_k} \alpha_{k,m}^2 \beta_{k,m}^2 |\Phi_{k,m}|^2, \quad (4.78)$$

where $|s_{k,m}|^2 = P_T/r_k$ due to the equal power allocation assumption at the BSs.

With respect to the effective noise vector in (4.76),

$$\mathbf{z}_k = \underbrace{\tilde{\Sigma}_{\tilde{\mathbf{G}}_k}}_{\Sigma \in \mathbb{C}^{r_k \times r_k}} \underbrace{\tilde{\Phi}_k}_{\tilde{\mathbf{C}}_k \in \mathbb{C}^{r_k \times M_R}} \mathbf{B}^+ \mathbf{U}_{\tilde{\mathbf{H}}_k}^H \mathbf{Q}_{\tilde{\mathbf{H}}_k}^H \mathbf{n}_R + \tilde{\mathbf{n}}_k = \underbrace{\Sigma \tilde{\mathbf{C}}_k}_{\mathbf{Q}} \mathbf{n}_R + \tilde{\mathbf{n}}_k = \mathbf{Q} \mathbf{n}_R + \tilde{\mathbf{n}}_k,$$

where $\Sigma = \text{diag}\{\Sigma_1, \Sigma_2, \dots, \Sigma_{r_k}\}$ with $\Sigma_m = \beta_{k,m} \Phi_{k,m}$. Then the (i, j) -th entry of \mathbf{Q} is written as

$$\begin{aligned} \mathbf{Q}_{i,j} &= \mathbf{q}_{i,j}^T \boldsymbol{\sigma}_k, \quad i = 1, 2, \dots, r_k, j = 1, 2, \dots, M_R \\ \mathbf{q}_{i,j} &= \left[\mathbf{0}_{1 \times (i-1)}, \quad \dots, \quad [\tilde{\mathbf{C}}_k]_{i,j}, \quad \dots, \quad \mathbf{0}_{1 \times (r_k-i)} \right]^T \in \mathbb{C}^{r_k}, \\ \boldsymbol{\sigma}_k &= \left[\Sigma_1, \quad \Sigma_2, \quad \dots, \quad \Sigma_{r_k} \right]^T \in \mathbb{C}^{r_k}. \end{aligned}$$

Therefore, the effective noise term \mathbf{z}_k for user k is

$$\mathbf{z}_k = \mathbf{Q} \mathbf{n}_R + \tilde{\mathbf{n}}_k = \begin{bmatrix} \mathbf{q}_{1,1}^T \boldsymbol{\sigma}_k & \cdots & \mathbf{q}_{1,M_R}^T \boldsymbol{\sigma}_k \\ \vdots & \ddots & \vdots \\ \mathbf{q}_{r_k,1}^T \boldsymbol{\sigma}_k & \cdots & \mathbf{q}_{r_k,M_R}^T \boldsymbol{\sigma}_k \end{bmatrix} \mathbf{n}_R + \tilde{\mathbf{n}}_k.$$

We assume that the noise at the relay \mathbf{n}_R and that at UTs \mathbf{n}_k for $k = 1, 2, \dots, K$ contain independent, identically distributed complex additive white Gaussian noise samples with variance σ_n^2 , i.e., $\mathbb{E}\{\mathbf{n}_R \mathbf{n}_R^H\} = \sigma_n^2 \mathbf{I}_{M_R}$ and $\mathbb{E}\{\mathbf{n}_k \mathbf{n}_k^H\} = \sigma_n^2 \mathbf{I}_{M_{U,k}}$. Then the noise variance at the UTs after applying the receive filter is $\mathbb{E}\{\tilde{\mathbf{n}}_k \tilde{\mathbf{n}}_k^H\} = \mathbb{E}\{\mathbf{A} \mathbf{U}_{\tilde{\mathbf{G}}_k} \mathbf{n}_k \mathbf{n}_k^H \mathbf{U}_{\tilde{\mathbf{G}}_k}^H \mathbf{A}^H\} = \sigma_n^2 \mathbf{I}_{r_k}$.

The power of the effective noise for the m -th stream of user k is derived as

$$\mathbb{E}|z_{k,m}|^2 = \sigma_n^2 \left| \underbrace{(\mathbf{q}_{m,1}^T + \cdots + \mathbf{q}_{m,M_R}^T)}_{\mathbf{q}_m^T} \boldsymbol{\sigma}_k \right|^2 + \sigma_n^2 = \sigma_n^2 \boldsymbol{\sigma}_k^H \mathbf{q}_m^* \mathbf{q}_m^T \boldsymbol{\sigma}_k + \sigma_n^2,$$

where

$$\boldsymbol{\sigma}_k = \left[\Sigma_1, \quad \Sigma_2, \quad \dots, \quad \Sigma_{r_k} \right]^T = \Sigma_{\tilde{\mathbf{G}}_k} \underbrace{\left[\Phi_{k,1}, \quad \dots, \quad \Phi_{k,r_k} \right]^T}_{\mathbf{w}_k}. \quad (4.79)$$

By incorporating (4.79) into (4.79), we get

$$\mathbb{E}\{|z_{k,m}|^2\} = \sigma_n^2 \mathbf{w}_k^H \underbrace{\Sigma_{\tilde{\mathbf{G}}_k} \mathbf{q}_m^* \mathbf{q}_m^T \Sigma_{\tilde{\mathbf{G}}_k}}_{\mathbf{R}_{k,m}} \mathbf{w}_k + \sigma_n^2. \quad (4.80)$$

By using (4.79) and (4.80), the SINR for each stream per user is obtained as

$$\text{SINR}_{k,m} = \frac{|r_{k,m}|^2}{|z_{k,m}|^2} = \frac{\frac{P_T}{r_k} \alpha_{k,m}^2 \beta_{k,m}^2 |\Phi_{k,m}|^2}{\sigma_n^2 \mathbf{w}_k^H \mathbf{R}_{k,m} \mathbf{w}_k + \sigma_n^2} = \frac{\frac{P_T}{r_k} \alpha_{k,m}^2 \beta_{k,m}^2 \mathbf{w}_k^H \mathbf{S}_{k,m} \mathbf{w}_k}{\sigma_n^2 \mathbf{w}_k^H \mathbf{R}_{k,m} \mathbf{w}_k + \sigma_n^2}, \quad (4.81)$$

where

$$\mathbf{S}_{k,m} = \begin{bmatrix} \mathbf{0}, & \dots, & \mathbf{0} \\ \vdots & 1 & \vdots \\ \mathbf{0}, & \dots, & \mathbf{0} \end{bmatrix} \in \mathbb{C}^{r_k \times r_k}.$$

The matrix $\mathbf{S}_{k,m}$ has only a single non-zero entry $[\mathbf{S}_{k,m}]_{m,m} = 1$ with all other elements equal to zero. Similarly as in Section 4.3.2, the objective is to minimize the average relay transmit power, which is equal to minimize the relay transmit power for each operator after the system is decoupled into multiple independent pairs. Assuming equal power allocation for each data stream per user $\mathbb{E}\{\mathbf{s}_k \mathbf{s}_k^H\} = \frac{P_T}{r_k} \mathbf{I}_{r_k}$, the relay transmit power for each operator is written as

$$\begin{aligned} P_{R,k} &= \mathbb{E}\left\{ \left\| \mathbf{F}_{R,k} \mathbf{H}_k \mathbf{s}_k + \mathbf{F}_{R,k} \mathbf{n}_R \right\|^2 \right\} \\ &= \frac{P_T}{r_k} \text{tr}(\mathbf{F}_{R,k} \mathbf{H}_k \mathbf{H}_k^H \mathbf{F}_{R,k}^H) + \sigma_n^2 \text{tr}(\mathbf{F}_{R,k} \mathbf{F}_{R,k}^H). \end{aligned} \quad (4.82)$$

The matrix

$$\mathbf{F}_{R,k} = \mathbf{F}_{BC,k} \mathbf{F}_{S,k} \mathbf{F}_{MAC,k} = \mathbf{Q}_{\hat{\mathbf{G}}_k} \mathbf{V}_{\hat{\mathbf{G}}_k} \Phi_k \mathbf{U}_{\hat{\mathbf{H}}_k}^H \mathbf{F}_{MAC,k} \quad (4.83)$$

is the relay amplification matrix for the k -th user and $\mathbf{F}_R = \sum_{k=1}^K \mathbf{F}_{R,k}$. By incorporating (4.83) and $\hat{\mathbf{H}}_k = \mathbf{F}_{MAC,k} \mathbf{H}_k = \mathbf{U}_{\hat{\mathbf{H}}_k} \Sigma_{\hat{\mathbf{H}}_k} \mathbf{V}_{\hat{\mathbf{H}}_k}^H$, the relay transmit power (4.82) is rewritten as follows,

$$\begin{aligned} P_{R,k} &= \mathbb{E}\left\{ \left\| \mathbf{F}_{R,k} \mathbf{H}_k \mathbf{s}_k + \mathbf{F}_{R,k} \mathbf{n}_R \right\|^2 \right\} \\ &= \text{tr}\left(\mathbf{Q}_{\hat{\mathbf{G}}_k} \mathbf{V}_{\hat{\mathbf{G}}_k} \left(\frac{P_T}{r_k} \Phi_k \Sigma_{\hat{\mathbf{H}}_k}^2 \Phi_k^H + \sigma_n^2 \Phi_k \Phi_k^H \right) \mathbf{V}_{\hat{\mathbf{G}}_k}^H \mathbf{Q}_{\hat{\mathbf{G}}_k}^H \right) \\ &= \text{tr}\left(\frac{P_T}{r_k} \Phi_k \Sigma_{\hat{\mathbf{H}}_k}^2 \Phi_k^H + \sigma_n^2 \Phi_k \Phi_k^H \right). \end{aligned} \quad (4.84)$$

Due to the fact that Φ_k has r_k elements on its main diagonal and based on (4.77), (4.84) can be further expressed as

$$\begin{aligned} P_{R,k} &= \text{tr}\left\{ \frac{P_T}{r_k} \Phi_k \Sigma_{\hat{\mathbf{H}}_k}^2 \Phi_k^H + \sigma_n^2 \Phi_k \Phi_k^H \right\} \\ &= \text{tr}\left\{ \frac{P_T}{r_k} \tilde{\Phi}_k \tilde{\Sigma}_{\hat{\mathbf{H}}_k}^2 \tilde{\Phi}_k^H + \sigma_n^2 \tilde{\Phi}_k \tilde{\Phi}_k^H \right\} \\ &= \underbrace{\begin{bmatrix} \Phi_{k,1}, \dots, \Phi_{k,r_k} \end{bmatrix}}_{\mathbf{w}_k^T} \underbrace{\left\{ \frac{P_T}{r_k} \alpha_{k,1}^2 + \sigma_n^2, \dots, \frac{P_T}{r_k} \alpha_{k,r_k}^2 + \sigma_n^2 \right\}}_{\mathbf{P}_k} \underbrace{\begin{bmatrix} \Phi_{k,1}^*, \dots, \Phi_{k,r_k}^* \end{bmatrix}^T}_{\mathbf{w}_k^*} \\ &= \mathbf{w}_k^T \mathbf{P}_k \mathbf{w}_k^* \end{aligned} \quad (4.85)$$

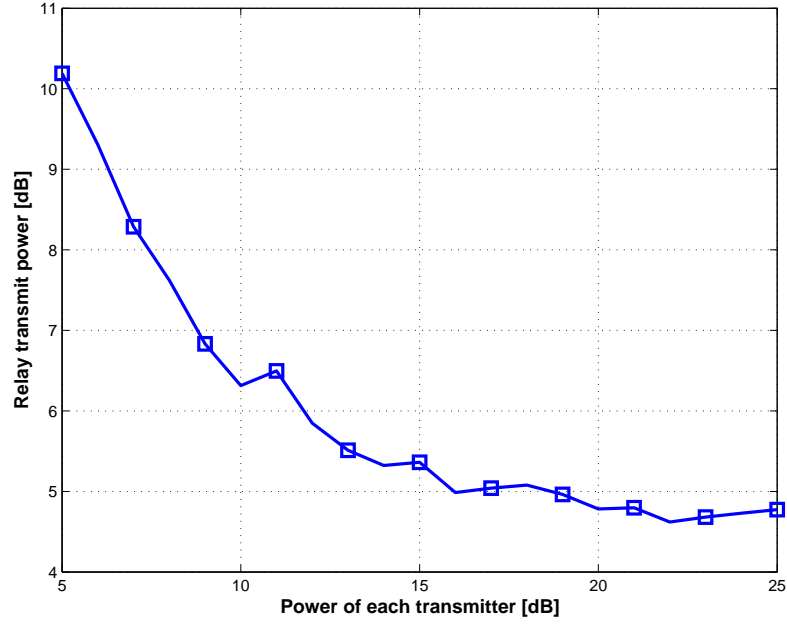


Figure 4.14.: P_R versus SNR with target SINR = 0 dB, $K = 2$, $r_k = 2$, $M_R = 8$

Our problem turns out to find a solution \mathbf{w} to the problem formulated as

$$\begin{aligned}
 \min_{\mathbf{w}_k} \quad & \mathbf{w}_k^T \mathbf{P}_k \mathbf{w}_k^* \\
 \text{s.t.} \quad & \frac{\frac{P_T}{r_k} \alpha_{k,m}^2 \beta_{k,m}^2 \mathbf{w}_k^H \mathbf{S}_{k,m} \mathbf{w}_k}{\sigma_n^2 \mathbf{w}_k^H \mathbf{R}_{k,m} \mathbf{w}_k + \sigma_n^2} \geq \gamma_{k,m}, m = 1, 2, \dots, r_k.
 \end{aligned} \tag{4.86}$$

By defining $\mathbf{W}_k = \mathbf{w}_k \mathbf{w}_k^H$, we rewrite (4.86) as

$$\begin{aligned}
 \min_{\mathbf{W}_k} \quad & \text{tr}(\mathbf{P}_k \mathbf{W}_k^T) \\
 \text{s.t.} \quad & \text{tr}\left(\left(\frac{P_T}{r_k} \alpha_{k,m}^2 \beta_{k,m}^2 \mathbf{S}_{k,m} - \gamma_{k,m} \sigma_n^2 \mathbf{R}_{k,m}\right) \mathbf{W}_k\right) \geq \gamma_{k,m} \sigma_n^2, m = 1, 2, \dots, r_k \\
 & \text{rank}(\mathbf{W}_k) = 1.
 \end{aligned} \tag{4.87}$$

Without considering the constraint $\text{rank}(\mathbf{W}_k) = 1$, \mathbf{W}_k can be computed effectively by semi-definite relaxation (SDR) using the convex optimization toolbox cvx [BV04, GBY09]. To retrieve \mathbf{w}_k from \mathbf{W}_k , the rank-1 decomposition is performed using the theorem [AHZ11]. In our case, if the number of data streams per user is less or equal than 4, an optimum \mathbf{w} can be reconstructed from \mathbf{W}_k .

After obtaining \mathbf{w} from the rank-1 decomposition, we design Φ_k by putting the elements of \mathbf{w} on the main diagonal, written as $\Phi_k = \text{diag}(\mathbf{w})$. The matrix $\mathbf{F}_{S,k}$ is obtained as $\mathbf{F}_{S,k} = \mathbf{V}_{G_k} \Phi_k \mathbf{U}_{H_k}^H$ and $\mathbf{F}_S = \text{diag}\{\mathbf{F}_{S,1}, \dots, \mathbf{F}_{S,K}\}$. The relay amplification matrix is finally obtained as $\mathbf{F}_R = \mathbf{F}_{BC} \mathbf{F}_S \mathbf{F}_{MAC}$, where \mathbf{F}_{MAC} and \mathbf{F}_{BC} are defined in (4.66) and (4.68).

Simulation results

A two operator system with a shared AF relay is considered for multiple stream transmission.

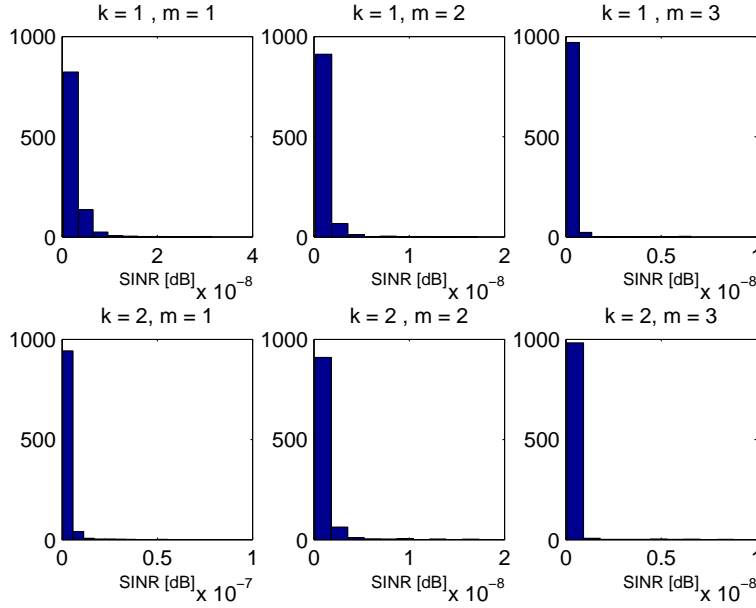


Figure 4.15.: histogram of SINR at $P_T = 25$ dB with target SINR = 0 dB, $K = 2$, $M_{T,k} = 3$, $M_{U,k} = 3$, $M_R = 8$, $r_k = 3$

Fig. 4.14 depicts the average total relay transmit power $P_R = \mathbb{E}\left\{\|\mathbf{F}_R \mathbf{H} \bar{\mathbf{s}} + \mathbf{F}_R \mathbf{n}_R\|^2\right\}$ and the sum of the relay transmit power from each operator $\sum_k P_{R,k}$ versus the transmit power P_T for a two operator AF relay sharing system. Each BS and UT are equipped with 3 antennas and the relay has $M_R = 8$ antennas. Unit noise variance is assumed at a single antenna of the relay and the UTs. The results are based on 1000 channel realizations. It can be seen that the total relay transmit power P_R decreases as P_T increases. Furthermore, the histogram of the SINR for each data stream per user is plotted in Fig. 4.15 at SNR = 25 dB. Here 3 data streams are transmitted for each user. It is seen that the $\text{SINR}_{k,m}$, $k = 1, 2$, $m = 1, 2, 3$, is always above the target threshold $\gamma_{k,m} = 0$ dB, which verifies that the SINR requirements are always satisfied.

To summarize, an effective algorithm is proposed in this section to achieve power efficiency for multiple stream transmission in multiple operator AF relay sharing system. The BSs, the UTs and the relay are equipped with multiple antennas. The inter-operator interference is first removed by using zero-forcing method. Following that, the structure of the relay precoder is exploited using the convex optimization tool. Simulation results show that the SINR requirement per stream can be always satisfied. As a continuous work, it would be interesting to investigate the relay amplification matrix design under imperfect channel state information at the relay.

5. Multiple Operator One-Way Relaying with Direct Link

In Chapter 4, the direct links between the BSs and the UTs are neglected because we assume that the signals are weak due to large path loss or shadowing. In this chapter, we deal with the scenario where the direct link is not negligible, where the relay is used to assist the pairwise concurrent point to point transmission. This scenario is called interference relay channel (IRC) as firstly defined in [SE07], which is another fundamental building block including both spectrum and infrastructure sharing. Some pioneering works have studied the impact of a full duplex decode and forward (DF) relay with a single antenna in such a scheme. In [SES09], the impact of relaying in a two-user Gaussian interference channel is studied. Various models for relay reception and transmission are considered. The relay can receive and transmit in the same band as the BSs (in-band relay reception and transmission), or both reception and transmission take place over orthogonal links (out-of-band relay reception and transmission). Further, [SSE09] presents a general achievable rate region and discusses a number of regimes of interest where either signal relaying only or both signal relaying and interference forwarding are optimal. In addition, [TY09] provides an outer bound for the Gaussian interference relay channel with finite relay power.

In contrast to this, we consider the linear precoding design for the amplify and forward (AF) relaying strategy in Chapter 5, assuming multiple antennas employed at all BSs, UTs, and the AF relay. Two cases are studied. We first investigate single stream transmission to achieve a good signal to noise ratio (SNR) at the UTs [LRH11b, LZR⁺11]. Following that a more general multiple stream transmission is considered and an improved spatial multiplexing gain is expected. [LSH11]. In both cases, the SAPHYRE sharing gain is exploited as defined in equation (2.1), showing the advantage of spectrum and relay sharing in comparison with the exclusive access of the resources.

The structure of this chapter is arranged as follows. The precoding design for single stream transmission in the IRC system is discussed in Section 5.1. To do that, we first investigate the efficient design of relay amplification matrices in Section 5.1.1. Following that, we design the precoding at the BSs in Section 5.1.2. After that, Section 5.2 extends the work to multiple stream transmission for the more general case, where a two-step algorithm is proposed. To this end, Section 5.2.1 addresses the relay matrix design while precoding at BSs is discussed in Section 5.2.2.

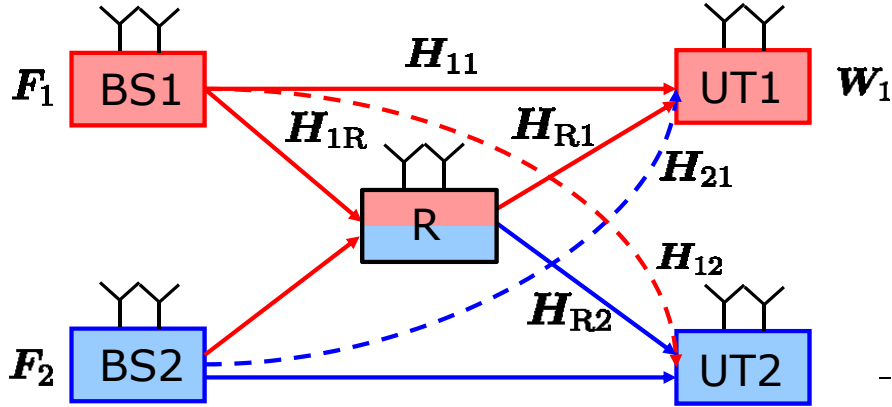


Figure 5.1.: Block Diagram of the Interference Relay Channel where the relay R (infrastructure) and spectrum are shared between two operators

5.1. System Sum Rate Maximization for Single Stream Transmission

In this section, single stream transmission for the interference relay channel (IRC) system is studied. It is shown that the IRC can be simplified to the interference channel (IC) as long as the relay precoder is fixed. First, we summarize several relaying algorithms which are adapted to the IRC. After that precoders designed for the IC can be applied at the transceivers. Inspired by the idea from [SRH10], we propose a linear suboptimal precoding method. The recent work [CHHT12] is taken as a benchmark, where a linear coordinated beamformer was designed under zero interference constraints. Simulations demonstrate that our proposed algorithm IRC flexible coordinated beamforming (IRC FlexCoBF) achieves a better sum rate performance. Furthermore, the robustness to the near-far problem is investigated for the IRC FlexCoBF as well as previous methods. Finally, we exploit the SAPHYRE sharing gain, showing the advantage of spectrum and relay sharing between multiple operators in comparison with the exclusive access of the spectrum and the infrastructure (relay) by each operator. This section is organized as follows. The system model of the IRC is first introduced. We first investigate the efficient design of the relay amplification matrices. As soon as the relay amplification matrix is determined, the IRC is converted into the IC and the precoder design at the BS is explained. All the simulation results will be presented and finally we give a summary on this section. The main contributions of this section have been published in references [LRH11b, LZR⁺11].

The system model is shown in Fig. 5.1, where two base stations (BSs) belonging to two operators transmit data to their target user terminals (UTs) with the assistance of a shared relay. Throughout this chapter, a half-duplex and amplify-and-forward (AF) relay is utilized. The BSs and UTs are equipped with $M_{T,i}$ and $M_{U,i}$ antennas, respectively, where $i = 1, 2$ denotes the index of each transceiver pair. The relay has M_R antennas. We assume that a

single data stream per UT is transmitted.

The transmission process is divided into two phases. During the first phase, both BSs transmit to their desired UTs and the relay. The received signal at each UT and the relay is

$$\begin{aligned} \mathbf{y}_1^{(1)} &= \mathbf{H}_{11}\mathbf{f}_1s_1 + \mathbf{H}_{21}\mathbf{f}_2s_2 + \mathbf{n}_1^{(1)}, \\ \mathbf{y}_2^{(1)} &= \mathbf{H}_{22}\mathbf{f}_2s_2 + \mathbf{H}_{12}\mathbf{f}_1s_1 + \mathbf{n}_2^{(1)}, \\ \mathbf{y}_R &= \mathbf{H}_{1R}\mathbf{f}_1s_1 + \mathbf{H}_{2R}\mathbf{f}_2s_2 + \mathbf{n}_R, \end{aligned}$$

where $\mathbf{H}_{ij} \in \mathbb{C}^{M_{U,j} \times M_{T,i}}$, $i, j \in \{1, 2, R\}$ denotes the channel matrices between BSs, UTs, and relay, which are assumed to undergo frequency flat quasi static block fading. The precoder at each BS is $\mathbf{f}_i \in \mathbb{C}^{M_{T,i}}$ and the transmitted data signal is s_i . The transmit power at each BS is constrained by $P_{T,i}$, i.e., $\mathbb{E}\{\|\mathbf{f}_i s_i\|^2\} \leq P_{T,i}$. In the second phase, the BSs are silent and the relay amplifies the received signal from phase 1 and forwards it to the UTs. The signal vectors received at the UTs during phase 2 are given by

$$\begin{aligned} \mathbf{y}_1^{(2)} &= \mathbf{H}_{R1}\mathbf{F}_R\mathbf{y}_R + \mathbf{n}_1^{(2)}, \\ &= \mathbf{H}_{R1}\mathbf{F}_R\mathbf{H}_{1R}\mathbf{f}_1s_1 + \mathbf{H}_{R1}\mathbf{F}_R\mathbf{H}_{2R}\mathbf{f}_2s_2 \\ &\quad + \mathbf{H}_{R1}\mathbf{F}_R\mathbf{n}_R + \mathbf{n}_1^{(2)} \\ \mathbf{y}_2^{(2)} &= \mathbf{H}_{R2}\mathbf{F}_R\mathbf{y}_R + \mathbf{n}_2^{(2)}, \\ &= \mathbf{H}_{R2}\mathbf{F}_R\mathbf{H}_{2R}\mathbf{f}_2s_2 + \mathbf{H}_{R2}\mathbf{F}_R\mathbf{H}_{1R}\mathbf{f}_1s_1 \\ &\quad + \mathbf{H}_{R2}\mathbf{F}_R\mathbf{n}_R + \mathbf{n}_2^{(2)} \end{aligned}$$

where $\mathbf{F}_R \in \mathbb{C}^{M_R \times M_R}$ is the relay amplification matrix. Applying the linear receive filters $\mathbf{w}_1 \in \mathbb{C}^{2M_{U,1}}$ and $\mathbf{w}_2 \in \mathbb{C}^{2M_{U,2}}$ at each UT, we finally get the received signals expressed as follows,

$$\begin{aligned} y_1 &= \mathbf{w}_1^H \begin{bmatrix} \mathbf{y}_1^{(1)} \\ \mathbf{y}_1^{(2)} \end{bmatrix} \\ &= \mathbf{w}_1^H \underbrace{\begin{bmatrix} \mathbf{H}_{11} \\ \mathbf{H}_{R1}\mathbf{F}_R\mathbf{H}_{1R} \end{bmatrix}}_{\mathbf{H}_1} \mathbf{f}_1s_1 + \mathbf{w}_1^H \underbrace{\begin{bmatrix} \mathbf{H}_{21} \\ \mathbf{H}_{R1}\mathbf{F}_R\mathbf{H}_{2R} \end{bmatrix}}_{\mathbf{G}_1} \mathbf{f}_2s_2 + \mathbf{w}_1^H \underbrace{\begin{bmatrix} \mathbf{n}_1^{(1)} \\ \mathbf{H}_{R1}\mathbf{F}_R\mathbf{n}_R + \mathbf{n}_1^{(2)} \end{bmatrix}}_{\mathbf{e}_1} \end{aligned} \quad (5.1)$$

$$\begin{aligned} y_2 &= \mathbf{w}_2^H \begin{bmatrix} \mathbf{y}_2^{(1)} \\ \mathbf{y}_2^{(2)} \end{bmatrix} \\ &= \mathbf{w}_2^H \underbrace{\begin{bmatrix} \mathbf{H}_{22} \\ \mathbf{H}_{R2}\mathbf{F}_R\mathbf{H}_{2R} \end{bmatrix}}_{\mathbf{H}_2} \mathbf{f}_2s_2 + \mathbf{w}_2^H \underbrace{\begin{bmatrix} \mathbf{H}_{12} \\ \mathbf{H}_{R2}\mathbf{F}_R\mathbf{H}_{1R} \end{bmatrix}}_{\mathbf{G}_2} \mathbf{f}_1s_1 + \mathbf{w}_2^H \underbrace{\begin{bmatrix} \mathbf{n}_2^{(1)} \\ \mathbf{H}_{R2}\mathbf{F}_R\mathbf{n}_R + \mathbf{n}_2^{(2)} \end{bmatrix}}_{\mathbf{e}_2}, \end{aligned} \quad (5.2)$$

where $\mathbf{n}_1^{(i)}$, $\mathbf{n}_2^{(i)}$ and \mathbf{n}_R contain independent, identically distributed additive white Gaussian noise samples with the variance σ_n^2 . It can be seen that the system model can be simplified to

a classical two-user IC based on the equivalent channels $\mathbf{H}_1, \mathbf{H}_2, \mathbf{G}_1$, and \mathbf{G}_2 , which requires the relay precoder \mathbf{F}_R to be designed first.

5.1.1. Relay Amplification Matrix Design

In the section, we propose a relay amplification matrix design so that the IRC is converted to an IC. To start, we derive a relay amplification matrix which is inspired by the algebraic norm maximization method (ANOMAX) [RH09]. Since \mathbf{H}_1 and \mathbf{H}_2 are the equivalent channels for the desired signals, maximizing the norm $\beta^2 \|\mathbf{H}_1\|_F^2 + (1 - \beta)^2 \|\mathbf{H}_2\|_F^2$ enhances the desired signal's energy and therefore improves the SNR, where β is the weighting factor ranging between 0 and 1. With $\mathbf{F}_{R,n}$ denoting the normalized relay amplification matrix, the solution of the one-way ANOMAX (OW-ANOMAX) is given by

$$\begin{aligned}
& \arg \max_{\mathbf{F}_{R,n}, \|\mathbf{F}_{R,n}\|_F=1} \beta^2 \|\mathbf{H}_1\|_F^2 + (1 - \beta)^2 \|\mathbf{H}_2\|_F^2 \\
&= \arg \max_{\mathbf{F}_{R,n}, \|\mathbf{F}_{R,n}\|_F=1} \beta^2 \|\mathbf{H}_{R1} \mathbf{F}_{R,n} \mathbf{H}_{1R}\|_F^2 + (1 - \beta)^2 \|\mathbf{H}_{R2} \mathbf{F}_{R,n} \mathbf{H}_{2R}\|_F^2 \\
&= \arg \max_{\mathbf{F}_{R,n}, \|\mathbf{F}_{R,n}\|_F=1} \left\| \begin{bmatrix} \beta(\mathbf{H}_{1R}^T \otimes \mathbf{H}_{R1}) \\ (1 - \beta)(\mathbf{H}_{2R}^T \otimes \mathbf{H}_{R2}) \end{bmatrix} \text{vec}\{\mathbf{F}_{R,n}\} \right\|_2^2 \\
&= \arg \max_{\mathbf{F}_{R,n}, \|\mathbf{F}_{R,n}\|_F=1} \left\| \underbrace{\left[\beta(\mathbf{H}_{1R} \otimes \mathbf{H}_{R1}^T), (1 - \beta)(\mathbf{H}_{2R} \otimes \mathbf{H}_{R2}^T) \right]}_{\mathbf{K}_\beta} \underbrace{\text{vec}\{\mathbf{F}_{R,n}\}}_{\mathbf{f}_R} \right\|_2^2 \\
&= \arg \max_{\mathbf{f}_R, \|\mathbf{f}_R\|_2=1} \frac{\mathbf{f}_R^H \mathbf{K}_\beta^* \mathbf{K}_\beta^T \mathbf{f}_R}{\mathbf{f}_R^H \mathbf{f}_R} \\
&= \lambda_{\max}(\mathbf{K}_\beta^* \mathbf{K}_\beta^T)
\end{aligned}$$

Here, the Kronecker product between two matrices \mathbf{A} and \mathbf{B} is symbolized by $\mathbf{A} \otimes \mathbf{B}$ and we use the property of $\mathbf{A}\mathbf{X}\mathbf{B} = (\mathbf{B}^T \otimes \mathbf{A})\text{vec}(\mathbf{X})$. The matrix \mathbf{K}_β is defined as $\mathbf{K}_\beta = \begin{bmatrix} \beta(\mathbf{H}_{1R} \otimes \mathbf{H}_{R1}^T), & (1 - \beta)(\mathbf{H}_{2R} \otimes \mathbf{H}_{R2}^T) \end{bmatrix}$. By performing a singular value decomposition (SVD) $\mathbf{K}_\beta = \mathbf{U}_\beta \cdot \boldsymbol{\Sigma}_\beta \cdot \mathbf{V}_\beta^H$, the vectorized relay amplification matrix is designed as $\mathbf{f}_R = \text{vec}\{\mathbf{F}_{R,n}\} = \mathbf{u}_1^*$, where \mathbf{u}_1 is the first column of \mathbf{U}_β , i.e., the dominant left singular vector of \mathbf{K}_β . The normalized relay amplification matrix is obtained as $\mathbf{F}_{R,n} = \text{unvec}\{\mathbf{f}_R\} \in \mathbb{C}^{M_R \times M_R}$ and we compute \mathbf{F}_R as $\mathbf{F}_R = \gamma \mathbf{F}_{R,n}$, where γ is a scalar to fulfill the transmit power constraint at the relay. Inspired by the well-known two-way relaying strategies, we also modify some alternatives to adapt to the one-way relaying scheme. These strategies are shown as follows.

- Dual Channel Matching (DCM) [VH11]

$$\tilde{\mathbf{F}}_R = \mathbf{H}_{R1}^H \mathbf{H}_{1R}^H + \mathbf{H}_{R2}^H \mathbf{H}_{2R}^H$$

- Discrete Fourier Transform (DFT) matrix

$$\tilde{\mathbf{F}}_R = \text{DFT}(\mathbf{I}_{M_R})$$

- MMSE [UK08]

$$\begin{aligned}\tilde{\mathbf{F}}_{\text{R}} &= \mathbf{F}_{\text{R},\text{Tx}}\mathbf{F}_{\text{R},\text{Rx}} \\ \mathbf{F}_{\text{R},\text{Rx}} &= \mathbf{H}_{\text{Rx}}^{\text{H}}\left(\mathbf{H}_{\text{Rx}}\mathbf{H}_{\text{Rx}}^{\text{H}} + \frac{\sigma_n^2}{P_{\text{T1}}+P_{\text{T2}}}\mathbf{I}_{M_{\text{R}}}\right)^{-1} \\ \mathbf{F}_{\text{R},\text{Tx}} &= \left(\mathbf{H}_{\text{Tx}}^{\text{H}}\mathbf{H}_{\text{Tx}} + \frac{\sigma_n^2}{P_{\text{T1}}+P_{\text{T2}}}\mathbf{I}_{M_{\text{R}}}\right)^{-1}\mathbf{H}_{\text{Tx}}^{\text{H}} \\ \text{where } \mathbf{H}_{\text{Tx}} &= \begin{bmatrix} \mathbf{H}_{\text{R1}} \\ \mathbf{H}_{\text{R2}} \end{bmatrix} \text{ and } \mathbf{H}_{\text{Rx}} = \begin{bmatrix} \mathbf{H}_{\text{1R}} & \mathbf{H}_{\text{2R}} \end{bmatrix}.\end{aligned}$$

- ZF [UK08]

$$\tilde{\mathbf{F}}_{\text{R}} = \mathbf{H}_{\text{Rx}}^+ \mathbf{H}_{\text{Tx}}^+$$

The superscript + represent the pseudo inverse. The same \mathbf{H}_{Rx} and \mathbf{H}_{Tx} are used as for MMSE.

We compute \mathbf{F}_{R} as $\mathbf{F}_{\text{R}} = \gamma \mathbf{F}_{\text{R},n}$, where $\mathbf{F}_{\text{R},n}$ is the normalized relay amplification matrix of $\tilde{\mathbf{F}}_{\text{R}}$ obtained by one of the aforementioned methods such that $\|\mathbf{F}_{\text{R},n}\| = 1$. For all the designs of the relay amplification matrix mentioned above, the scalar γ guarantees that the relay transmit power constraint remains satisfied. Let $P_{\text{T,R}}$ be the available transmit power at the relay. A simple method is upper-bounding the relay transmit power and then constraining this upper bound to $P_{\text{T,R}}$. Using the Cauchy-Schwarz inequality on the relay transmit signal $\gamma \mathbf{F}_{\text{R},n} \mathbf{y}_{\text{R}}$, we obtain that

$$\|\gamma \mathbf{F}_{\text{R},n} \mathbf{y}_{\text{R}}\|_2^2 = \gamma^2 \|\mathbf{y}_{\text{R}}\|_2^2 \leq \gamma^2 (M_{\text{T},1} M_{\text{R}} P_{\text{T},1} + M_{\text{T},2} M_{\text{R}} P_{\text{T},2} + M_{\text{R}} \sigma_n^2) = P_{\text{T,R}}.$$

Here, we have applied the fact that each entry of the channel matrices \mathbf{H}_{1R} and \mathbf{H}_{2R} is Gaussian distributed with unit variance and that each entry of the noise vector \mathbf{n}_{R} is Gaussian distributed with variance σ_n^2 . The transmit signals are assumed to be uncorrelated with each other and with the noise at the relay. The transmit power at each BS is constrained by $P_{\text{T},i}$, i.e., $\mathbb{E}\{\|\mathbf{f}_i s_i\|^2\} \leq P_{\text{T},i}$. Then we choose γ as

$$\gamma = \sqrt{\frac{P_{\text{T,R}}}{M_{\text{T},1} M_{\text{R}} P_{\text{T},1} + M_{\text{T},2} M_{\text{R}} P_{\text{T},2} + M_{\text{R}} \sigma_n^2}}$$

In general, the actual consumed power at the relay is less than $P_{\text{T,R}}$. However, the advantage is that it is very easy to compute γ as it does not depend on the UTs' transmit covariance matrices nor on the strategy of the relay. We therefore use it in the following analysis.

5.1.2. Precoder Design at the BSs

After the design of \mathbf{F}_{R} , all the equivalent channel matrices \mathbf{H}_i and the interference matrices \mathbf{G}_i can be estimated from the downlink dedicated pilot transmission. Then the IRC corresponds to a conventional IC model. We assume that \mathbf{H}_i and \mathbf{G}_i are available at the BSs. At this point, no path loss is considered.

Since the system is now converted to the IC model, the efficient precoding introduced in Section 3.3 can be applied in the IRC system, i.e., either BD or RBD is used at the BSs

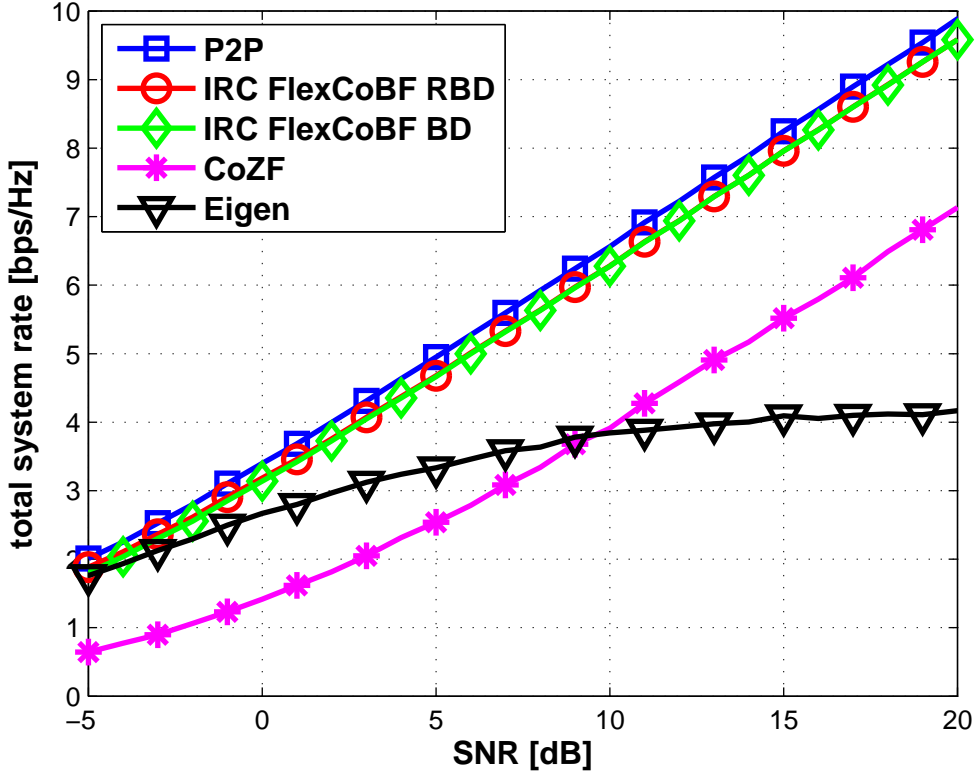


Figure 5.2.: Sum rate vs SNR for the interference relay channel, the DFT matrix is applied at the relay, $M_{T,i} = M_{U,i} = M_R = 4$

combined with MRC at the UTs and the precoding matrices IRC FlexCoBF is designed iteratively until the power of the residual interference is below a predefined threshold. The only difference compared to the method in Section 3.3 is that no power loading is necessary in designing the precoding vector because a single stream transmission is considered here. The algorithm is summarized in Table 5.1.

Simulation results

We assume that perfect link adaptation and perfect synchronization can be achieved. Each element of the \mathbf{H}_{ij} is a zero mean circularly symmetric complex Gaussian random variable with unit variance $\mathcal{CN}(0,1)$. The BSs, the UTs, and the relay are equipped with 4 antennas. The transmit power of the BSs is $P_{T1} = P_{T2} = P_T$ and the SNR is defined as P_T/σ_n^2 .

At first, we want to compare different precoding strategies applied at the BSs by fixing the relay precoder. Without loss of generality, we choose a simple DFT matrix at the relay. The sum rate performance of the IRC system is given in Fig. 5.2, including our proposed IRC FlexCoBF as well as the recent work coordinated zero-forcing (CoZF) [CHHT12]. As a reference, we also include an upper bound called point-to-point (P2P) transmission, which is an ideal case without taking into account the interference between the two concurrent transmission. It uses also the DFT matrix at the relay and applies eigen-beamforming at

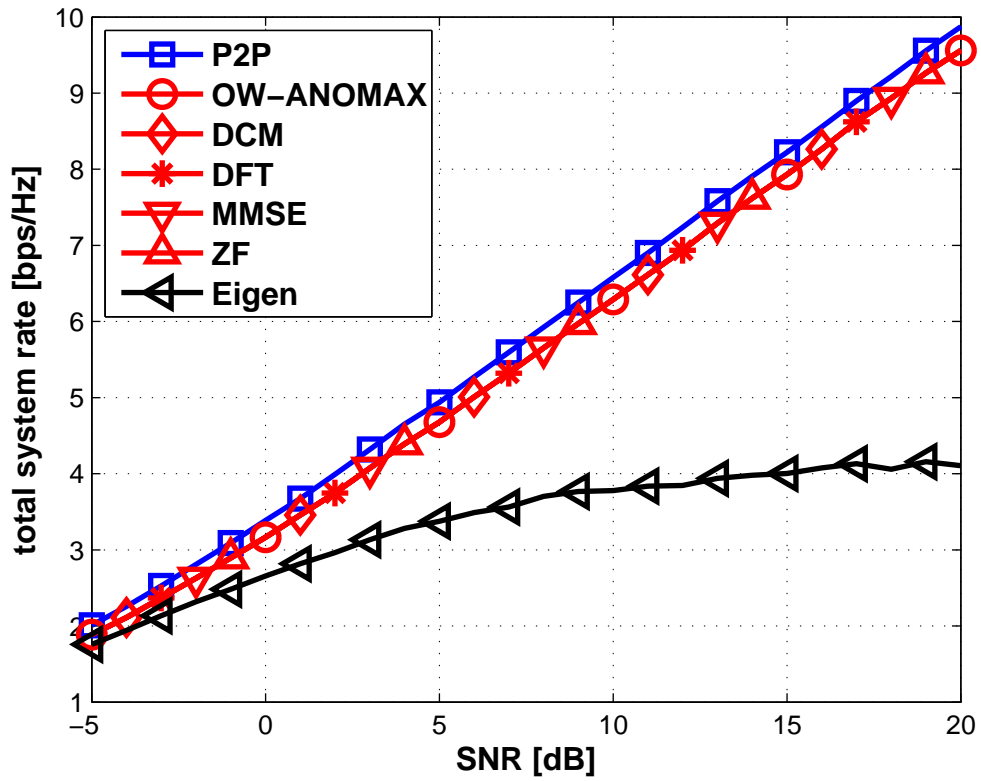


Figure 5.3.: Sum rate of the interference relay channel for different relaying strategies, IRC FlexCoBF RBD is applied at BSs, $M_{T,i} = M_{U,i} = M_R = 4$

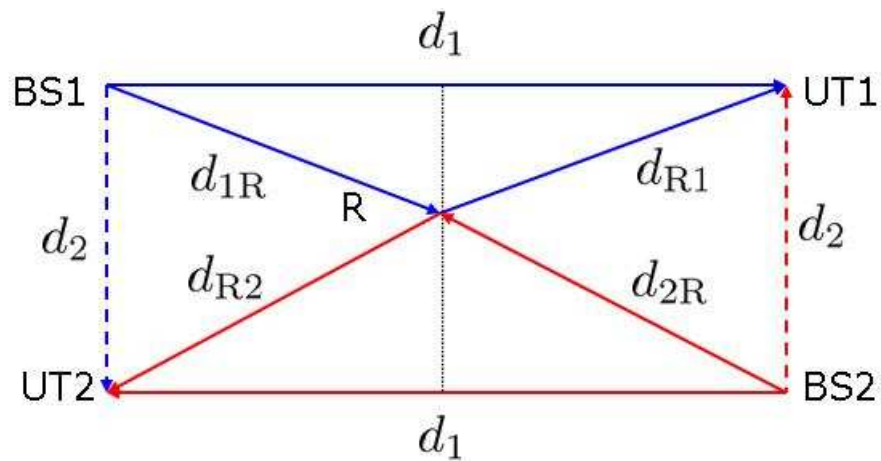


Figure 5.4.: Path loss model of the interference relay channel, d_1 denotes the distance between the BSs and their desired UTs and d_2 is the distance between the two interfering links

Table 5.1.: Precoding design at the BSs for IRC FlexCoBF [LRH11b]

<p>the receive beamformers $\mathbf{w}_1, \mathbf{w}_2$ are initialized as all-ones vectors</p> <p>- BD</p> <p>Step 1: compute the SVD of the equivalent interference channel of operator j caused by operator i</p> $\tilde{\mathbf{g}}_j^T = \mathbf{w}_j^H \mathbf{G}_j = \mathbf{1} \cdot \tilde{\boldsymbol{\sigma}}_j^T \cdot \begin{bmatrix} \tilde{\mathbf{v}}_j^{(1)}, & \tilde{\mathbf{V}}_j^{(0)} \end{bmatrix}^H,$ $\tilde{\mathbf{v}}_j^{(1)} \in \mathbb{C}^{M_T}: \text{signal space of } \tilde{\mathbf{g}}_j^T$ $\tilde{\mathbf{V}}_j^{(0)} \in \mathbb{C}^{M_T \times (M_T - 1)}: \text{null space of } \tilde{\mathbf{g}}_j^T$ <p>Step 2: compute the SVD on the equivalent channel for operator i to maximize its sum rate</p> $\mathbf{w}_i^H \mathbf{H}_i \tilde{\mathbf{V}}_j^{(0)} = \mathbf{1} \cdot \tilde{\boldsymbol{\sigma}}_i^T \cdot \tilde{\mathbf{V}}_i^H$ $\mathbf{f}_i = \tilde{\mathbf{V}}_j^{(0)} \tilde{\mathbf{v}}_i,$ $\tilde{\mathbf{v}}_i: \text{dominant singular vector of } \tilde{\mathbf{V}}_i$ <p>Step 3: the receiver beamformer is updated as $\mathbf{w}_i = \mathbf{H}_i \mathbf{f}_i$ and go back to Step 1</p> <p>- RBD</p> <p>Step 1: compute the SVD of the equivalent interference channel of operator j caused by operator i</p> $\tilde{\mathbf{g}}_j^T = \mathbf{w}_j^H \mathbf{G}_j = \mathbf{1} \cdot \tilde{\boldsymbol{\sigma}}_j^T \cdot \tilde{\mathbf{V}}_j^H,$ $\mathbf{F}_{i,a} = \mathbf{M}_{i,a} \mathbf{D}_{i,a}$ $\mathbf{M}_{i,a} = \tilde{\mathbf{V}}_j$ $\mathbf{D}_{i,a} = (\tilde{\boldsymbol{\sigma}}_j \tilde{\boldsymbol{\sigma}}_j^T + \frac{M_{U,j} \sigma_n^2}{P_{T,i}} \mathbf{I}_{M_{T,i}})^{-1/2}$ <p>Step 2: compute the SVD on the equivalent channel for operator i to maximize its sum rate</p> $\mathbf{w}_i^H \mathbf{H}_i \mathbf{F}_{i,a} = \mathbf{1} \cdot \tilde{\boldsymbol{\sigma}}_i^T \cdot \tilde{\mathbf{V}}_i^H$ $\mathbf{f}_{i,b} = \tilde{\mathbf{v}}_i$ $\tilde{\mathbf{v}}_i: \text{dominant singular vector of } \tilde{\mathbf{V}}_i$ $\mathbf{f}_i = \alpha \mathbf{F}_{i,a} \mathbf{f}_{i,b}$ $\alpha: \text{scalar to fulfill transmit power constraint, } \alpha = P_{T,i} / \text{tr}\{\mathbf{F}_{i,a} \mathbf{F}_{i,a}^H\}$ <p>Step 3: the receiver beamformer is updated as $\mathbf{w}_i = \mathbf{H}_i \mathbf{f}_i$ and go back to Step 1</p> <p>The iterative procedure for BD or RBD continues until the power of the residual interference is below a predefined threshold</p>
--

the BSs to maximize the system sum rate. Another reference scheme named Eigen is also used as a benchmark. Differently to P2P, the interference is treated as noise. It is observed that IRC FlexCoBF with either RBD or BD performs much better than CoZF within all SNR ranges. Especially at low SNRs, CoZF performs even worse than Eigen. IRC FlexCoBF RBD improves the sum rate compared to BD because it allows some residual interferences to balance with the noise enhancement.

By selecting the best precoder at the BSs using IRC FlexCoBF RBD, different relaying strategies are compared, as shown in Fig. 5.3. We observe that all the proposed AF relay precoders almost give the same sum rate, of which OW-ANOMAX with $\beta = 0.5$ performs slightly better than others. With respect to the complexity consideration, we propose to use the DFT as the relay amplification matrix and use it in the following simulations.

Furthermore, a path loss model is introduced to test the robustness to the interference of the proposed method compared to the CoZF in [CHHT12]. As shown in Fig. 5.4, the distance between the BSs and the UTs is d_1 and the distance between these two interfering links is d_2 . The relay is assumed to be in the center of the two interfering links, which means that

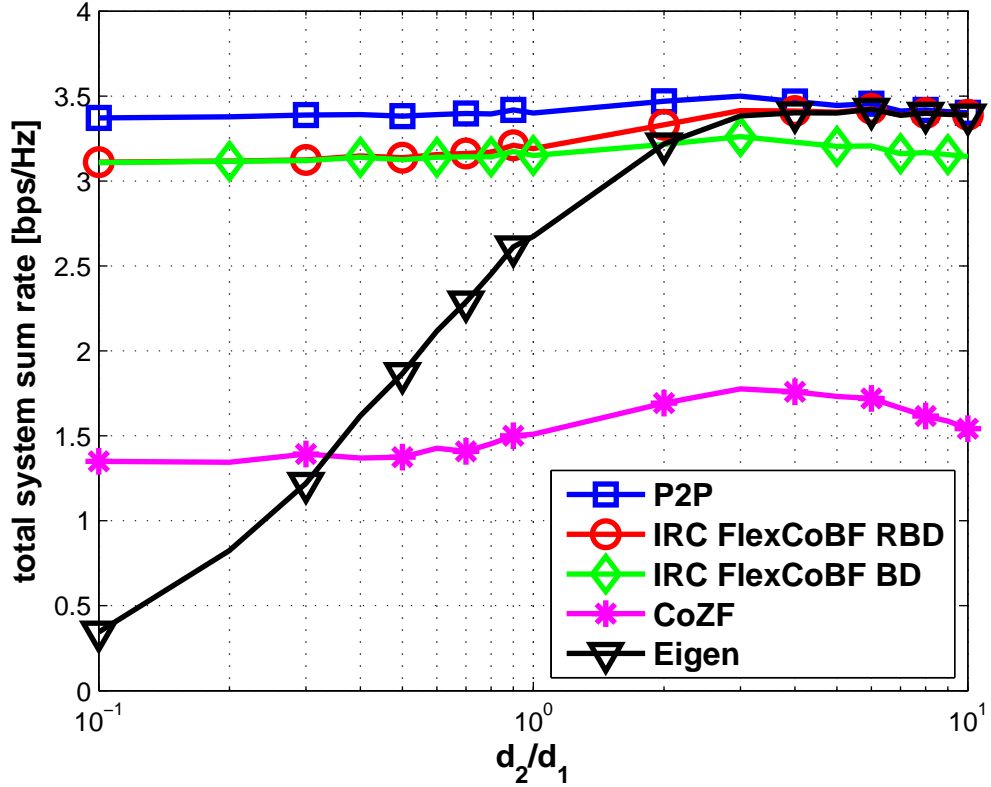


Figure 5.5.: Sum rate for interference relay channel path loss model at SNR = 0 dB, the DFT matrix is applied at the relay, $M_{T,i} = M_{U,i} = M_R = 4$

$d_{1R} = d_{R1} = \frac{\sqrt{d_1^2 + d_2^2}}{2}$ and $d_{2R} = d_{R2} = \frac{\sqrt{d_1^2 + d_2^2}}{2}$. The channel is constructed by scaling the channel matrix by $d^{-\frac{\alpha}{2}}$, i.e., $\mathbf{H}_{ij,PL} = \mathbf{H}_{ij} \cdot d^{-\frac{\alpha}{2}}$, where $\alpha = 2$ is the path loss exponent.

Fig. 5.5 and Fig. 5.6 depict the sum rate depending on the ratio of d_2/d_1 for the path loss model of the IRC for SNR = 0 dB and SNR = 20 dB, respectively. The DFT matrix is used at the relay. When d_2/d_1 is small, it means that strong interferences exist between the two transceiver pairs. On the other hand, a larger d_2/d_1 results in weaker interferences. It can be seen that all types of the precoders except Eigen are resistant to the interferences. Furthermore, as d_2/d_1 increases, we have less interference, noise dominates, and IRC FlexCoBF RBD performs better than IRC FlexCoBF BD. When the interference is quite small, IRC FlexCoBF RBD converges to the P2P bound at SNR = 0 dB.

In our IRC scenario, the spectrum and the relay are shared by both users. We want to compare this case to the exclusive use of the spectrum and the relay, which is defined as the relay channel (RC). We refer to the ratio of throughput (TP) obtained by the IRC TP_{IRC} over that obtained by the RC TP_{RC} as the *sharing gain* due to the use of the shared relay instead of accessing the spectrum and the relay in a TDMA mode. This sharing gain of the IRC over the RC is shown in Fig. 5.7, where IRC FlexCoBF and eigen-beamforming are applied at the BSs for the IRC and the RC, respectively. It can be seen that the IRC utilizing either

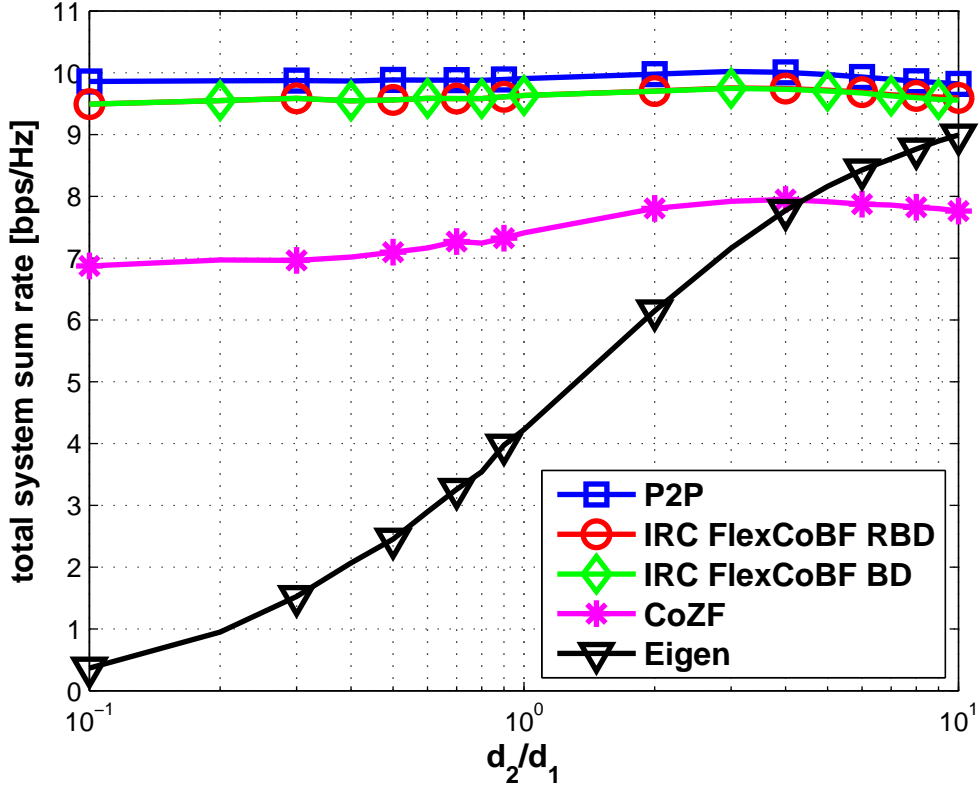


Figure 5.6.: Sum rate for interference relay channel path loss model at SNR = 20 dB, the DFT matrix is applied at the relay, $M_{T,i} = M_{U,i} = M_R = 4$

IRC FlexCoBF RBD or IRC FlexCoBF BD provides a sharing gain over the RC which uses the relay exclusively. For IRC FlexCoBF BD, the sharing gain becomes larger as the SNR increases. When IRC FlexCoBF RBD is applied, there is even an improvement at low SNRs due to the regularization of RBD. This shows that the spectrum and the relay sharing is more advantageous compared to the exclusive use of the physical resources.

To summarize, a linear precoding design for the MIMO interference relay channel is studied, where the spectrum and an AF relay with multiple antennas are shared between two operators. Various relaying strategies are investigated for this scenario. We first consider the conversion of the interference relay channel (IRC) to the interference channel (IC), where we propose to use the DFT matrix as the relay amplification matrix. After that we recommend the precoding method IRC FlexCoBF at the BSs, which achieves a better sum rate performance compared to coordinated zero-forcing (CoZF) beamforming as well as eigen-beamforming [CHHT12]. IRC FlexCoBF is also more robust to the interference. Last but not least, the sum rate performance of the IRC is compared to the relay channel and there exists a large sharing gain, which strongly supports the use of a shared spectrum and the relay instead of operating in the time division multiple access (TDMA) mode.

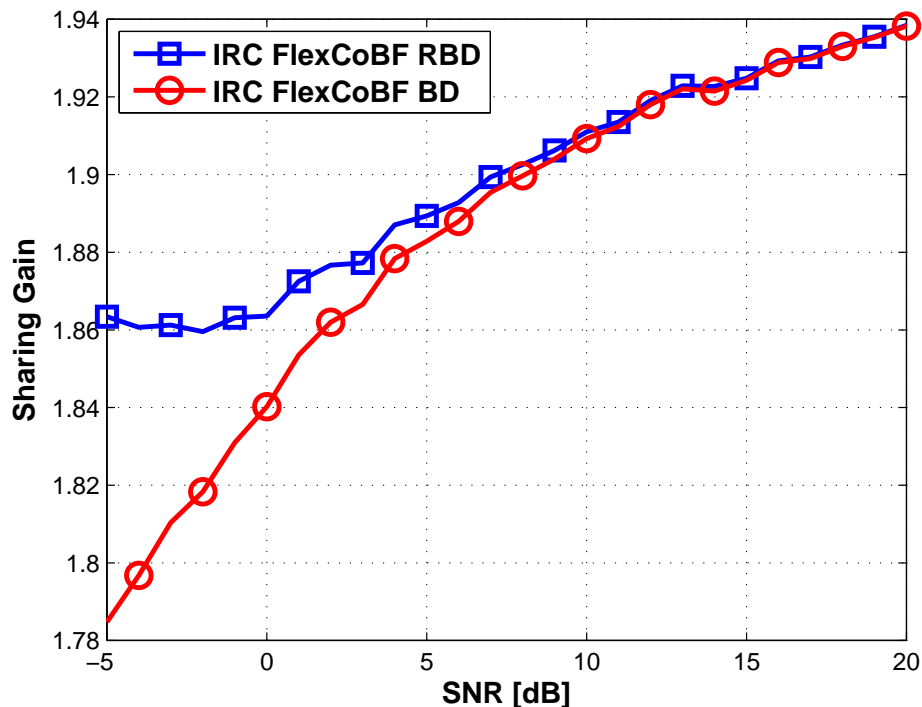


Figure 5.7.: Sharing gain of the IRC over the RC, the DFT matrix is used at the relay, IRC FlexCoBF and eigen-beamforming are used for IRC and RC, respectively

5.2. System Sum Rate Maximization for Multiple Stream Transmission

In this section, we extend our work of Section 5.1 to investigate multiple data stream transmission per user for the IRC [LSH11]. It is shown that the IRC can be simplified to the IC as long as the relaying strategy is predefined. Although many relaying strategies have been proposed for the RC [TW09], they are not straightforward to extend explicitly to our scenario. To start, we first derive a relay amplification matrix which is inspired by [RH09]. After that, precoders that facilitate multiple stream transmission in case of the IC are applied. The stream control approach of [DI03] is used for comparison. Although the system throughput using the stream control method almost coincides with that employing the optimum stream control, [DI03] designs the precoder only to strengthen the desired signal without suppressing the interferences between the two transceiver pairs. Inspired by the idea from [SRH10, SRH13], we propose the IRC-FlexCoBF to further improve the system sum rate. Furthermore, the robustness to strong interference is investigated for the IRC-FlexCoBF compared to [DI03]. Finally, we demonstrate that there is a sum rate gain by sharing the relay instead of accessing the relay exclusively.

The system model is the same as before, as shown in Fig. ??, where two base stations (BSs) transmit data to their target user terminals (UTs) separately with the assistance of a shared relay. Again a half-duplex AF relay is utilized. The BSs and UTs are equipped with $M_{T,i}$

and $M_{U,i}$ antennas, respectively, where $i = 1, 2$ denotes the transceiver pair index. The relay has M_R antennas. It is possible to transmit several data streams and the maximum of data streams for UT_i is equal to $\min(M_{T,i}, M_{U,i})$.

The transmission process is divided into two phases. During the first phase, both BSs transmit to their desired UTs and the relay. The received signal at each UT and the relay is given by

$$\begin{aligned} \mathbf{y}_1^{(1)} &= \mathbf{H}_{11}\mathbf{F}_1\mathbf{s}_1 + \mathbf{H}_{21}\mathbf{F}_2\mathbf{s}_2 + \mathbf{n}_1^{(1)} \\ \mathbf{y}_2^{(1)} &= \mathbf{H}_{22}\mathbf{F}_2\mathbf{s}_2 + \mathbf{H}_{12}\mathbf{F}_1\mathbf{s}_1 + \mathbf{n}_2^{(1)} \\ \mathbf{y}_R &= \mathbf{H}_{1R}\mathbf{F}_1\mathbf{s}_1 + \mathbf{H}_{2R}\mathbf{F}_2\mathbf{s}_2 + \mathbf{n}_R \end{aligned}$$

where $\mathbf{H}_{ij} \in \mathbb{C}^{M_{U,j} \times M_{T,i}}$, $i, j \in \{1, 2, R\}$ denotes the channel matrices between the BSs, the UTs, and the relay, which are assumed to be frequency flat and quasi static block fading. The precoder at each BS is $\mathbf{F}_i \in \mathbb{C}^{M_{T,i} \times r_i}$, $i \in \{1, 2\}$, where r_i denotes the number of data streams for each user. The data vector is $\mathbf{s}_i \in \mathbb{C}^{r_i}$. In the second phase, the relay amplifies the received signal from phase 1 and forwards it to the UTs while the BSs stay silent. The received signal vectors during the second phase are given by

$$\begin{aligned} \mathbf{y}_1^{(2)} &= \mathbf{H}_{R1}\mathbf{F}_R\mathbf{y}_R + \mathbf{n}_1^{(2)}, \\ \mathbf{y}_2^{(2)} &= \mathbf{H}_{R2}\mathbf{F}_R\mathbf{y}_R + \mathbf{n}_2^{(2)}, \end{aligned}$$

where $\mathbf{F}_R \in \mathbb{C}^{M_R \times M_R}$ is the relay amplification matrix. The total received signals at both UTs are expressed in equations (5.3) and (5.4). The vectors $\mathbf{n}_1^{(i)}$, $\mathbf{n}_2^{(i)}$ and \mathbf{n}_R contain independent, identically distributed additive white Gaussian noise samples with the variance σ_n^2 . With (5.3) and (5.4), the system is simplified to a classical two-user IC as long as the equivalent channels $\mathbf{H}_1, \mathbf{H}_2, \mathbf{G}_1$, and \mathbf{G}_2 are known, which requires the relay precoder \mathbf{F}_R to be designed first.

$$\begin{aligned} \mathbf{y}_1 &= \begin{bmatrix} \mathbf{y}_1^{(1)} \\ \mathbf{y}_1^{(2)} \end{bmatrix} \\ &= \underbrace{\begin{bmatrix} \mathbf{H}_{11} \\ \mathbf{H}_{R1}\mathbf{F}_R\mathbf{H}_{1R} \end{bmatrix}}_{\mathbf{H}_1} \mathbf{F}_1\mathbf{s}_1 + \underbrace{\begin{bmatrix} \mathbf{H}_{21} \\ \mathbf{H}_{R1}\mathbf{F}_R\mathbf{H}_{2R} \end{bmatrix}}_{\mathbf{G}_1} \mathbf{F}_2\mathbf{s}_2 + \underbrace{\begin{bmatrix} \mathbf{n}_1^{(1)} \\ \mathbf{H}_{R1}\mathbf{F}_R\mathbf{n}_R + \mathbf{n}_1^{(2)} \end{bmatrix}}_{\mathbf{e}_1} \end{aligned} \quad (5.3)$$

$$\begin{aligned} \mathbf{y}_2 &= \begin{bmatrix} \mathbf{y}_2^{(1)} \\ \mathbf{y}_2^{(2)} \end{bmatrix} \\ &= \underbrace{\begin{bmatrix} \mathbf{H}_{22} \\ \mathbf{H}_{R2}\mathbf{F}_R\mathbf{H}_{2R} \end{bmatrix}}_{\mathbf{H}_2} \mathbf{F}_2\mathbf{s}_2 + \underbrace{\begin{bmatrix} \mathbf{H}_{12} \\ \mathbf{H}_{R2}\mathbf{F}_R\mathbf{H}_{1R} \end{bmatrix}}_{\mathbf{G}_2} \mathbf{F}_1\mathbf{s}_1 + \underbrace{\begin{bmatrix} \mathbf{n}_2^{(1)} \\ \mathbf{H}_{R2}\mathbf{F}_R\mathbf{n}_R + \mathbf{n}_2^{(2)} \end{bmatrix}}_{\mathbf{e}_2} \end{aligned} \quad (5.4)$$

5.2.1. Relay Amplification Matrix Design

In this section, several relay amplification matrices are proposed and investigated to convert the IRC to the IC. To start, a simple discrete Fourier Transform (DFT) matrix is utilized as $\tilde{\mathbf{F}}_R = \text{DFT}(\mathbf{I}_{M_R})$, where no channel state information is required. We normalize $\tilde{\mathbf{F}}_R$ as $\mathbf{F}_{R,n} = \tilde{\mathbf{F}}_R / \|\tilde{\mathbf{F}}_R\|_F$ and compute the relay amplification matrix as $\mathbf{F}_R = \gamma \mathbf{F}_{R,n}$. The scalar γ is to fulfill the transmit power constraint.

Furthermore, the method named one-way rank-restored algebraic norm maximization (OW-RR-ANOMAX) is investigated. The original ANOMAX [RH09] is a low rank solution and is not good for multiple stream transmission. Therefore, the RR-ANOMAX [RH10] is designed to get a full rank solution. Here we extend the work [RH10] which is originally applied in two-way relaying to our IRC scenario. The OW-RR-ANOMAX is based on the OW-ANOMAX method as introduced in Section 5.1.1, which maximizes the weighted Frobenius norm of the equivalent channel $\beta^2 \|\mathbf{H}_1\|_F^2 + (1 - \beta)^2 \|\mathbf{H}_2\|_F^2$. The scalar β is the weighting factor ranging between 0 and 1. Then based on the normalized relay amplification matrix $\mathbf{F}_{R,\text{ANOMAX}}$ obtained from OW-ANOMAX, we adjust the singular values of $\mathbf{F}_{R,\text{ANOMAX}}$ so that the spatial multiplexing gain is fully exploited. To be more specific, the SVD of the relay amplification matrix $\mathbf{F}_{R,\text{ANOMAX}}$ obtained from OW-ANOMAX is first calculated as $\mathbf{F}_{R,\text{ANOMAX}} = \mathbf{U} \cdot \mathbf{\Sigma} \cdot \mathbf{V}^H$. Then we preserve the singular vectors \mathbf{U} and \mathbf{V} and the singular value profiles need to be adjusted using a heuristic method similar to water filling. To do that, the virtual eigenvalue profiles are formed as

$$\lambda_i = (\lambda_{1R,i} + \delta)(\lambda_{2R,i} + \delta)(\lambda_{R1,i} + \delta)(\lambda_{R2,i} + \delta),$$

where $\lambda_{1R,i}$, $\lambda_{2R,i}$, $\lambda_{R1,i}$ and $\lambda_{R2,i}$ are the singular values of the channels \mathbf{H}_{1R} , \mathbf{H}_{2R} , \mathbf{H}_{R1} and \mathbf{H}_{R2} with $i = 1, 2, \dots, r$. The scalar $\delta = 2^{-1}$ is a positive constant to assure that there exist r non-zero eigenvalues at high SNRs, where r is the number of transmitted data streams and $r = \min(M_R, M_{T,k}, M_{U,k})$. Then water filling based power allocation is implemented as $\gamma_i = \left(\mu - \frac{1}{\text{SNR} \lambda_i} \right)_+$, where the water level is given by $\mu = \frac{1}{r} \left(1 + \frac{1}{\text{SNR}} \sum_i \frac{1}{\lambda_i} \right)$ with $\text{SNR} = \frac{P_T}{\sigma_n^2}$, $(x)_+ = \max\{0, x\}$. Then the rank restored solution is given by

$$\tilde{\mathbf{F}}_{R,\text{OW-RR-ANOMAX}} = \mathbf{U} \cdot \text{diag}\{\gamma\} \cdot \mathbf{V}^H \in \mathbb{C}^{M_R \times M_R}$$

with $\gamma = \left[\sqrt{\gamma_1}, \sqrt{\gamma_1}, \dots, \sqrt{\gamma_r} \right]$. We also need a scalar γ to adjust the relay transmit power level to get

$$\mathbf{F}_{R,\text{OW-RR-ANOMAX}} = \gamma \frac{\tilde{\mathbf{F}}_{R,\text{OWRRANOMAX}}}{\|\tilde{\mathbf{F}}_{R,\text{OWRRANOMAX}}\|_F},$$

such that the relay transmit power constraint is satisfied. Similarly as in Section 5.1.1, we choose γ using a simple method by upper-bounding the relay transmit power and constraining

¹ δ should be large enough to ensure that there exist r non-zero eigenvalues.

this upper bound to $P_{T,R}$. Using the Cauchy-Schwarz inequality on the relay transmit signal $\gamma \mathbf{F}_{R,n} \mathbf{y}_R$, we obtain that

$$\|\gamma \mathbf{F}_{R,n} \mathbf{y}_R\|_2^2 = \gamma^2 \|\mathbf{y}_R\|_2^2 \leq \gamma^2 (M_{T,1} M_R P_{T,1} + M_{T,2} M_R P_{T,2} + M_R \sigma_n^2) = P_{T,R}.$$

Here, we have applied the fact that each entry of the channel matrices \mathbf{H}_{1R} and \mathbf{H}_{2R} is Gaussian distributed with unit variance and that each entry of the noise vector \mathbf{n}_R is Gaussian distributed with variance σ_n^2 . The transmit signals are assumed to be uncorrelated with each other and with the noise at the relay. The transmit power at each BS is constrained by $P_{T,i}$, i.e., $\mathbb{E}\{\|\mathbf{f}_i s_i\|^2\} \leq P_{T,i}$. Then we choose γ as

$$\gamma = \sqrt{\frac{P_{T,R}}{M_{T,1} M_R P_{T1} + M_{T,2} M_R P_{T2} + M_R \sigma_n^2}}$$

In general, the actual consumed power at the relay is less than $P_{T,R}$. However, the advantage is that it is very easy to compute γ as it does not depend on the UTs' transmit covariance matrices nor on the strategy of the relay. We therefore use it in the following analysis.

5.2.2. Precoder Design at the BSs

Once \mathbf{F}_R is obtained, the IRC is converted to IC and we use precoders supporting multiple data stream transmission in the IC.

In [DI03], a stream control method is proposed using the classical water filling solution, where the MIMO IC is treated as two parallel single-user MIMO links. The scheme in [DI03] works as follows. The SVD of \mathbf{H}_i is denoted as $\mathbf{H}_i = \tilde{\mathbf{U}}_i \cdot \tilde{\boldsymbol{\Sigma}}_i \cdot \tilde{\mathbf{V}}_i^H$, $i = 1, 2$. Assuming that the system is initially free of interference, the precoder at each BS is initialized as $\mathbf{F}_i = \tilde{\mathbf{V}}_i \tilde{\mathbf{A}}_i^{\frac{1}{2}}$ to maximize the sum rate for each link, where $\tilde{\mathbf{A}}_i$ is the diagonal power allocation matrix using water filling. At the receiver, a prewhitening matrix is applied $\mathbf{D}_i = (\mathbf{I}_{2M_{U,i}} + \frac{1}{\sigma_n^2} \mathbf{K}_{i,j})^{-\frac{1}{2}}$, where $\mathbf{K}_{i,j} = \mathbf{G}_i \mathbf{F}_j \mathbf{F}_j^H \mathbf{G}_i^H$ denotes the interference covariance. When one link tries to add an extra data stream, it compares its capacity increment with the capacity loss of the other transceiver pair due to the additional interference. Based on this, a distributed stream control algorithm is designed such that an extra data stream is allowed only if the total system throughput obtains a positive gain. Although this method achieves almost the same sum rate as the optimum stream control, the precoder is designed only to strengthen the desired signal without taking the interference into account.

Instead of the stream control method, we propose the IRC FlexCoBF RBD method, which utilizes the regularized block diagonalization (RBD) algorithm [SH08] as the precoders $\mathbf{F}_i \in \mathbb{C}^{M_{T,i} \times r_i}$ at the BSs combined with maximum ratio combining (MRC) as receive filters $\mathbf{W}_i = \mathbf{H}_i \mathbf{F}_i \in \mathbb{C}^{M_{U,i} \times r_i}$ at the UTs, as described in Chapter 3. The precoders \mathbf{F}_i and receive filters \mathbf{W}_i , $i \in \{1, 2\}$ are jointly designed to iteratively suppress the interferences as well as to improve the system sum rate. Furthermore, inspired by the stream control method [DI03], a greedy search can be combined with the IRC FlexCoBF algorithm, named as IRC FlexCoBF greedy

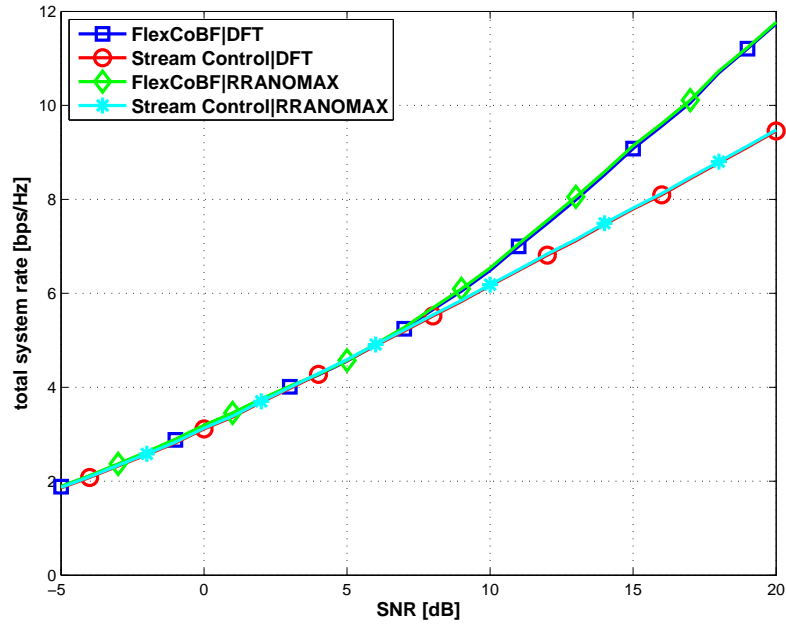


Figure 5.8.: Sum rate for different relay strategies, $M_{T,i} = M_{U,i} = M_R = 4$

search, to find the optimum number of data streams to be transmitted so as to maximize the system sum rate. In the IRC FlexCoBF algorithm, we use water filling for power allocation to determine the number of data streams, as described in Section 3.3. Differently to that, for the IRC FlexCoBF greedy search method, we apply the IRC FlexCoBF RBD algorithm with equal power allocation at both BSs. Then we start with a single stream transmission for both links and add additional data streams step by step to see if the system sum rate improves. In this way, we determine the optimum number of data streams to be transmitted throughout all possible combinations.

For the simulations, we assume that perfect link adaptation and perfect synchronization can be achieved. Each BS, relay, and user know the channel state information perfectly. Each element of \mathbf{H}_{ij} is a zero mean circularly symmetric complex Gaussian random variable with unit variance $\mathcal{CN}(0,1)$. The transmit power of the BSs is $P_{T,1} = P_{T,2} = P_T$ and the SNR is defined as P_T/σ_n^2 .

First of all, by utilizing a DFT matrix or the OW-RR-ANOMAX strategy at the relay, the sum rate are compared for $M_{T,i} = 4, M_{U,i} = 4, M_R = 4$ for $i = 1, 2$. Both schemes are combined either with IRC-FlexCoBF or the stream control method of [DI03]. As shown in Fig. 5.8, OW-RR-ANOMAX performs only slightly better than the DFT matrix. It indicates that the relaying strategies do not play a key role in the system sum rate rather than the precoding matrix used at the BSs. Therefore, compromising between the performance and the complexity, we choose the simple DFT matrix in the following analysis due to its lower computational complexity.

Fixing the DFT matrix at the relay, Fig. 5.9 gives the sum rate of the IRC for $M_{T,i} = 4, M_{U,i} = 4, M_R = 4$ for $i = 1, 2$. It is observed that IRC FlexCoBF results in a much better

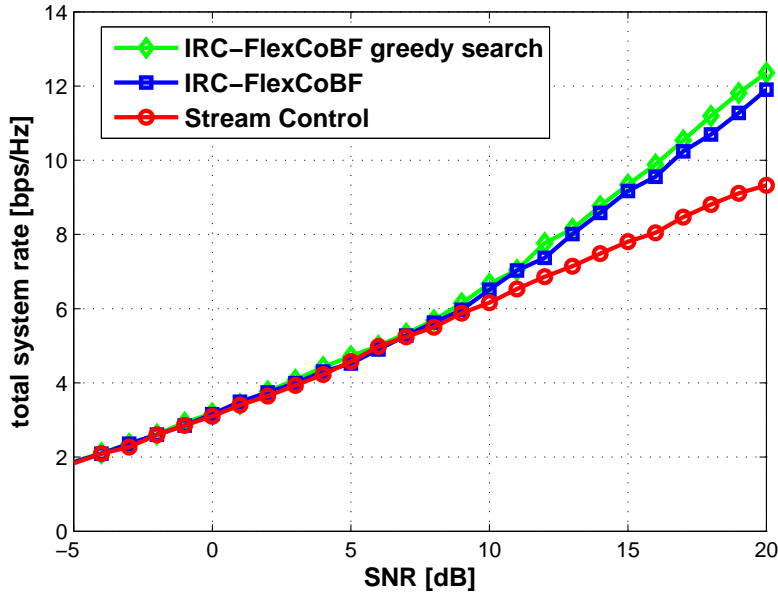


Figure 5.9.: Sum rate vs SNR for $M_{T,i} = M_{U,i} = M_R = 4$, DFT matrix is applied at the relay

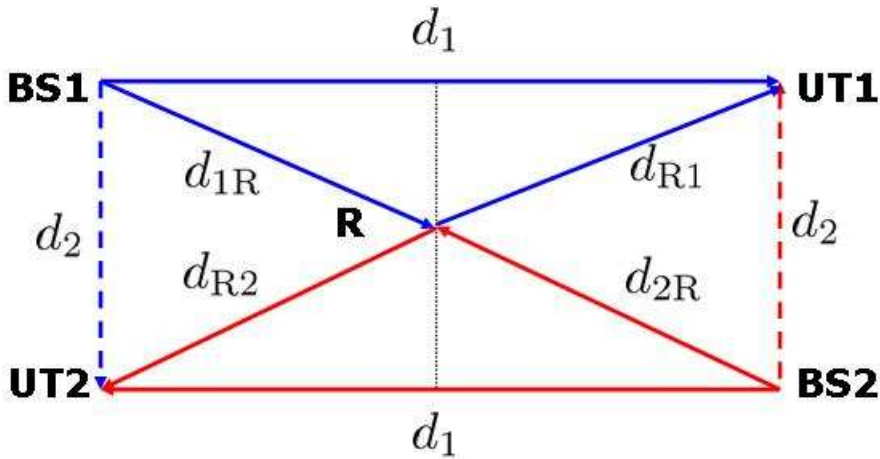


Figure 5.10.: Path loss model for IRC

performance than the stream control method [DI03] at high SNRs. It is because IRC FlexCoBF is designed not only to enhance the desired signal of the respective links but also to effectively mitigate the interference to each other. Comparing to IRC FlexCoBF, the combination of IRC FlexCoBF and a greedy search even further improves the sum rate at high SNRs because the optimum number of data streams is selected so as to maximize the spatial multiplexing gain. However, the computational complexity is very high when performing the greedy search. Compromising between the performance and the complexity, IRC-FlexCoBF is used in the following analysis.

A path loss model is further introduced to test the robustness to the interferences of the IRC FlexCoBF compared to the stream control method. As shown in Fig. 5.10, suppose that

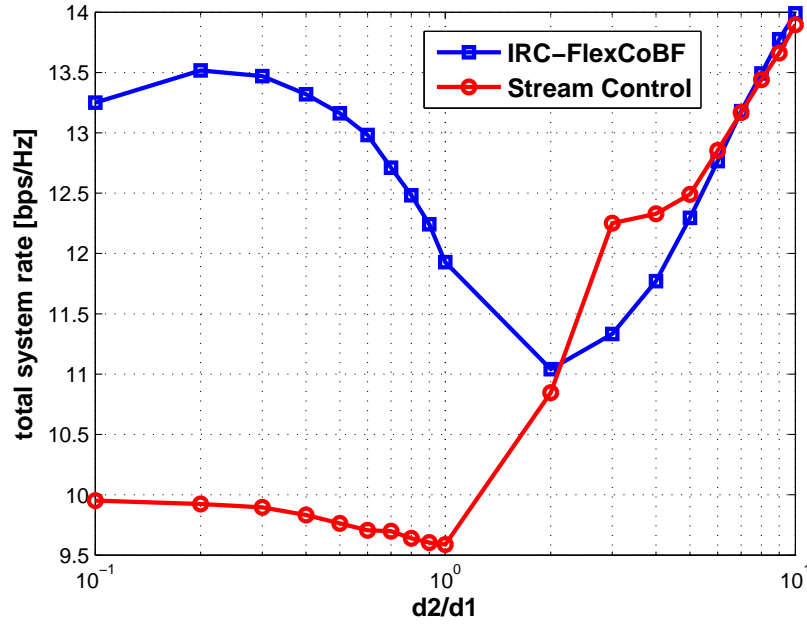
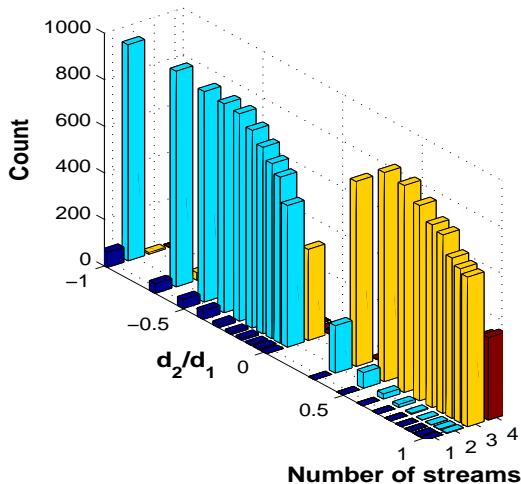


Figure 5.11.: Sum rate for the path loss model at SNR = 20 dB for $M_{T,i} = M_{U,i} = M_R = 4$

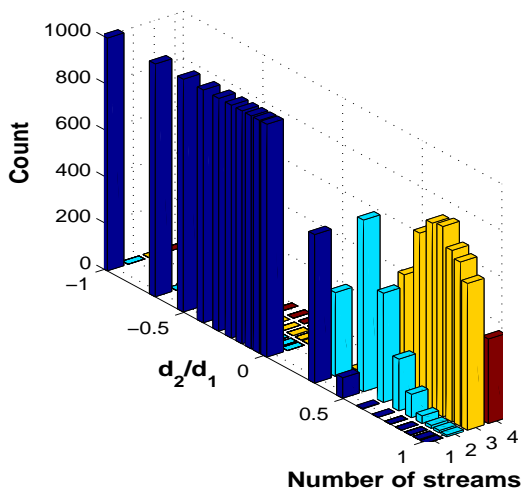
the distance between the BSs and the UTs is d_1 and that the distance between these two interfering links is d_2 . The relay is located in the centre of the two transceiver pairs. The channel is constructed by scaling the channel matrix with unit variance channel coefficients by $d^{-\frac{\alpha}{2}}$, where α is the path loss exponential factor and is set to $\alpha = 2$ in the simulations.

Based on this model, Fig. 5.11 gives the sum rate depending on the ratio of d_2/d_1 at SNR = 20 dB. The sum rate decreases until $d_2/d_1 \approx 1$ and increases when $d_2/d_1 \gg 1$. On one side, increasing d_2/d_1 will decrease the interferences between the two transceiver pairs. On the other side, the signal transmitted via the relay becomes weak. This implies that the relay assisted transmission dominates when $d_2/d_1 \ll 1$ while the direct transmission plays the key role when d_2/d_1 is large. There is not much difference in sum rate for both the IRC FlexCoBF and the stream control method at high d_2/d_1 or weak interferences. On the other hand, when d_2/d_1 is small, we have high interferences, IRC FlexCoBF uses more data streams to transmit than the stream control method. Therefore, it exhibits a great improvement of the sum rate over the stream control method, which shows its higher robustness to strong interferences. Fig. 5.12 further explains the reason explicitly. It shows the histogram of the number of streams for one user at different d_2/d_1 values over 1000 channel realizations. Due to the effective interference mitigation, especially at low d_2/d_1 , the IRC FlexCoBF can exploit more degrees of freedom to dramatically increase the system throughput.

Finally, the sum rate performance of the IRC is compared to the traditional RC where the transmission takes place between only one transceiver pair assisted by a relay without interfered from the other. The RC is taken as a reference, where the iterative water filling solution with optimum stream control is applied at the BS while the relay utilizes the DFT



(a) IRC-FlexCoBF



(b) Stream Control

Figure 5.12.: Histogram of the number of streams at different d_2/d_1 values for $M_{T,i} = M_{U,i} = M_R = 4$

matrix as the relay amplification matrix. We refer to this ratio of throughput (TP) TP_{IRC} / TP_{RC} as the sharing gain due to the use of the shared relay instead of accessing the relay in a TDMA mode, shown in Fig. 5.13. It can be seen that the proposed IRC FlexCoBF with RBD provides a larger sharing gain than the stream control method. We conclude that the relay sharing is more advantageous than the exclusive use of infrastructure resources, of which IRC FlexCoBF with RBD provides a larger sharing gain than the stream control method.

In this section, we have studied coordinated beamforming for multiple data stream transmission in the MIMO interference relay channel (IRC). Two AF relaying strategies are investigated first for the conversion from the IRC to the interference channel, of which the DFT matrix is recommended as the relay amplification matrix due to its simplicity. After that

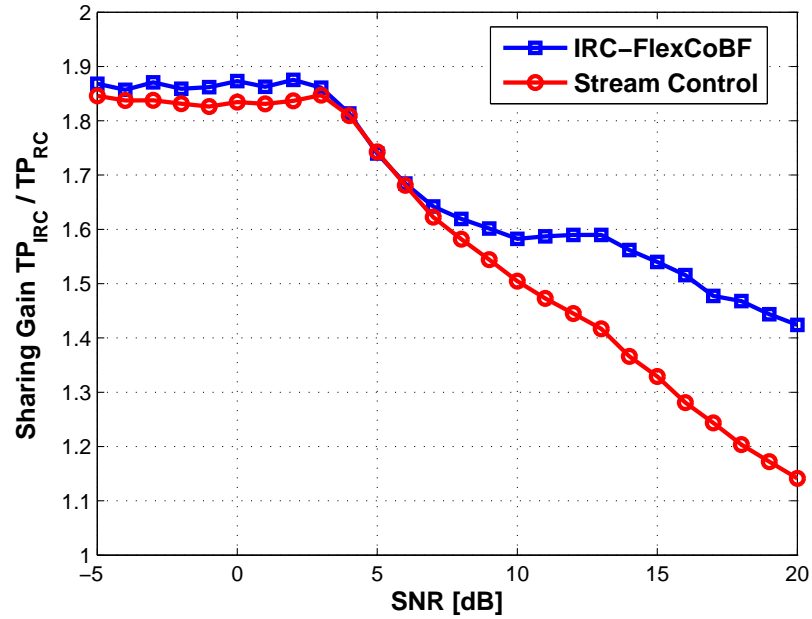


Figure 5.13.: sharing gain due to the use of the shared relay instead of accessing the relay in a TDMA mode

we propose the precoding algorithm IRC FlexCoBF with RBD at the BSs, which achieves a better sum rate performance compared to the approach in [DI03]. Furthermore, simulation results show that the IRC FlexCoBF RBD is more robust to strong interference than the approach in [DI03]. In addition to this, the sum rate performance of the IRC is compared to the relay channel and there exists a large sharing gain, which strongly supports the use of a relay shared by two base stations instead of accessing the relay in the time division multiple access (TDMA) mode.

Part II.

Home Gigabit Access (OMEGA)

6. OMEGA Concept

The rapidly increasing demand for convenient resource sharing on the Internet prompts the future vision of home area networks operating at several Gigabits per second (Gbps). As a part of the EU seventh framework R&D programme (FP7), the hOME Gigabit Access (OMEGA) project (www.ict-omega.eu) aims at bridging the gap between mobile broadband terminals and the wired backbone at home. To provide Gbps connectivity within the home area network, a large number of different complementary access techniques are considered. In addition to the wired power line communications, the wireless links will use radio frequency (RF), infrared (IR) as well as the visible light transmission to fulfill the vision of broadband home networking without adding new wires as shown in Fig. 1.4. Part II of this dissertation is focused on wireless infrared communications and it presents the physical layer analysis on integration and feasibility investigation of Gbps IR system.

As an alternative to RF for short range indoor communications, IR exhibits several advantages. Since there is a rapid growth in wireless communications, the RF resources become more and more rare. To overcome the spectral limitations, there is a trend in RF to move to higher frequencies such as 60 GHz, where the propagation is similar to that of IR radiation. Compared to RF, the unregulated bandwidth offers IR overwhelming dominance, which qualifies it as an competitive candidate for indoor transmission. Moreover, IR transceivers employing intensity modulation and direct detection avoid multipath fading that occurs in RF. This is because the detector usually has a large area compared to the short wavelength such that efficient spatial diversity reception is exploited [WK03]. Since IR radiation does not pass through walls, the signal is confined within a room to ensure a secure transmission which is immune to eavesdropping. The reuse of the same bandwidth is possible throughout a building. Last but not least, low cost IR transceivers are available on the market that are capable of high speed transmission.

In the previous work, infrared transmission operating at 100 Mbps [AK95] has been investigated in the indoor environment. However, when switching the data rate from 100 Mb/s to 1 Gbps, the design of an indoor infrared wireless system operating at Gbps is quite challenging. This is because the system operating at Gbps is mainly constrained by the receiver frontend noise [LGB⁺08], which increases by a factor of 1000. In addition to that, it is also required that the system provides a typical 90 degrees of coverage both at the transmitter and receiver. This wide coverage for robust indoor coverage makes the system considerably more challenging. If we increase the transmitter and receiver coverage by a factor of two while keeping the photodiode area unchanged, we need to increase the transmit power by a factor of 16, which imposes a very strict limit on the eye safety of the laser driver. Thus multiple links with a narrow coverage will be required to cover the target coverage, and the control

and management of these is to be where most of the innovation in OMEGA lies, as the state of the art is relatively undeveloped.

In particular, the basic IR system topology is categorized into diffuse and line of sight (LOS) systems [KB97]. The diffuse system creates a large number of paths from the transmitter to the receiver, which makes the system robust and prevents it from getting blocked. However, it suffers from multipath dispersion, which causes pulse spread and significant inter-symbol interference, in addition to higher path losses compared to direct LOS links. To fulfill the Gbps data transmission requirement, OMEGA adopts a LOS system topology. Direct LOS links improve the power efficiency and reduce the multipath dispersion, but require an inherent alignment between the transmitter and the receiver in order to establish a reliable communication. The path loss combined with the narrow transmitter and receiver field of view (FOV) determine the link budget and the available data rate of the system. In general, the narrower the FOV, the higher is the data rate that is achievable. However, such narrow links do not provide coverage, and thus cellular systems using a number of LOS links are employed in order to increase the coverage and achieve high data rates. Generally speaking, there are two approaches to implement multiple element transmitters and receivers. One is to use imaging transmitters and receivers, where light beams are transmitted at different angles within the desired coverage area while the receiver uses a detector array so that radiations from different angles reach particular elements within the range of the detector [PFOE01, WN97, OFJ+03]. An alternative is to build an angle diversity system where individual transmitters and receivers are arranged to point at different angles to provide the desired coverage [CK00]. In OMEGA, the latter choice is made since there are not sufficient resources within the project to fabricate the necessary custom devices for the imaging solution.

In Part II of this thesis, the physical layer design for a high speed line-of-sight (LOS) IR system is considered, which consists of a base station located at the ceiling and terminals that move around at the ground, as illustrated in Fig. 7.1. Both transmitters and receivers have multiple elements, where each element covers a relatively narrow FOV. By switching on/off different transmit/receive elements, different fractions of the solid angle will be covered. This part is organized as follows. In Chapter 7, the system model of the high speed IR transmission is introduced, where individual components suitable for Gbps IR system are analyzed and specified. To be more specific, the modulation scheme that fits for Gbps IR transmission is briefly discussed in Section 7.1. To overcome the baseline wander effect of the highpass filter, a new line coding scheme is proposed in Section 7.2. Following that, the low-pass filter applied and high-pass filter are further discussed in Section 7.3 and Section 7.4, which are applied to reject the noise and block the DC photocurrent generated by the received ambient light as well as to reduce the harmonics caused by the fluorescent lighting, respectively. The photodiode detectors are specified in Section 7.5, including PIN photodiodes and Avalanche types. Various noise sources generated in the IR system are discussed in Section 7.6. Based on all the above mentioned analysis and specification of the individual components, the link budget for a LOS Gbps IR transmission with a narrow angle FOV is given in Chapter 8. At last, the transmit and receive angle diversity are discussed in Chapter 9, in order to further extend the system FOV.

7. System Model

The block diagram of the Gbps infrared (IR) system for line-of-sight (LOS) based single link is shown in Fig. 7.2. Information bits are first fed into the line encoder. Then the output is non-return-to-zero (NRZ) on-off-keying (OOK) modulated and drives the laser diode. The intensity modulated optical signal passes through an LOS channel which is assumed to be ideal and characterized by the impulse response $h_c(t) = c\delta(t)$, where c denotes a path loss constant. The incoming optical signal is converted into an electrical signal by a positive-intrinsic-negative (PIN) photodiode that forms a p-type /intrinsic/n-type structure, or an Avalanche photodiode (APD) using direct detection [KB97]. This electrical signal is comprised of the transmitted signal and the ambient light induced shot noise that is essentially white Gaussian and independent of the desired signal. An ideal preamplifier at the receiver frontend is assumed to have the transfer function $|H_{\text{preamp}}(f)| = 1$. Additional noise is induced by this preamplifier, which consists of thermal noise with constant power spectral density (PSD) and so-called f^2 noise with a PSD increasing with the square of the frequency [Muo84]. A

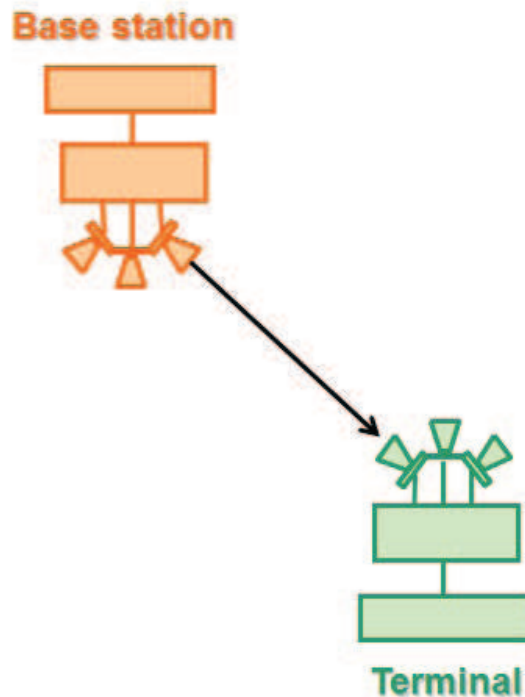


Figure 7.1.: Gbps LOS infrared system concept

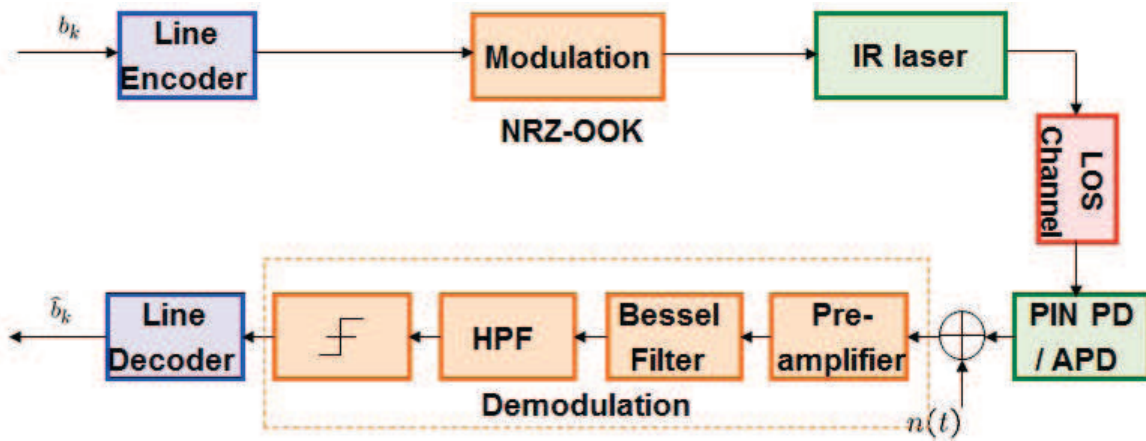


Figure 7.2.: Block diagram of the Gbps wireless IR system

fifth-order Bessel filter with a cut-off frequency f_{3dB} is then applied for noise rejection. The high-pass filter (HPF) before demodulation, which is modeled as a first-order RC filter, is supposed to mitigate all the fluorescent light induced periodic interferences completely. At last, a hard decision is made after the filtering and the information is retrieved at the output of the line decoder.

In the following sections, we will describe each component in the Gbps wireless IR system respectively.

7.1. Modulation

As [WGL09, GLWH09] shows, non-return-to-zero (NRZ) on-off-keying (OOK) offers several advantages compared to other popular modulation schemes used in indoor infrared transmission. The signal at each laser driver input exhibits only two amplitude levels, the laser drivers are much easier to build and much more power efficient than linear drivers required for subcarrier or pulse amplitude modulation (PAM). Moreover, it is not required to derive the decision threshold from the received signal as for pulse position modulation (PPM) or return-to-zero (RZ) OOK. In the Gbps IR system, NRZ OOK modulation is performed on the coded bits which are DC-balanced after the line encoder (see Section 7.2), the optimum decision threshold with respect to the high-pass filtered signal is equal to zero. To conclude, NRZ OOK gives a good compromise between power and bandwidth efficiency and facilitates the extremely simple implementation, which makes it preferred for Gbps system.

7.2. Line Coding

A major motivation for line coding in direct detection optical systems is the baseline wander effect [AK95, Gha08] induced by the AC-coupling inherent in the receiver's preamplifier. AC-

coupling blocks the DC photocurrent generated by the received ambient light and removes DC-couplings between different amplifier stages. Furthermore, a high-pass characteristic is also required to reduce harmonics caused by fluorescent lighting [SOSE98]. In modern compact tubes with electronic ballasts, the electrical spectrum of the harmonics may extend up to 1 MHz [NAK96], [Bou96]. Although a large cut-on frequency is desirable to effectively attenuate this interference¹, it may be undesirable from a signal distortion point of view. More precisely, if the short time average of the signal (i.e., the “baseline”) is not constant, the high-pass filter (HPF) will introduce a significant amount of inter-symbol-interference (ISI) [SSOE97].

The effect of the transient baseline wander can also be mitigated by active baseline restoration. However, line coding is particularly attractive if the receiver implementation complexity should remain low [AK95]. By means of additional redundancy, a line code is able to control the statistics of the data symbols to be transmitted and is thereby capable of reducing the baseline wander effect. Meanwhile, line coding ensures a reliable synchronization of the receiver clock due to sufficient binary state transitions, which are either from “1” to “0” or from “0” to “1”. There are many types of line coding commonly used in telecommunications, such as the unipolar non-return-to-zero code, the Manchester code, the alternate mark inversion (AMI) code [Com11], etc. With respect to byte oriented transmission, we consider the 8B10B line code in this section, where the 8 information bits are mapped into 10 coded bits.

This section focuses on the DC-balanced low redundancy binary line codes to be combined with NRZ-OOK modulation. Such codes can be potentially applied to Gbps wireless IR transmission. The remainder of this section is organized as follows. In Section 7.2.1, important characteristics of line codes are presented. Two 8B10B block codes are proposed and analyzed in Section 7.2.2. One is the well-known IBM code [WF83] while the other is a new alternative 8B10B code, which can achieve a comparable performance while its implementation is less complex. Simulation results are given in Section 7.2.3, where the baseline wander effect is investigated for both proposals. Finally, conclusions are drawn on this section. The main contribution of this section has been published in reference [LWH09].

7.2.1. Desirable Line Code Properties

As will be shown in Section 7.6, the so-called f^2 noise plays an important role on the Gbps IR transmission system [LGB⁺08], whose variance depends on the third power of the data rate [LGB⁺08], which means that it increases by a factor 1000 when switching the data rate from 100 Mb/s to 1 Gbps. As for line code considerations, it implies that the power (second moment) of the photocurrent’s f^2 noise component decreases with the *third power* of the code rate

$$r_c = \frac{m}{n},$$

¹For packet oriented transmission, a large cut-on frequency is also very important to keep the duration of the baseline wander subsequent to idle periods short. The longer the baseline wander extends, the more extra training bits are required at the beginning of a packet.

where m is the number of information bits at the input of the line encoder and n the number of bits at its output. This shows directly that a low redundancy is a primary design issue for the line code. Moreover, the limited speed of the individual components for Gbps IR transmission will be another reason demanding for the low-redundancy design.

At a given r_c , the following properties can be considered to evaluate a line code.

- Maximum run-length r_{\max} : defined as the maximum number of consecutive ones or zeros in the data stream that needs to be limited to provide a regular clock information. The receiver's phase locked loop (PLL) bandwidth can be increased by decreasing the maximum run-length, which ensures a fast acquisition time with respect to the receiver clock.
- Short time average variation σ_N : It is assumed that the receiver's high-pass characteristic can be modeled as a first-order RC filter with the impulse response

$$g(t) = \delta(t) - \frac{1}{\tau} \exp\left(-\frac{t}{\tau}\right) \quad \text{for } t \geq 0, \quad (7.1)$$

where $1/(2\pi\tau)$ is the cut-on frequency. The expression shows that the high-pass filter (HPF) basically removes the short time average from the signal. Since there is an exponentially decreasing weighting factor within the integration interval, the effect of the baseline wander on the eye-opening can only be estimated through a numerical simulation (cf. Section 7.2.3).

However, the baseline wander effect can still be estimated roughly, if a constant weighting factor is assumed within the integration interval. With $c_n \in \{0, 1\}$ being the coded bits at the line encoder output, we define

$$\mu_N[n] = \frac{1}{N} \sum_{k=n}^{n+N-1} c_k, \quad n \in \mathbb{N}$$

as the short time average over N bits. With

$$\mu_{N,\max} = \max_{\forall n} \mu_N[n] \quad \text{and} \quad \mu_{N,\min} = \min_{\forall n} \mu_N[n]$$

denoting the maximum and minimum short time average over N bits respectively, the relative vertical eye-opening at the receiver can be estimated as

$$(1 - \mu_{N,\max}) - (0 - \mu_{N,\min}) = 1 - \underbrace{(\mu_{N,\max} - \mu_{N,\min})}_{\sigma_N}.$$

The parameter σ_N is the maximum variation of the short time average and it is a direct measure of the loss with respect to the vertical eye-opening. For example, $\sigma_{10} = 1/5$ and $\sigma_{20} = 1/10$ are obtained for 4-PPM, which can be considered as OOK with additional line coding, showing that the baseline wander effect decreases with an increasing integration interval.

- DC-balance: DC balance is preferable, i.e., $E\{\mu_N[n]\} = N/2$. It ensures that the optimum decision threshold corresponds to zero with respect to the high-pass filtered signal, which is advantageous from the implementation point of view.
- Error propagation: High-redundancy codes may exploit their code redundancy for error detection and correction. However, such properties are hardly achievable by line codes that fit Gbps IR links due to the low-redundancy constraint discussed at the beginning of Section 7.2.1. We should minimize the error probability after line coding.
- Implementation complexity: The implementation aspect is also an important figure of merit to judge a line code.

7.2.2. 8B10B Codes

Byte orientation is considered as a further favorable property of line codes since 8 input bits correspond to the natural data units at the interface to the multiple access (MAC) layer.

To obtain a small variation of the short time average, a first design approach could rely upon the usage of codewords with a constant Hamming weight, just as in multiple PPM [PB95]. With respect to $m = 8$ input bits, it is not possible to construct such a code for $n = 9$ or for $n = 10$ output bits, since there are not enough codewords to be utilized: $\binom{9}{5}$ or $\binom{9}{4}$ gives only 126, while $\binom{10}{5}$ gives 252. However, two solutions can be used to increase the alphabet size. One is to use a codeword length of $n = 11$ which is not considered here since it will further increase the required bandwidth. Another method can be applied to $n = 10$, if not only codewords with a Hamming weight of 5 but also with that of 4 or 6 are used. The alphabet can be extended by $\binom{10}{4} = 210$ additional codewords, which is more than enough. This approach is not adaptable for $n = 9$, since $\binom{9}{4} + \binom{9}{5}$ or $\binom{9}{4} + \binom{9}{3}$ is still less than $2^8 = 256$.

Let us define the codeword disparity (CDP) as the count of ones minus the count of zeros. The 8B10B coding with varying Hamming weights (number of ones in a codeword) can still guarantee DC balance, if the output with a CDP of +2 (Hamming weight of 6) and its complementary with a CDP of -2 are assigned to the same input. The rule of running disparity has to be fulfilled during the transmission such that these codewords appear alternately to ensure the DC balance.

Furthermore, an 8B10B code can be a concatenation of a 5B6B code and a 3B4B code, where sufficient codewords with $CDP = 0, \pm 2$ can be used with respect to the input information through a similar analysis as mentioned above. Moreover, their coding tables are easier to design with 32 and 8 entries respectively, compared to a single 8B10B code holding a total of 256 entries. In the following, two 8B10B line codes are going to be investigated.

A. IBM

The first line code considered here is the well-known IBM 8B10B code [WF83]. The IBM code has already been used in many systems including the Gigabit Ethernet.

Table 7.1.: Rule of Running Disparity for IBM Code

Previous RD	Current CDP	Next RD
-1	0	-1
+1	0	+1
-1	+2	+1
+1	-2	-1

A main feature of this code is that it is a concatenation of a 5B6B code and a 3B4B code as described above. Encoding and decoding are performed independently for each 6B or 4B subblock. Moreover, all 6B and 4B subblocks individually, and the complete 10-bit codeword hold a disparity of either 0 or ± 2 , which ensures quite a small transient baseline wander.

During the transmission, the rule of running disparity (RD) has to be fulfilled for each encoded 6B or 4B subblock. As already described previously, an input may be assigned to two complementary output codewords. As shown in Table 7.1, the current codeword is chosen depending on the CDP and the previous RD. Since the RD is initialized to -1 or +1 at the beginning, the RD is always bounded to ± 1 during the transmission. It should be noted that there are additional constraints with respect to the concatenation of the 3B4B code with the 5B6B code. To ensure a maximum run-length of 4, some specific 6B codewords are followed by alternative 4B codewords [WF83].

Considering those special cases and constrains, it would be a straightforward way to implement the IBM code through two look-up tables instead of sophisticated logic circuits as many researchers complained [KSK08], [Krz89], [JKJC01]. If an invalid codeword is received, the decoder will try to find a valid codeword that has a minimum Hamming distance with it and performs demapping. However, this mapping ROM table has the potential of limiting the operating speed.

With respect to the code design, codewords are actually elaborately selected for the sake of good DC-balance and reasonable transitions as observed from the code table, though it was not mentioned in [WF83]. Take the 5B6B code, for instance, concerning the $2^5 = 32$ input information, it first chooses all $\binom{6}{3} = 20$ codewords with a disparity of zero (Hamming weight of 3). These 20 codewords are assigned to 19 input information, with the exception that (000111) and (111000) are assigned to the same inputs for the sake of r_{\max} . Then the residual 13 inputs are assigned to 2·13 codewords with minimum possible nonzero disparity of ± 2 (Hamming weight of 4 or 2), which are selected from $\binom{6}{4} + \binom{6}{2} = 2 \cdot 15$ possible codewords, discarding (111100), (001111) and their complements also due to the maximum run-length consideration.

B. CFBI

Inspired by the elaborate code design of this IBM code as well as the simplicity and efficiency of the bit insertion code [Krz89], a new code named concatenated flipped bit insertion (CFBI) is designed to couple both advantages. It also consists of a 5B6B and a 3B4B code, each of

which can be viewed as an improved version of the bit insertion and manipulation (BIM) code [JKJC01].

At the first step, the CFBI 5B6B code is to be designed. With respect to a total of $2^5 = 32$ entries, it first chooses all $\binom{6}{3} = 20$ codewords with disparity of zero for maintaining a good DC-balance. The 12 residual entries are assigned by $2 \cdot 12$ complementary pairs with disparity of ± 2 . Unlike the BIM 5B6B code, the codewords (001111), (111100) and their complementary counterparts contain long consecutive ones and zeros, and they are not well suited to retrieve the clock information at the receiver. Therefore, they are not included in our CFBI code. When the codewords are selected, the mapping table is generated by means of simply adding a bit to the original information followed by some partial flipping afterwards.

Depending on the disparity of the input information, the CFBI 5B6B precoding table is basically divided into 3 classes as shown in Table 7.2.

(1) If $DP = \pm 1$ or $+3$, the codeword is produced either by inserting a 0-bit for $DP > 0$ or 1 for $DP < 0$ in the position between b_3 and b_2 , so that the codeword disparity is maintained

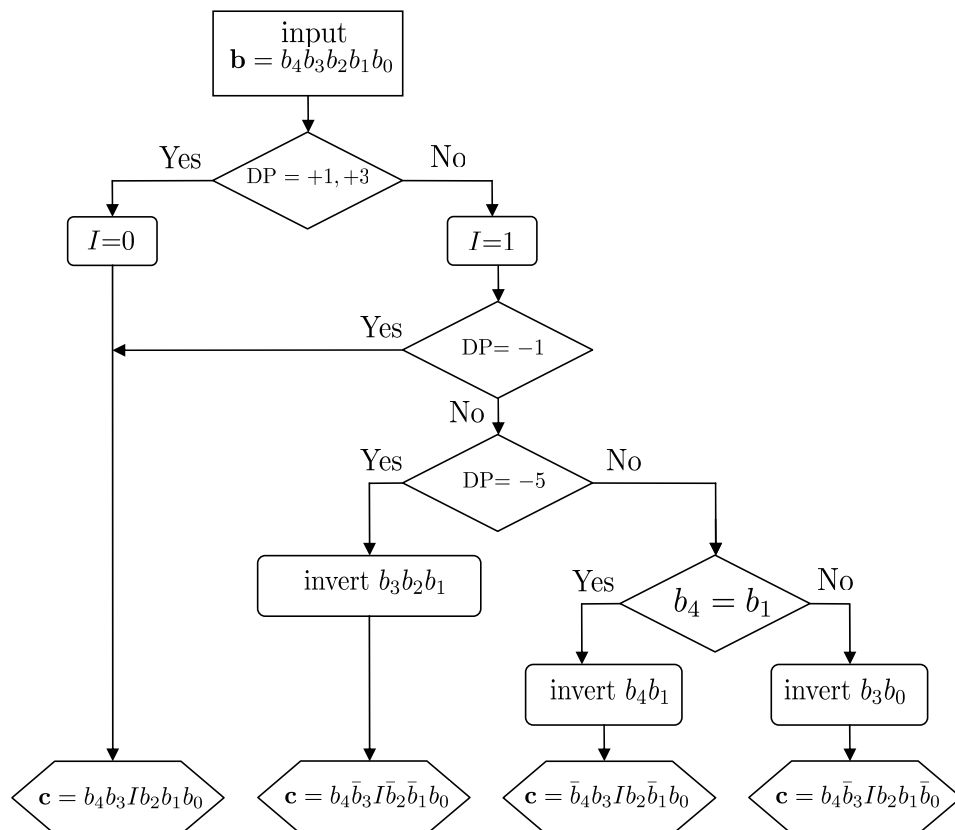


Figure 7.3.: Flowchart of CFBI 5B6B encoder

Table 7.2.: Precoding Table of CFBI 5B6B

Classification		$b_4b_3b_2b_1b_0$	DP	\mathbf{c}	CDP		
Class 1 DP= $\pm 1, +3$ $\mathbf{c} = b_4b_3Ib_2b_1b_0$ $I=1$ for DP= -1 $I=0$ for DP= $+1, +3$		0 0 0 1 1	-1	0 0 1 0 1 1	0		
		0 0 1 0 1	-1	0 0 1 1 0 1	0		
		0 0 1 1 0	-1	0 0 1 1 1 0	0		
		0 1 0 0 1	-1	0 1 1 0 0 1	0		
		0 1 0 1 0	-1	0 1 1 0 1 0	0		
		0 1 1 0 0	-1	0 1 1 1 0 0	0		
		1 0 0 0 1	-1	1 0 1 0 0 1	0		
		1 0 0 1 0	-1	1 0 1 0 1 0	0		
		1 0 1 0 0	-1	1 0 1 1 0 0	0		
		1 1 0 0 0	-1	1 1 1 0 0 0	0		
		0 0 1 1 1	+1	0 0 0 1 1 1	0		
		0 1 0 1 1	+1	0 1 0 0 1 1	0		
		0 1 1 0 1	+1	0 1 0 1 0 1	0		
		0 1 1 1 0	+1	0 1 0 1 1 0	0		
		1 0 0 1 1	+1	1 0 0 0 1 1	0		
		1 0 1 0 1	+1	1 0 0 1 0 1	0		
		1 0 1 1 0	+1	1 0 0 1 1 0	0		
		1 1 0 0 1	+1	1 1 0 0 0 1	0		
		1 1 0 1 0	+1	1 1 0 0 1 0	0		
		1 1 1 0 0	+1	1 1 0 1 0 0	0		
0 1 1 1 1	+3	0 1 0 1 1 1	+2				
1 0 1 1 1	+3	1 0 0 1 1 1	+2				
1 1 0 1 1	+3	1 1 0 0 1 1	+2				
1 1 1 0 1	+3	1 1 0 1 0 1	+2				
1 1 1 1 0	+3	1 1 0 1 1 0	+2				
Class 2 DP= -5 $I=1$		0 0 0 0 0	-5	0 1 1 1 1 0	+2		
Class 3 DP= $-3, 5$ $I=1$		$b_4 = b_1$ $\mathbf{c} = \bar{b}_4b_3Ib_2\bar{b}_1b_0$		0 0 0 0 1	-3	1 0 1 0 1 1	+2
				0 0 1 0 0	-3	1 0 1 1 1 0	+2
				0 1 0 0 0	-3	1 1 1 0 1 0	+2
				1 1 1 1 1	5	0 1 1 1 0 1	+2
		$b_4 \neq b_1$ $\mathbf{c} = b_4\bar{b}_3Ib_2b_1\bar{b}_0$		0 0 0 1 0	-3	0 1 1 0 1 1	+2
				1 0 0 0 0	-3	1 1 1 0 0 1	+2

as 0 for DP = ± 1 while generating codewords with the possible minimum positive disparity of +2 for DP = +3. The output codeword is $\mathbf{c} = b_4b_3Ib_2b_1b_0$, with I denoting the insertion bit.

(2) If DP = -5 , insertion bit $I = 1$ and b_3, b_2, b_1 are inverted aiming to get a codeword also constrained to the disparity of +2.

(3) If DP = -3 or 5 , a 1-bit is inserted first. Following that the codeword is obtained either by inverting b_4 and b_1 when $b_4 = b_1$, which is denoted as $\mathbf{c} = \bar{b}_4b_3Ib_2\bar{b}_1b_0$, or by inverting b_3 and b_0 for other cases $\mathbf{c} = b_4\bar{b}_3Ib_2b_1\bar{b}_0$. This also results in a cluster of codewords with disparity of +2.

Compared to the BIM 5B6B code, since the codewords (001111) and (111100) are not included in this new code, the maximum run-length is reduced from 7 to 6, which determines

the worst case of clock recovery so that more timing information can be extracted. Moreover, the complexity of this new CFBI 5B6B code is reduced, which could be clearly illustrated in Fig. 7.3 and Fig. 7.4. First of all, this CFBI code does not use the coding apparatus CDP in deciding a 1-bit or a 0-bit to insert. It simplifies the bit insertion manipulation by only considering whether $DP = +1$ or $+3$. If such case is satisfied, a 0-bit is inserted while a 1-bit is added under other conditions. Secondly, there are more judging constrains in mapping the information to the pre-codewords for the BIM code. Last but not least, CFBI 5B6B produces 4 possible codeword formats instead of 5 as in the case of the BIM code, which indeed facilitates the bit flipping control in a hardware implementation.

It is clearly seen that the disparity of a valid codeword is either 0 or $+2$ through the above precoding. After that those codewords are sent either unchanged or totally inverted depending on the following simple rule of running disparity: $RDS \cdot CDP \leq 0$, which implies that

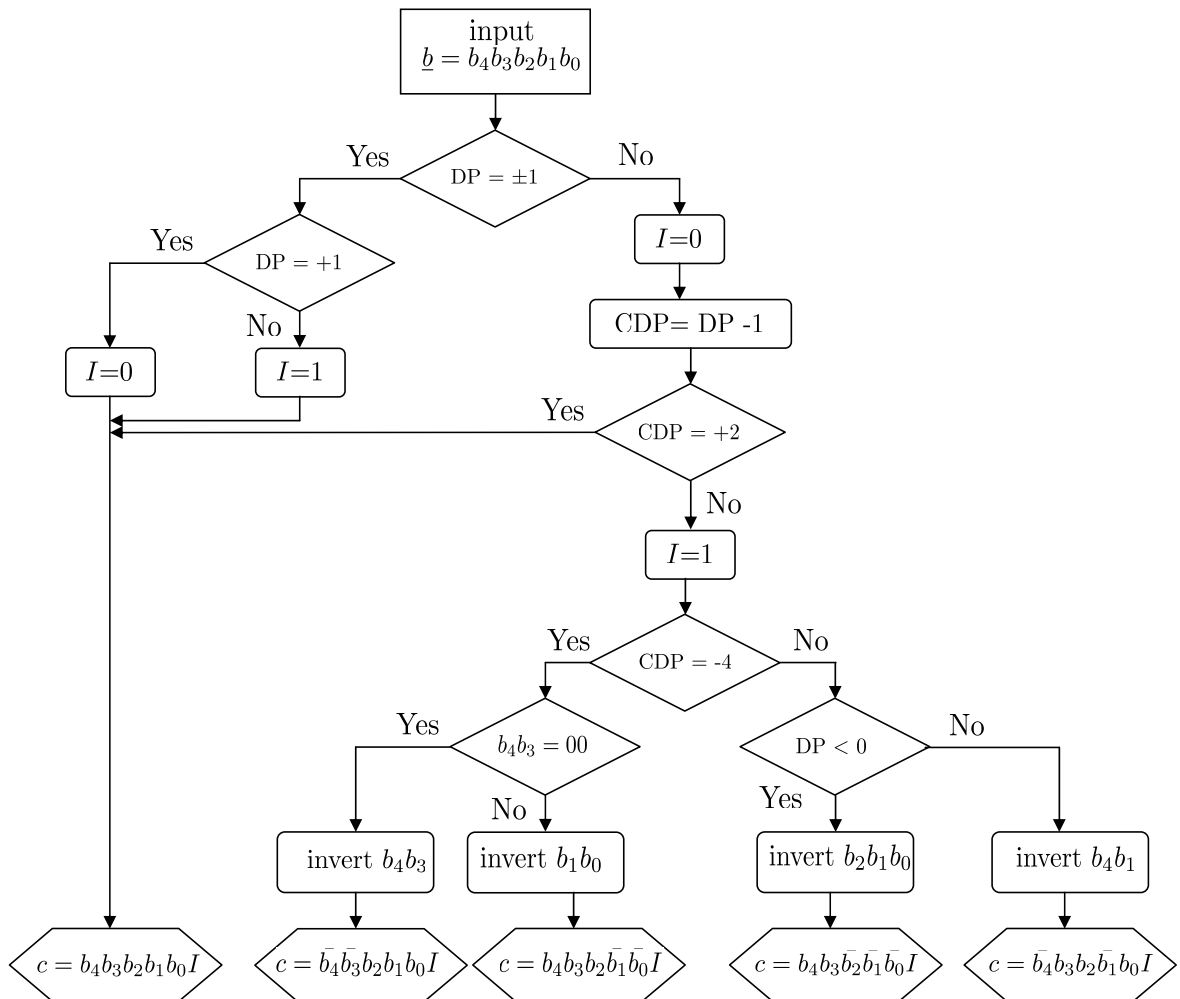


Figure 7.4.: BIM 5B6B encoder flowchart

the precoding codewords \mathbf{c} only require inversion if the polarity of the previous accumulated RDS differs from that of the current codeword disparity. This disparity rule is much simpler to implement than that of the IBM code mentioned before, where no complementary counterparts are required for zero-disparity codewords.

The 6B5B decoding procedure is an inverse process of encoding, as shown in the Fig. 7.5. The received 6-bit subblock is denoted as $c_5c_4c_3c_2c_1c_0$. First the codeword disparity is calculated.

(1) If $CDP = 0$, which corresponds to $DP = \pm 1$, the applied insertion bit c_3 is removed and the decoded information is $\hat{\mathbf{b}} = c_5c_4c_2c_1c_0$

(2) When $CDP < 0$, it means the codeword has already been inverted due to the rule of running disparity and needs to be inverted again. In the case of positive polarity, no inversion is required.

(3) After (2) finishes, the insertion bit c_3 value is examined.

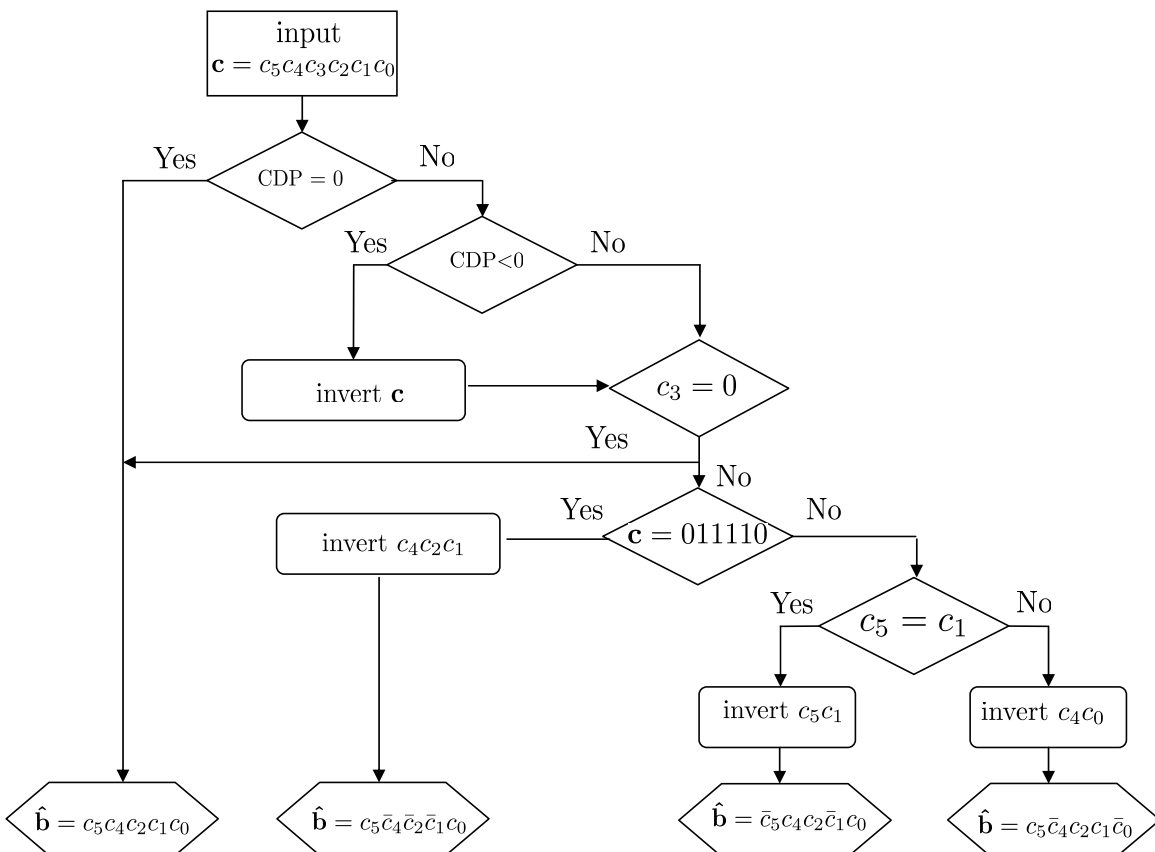


Figure 7.5.: Flowchart of CFBI 5B6B decoder

Table 7.3.: Precoding Table of CFBI 3B4B

Classification	$b_2b_1b_0$	DP	\mathbf{c}	CDP
Class 1 DP= $\pm 1, +3$ $\mathbf{c} = b_2b_1Ib_0$ $I = 1$ for DP= -1 $I = 0$ for DP= $+1, +3$	0 0 1	-1	0 0 1 1	0
	0 1 0	-1	0 1 1 0	0
	1 0 0	-1	1 0 1 0	0
	0 1 1	+1	0 1 0 1	0
	1 0 1	+1	1 0 0 1	0
	1 1 0	+1	1 1 0 0	0
	1 1 1	+3	1 1 0 1	+2
Class 2 DP= $-3, I=1$	0 0 0	-3	1 0 1 1	+2

- $c_3 = 0$ corresponds to the case that the original information data is mapped to a codeword with CDP = +2 only by a 0-bit insertion. Thereby only this insertion bit c_3 needs to be removed to retrieve the original information.
- If c_3 is found to be 1, the decoder firstly checks whether the obtained codeword \mathbf{c} is equal to (011110). If it is satisfied, $c_4c_2c_1$ are inverted after removing c_3 and the decoded data is $\widehat{\mathbf{b}} = c_5\bar{c}_4\bar{c}_2\bar{c}_1c_0$. When it is not the above case, c_5c_1 are examined to check if they are equal. The positive answer leads to the inversion of c_5c_1 and thereby the decoded data is $\widehat{\mathbf{b}} = \bar{c}_5c_4c_2\bar{c}_1c_0$. Regarding the other cases c_4c_0 are inverted to obtain decoded data $\widehat{\mathbf{b}} = c_5\bar{c}_4c_2c_1\bar{c}_0$.

The complexity of CFBI decoding is also lower than that of the BIM code not only due to the reduced demapping constraints but also as a result of the simplified bit inversion control.

A similar encoding and decoding process can also be realized for an CFBI 3B4B code shown in Table 7.3, so that it concatenates with the 5B6B code together to form a compound CFBI 8B10B line code for the sake of byte-orientation. It is emphasized that there is no alternate codeword included in this 3B4B code for concatenation purposes as in the IBM code, which also simplifies the implementation aspects.

Since only bit insertion and flipping as well as simple disparity control are required for encoding and decoding of this CFBI code, it would be much easier and faster than the IBM code in terms of hardware implementation.

7.2.3. Simulation Results

a) A first estimation is obtained by means of the short time average variation σ_N , where $N = 20$ corresponds to a time constant $\tau = 20 \cdot \frac{r_c}{R_b} = 20 \cdot \frac{1}{R_{\text{line}}}$. The parameter R_{line} denotes the data rate including line coding. The short time average variation σ_{20} is equal to 0.3 and 0.4 for the IBM and the CFBI code, respectively.

The parameter σ_N is only a measure of the minimum eye-opening $1 - \sigma_N$ at the sampling time. To obtain the statistics of the high-pass filter (HPF) output at the sampling time, a simulation needs to be performed. Fig. 7.6 shows the histogram for a HPF with the impulse

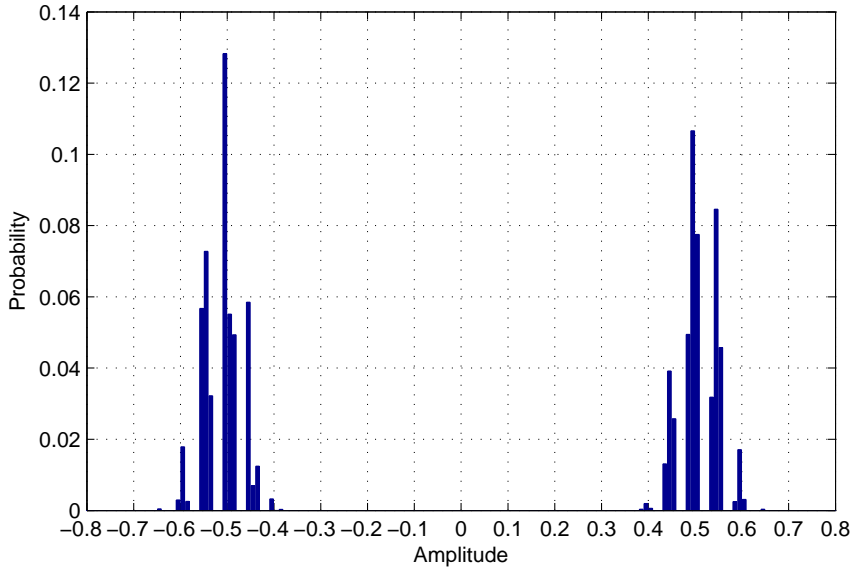


Figure 7.6.: Histogram of HPF output using IBM 8B10B

Table 7.4.: Comparison of IBM code and CFBI code

	σ_{20}	r_{\max}	DP control	decoding
IBM	0.3	4	complex	complex
CFBI	0.4	5	simple	medium

response $g(t) = \delta(t) - \text{rect}((t - \tau/2)/\tau)$ to obtain σ_N , where the IBM code is utilized. Although the rectangular transmit pulse shape is also incorporated into the simulation, the minimum eye opening indeed corresponds to our estimation of about $1 - \sigma_{20} = 0.7$.

b) Fig. 7.7 shows the simulated histograms, when a realistic first-order RC-HPF with the impulse response in (7.1) and a fifth-order Bessel low-pass filter are incorporated into the system, cf. Fig. 7.2. The Bessel filter is used for noise rejection, where a cut-off frequency $f_{3\text{dB}} = \frac{1}{2}R_{\text{line}}$ is selected to give a good compromise between noise rejection and the vertical eye-opening as discussed in Section 7.3. The time constant τ of the RC-HPF is chosen as the same in a), i.e., $\tau = 20/R_{\text{line}}$, which corresponds to $f_c = 0.008R_{\text{line}}$.

Fig. 7.7(a) shows the result without line coding. Fig. 7.7(b) and Fig. 7.7(c) illustrate the histograms for the IBM code and the CFBI code, respectively. Here, ± 0.5 denote the desired amplitudes in the absence of a baseline wander. From Fig. 7.7(a) it can be seen that the eye-diagram is almost closed when no line coding is applied. Fig. 7.7(b) and Fig. 7.7(c) show that the baseline wander effect is effectively suppressed if either the IBM code or the CFBI code is utilized. Actually, compared to the estimation of the minimum eye-opening using σ_{20} , a smaller eye-opening penalty is achieved. This is due to a longer total integration interval of the RC-HPF, which is about 3τ to 4τ .

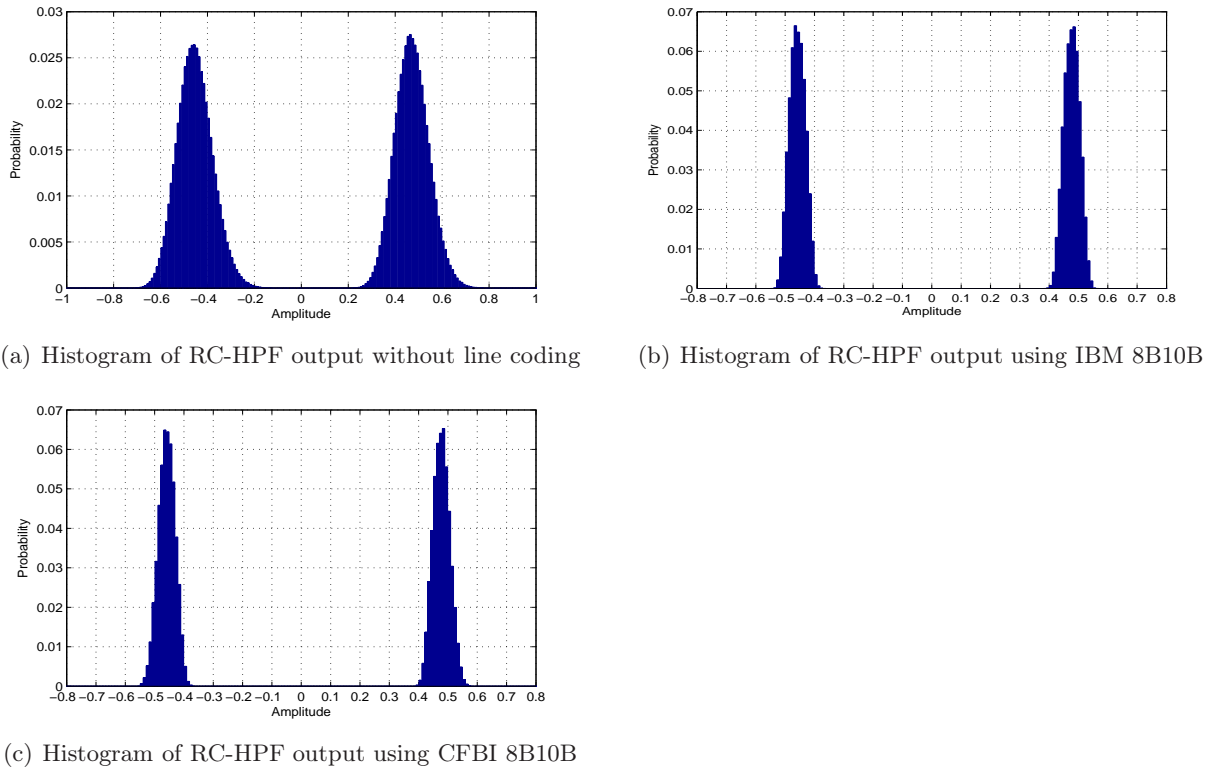


Figure 7.7.: Baseline wander reduction using line coding

Secondly, the IBM code has at least 30 transitions per 100 bits in the worst case while the CFBI code exhibits 20 transitions due to the maximum run-length constraint. Both of them have on the average 5 transitions per 10 bits, which ensures sufficient timing information for the receiver's clock recovery.

The bit error rate (BER) is another important property to judge the line code performance. The error propagation assuming a binary symmetric channel is investigated for both the IBM and the CFBI code. Fig. 7.8 shows that for both codes the output BER is approximately 2.5 times larger than the input BER.

In summary, Table 7.4 gives the comparison of these two proposed line codes.

To conclude this section, we proposed two DC-balanced line codes which are suitable for Gbps wireless infrared transmission. Both codes are byte-oriented and offer a comparable susceptibility to the transient baseline wander. Our results reveal that both codes ensure regular transitions from "1" to "0" or from "0" to "1", which is important from the clock recovery point of view. Both line codes are feasible in terms of hardware complexity. Due to the complicated mapping table, the IBM code can only be implemented via look-up table. In contrast to this, the novel CFBI code can either be implemented via look-up table or logic circuits because of its simple logic mapping.

7.3. Bessel filter

As shown in Fig. 7.2, a low-pass Bessel filter is required at the receiver of the Gbps infrared system for noise rejection.

The Bessel low-pass filter is characterized by the maximum flat group delay across the entire pass-band and near the cut-off frequency, which is usually applied for the noise rejection in an IR system. A high order Bessel filter is required so as to better approximate the constant group delay up to a desired frequency. However, it becomes also more difficult for this analog Bessel filter implementation as the filter order increases. In OMEGA, we choose a 5th order Bessel filter to perform noise rejection. Further, the choice of a proper 3 dB cut-off frequency (a frequency at which the magnitude of the transfer function of a low-pass filter is half of its pass-band value), denoted by $f_{3\text{dB}}$, plays a key role on the system performance since a compromise has to be balanced between the noise rejection and the induced inter-symbol-interference (ISI). It is shown in [OME10] that a 5th order Bessel filter with $f_{3\text{dB}} = R_{\text{line}}/2 = 625$ MHz provides a very good tradeoff between the vertical eye-opening and the noise rejection, where R_{line} denotes the data rate including the 8B10B line coding as introduced in Section 7.2. In this case, the ISI causes only 10 % degradation of the vertical eye-opening.

In theory, the transfer function of an ideal 5th order Bessel filter is given as

$$H_{\text{Bessel}}(f) = H_{\text{Bessel}}(p) \Big|_{p=j2\pi f}, \quad (7.2)$$

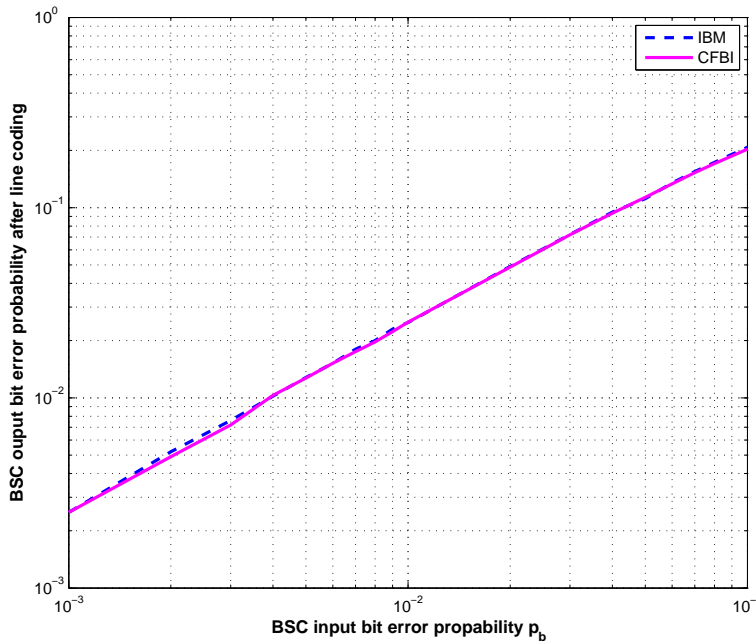
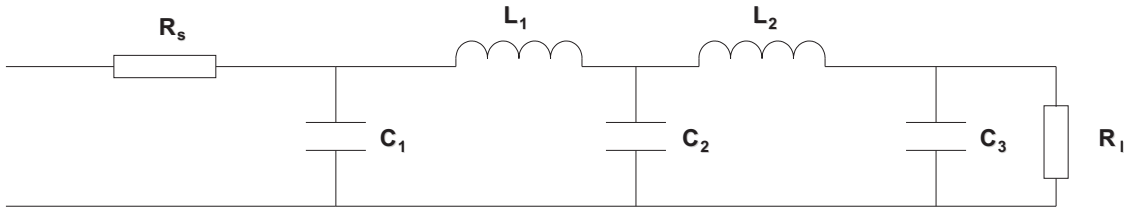
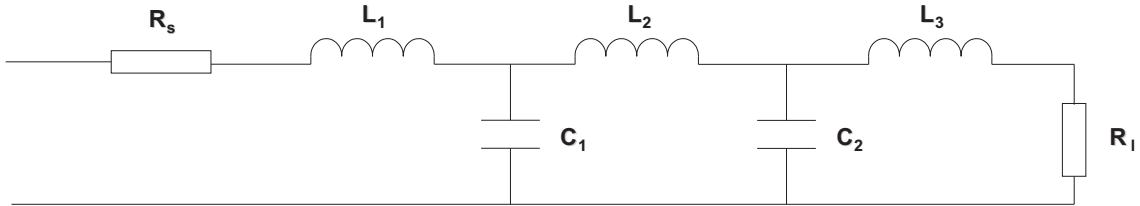


Figure 7.8.: BER comparison of IBM 8B10B and CFBI 8B10B

Figure 7.9.: 5th order Bessel filter configuration for $R_s \geq R_l$ Figure 7.10.: 5th order Bessel filter configuration for $R_s < R_l$

$R_s = R_l, R_l^* = 1$				
C_1^*	L_1^*	C_2^*	L_2^*	C_3^*
2.2582	1.1110	0.8040	0.5072	0.1743

Table 7.5.: normalized RLC-Values for $R_s = R_l$.

$R_s < R_l, R_l^* = 1$					
R_s/R_l	L_1^*	C_1^*	L_2^*	C_2^*	L_3^*
1/2	1.9039	1.0764	0.7836	0.4930	0.1690
1/4	1.7090	1.0493	0.7678	0.4820	0.1652
1/8	1.6102	1.0360	0.7598	0.4762	0.1634

Table 7.6.: normalized RLC-Values for $R_s < R_l$.

where $H_{\text{Bessel}}(p) = \frac{945}{p^5 + 15p^4 + 105p^3 + 420p^2 + 945p + 945}$ [Bes]. An ideal Bessel filter is an infinite impulse response (IIR) filter. In OMEGA, to approximate a 5th order Bessel filter with the 3 dB cut-off frequency $f_{3\text{dB}} = 625$ MHz, we use a passive RLC-network [Win02] consisting of resistances, inductances, and capacitors, as illustrated in Fig. 7.9 and Fig. 7.10. The parameters R_s and R_l denote the series resistance and the load resistance, respectively. If $R_s \geq R_l$, the LC ladder uses 3 capacitors and 2 inductors. If $R_s < R_l$, 3 inductors and 2 capacitors are utilized.

The RLC-values can be obtained from the filter catalogs. The normalized component values L^* , C^* which are indicated by an additional asterisk *, correspond to the normalization $R_l^* = 1$ and $2\pi f_{3\text{dB}} = 1$ Hz. The normalized RLC-values are given in Table 7.5 and Table 7.6, which discusses the cases $R_s = R_l$ and $R_s < R_l$ separately [Win02].

For a given 3 dB cut-off frequency $f_{3\text{dB}}$ and load resistance R_l , the denormalized values are

$R_s/R_l = 1, R_l = 50 \Omega$					
$f_{3dB}(\text{GHz})$	C_1	L_1	C_2	L_2	C_3
0.5	14.3762 pF	17.6821 nH	5.1184 pF	8.0724 nH	1.1096 pF
0.625	11.5010 pF	14.1457 nH	4.0948 pF	6.4578 nH	0.8878 pF

Table 7.7.: denormalized RLC-Values for $R_s = R_l$ assumed $R_l = 50 \Omega$.

$R_s/R_l = 1/8, R_l = 100 \Omega$					
$f_{3dB}(\text{GHz})$	L_1	C_1	L_2	C_2	L_3
0.5	25.6272 nH	6.5954 pF	12.0926 nH	3.0316 pF	2.6006 nH
0.625	20.5017 nH	5.2764 pF	9.6740 nH	2.4252 pF	2.0804 nH

Table 7.8.: denormalized RLC-Values for $R_s = 1/8 \cdot R_l$ assumed $R_l = 50 \Omega$.

given by

$$L_i = L_i^* \cdot \frac{R_l}{2\pi f_{3dB}}, \quad C_i = C_i^* \cdot \frac{1}{2\pi f_{3dB} R_l}.$$

Assuming $R_l = 50 \Omega$, Table 7.7 and Table 7.8 show the denormalized values for $R_s = R_l$ and $R_s = 1/8 \cdot R_l$.

With the LC values given in Table 7.7 and Table 7.8, the Bessel filter transfer function $H_{\text{Bessel}}(f)$ is acquired. Taking the case $R_s < R_l$ for example, $H_{\text{Bessel}}(f)$ is obtained as follows.

$$H_{\text{Bessel}}(f) = \frac{U_{\text{out}}}{U_{\text{in}}} = \frac{Z_l}{Z_5} \cdot \frac{Z_4}{Z_3} \cdot \frac{Z_2}{Z_1},$$

where

$$\begin{aligned} Z_1 &= Z_2 + jwL_1, \\ Z_2 &= \frac{1}{jwC_1 + \frac{1}{Z_3}}, \\ Z_3 &= Z_4 + jwL_2, \\ Z_4 &= \frac{1}{jwC_2 + \frac{1}{Z_5}}, \\ Z_5 &= R_l + jwL_3. \end{aligned}$$

The parameter w stands for the angular frequency and $w = 2\pi f$. The magnitude of the Bessel filter transfer function is plotted in Fig. 7.11. The ideal 5th order Bessel filter with cut-off frequency $f_{3dB} = 0.5 \cdot R_{\text{line}} = 625 \text{ MHz}$ is taken as a benchmark, which is drawn by using the besself function in MATLAB. In our approximation, R_l is kept 50Ω . It is noted that the setting of $R_s = R_l$ leads to a 6 dB loss in the pass band, which is not desirable. By adjusting $R_s = \frac{1}{8} \cdot R_l$, this loss is decreased to about 1 dB, which is a good approximation of an ideal 5th order Bessel filter.

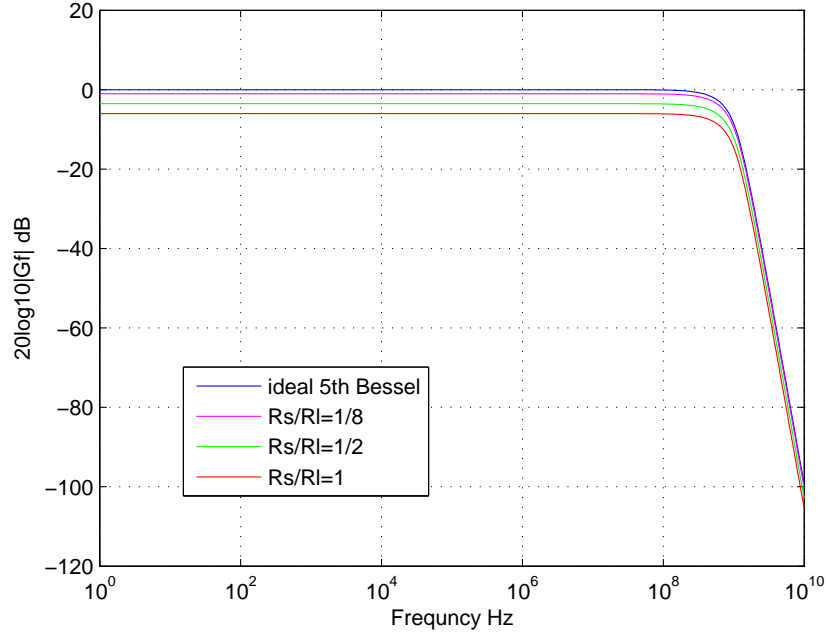


Figure 7.11.: 5th Order Bessel Filter transfer function

Using this transfer function, the noise power after the Bessel filter is calculated as

$$\sigma_n^2 = \int_0^{\infty} \Phi_{NN}(f) |H_{rx}(f)|^2 df, \quad (7.3)$$

where $\Phi_{NN}(f)$ represents the noise power density spectrum (PSD) and $H_{rx}(f)$ is the combination of the transfer function of the ideal preamplifier with $|H_{preamp}(f)| = 1$ and the Bessel filter $H_{Bessel}(f)$. As mentioned at the beginning of this chapter, in Gbps IR systems, the noise is divided into two categories. One is the white noise with constant PSD, which consists of the background light induced shot noise, signal induced shot noise, and the thermal noise caused by the preamplifier at the receiver frontend, denoted by N_{bg} , N_s , and N_0 , respectively. The other one is called f^2 noise with a PSD increasing with the square of the frequency that is generated by the preamplifier, denoted by $N_2 f^2$. Therefore, we write $\Phi_{NN}(f)$ as

$$\Phi_{NN}(f) = N_{bg} + N_s + N_0 + N_2 f^2. \quad (7.4)$$

Taking (7.4) into (7.3), it is further obtained that

$$\sigma_n^2 = \int_0^{\infty} N_0 |H_{rx}(f)|^2 df + \int_0^{\infty} N_2 f^2 |H_{rx}(f)|^2 df.$$

By substituting f into $f' = f/R_{line}$, the noise power is finally calculated as

$$\sigma_n^2 = N_0 R_{line} \underbrace{\int_0^{\infty} |H_{rx}(f')|^2 df'}_{I_2} + N_2 R_{line}^3 \underbrace{\int_0^{\infty} f'^2 |H_{rx}(f')|^2 df'}_{I_3},$$

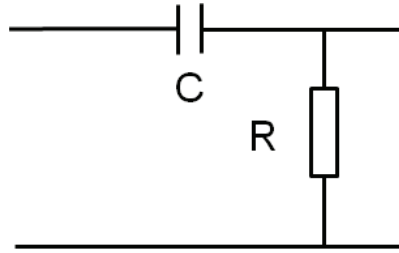


Figure 7.12.: First order high-pass filter

where I_0 and I_2 denote the Personick-integrals for the white noise and the f^2 noise respectively. Personick-integrals [Per77] are usually used in optical communications to indicate noise bandwidths. These integrals are denoted by I_2 and I_3 and are defined such that the input noise power can be written as $\sigma_n^2 = \alpha I_2 R_{\text{line}} + \beta I_3 R_{\text{line}}^3$, where α and β are constant values and R_{line} is the data rate including line coding. Considering a 5th order Bessel filter with $f_{3\text{dB}} = R_{\text{line}}/2$, there parameters are given as $I_2 = 0.52$ and $I_3 = 0.843$.

7.4. High-pass filter

At the receiver of the IR system, the photodiode is always connected with the preamplifier via coupling capacitors to block the DC photocurrent generated by the received ambient light as well as to remove the DC couplings between different stages of the preamplifier. This transmission characteristic is usually modeled as a first order RC high-pass filter, as shown in Fig. 7.12. Furthermore, this high-pass characteristic is also required to reduce harmonics caused by fluorescent lighting [SOSE98] since the electrical spectrum of the harmonics may extend up to 1 MHz in modern compact tubes with electronic ballasts [Bou96, NAK96].

The choice of the cut-on frequency f_c of the high-pass filter plays an important role on the Gbps wireless IR system. On one side, a large f_c is desired since it reduces the length of the training sequence required at the beginning of a transmission. However, if f_c is too high, it will induce significant inter-symbol-interference (ISI).

More explicitly, the channel impulse response of the high-pass filter is given as

$$h_{\text{HP}}(t) = \delta(t) - \frac{1}{\tau} e^{-\frac{t}{\tau}},$$

where $\tau = RC = 1/(2\pi f_c)$ denotes the time constant required for the settling down of a high-pass filter. The larger the f_c , the shorter the high-pass impulse response and thus the length of the training sequence. To show the ISI effect clearly, the combined impulse response of a first order high-pass filter and a 5th order Bessel filter with $f_{3\text{dB}} = /2$ introduced in Section 7.3 is depicted in Fig. 7.13. The amplitude of $\frac{1}{\tau}$, which is proportional to f_c , determines the fluctuations of the “tail” of the impulse response and thus the amplitude of the ISI, shown as the portion starting from $2 T_b$ to $20 T_b$ in Fig. 7.13. That means, the system may suffer from a severe ISI due to a large f_c . Therefore, it is critical to choose a proper f_c of the high-pass

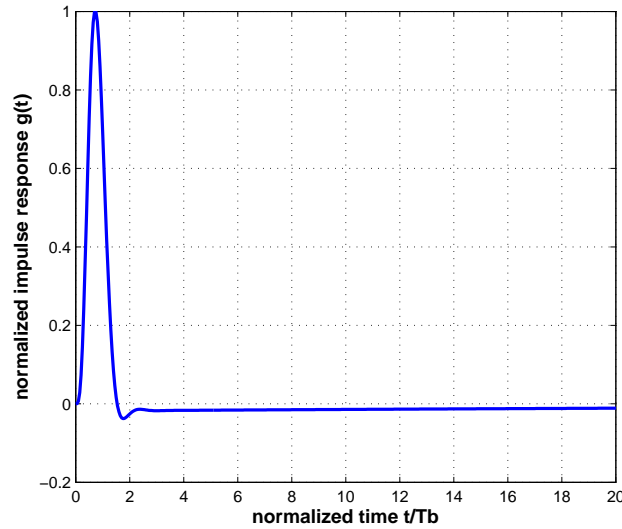


Figure 7.13.: Impulse response of the high-pass filter combined with the 5th order Bessel filter, $f_{3dB} = R_{line}/2 = 625$ MHz, $f_c = 0.004 \cdot R_{line} = 5$ MHz

filter compromising between the settling down time and the ISI. It is shown in [OME10] that a first order high-pass filter with $f_c = 0.004 \cdot R_{line}$ provides a very good tradeoff between the vertical eye-opening and the high-pass filter settling time, where the ISI causes only 10 % eye opening penalty combined with the Bessel filter and an 8 byte training sequence is required for the high-pass to settle down.

7.5. Photodiode for Gbps system

In an IR system, the wavelength at which the transmission takes place determines the choice of the individual components, especially for the choice of a photodiode. Further, it also affects the received noise power to a large extent, which is an important factor for achieving a reasonable link budget. In particular, the wavelength directly effects the quantum efficiency and the responsivity of a photodiode. Depending on the range of the wavelength, different photodiode materials can be used, which determine the photodiode capacitance and thus the power of the f^2 noise, as will be addressed in Section 7.6. Meanwhile, the spectral density of the received sun light that usually induces shot noise decreases as the wavelength increases. Therefore, the wavelength for a Gbps system must be carefully chosen, which plays a key role on the choice of the photodiode.

Two wavelength ranges are of particular interest for Gbps IR transmission. The range between 750 nm and 900 nm is especially suitable for the cheap and fast silicon (Si) photodiodes, which provide a reasonable quantum efficiency as well as a fast transit time of less than 1 ns. In addition to that, 1300 nm and 1500 nm are also alternatives since the permitted radiant intensity of the laser source is several times higher than that between 750 nm and 900 nm

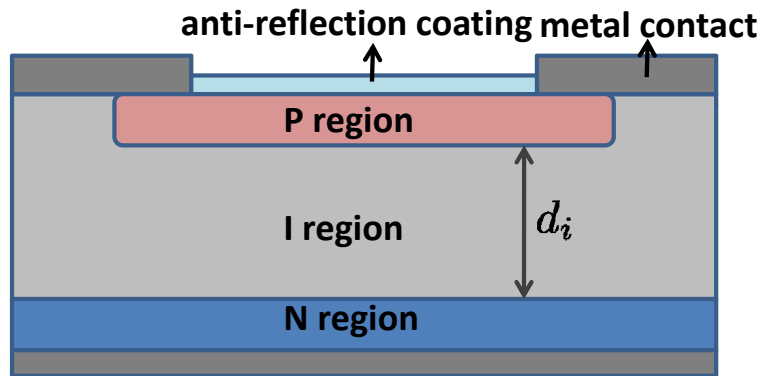


Figure 7.14.: PIN photodiode

from the eye safety point of view. Also the Indium-Gallium-Arsenic (InGaAs) photodiodes are available at these wavelengths with high quantum efficiency.

In addition to the wavelength dependent property, the requirement of achieving a satisfactory link budget for the Gbps IR system also pushes a harsh constraint on the photodiode choice. It is desired that the photodiodes used for Gbps transmission ensure a short rise time for fast response, exhibit a large detection area as well as a low capacitance for obtaining a high SNR, which is more related with the inherent property of the photodiodes depending on the component material. There is a trade-off to compromise these desired properties. Therefore, the parameters of the photodiodes need to be analyzed.

In this section, we will analyze and propose available photodiodes for Gbps IR systems. Two basic categories of photodiodes will be considered, including the positive-intrinsic-negative (PIN) photodiode and the Avalanche photodiode (APD), which are discussed subsequently.

7.5.1. PIN photodiode

Fig. 7.14 shows a typical PIN photodiode structure, which is simply a P-N junction diode. The PIN photodiode basically consists of 3 regions, P-region, N-region as well as the intrinsic region (I-region). Its most important parameters are listed in the following [WLG⁺10]:

- the quantum efficiency η

It describes the percentage of photons hitting the photodiode's surface that produce charge carriers. In the ideal case, which means no reflections on the surface, no carrier recombination, no carrier absorption in the upper P-region, the quantum efficiency η is given by

$$\eta = 1 - e^{-\alpha d_i}$$

where α is the wavelength dependent intensity absorption coefficient and it decreases with increasing wavelength. The parameter d_i denotes the thickness of the I-region.

- the diode responsivity R_λ

It measures the electrical output per optical input of a photodiode.

$$R_\lambda = \eta \frac{q\lambda}{hc} = \eta \frac{\lambda}{1.24 \mu\text{m}} \text{ A/W} \quad \text{for} \quad \lambda \leq \lambda_c$$

The parameter λ_c is the cutoff wavelength of the semiconductor and q , h , and c denote the elementary charge, the Planck constant, and the speed of light, respectively.

- capacitance C_D per area A_D

When the I-region is fully depleted, the diode capacitance per unit diode area C_D/A_D is given by

$$\frac{C_D}{A_D} = \frac{1}{d_i} \epsilon_0 \epsilon_r ,$$

where A_D is the active area of the photodiode and d_i is the thickness of the I-region. The constant ϵ_0 is the permittivity of free-space and ϵ_r is the relative permittivity of the semiconductor. For example, $\epsilon_r = 11.9$ for Si, 13.1 for InGaAs and 16 for Ge.

- the transit time

Assuming that photons are still absorbed just above the N-region, the maximum transit time τ_{max} is dominated by the slower holes and is given by

$$\tau_{\text{max}} = \frac{d_i}{v_h} ,$$

where v_h is the drift velocity of the holes that is proportional to the strength of the electrical field. That means, $v_h \sim \frac{U_{\text{bias}}}{d_i}$ with U_{bias} denoting the applied biased voltage and d_i the thickness of the I-region.

To summarize, the first two items are wavelength dependent while the latter two are determined by the thickness d_i of the I-region. Based on these parameters, several PIN photodiodes will be analyzed in the following.

(1) Si PIN photodiode

In order to achieve the 1 Gbps data rate, the transit time of the photodiode must be fast enough, which is usually constrained in the range of 0.4 ns \sim 0.8 ns. In order to fulfill such a requirement, the I-region thickness d_i of the Si PIN must be carefully chosen, which is usually designed varying from about 10 μm to a few hundreds micrometers. For example, we choose $d_i = 25 \mu\text{m}$ and a reverse voltage of 50 V is assumed. Then the strength of the electric field is obtained as 2 V/ μm , which gives the velocity of the 50 $\mu\text{m}/\text{ns}$, leading to the transit time 0.5 ns. Fig. 7.15 shows the maximum transit time and diode capacitance per unit area versus the I-region thickness for a reasonable biased voltage range $U_{\text{bias}} = 30 \text{ V} \dots 50 \text{ V}$. Due to the maximum transit time constraint, d_i is limited between 20 μm and 30 μm , which thereby restricts the capacitance per unit area C_D/A_D in the range 3.5 \sim 5 pF/(mm²). In the following, we choose $d_i = 25 \mu\text{m}$ and 30 μm , corresponding to $C_D/A_D = 4.2$ and 3.51 pF/(mm²), to further investigate the responsivity and quantum efficiency requirement for

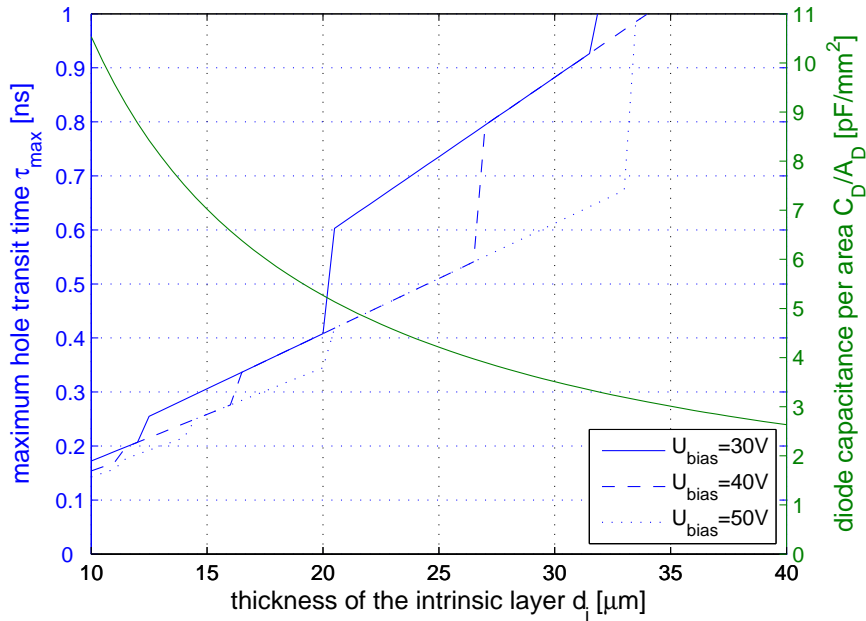


Figure 7.15.: Maximum transit time and diode capacitance per area versus the intrinsic layer thickness for Si PIN at reasonable biased voltages

Gbps IR transmission.

Another factor to be considered for diode choice is the responsivity R_λ , which is depending on the wavelength and d_i . Table 7.9 contains theoretical values for R_λ and η varying with wavelength with respect to some particular d_i and C_D/A_D . Because the quantum efficiency η decreases with λ , the useful wavelength range of such fast diodes is restricted to about 900 nm, where the responsivity falls off rapidly. As seen from Table 7.9, the peak responsivity is obtained between 750 nm and 780 nm.

To conclude, a Si PIN photodiode suitable for Gbps infrared transmission is desired to possess a C_D/A_D of less than 5 pF/mm 2 and a peak responsivity in the range of 750 ~ 780 nm, which are commercially available on the market. For a more practical case, a Si PIN with $C_D/A_D = 5$ pF/(mm 2) operating at 750 nm is considered for the link budget analysis in Chapter 8.

(2) InGaAs PIN photodiodes

As written in [WLG $^+$ 10], InGaAs devices exhibit a maximum possible thick I-region of 5 μm . Definitely it requires a much shorter transit time than Si PIN photodiode and fulfill the transit speed requirement. However, it means at the same time a much larger C_D/A_D , which will cause a much larger f^2 noise induced by the preamplifier as shown in Section 7.6. Theoretically, this InGaAs photodiodes with 5 μm thickness corresponds to a minimum possible capacitance of 23.2 pF/mm 2 . Typical InGaAs devices usually have a much larger capacitance per unit area of 60 pF/mm 2 [WLG $^+$ 10].

Table 7.9.: Theoretical parameters of Si photodiodes with transit times of less than 1 ns.

λ in nm	750	780	820	850	880	900
$1/\alpha$ μm	7.7	9.9	14.1	18.7	26.1	32.7
Si PIN-photodiode with $d_i = 30 \mu\text{m}$						
C_D/A_D in pF/mm ²	3.51					
η	0.98	0.95	0.88	0.80	0.68	0.60
R_λ in A/W	0.59	0.60	0.58	0.55	0.48	0.43
Si PIN-photodiode with $d_i = 25 \mu\text{m}$						
C_D/A_D in pF/mm ²	4.2					
η	0.96	0.92	0.83	0.74	0.62	0.53
R_λ in A/W	0.58	0.58	0.55	0.50	0.44	0.39

Concerning the responsivity, InGaAs may have $R_{1.3\mu\text{m}} \approx 1$ A/W at 1300 nm, which is almost twice as large as $R_{850\text{nm}}$ for Si PIN. In addition to that, another advantage of using 1300 nm over 750 nm is that there is a much lower sunlight induced noise power at this wavelength, as shown in Section 7.6, which supports the InGaAs photodiodes as a candidate operating at higher wavelengths for high-speed infrared transmission. The typical responsivity range of the InGaAs photodiodes is from about 0.6 A/W to 0.9 A/W [Agr05]. For link budget estimation, we take 0.8 A/W for 1300 nm and 0.95 for 1550 nm.

7.5.2. Avalanche photodiode (APD)

As shown in [WLG⁺10], a PIN-diode based detector operating at 1 Gbps will be limited by f^2 noise and not by the background light induced shot noise. For this reason, the receiver sensitivity can be increased by utilization of APDs. An important characteristic of APDs is the excess noise, which is characterized by the excess noise factor $F(M)$ given by [Agr05]

$$F(M) = M^{x_{\text{APD}}},$$

where M is the average multiplication gain that ranges from 1 to 100. Typical values of x_{APD} are given in Table 7.10.

7.6. Noise

The noise for the infrared system may come from the received background light, which will lead to shot noise as well as low frequency interference induced by fluorescent light or incandescent light. Another important source is the preamplifier frontend, which generates thermal noise with constant power density spectrum (PSD) as well as the f^2 noise whose PSD increases with the square of the frequency. The received signal itself will also contribute to the shot noise. In the following, we will specify each type of noise in the Gbps infrared system.

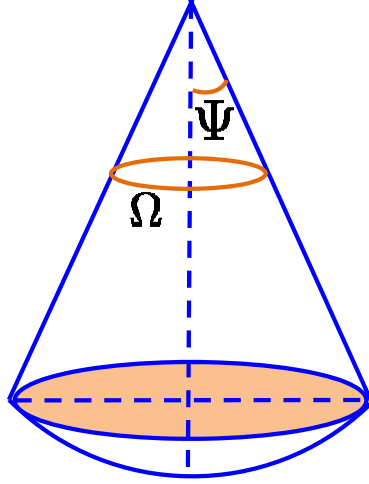


Figure 7.16.: Illustration of the solid angle

7.6.1. Shot noise

(1) Background light induced shot noise

The PSD of the background light induced shot noise N_{bg} depends directly on the received optical power P_{bg} of the background light, shown as follows

$$N_{\text{bg}} = 2qR_{\lambda}P_{\text{bg}}M^2F(M),$$

where R_{λ} , M and $F(M)$ denote the photodiode responsivity, multiplication gain, and the excess noise factor, respectively. The constant q is the electronic charge. The optical power $P_{\text{bg}}(\lambda)$ is calculated as follows.

$$P_{\text{bg}}(\lambda) = \int_0^{\Omega_{\text{rx}}} L_{\text{bg}}(\lambda)A_{\text{rx,eff}}d\Omega, \quad (7.5)$$

where $L_{\text{bg}}(\lambda)$ is the irradiance of the received background light and $A_{\text{rx,eff}}$ is the effective detector area within the receiver solid angle Ω_{rx} . Given a random solid angle $\Omega \in [0, 4\pi]$ sr and its corresponding colatitude $\Psi \in [0, 2\pi]$, as shown in Fig. 7.16, we have $\Omega = 2\pi(1 - \cos\Psi)$ and thus $d\Omega = 2\pi\sin\Psi d\Psi$. The notation *sr* stands for steradian, which is a measure of the solid angle. Moreover, the effective detector area is $A_{\text{rx,eff}} = A_{\text{rx}}\cos\Psi$. Therefore, denoting the colatitude of the receiver field-of-view (FOV) as Ψ_{rx} , (7.5) can be further manipulated as

$$\begin{aligned} P_{\text{bg}}(\lambda) &= \int_0^{\Psi_{\text{rx}}} L_{\text{bg}}(\lambda)A_{\text{rx}}\cos\Psi \cdot 2\pi \cdot \sin\Psi d\Psi \\ &= 2\pi L_{\text{bg}}(\lambda)A_{\text{rx}} \int_0^{\Psi_{\text{rx}}} \sin\Psi \cos\Psi d\Psi \\ &= L_{\text{bg}}(\lambda)A_{\text{rx}}\sin^2(\Psi_{\text{rx}})\pi. \end{aligned} \quad (7.6)$$

A value of $2 \mu\text{W}/(\text{mm}^2 \cdot \text{sr})$ is chosen according to [DK00] as the typical $L_{\text{bg}}(\lambda)$ at $\lambda = 850 \text{ nm}$, assuming the background light noise is dominated by the diffuse skylight and the receiver incorporates an optical filter with 50 nm bandwidth. Based on the model in [RG98], the wavelength dependent irradiance of the sunlight can be modeled as a thermal radiator operating at the temperature 5500 K , which is calculated according to Planck's law

$$L_{\text{bg}}(\lambda) = \frac{8\pi hc}{\lambda^5 (e^{\frac{hc}{\lambda k_B T}} - 1)}.$$

The constant is calculated as $hc/(k_B T) = 2.619 \cdot 10^{-6}$, where h , c , K_B , and T denote the Planck constant, the speed of light, the Boltzmann constant, and the absolute temperature, respectively. Due to this wavelength dependence, an estimate of $2.44 \mu\text{W}/(\text{mm}^2 \cdot \text{sr})$ is obtained for $L_{\text{bg}}(\lambda)$ at $\lambda = 750 \text{ nm}$ and the irradiance is about a factor 3.19 and 5.23 times less at 1300 nm and 1550 nm , as shown in Table 7.10. As for the detector area A_{rx} , we calculate it as

$$A_{\text{rx}} = A_{\text{D}} \frac{n_c^2}{\sin^2(\Psi_{\text{rx}})},$$

where A_{D} is the actual photodiode area and $n_c = 1.5$ is assumed for the refraction index of an ideal concentrator, which restricts the receive field of view assuming the use of a lossless optical filter.

(2) Signal shot noise

The PSD of the signal shot noise N_s is a function of the peak received signal power \widehat{P}_{rx} , i.e.,

$$N_s = 2qR_\lambda \widehat{P}_{\text{rx}} M^2 F(M),$$

For NRZ OOK modulation scheme, $\widehat{P}_{\text{rx}} = 2P_{\text{rx}}$ with P_{rx} denoting the average received signal power. Then the receive SNR ϱ is obtained as

$$\varrho = \frac{(R_\lambda P_{\text{rx}} M)^2}{N_s I_2 R_{\text{line}} + \sigma_n'^2}, \quad (7.7)$$

where $\sigma_n'^2$ represents the noise power excluding the power of the signal shot noise. $\sigma_n'^2 = N_{\text{bg}} I_2 R_{\text{line}} + N_0 I_2 R_{\text{line}} + N_2 I_3 R_{\text{line}}^3$ with N_{bg} , N_0 and N_2 denoting the PSD of the background light induced noise, preamplifier thermal noise, and the preamplifier f^2 noise, separately.

It is clear from (7.7) that the SNR ϱ is a quadratic function of P_{rx} , the solution is given as

$$P_{\text{rx}} = -\frac{a}{2} + \sqrt{\left(\frac{a}{2}\right)^2 - b},$$

where $a = -\varrho 4qF(M) I_2 R_{\text{line}} / R_\lambda$ and $b = -\varrho \sigma_n'^2 / (R_\lambda M)^2$.

7.6.2. Preamplifier frontend noise

In addition to the shot noise, there are two types of noise caused by the preamplifier frontend. One is the thermal noise with constant power density spectrum (PSD), denoted as N_0 . The other one is called the f^2 noise whose PSD increases with the square of the frequency, denoted by N_2 . The constants N_0 and N_2 are given as follows [Muo84]

$$N_0 = 2qI_b + \frac{4k_B T}{R_L},$$

$$N_2 = \frac{2qI_c(2\pi C_{\text{tot}})^2}{S^2} + 4k_B T(R_{\text{bb}} + R_s)(2\pi C_D)^2.$$

- q electronic charge; k_B Boltzmann constant; T absolute temperature
- I_c collector current of the bipolar junction transistor (BJT); $I_b = I_c/\beta$ base current with β denoting the current gain
- C_D photodiode capacitance; $C_{\text{tot}} \approx C_D$ the total capacitance at the first stage of the preamplifier
- R_L load resistor; $R_{\text{bb}} + R_s$ sum of the photodiode series resistance and the BJT spreading resistance

The total PSD of the noise is calculated as

$$\Phi_{NN}(f) = N_{\text{bg}} + N_s + N_0 + N_2 f^2. \quad (7.8)$$

The parameter values used for the link budget analysis are summarized in Table 7.10. Si as well as InGaAs photodiodes are utilized operating at 800 nm, 1300 nm, and 1550 nm, respectively. A Si PIN diode with $C_D/A_D = 5$ pF/(mm²) is considered while 60 pF/(mm²) is taken into account for InGaAs photodiodes. An optical bandpass filter with the spectral width of 50 nm is assumed.

7.6.3. Artificial light

In addition to the previously mentioned noise, there is also artificial light induced interference, which is addressed in this subsection.

The fluorescent lights with conventional, electromagnetic ballasts contain the electrical spectrum up to 500 kHz [Bou96]. In modern compact tubes with electronic ballasts, the electrical spectrum of the harmonics may extend up to 1 MHz [NAK96]. This may be an issue if transmission at about 750 nm is considered, since the optical spectrum still contains significant energy in contrast to transmission at 1300 or 1550 nm. However, [Bou96] investigated that this interference can be reduced by about 60 dB, if the receiver uses a high-pass filter with a cut-on frequency of 500 kHz. Thereby, the low-frequency interference induced by the artificial light is skipped due to the application of the high-pass filter.

Table 7.10.: Parameters used for link budget analysis

bit rate R_{line} (Mbit/s)	1250	
bit error rate p_b	10^{-9}	
receiver FOV (half cone angle) ϕ (°)	5	
photodiode	Si	InGaAs
wavelength (nm)	800	1300
capacitance per area C_D/A_D (pF/mm ²)	5	60
responsivity R_λ (A/W)	0.5	0.8
APD gain M	optimized between 1 and 100	
APD excess noise factor exponent x_{APD}	0.3	0.7
refraction index n_c	1.7	
background light radiance $L_{\text{bg}}(\lambda)$ ($\mu\text{W}/(\text{mm}^2 \cdot \text{sr} \cdot \text{nm})$)	0.0443	0.0443/2.9
optical filter bandwidth δ_λ (nm)	10	
absolute temperature T (K)	330	
collector current I_c (mA)	optimized between 0.5 mA and 5 mA	
current gain β	180	
feedback resistance R_L (Ω)	$10 \text{ k}\Omega \cdot 1\text{pF}/C_D$	
series resistance $R_{\text{bb}} + R_s$ (Ω)	10	
Personick integrals	$I_2 = 0.502, I_3 = 0.0843$	

To summarize this section, assuming a BJT-based input stage, the noise variance σ_n^2 after the 5th order Bessel filter with $f_{3\text{dB}} = R_{\text{line}}/2$ is given as [Muo84]

$$\begin{aligned}
\sigma_n^2 = & \underbrace{\left(\underbrace{2q(P_{\text{bg}} + 2P_{\text{rx}})R_\lambda M^2 F(M)}_{\text{shot noise } \sigma_{\text{bg}}^2 + \sigma_s^2} + \underbrace{2qI_b + \frac{4k_B T}{R_L}}_{\text{preamp white noise } \sigma_w^2} \right)}_{\text{white noise}} I_2 R_b + \\
& \underbrace{\left(\frac{2qI_c(2\pi C_{\text{tot}})^2}{S^2} + 4k_B T(R_{\text{bb}} + R_s)(2\pi C_D)^2 \right)}_{\text{preamp } f^2 \text{ noise } \sigma_{f^2}^2} I_3 R_b^3. \tag{7.9}
\end{aligned}$$

8. Link Budget

Based on the system model introduced in Chapter 7, the link budget for Gbps infrared (IR) transmission is investigated in this chapter. In Section 8.1, the receiver sensitivity limits for both PIN diodes and Avalanche photodiodes (APDs) are first discussed and different types of noise dominate for PINs and APDs in Gbps IR transmission. Then the link budget is calculated for both PINs and APDs operating on different wavelengths in Section 8.2.

8.1. Receiver sensitivity limit with PIN and APD for Gbps transmission

For a non-return-to-zero on-off keying NRZ-OOK based scheme, the bit error ratio (BER) p_b can be expressed as a function of the signal-to-noise ratio (SNR) ϱ [Pro00] for the additive Gaussian channel

$$p_b = \frac{1}{2} \operatorname{erfc}\left(\sqrt{\frac{\varrho}{2}}\right) \quad \text{with} \quad \varrho = \frac{(d_{\text{eucl}}/2)^2}{\sigma_n^2},$$

where d_{eucl} is the Euclidian distance of the signal constellation and σ_n^2 denotes the total noise variance. Assuming NRZ-OOK based on rectangular pulses with an average optical power P_{rx} at the receiver, the Euclidian distance is

$$d_{\text{eucl,ideal}} = 2P_{\text{rx}}R_\lambda M.$$

The parameter R_λ is the photodiode responsivity in A/W and M is the multiplication gain (APD gain) with $M = 1$ for the positive-intrinsic-negative layer (PIN) photodiodes and M ranges from 1 to 100 for typical APDs, respectively. The total noise σ_n^2 is given in (7.9).

For the Gbps line of sight (LOS) transmission, a Lambertian source with a radiant intensity of $I(\theta) = (n+1)/(2\pi) \cdot \cos^n(\theta)$ is assumed, where $n = \ln(0.5)/\ln(\cos\theta_{\text{HP}})$ with θ_{HP} denoting the half power angle. For the receiver located at distance d with receive angle ϕ_{rx} , the irradiance is $P_{\text{tx}}I(\theta)/d^2$. The received power is thereby obtained as follows

$$\begin{aligned} P_{\text{rx}} &= P_{\text{tx}}I(\theta) \frac{A_{\text{rx}}}{d^2} \\ &= P_{\text{tx}} \frac{n+1}{2\pi} \cos^n(\theta) \frac{A_{\text{rx}}}{d^2} \\ &= P_{\text{tx}} \frac{n+1}{2\pi} \cos^n(\theta) \frac{1}{d^2} \frac{n_c^2}{\sin(\phi_{\text{rx}})^2} A_{\text{D}}, \end{aligned} \quad (8.1)$$

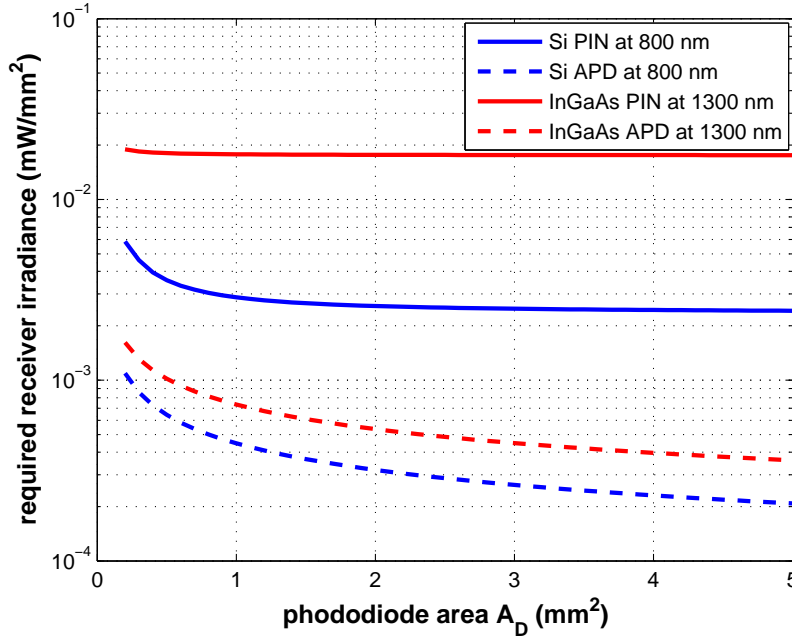


Figure 8.1.: Required receiver irradiance with the photodiode area

where n_c denotes the refraction index of the concentrator. From (8.1) we see that the receiver irradiance P_{rx}/A_D can be deemed as a preliminary measure of the required transmitter power. In the following, we will estimate P_{rx}/A_D analytically for PIN and APD photodiodes.

For a given bit error probability p_b , the corresponding SNR is proportional to the following factor,

$$\varrho \sim R_\lambda^2 \frac{P_{\text{rx}}^2}{\sigma_n^2}.$$

The total noise variance $\sigma_n^2 \approx \sigma_{\text{bg}}^2 + \sigma_w^2 + \sigma_{f^2}^2$, where the signal shot noise variance σ_w^2 can be skipped since it is quite small. In the following, we analyze two cases separately. On one hand, if the f^2 -noise dominates, whose variance is proportional to C_D^2 , then the SNR is proportional to the following factor,

$$\varrho \sim R_\lambda^2 \frac{P_{\text{rx}}^2}{C_D^2} = R_\lambda^2 \left(\frac{P_{\text{rx}}}{A_D} \right)^2 \cdot \left(\frac{A_D}{C_D} \right)^2.$$

Since C_D/A_D is a constant as soon as the photodiode is manufactured, the required receiver irradiance P_{rx}/A_D is more or less unchanged when the photodiode area increases. On the other hand, we consider the case that the white noise dominates, which consists of the background light induced shot noise as well as the white noise caused by the preamplifier. The variance of the background light induced shot noise is proportional to A_D , $\sigma_{\text{bg}}^2 \sim P_{\text{bg}} \sim A_D$. Meanwhile, the main part of the preamplifier white noise is also proportional to A_D , $\frac{4k_B T}{R_L} \sim C_D = (C_D/A_D) \cdot A_D \sim A_D$. Then the SNR is depending on the following factor,

$$\varrho \sim R_\lambda^2 \frac{P_{\text{rx}}^2}{A_D} = R_\lambda^2 \left(\frac{P_{\text{rx}}}{A_D} \right)^2 \cdot A_D.$$

As the photodiode area increases by 4 times, the required $P_{\text{rx}}/A_{\text{D}}$ is decreased by a factor of two, which indicates a 3 dB gain.

Fig. 8.1 shows the required irradiance at the receiver $P_{\text{rx}}/A_{\text{D}}$ in mW/mm^2 as a function of the photodiode area A_{D} with respect to Si and InGaAs photodiodes separately, using the parameters in Table 7.10. All the noise sources, including the ambient light induced shot noise, signal shot noise as well as the preamplifier noise, are incorporated into our analysis.

Let us first focus on the performance of PIN diodes, which are plotted in solid lines. It shows that an increase of A_{D} brings almost no gain with respect to the required receiver irradiance. It clearly illustrates that the PIN photodiodes are f^2 -noise limited as analyzed in the first case above. Thereby, the gain due to the increased area of the photodiode is almost compensated by the increased f^2 -noise, whose power increases rapidly with the increasing photodiode area A_{D} . Furthermore, as observed from Fig. 8.1, there is around 3 dB gain when increasing the photodiode area from 1 mm^2 to 4 mm^2 for APDs, which verifies that the APDs are constrained by the white noise. Moreover, when comparing the receiver irradiance of InGaAs PIN to Si PIN, InGaAs diodes have 12 times larger capacitance per unit area $C_{\text{D}}/A_{\text{D}}$ than Si PIN while it exhibits a $0.8 \text{ (A/W)} / 0.5 \text{ (A/W)} = 1.6$ times larger responsivity. Thereby, there is around a factor of $12/1.6$, i.e., 8.8 dB loss with respect to the required receiver irradiance, which is observed in Fig. 8.1. For APDs, Si still outperforms its InGaAs counterpart due to the much larger $C_{\text{D}}/A_{\text{D}}$.

To summarize, PIN photodiodes are mainly limited by f^2 -noise for Gbps transmission while the receiver sensitivity of APDs are constrained by the white noise. Si outperforms its InGaAs counterpart and is a good choice for Gbps infrared transmission.

8.2. Link budget for Gbps transmission

In this section, we will investigate the real link budget applying both PINs and APDs for Gbps infrared system. Let us first take a look at Si PIN operating at 800 nm for 1 m LOS link configuration, where a single transmitter and single receiver are perfectly aligned to each other. Both transmitter and receiver are assumed to have 5° half power angle. The 8B10B line coding scheme is incorporated into the system and all the noise sources are taken into account. A typical background light radiance of $L_{\text{bg}} = 0.0443 \text{ } \mu\text{W}/(\text{mm}^2 \cdot \text{sr} \cdot \text{nm})$ at 800 nm is adopted as demonstrated in Section 7.6.1. Further simulation parameters can be found in Table 7.10. Around 7 (mW/sr) is observed for Si PIN for establishing a 1 m Gbps LOS link as shown in Fig. 8.2. There is hardly any difference when increasing the photodiode area since the PIN photodiode is f^2 -noise limited.

Since the f^2 -noise caused by the preamplifier dominates in PIN-based receivers operating at 1 Gbps, APDs may offer a performance improvement, which depends on the excess noise factor $F(M)$ of the APD, the received amount of background light P_{bg} and the amount of the residual preamplifier noise. The blue solid curve gives the require radiant intensity for Si APD. We assume that the optimum APD gain M_{opt} is selected in the range between 1 and

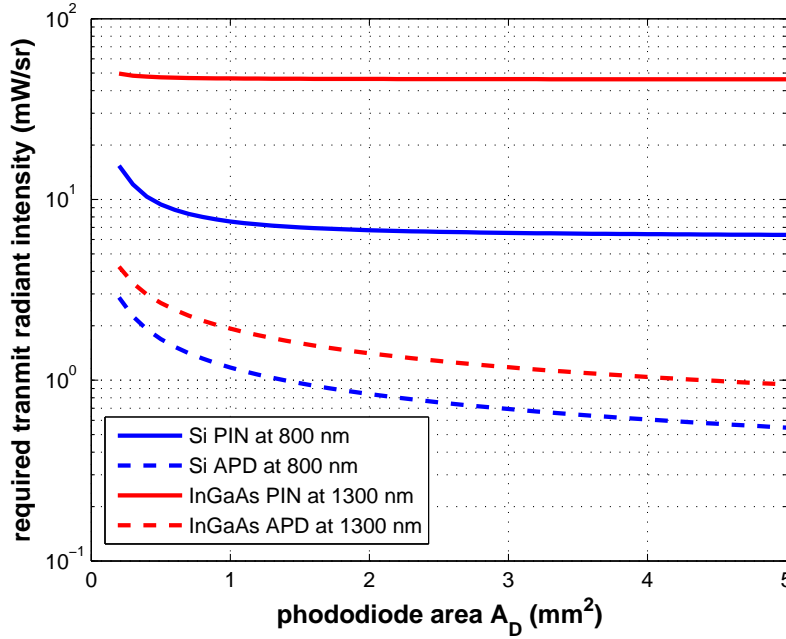


Figure 8.2.: Required radiant intensity with the photodiode area to obtain a 1 m LOS link, $C_D/A_D = 60\text{pF}/(\text{mm}^2)$ for InGaAs diodes

100. Compared to Si PIN, the required radiant intensity of Si APD is decreasing with an increased photodiode area and it would offer around 10 dB gain for $A_D = 5 \text{ mm}^2$.

The required radiant intensity of InGaAs photodiodes are plotted in red curves in Fig. 8.2, where a capacitance per unit area of $60 \text{ pF}/(\text{mm}^2)$ is assumed. As seen from Fig. 8.2, InGaAs PIN has around 9 dB loss due to a much larger C_D/A_D compared to Si PIN. Furthermore, InGaAs APD does not outperform its Si counterpart although it has a higher responsivity R_λ and a reduced background light induced irradiance L_{bg} at 1300 nm. In other words, there is not any advantage of InGaAs APD over Si APD, although its price is much higher. Therefore, Si APD would definitely be a good choice for Gbps infrared transmission.

The result in Fig 8.2 can be easily extended to the link budget estimation for larger distances d by a further $20 \cdot \log_{10}|d|$ dB loss. In the simulation, we assume that the transmitter and receiver are aligned both on-axis. If either the transmitter or receiver is operating in the half-power-angle instead of on-axis, there is a 3 dB further loss compared to the on-axis case.

To conclude, two statements are obtained. On one side, Si APD exhibits around 6 dB gain on the average compared to a Si PIN. On the other side, an InGaAS APD counterpart operating at 1300 nm cannot outperform a Si APD receiver operating at about 750 nm, if the same photodiode area A_D is considered.

Fig. 8.3 gives the receiver sensitivity to obtain a 1 m LOS IR link. The simulation parameters can be found in Table 7.10. It can be seen that the required receive power increases with the photodiode area due to the rapidly increasing f^2 noise in Gbps IR transmission. The PIN

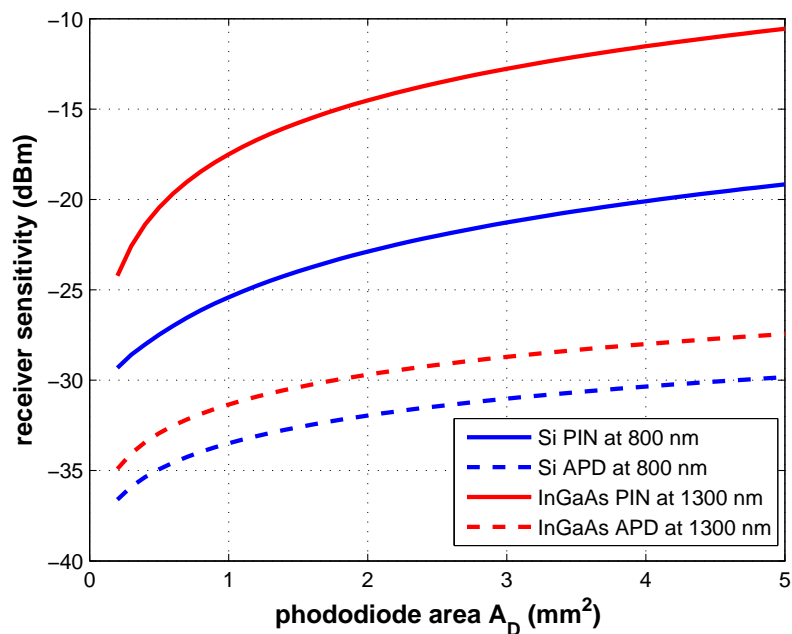


Figure 8.3.: Receiver sensitivity to obtain a 1 m LOS link,

photodiode does not outperform APDs and there exists around 8 dB loss when comparing InGaAs PIN to Si PIN. Furthermore, APDs offers further improvements while the Si APD gives the best performance. Therefore, the Si APD is strongly recommended for Gbps infrared systems.

9. Angle Diversity

As described in Chapter 8, a reasonable link budget is achievable for Gbps IR transmission, where both the transmitter and the receiver have narrow half power angles. A half power angle of 10° ¹ is used for our investigation. With seven laser diodes at the transmitter and seven APDs at the receiver at hand, an approximate 30° system FOV can be obtained. However, it is impossible to fulfill a 90° system FOV requirement by using these 7×7 system configuration. Thereby, a 30° half power angle for each transmitter and receiver element is proposed for further increasing the angular coverage, which definitely demands much more transmit power if the data rate R_b and the photodiode area A_D remains the same. In this chapter, we first illustrate the seven elements arrangement in Section 9.1 in order to achieve a 90° FOV. Based on this multi-element configuration, the transmit and receive gain is analyzed compared to a single transmitter and receiver with a wide angle and the link establishment process is analyzed in Section 9.2. Then depending on the different transmission phases for the link establishment, the required transmit radiant intensity is presented and a preliminary analysis on the challenges of achieving a large FOV in Gbps IR transmission is illustrated for a typical room in Section 9.3. Finally, the demonstrator of OMEGA project is briefly introduced in Section 9.4, which has been built by our project partner University of Oxford based on our physical layer design.

9.1. Multi-element configuration

Angle diversity in IR transmission is attainable via either a multi-element or an imaging transmitter and receiver. Due to the limited resources within OMEGA to fabricate the devices for imaging transceivers, we choose to use a multi-element transmitter and receiver, where each laser diode and APD has its own optics. It is assumed that each transmitter and receiver element exhibits a generalized Lambertian beam profile with a half power angle of 30° . Seven transmitter and receiver elements are used for demonstration. The elements are arranged as shown in Fig. 9.1. A central element points straight up. All the other 6 neighboring elements, each having an elevation of 30° compared to the central element, are separated by 60° in azimuth. To be more specific, the configuration is shown in Fig. 9.2, including two elements with 30° elevation as well as a central element each represented by an arrow. According to the law of cosine, it can be calculated that the angle between these two elements is less than 30° (marked in green), which ensures that the radiant intensity is always larger than half of the

¹All the angles mentioned throughout this chapter are full cone angles.

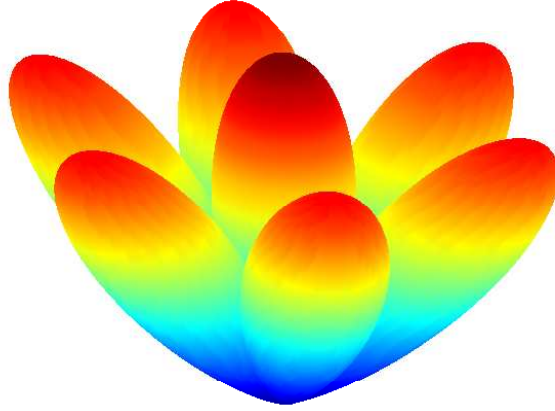


Figure 9.1.: Visualization of the transmit and receive beam pattern with 7 elements

peak value even at the edge between any two elements. The radiant intensity distribution is given in Fig. 9.3. The colorbar provides the normalized radiant intensity to the peak value of a single transmitter element. It can be larger than one in the middle area due to the overlap between the seven transmitter elements. It clearly verifies that the obtained radiance intensity is never less than half of the peak, even between the element edges. In the following, the advantage of using the 7 narrow angle elements configuration are addressed instead of a single transmitter and receiver element with a wide angle, in terms of the transmit and receive power gain, respectively.

Concerning the transmit power gain, a Lambertian source with a radiant intensity of $I(\theta) = I_0 \cos^n(\theta)$ is assumed, where $I_0 = P_{\text{tx}}(n+1)/(2\pi)$ denote the maximum radiant intensity at $\theta = 0$ and the order $n = \ln(0.5)/\ln(\cos\theta_{\text{HP}})$ with θ_{HP} denoting the half power angle. As shown in Fig. 9.4, by taking θ_{HP} as a reference, the transmitter power gain becomes larger with a decreasing θ_{HP} . When switching θ_{HP} from 45° to 15° , n varies from around 2 to 20 and there is a factor 7 (8.4 dB) reduction on the required transmit power in the main direction.

The receive power gain is discussed under the assumption that each photodiode with area A_{D} is equipped with an ideal optical concentrator. We first compare the required optical power obtained by an APD with 30° FOV to that with 90° FOV. When switching the half FOV ψ_{rx} from 45° to 15° , the received signal power increases by a factor $\sin^2(45^\circ)/\sin^2(15^\circ) \approx 7$ due to the increased detector area $A_{\text{rx}} = A_{\text{D}} \cdot \frac{n_c^2}{\sin^2(\psi_{\text{rx}})}$. With respect to the noise power (background light induced shot noise dominates in APDs), the received amount of diffusely scattered background light remains unchanged due to the fact that the detector area gain is compensated by the reduced FOV, which is given by $P_{\text{bg}} = L_{\text{bg}} A_{\text{rx}} \sin^2(\psi_{\text{rx}}) \pi$ with $A_{\text{rx}} = A_{\text{D}} \cdot \frac{n_c^2}{\sin^2(\psi_{\text{rx}})}$. This can be further illustrated in Fig. 9.5, where the required transmit radiant intensity is plotted for 1m LOS link with $A_{\text{D}} = 1 \text{ mm}^2$. There is around a factor of 7 reduction on the transmit

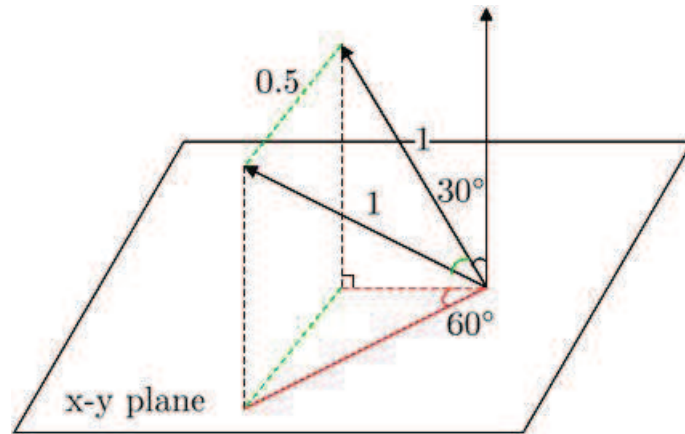


Figure 9.2.: Illustration of the seven element configuration. The central element points straight up and the six neighboring elements are uniformly placed around the central element with 30° elevation. It can be calculated that the angle between these two elements is less than 30° (marked in green) to ensure that the radiant intensity is always larger than half of the peak value even at the edge between any two elements.

radiant intensity when compare $\Psi_{rx} = 45^\circ$ to $\Psi_{rx} = 15^\circ$. Furthermore, in order to provide 90° coverage for fair comparison, 7 receiver elements as configured in Fig. 9.1 with narrow angle are compared to the case of that 7 APDs each having a wide angle of 90° and pointing in the same direction. Since the latter case has a factor of $\sqrt{7}$ gain compared to a single APD with 90° FOV, the effective receive power gain associated with 7 receiver elements is effectively $\sqrt{7}$.

9.2. Establishment of a link

Based on the configuration mentioned in Section 9.1, the transmitter and receiver block diagram are shown in Fig. 9.6. At the transmitter side, first the IBM 8B10B line encoding is performed. At each byte clock, 8 data bits at the encoder input are encoded to 10 bits at the output, which gives a rate of 1.25 Gb/s at the modulator inputs. This line encoding ensures DC-balance and enough state changes from 0 to 1 and from 1 to 0. These state changes are required to track the 1.25 GHz line clock at the receiver and to ensure a DC-balanced transmit signal. At the receiver, APDs are used to increase the receiver sensitivity compared to PIN photodiodes. All seven input signals are individually amplified by the transimpedance amplifiers (TIA). After that a first order high-pass (HP) filter is used to ensure an appropriate cut-on frequency. A low-pass (LP) filter is then applied for noise rejection. At each high-pass filter output, an analogue signal named received signal strength indicator (RSSI) is derived. If one or more RSSI-signals exceed a fixed threshold, which corresponds to the receiver sensitivity, the one with the maximum RSSI is fed into the clock and data recovering

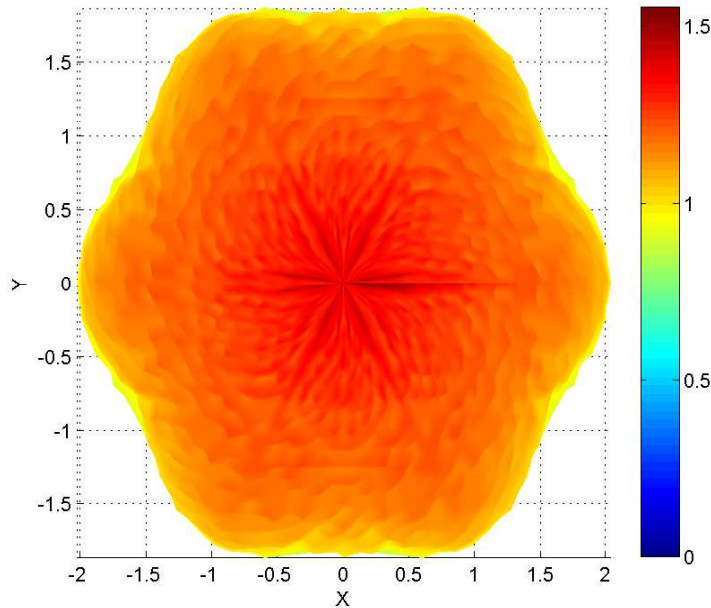


Figure 9.3.: Radiant intensity distribution with the proposed seven elements configuration. The colorbar provides the normalized radiant intensity to the peak value of a single transmitter element. It can be larger than one in the middle area due to the overlap between the seven elements. It clearly verifies that the obtained radiance intensity is never less than half of the peak, even between the element edges.

circuit (CDR) to accomplish receiver selection. On the other hand, if none of the RSSI-signals exceeds the threshold, a sequence of “101010 ...” is fed to the CDR to ensure that the CDR is always frequency synchronized and that no random bits are produced during idle periods.

Assume that there is only one transmitter and one receiver in the room and both of them consist of 7 elements as shown in Figure 9.1. Figure 9.7 illustrates the link establishment process during the beacon period by integration of the MAC layer and the PHY layer. The MAC layer first adjusts the beacon period start time (BPST) for synchronization and sends a beacon frame at the BPST. Meanwhile, it informs the PHY layer to start transmission within the beacon period (BP). As soon as being informed by the MAC layer, the optical wireless switch (OWS) switches on all the 7 control signals Laser On/Off on the base station and the transmitter starts transmission towards 7 different directions trying to reach a receiver. In order to avoid being disturbed by the transmitter’s own reflections of the transmitted signal, it is advised for the transmitter to stop receiving during the transmission. At the receiver side, only one element is active at one time and the received signal power is measured by the received signal strength indicator (RSSI). The OWS controls the 7 receiver elements selection and 7 RSSIs are obtained. At this point, these RSSIs will be compared to a predefined threshold. If these obtained RSSIs exceed the threshold, the OWS will select the strongest RSSI and use it for receiver selection during the data transmission period later on. If not,

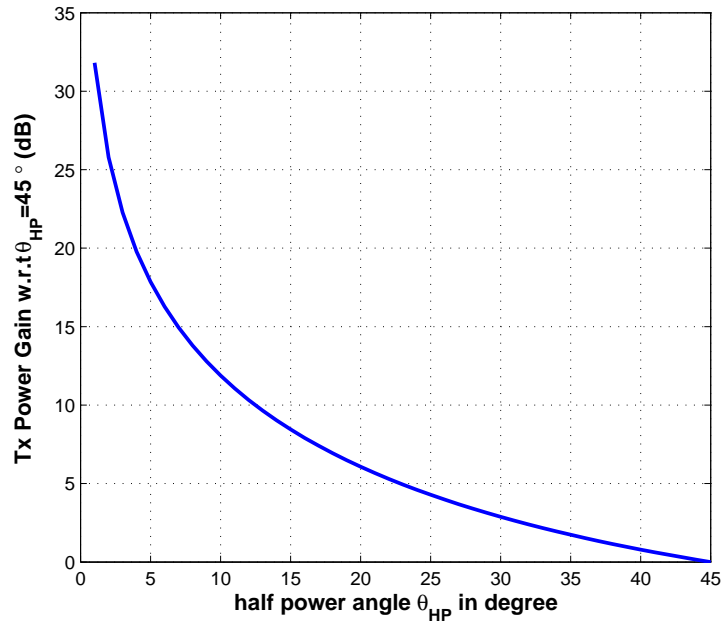


Figure 9.4.: Transmit power gain

none of these 7 received signals will be used for data recovery and a clean signal in the format of “101010 ...” will be fed into the input of the multiplexer to keep frequency synchronization. In the case that there is more than one RSSI exceeds the threshold, the receiver element with the strongest RSSI is selected for detection, which is called the best receiver element. Then this best receiver element starts transmission to the transmitter. A similar element selection procedure is performed at the transmitter and the best transmit element is chosen. After that the receiver gets the device address (DevAddr) of the best transmitter element from the MAC layer. Before the receiver sends the acknowledgement (ACK) to this best transmitter element, it scans the beacon signal for at least 2 superframes. If no further beacon frames are received, the receiver sends back the ACK to ensure that the link between the receiver and the transmitter is established. After the receiver element DevAddr is identified by the MAC layer, the OWS switches off all other 6 Laser On/Off at the transmitter except for the best transmitter element and starts data transmission to the best receiver element.

Concerning different phases of the link establishment procedure, we now investigate the power propagation in a typical indoor environment. A typical room dimension of (5 m \times 4 m \times 3 m) is assumed, where the transmitter is located at the ceiling center (2.5, 2, 3) m with the transmit power of 1 mW. The receiver moves around the room at 1 m height. The reflection coefficients are chosen for all walls and the ceiling 0.8 and for the floor 0.3 for the worst case consideration. Based on the channel model proposed in [BKK⁺93], 5 reflections are taken into account in the simulation.

The Rice factor is defined as $r = P_{LOS}/P_{refl}$, where P_{LOS} represents the received LOS power and P_{refl} denotes the received power from all the reflected components. Fig. 9.8 shows the

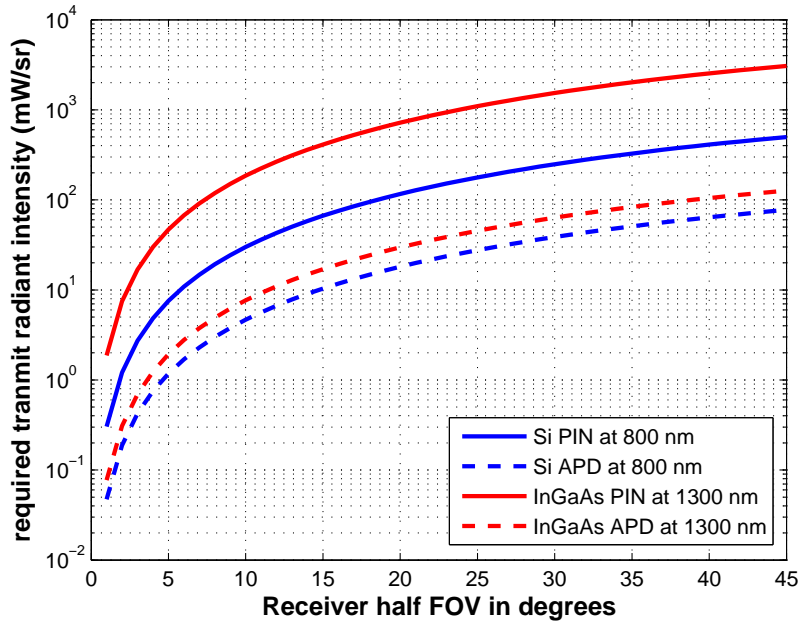


Figure 9.5.: Required transmit radiant intensity for a 1m LOS link

distribution of the Rice factor in dB within the room as the receiver moves around the room. The black circle indicates the intended FOV illuminated by the transmitter located at the ceiling center. During the beacon period, a wide beam transmitter with 90° half power angle is used, which consists of 7 transmitter elements each having a half power angle of 30° . As shown in Fig. 9.8(a), the Rice factor is never less than 10 dB within 90° FOV. Consider $r = 10$ dB, the diffused component caused by reflections contains only $1/10$ power of the LOS component. Roughly speaking, this will induce at maximum a factor of 0.2 vertical eye-opening reduction in the eye diagram concerning the worst case. Detection is possible in presence of multipath distortion. For the data period transmission, Fig. 9.8(b) illustrates that the Rice factor is always larger than 15 dB when each pair of the receiver element and the corresponding well-pointed transmitter element are activated, which implies that almost all of the received power is contained in the LOS component and the ISI caused by multiple reflections is not a big issue with this system configuration. To summarize, the multipath distortion will not cause an obstacle by using angle diversity for Gbps transmission.

9.3. Preliminary analysis on the required radiant intensity per transmitter element

We consider the best case configuration, where the transmitter is located in the ceiling center and the receiver is 3 m away straightly under the transmitter, as shown in Fig. 9.9. The transmitter and the receiver are aligned to each other. Suppose that a Si APD with a photodiode area of 0.6 mm^2 is used operating at 800 nm. By incorporating all the system parameters

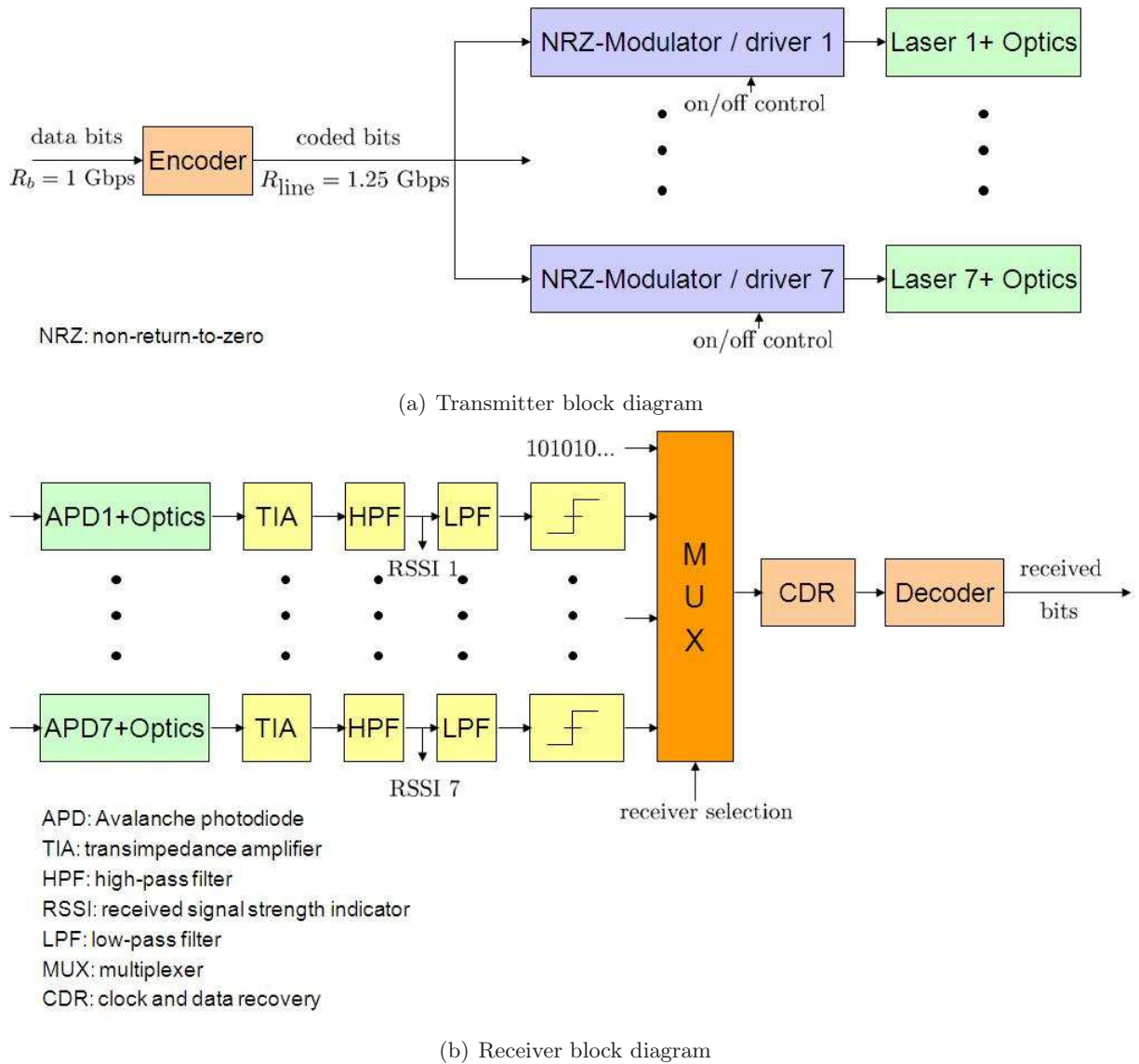


Figure 9.6.: Transmitter and receiver block diagram

in Table 7.10, the required radiant intensity for this best case arrangement would be 120 mW/srad, as shown in Fig. 9.10.

As the receiver moves around, more transmit radiant intensity is required due to the increased transmission distance. At the cell border with 90° system FOV, the receiver is located 3 m away horizontally compared to the central spot, shown as the dotted receiver block in Fig. 9.9. In this case, the additional loss is at least 9 dB, where a 3 dB loss is caused by the increased distance while the additional (2 × 3) dB loss is due to that both the transmitter and the receiver operate at their half power intensity angles. This means that around 1200 mW/srad on axis radiant intensity is required to cover a 90° system FOV without including the link margin, if the vertical separation between the transmitter and the receiver is 3 m. For a 30° angle, this corresponds to an average optical transmit power of about 360 mW, which is a big challenge given the current levels of the available transmitter power.

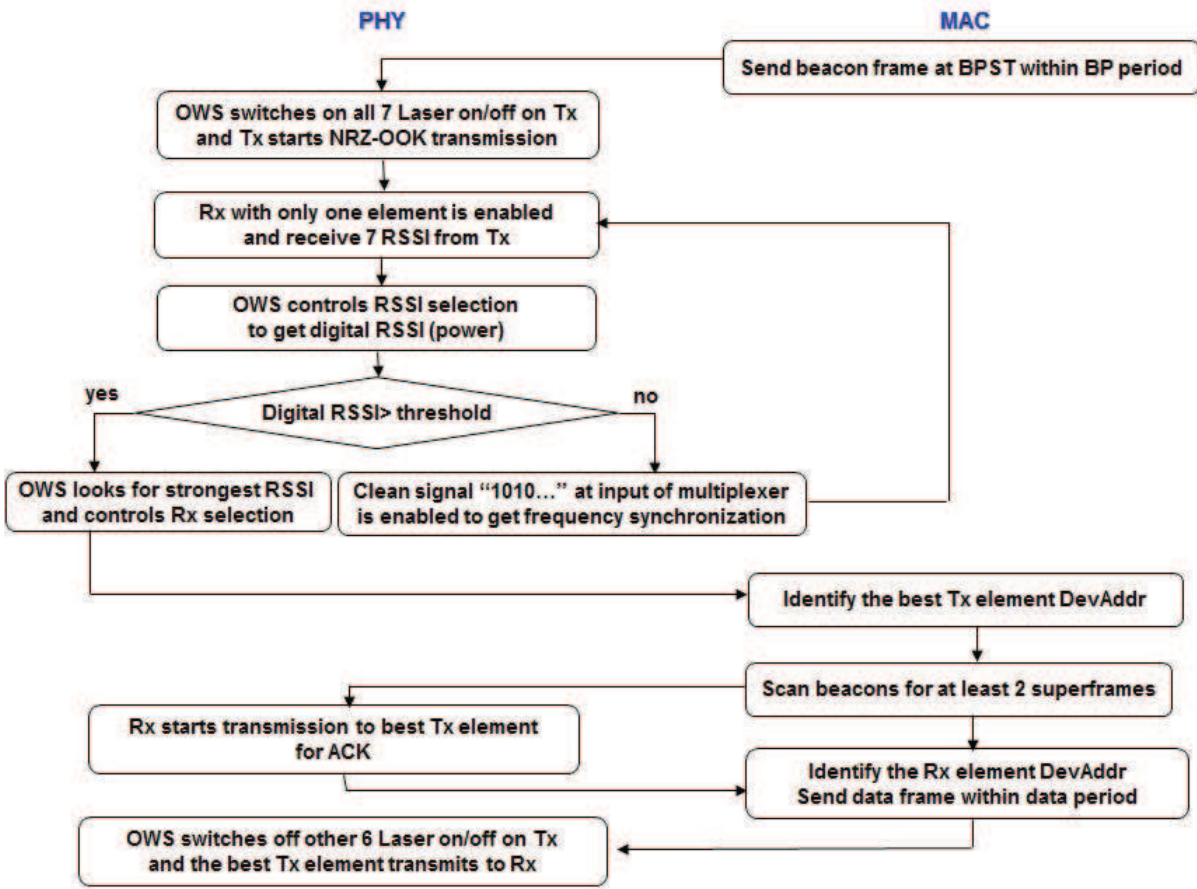
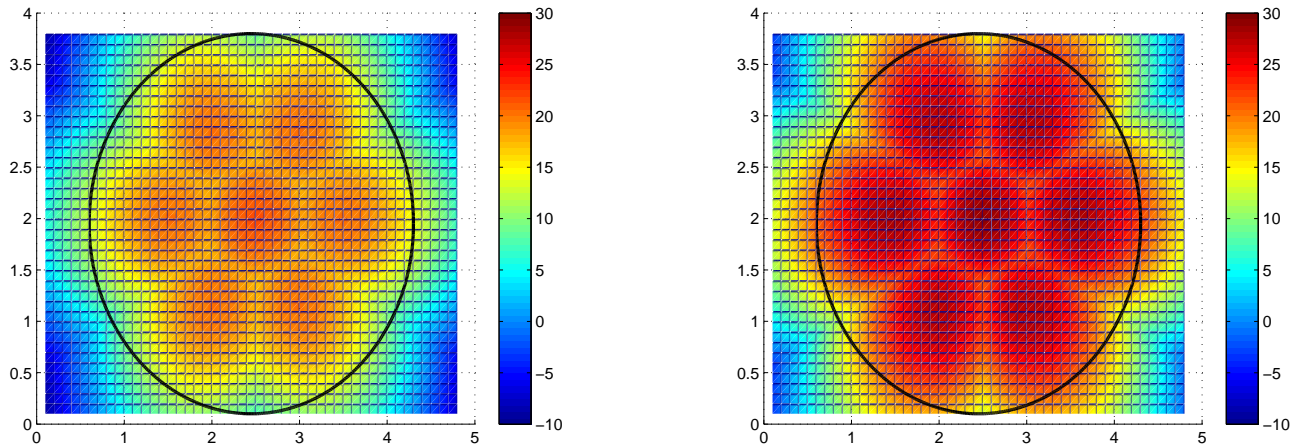


Figure 9.7.: Link establishment process

To overcome this problem, either the data rate has to be reduced or the photodiode area needs to be increased. We first consider the effect of the data rate on the required transmit power. Suppose a Si APD is used, then the shot noise dominates and its power increases proportionally with R_{line} , i.e., $\sigma_n^2 \approx N_0 I_2 R_{\text{line}}$. Given the BER, a factor of 2 reduction on R_{line} will bring a factor of $\sqrt{2}$ gain with respect to the required transmit power. On the other hand, when we increase the photodiode area A_D , both the received signal power P_{rx} and the noise variance σ_n^2 increase with A_D . Thereby, a factor of 2 increment on A_D will cause a factor of $\sqrt{2}$ on the required P_{rx} and thus a factor of $\sqrt{2}$ gain on the required transmit power due to the fact that the required transmit power is proportional to the required receive power and that the required receive power is inversely proportional to the photodiode area.



(a) beacon period: a single wide-beam transmitter and seven narrow-beam receiver elements (b) data period: seven narrow-beam transmitter elements and seven narrow-beam receiver elements

Figure 9.8.: Rice factor distribution in a typical room

9.4. Demonstrator

Within the OMEGA project, we at TU Ilmenau had been responsible for the physical layer design² for the 1 Gbps IR system. Based on our analysis and through intense cooperation with our partners, a 1 Gbps IR demonstrator was successfully built at the University of Oxford [MOF⁺10, OMF⁺10]. In the interest of time and cost, a three channel demonstrator was fabricated, achieving 1.25 Gb/s over a 3 m range and a coverage area of 1.3 m × 0.45 m with no forward error coding. The angle diversity is used at both the transmitter and the receiver, where the sub-sector half power angles are 5°. The 825 nm transmitter consists of 3 differently aligned lasers, each equipped with a holographic diffuser. The receiver uses 3 differently aligned 0.2 mm² Si APDs, each equipped with a lens offering a gain of 130 (linear scale). Without the background light, a sensitivity of -35 dBm was achieved. The demonstration clearly shows the possibility of optical indoor transmission at 1 Gbps. However, it emphasizes that a compact and lightweight angle diversity concept, which provides a large system FOV as required for networks, is really challenging to build [OTM⁺11, OTM⁺12].

²Physical layer design includes modulation, line coding, filter design, link budget analysis, etc. The optical elements are designed by our partner University of Oxford.

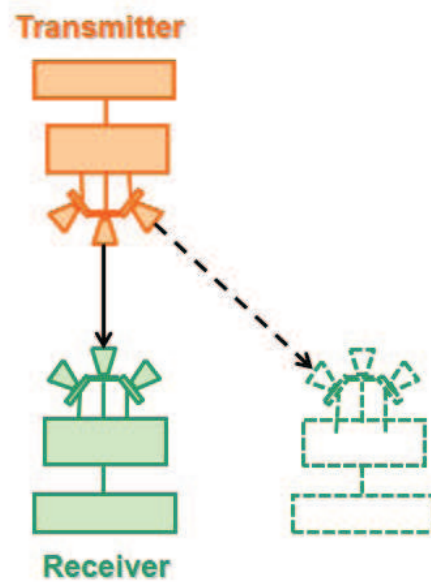


Figure 9.9.: The best case configuration, where the transmitter is located in the ceiling center and the receiver is 3 m away straightly under the transmitter. The transmitter and the receiver are aligned to each other.

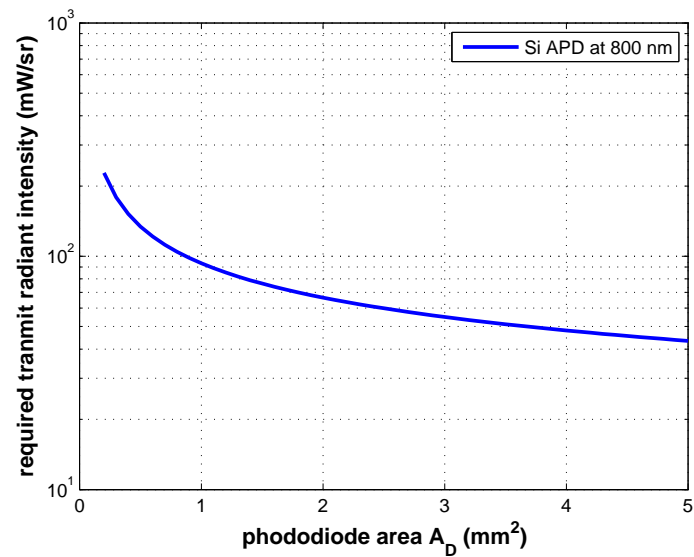


Figure 9.10.: Required radiant intensity for the transmission distance of 3 m

10. Conclusions and future work

In this thesis, we consider advanced signal processing for wireless communications at very high data rates, which consists of two application areas of high speed signal processing in the radio frequency (RF) and the infrared (IR) bands.

10.1. Part I: Sharing Physical Resources (SAPHYRE)

In the first part of this thesis, the concept of sharing the radio spectrum and the infrastructure between multiple operators is illustrated, which is within the vision of the European's seventh framework research project SAPHYRE (www.SAPHYRE.eu).

To start, the SAPHYRE concept is addressed. Two topologies are discussed that are defined within the scope of SAPHYRE. We first give an overview for the spectrum sharing only scenario. Following that, the model including both spectrum and infrastructure (relay) sharing is introduced. More specifically, we consider the relay assisted communication between multiple operators and various relaying operation modes are compared and discussed. Finally, to clearly illustrate the advantage of the sharing schemes compared to the traditional exclusive use of the physical resources, the SAPHYRE sharing gain is defined in terms of both spectral efficiency as well as power efficiency, which are used as a main performance metric in the following chapters, i.e., from Chapter 3 to Chapter 5.

Chapter 3 discusses precoding design for the non-orthogonal spectrum sharing between multiple operators. The downlink of the spectrum sharing scenario is considered, where two base stations (BSs) of different operators transmit over the same spectrum, each dedicated to its own user terminal (UT). Multiple antennas are employed at the BSs and UTs. This scenario is modeled as the interference channel with several concurrent point-to-point transmissions interfering with each other. We view this scenario as a special case of voluntary spectrum sharing in SAPHYRE. Two closed-form transmit beamforming schemes, i.e., block diagonalization (BD) for the interference channel (IC) and regularized block diagonalization (RBD) for the IC are first developed for this scenario. On a basis of that, a more flexible beamforming algorithm named flexible coordinated beamforming for the interference channel (IC FlexCoBF) [KGH⁺11, LKK⁺11] is designed to further enhance the system spectrum efficiency, which can be applied for any transmit and receive antenna configuration. Simulation results reveal that the proposed IC FlexCoBF improves the spectral efficiency dramatically compared to the state of the art work and a large sharing gain is observed by non-orthogonal spectrum sharing instead of an exclusive use of the spectrum.

Chapter 4 investigates relay assisted communications, where both the spectrum and an amplify and forward (AF) relay are shared between multiple operators without taking into

account the direct link between the BSs and the UTs. We propose several algorithms for the relay precoder design to further improve the system performance.

- Firstly, a set of algorithms named efficient relay sharing rate maximization (EReSh-RM) [LRH11a] is designed to improve the system sum rate under the relay transmit power constraint for both the single stream transmission and multiple stream transmission.
- Secondly, the relay precoder design is systematically studied for power efficient transmission, where an optimum algorithm and several suboptimal solutions are proposed. A special case is studied that the BSs and the UTs are equipped with single antennas, where only single stream transmission is possible. A global optimum solution is firstly derived, which uses a convex optimization tool to exploit the structure of the relay precoder. Taking this method as well as the work [LP10] as benchmarks, two suboptimal algorithms named efficient relay sharing power minimization (EReSh-PM) [LRH11a] and block diagonalization single channel algebraic norm maximization (BD/SC-ANOMAX) are proposed to find a compromise between the achievable power efficiency and the computational complexity, which are based on zero-forcing and block diagonalization techniques for interference mitigation. Both of them are closed-form solutions and no iteration is required. Compared to the optimum solution, both suboptimal algorithms achieve almost the same good performance and have only a degradation of 1 dB for the case that the number of relay $M_R = 4$ and the SINR constraint at each UT is 0 dB. Hence, EReSh-PM and BD/SC-ANOMAX methods are strongly recommended due to their extremely low computational complexity. Following that, the SAPHYRE sharing gain is investigated in terms of the required relay transmit power. In the case of two operators with $M_R = 8$, there is a 2 dB gain by sharing the spectrum and a 6 dB gain is observed by both the spectrum and relay sharing compared to the exclusive use of these physical resources.
- Third, a novel robust relay precoder design is proposed by considering imperfect channel state information (CSI) at the relay. In the case of two operators with $M_R = 8$ and the CSI error variance $\sigma_E = \sigma_F = 0.1$, there is a gain of around 5 dB by the shared use of the spectrum between the two operators at high SNRs. An additional 2 dB gain is obtained by an additional sharing of the relay compared to the exclusive access of the relay with half of the number of relay antennas.
- At last, we extend our study to the case where each pair of BSs and UTs are equipped with multiple antennas and a novel relay matrix design is derived for multiple stream transmission between multiple pairs of BSs and UTs. An effective algorithm is proposed to achieve power efficiency for multiple stream transmission in a multiple operator AF relay sharing system. The inter-operator interference is first removed by using a zero-forcing method. Following that, the relay precoder is designed using the convex optimization tool. Simulation results show that the SINR requirement per stream can be always satisfied. As a continuous work, it would be interesting to investigate the relay amplification matrix design under imperfect channel state information at the relay.
- Considering future work, it would be an open problem to investigate the joint precoding design of the BSs and the AF relay either to maximize the system sum rate or minimize

the required total power consumption. Furthermore, it would be interesting to see the results by including a path loss model into this system and a systematic study about the impact of relay transmit power and the relay location on the system performance would be useful.

Furthermore, when the direct link is not negligible, we study another spectrum and relay sharing scenario in Chapter 5, named interference relay channel (IRC). We consider the linear precoding design for the AF relaying strategy assuming multiple antennas employed at all BSs, UTs, and the AF relay. Two cases are studied, categorized into single stream and multiple stream transmission.

- For the single stream transmission, we first consider the conversion of the interference relay channel (IRC) to the interference channel (IC), where we propose to use the DFT matrix as the relay amplification matrix. After that we recommend the precoding method IRC FlexCoBF at the BSs, which achieves a better sum rate performance compared to the state-of-the-art work coordinated zero-forcing beamforming (CoZF) as well as eigen-beamforming [CHHT12]. Simulation results also show that IRC FlexCoBF is more robust to the interference. Last but not least, the sum rate performance of the IRC is compared to the relay channel and there exists a large sharing gain, which strongly supports the use of a shared spectrum and the relay instead of operating in the time division multiple access (TDMA) mode.
- For the multiple stream transmission, two AF relaying strategies are investigated first for the conversion from the IRC to the interference channel, of which the DFT matrix is recommended as the relay amplification matrix due to its simplicity. After that we propose the precoding algorithm IRC FlexCoBF with RBD at the BSs, which achieves a better sum rate performance compared to the approach in [DI03]. Furthermore, simulation results show that the IRC FlexCoBF RBD is more robust to strong interference than the approach in [DI03]. In addition to this, the sum rate performance of the IRC is compared to the relay channel and there exists a large sharing gain, which indicates the advantage of the use of a relay shared by two base stations instead of accessing the relay in the time division multiple access (TDMA) mode.
- As for the future work, it is interesting to study the precoding design to achieve the power efficiency of this system.

10.2. Part II: hOME Gigabit Access (OMEGA)

In the second part of this thesis, the physical layer design for a high speed infrared (IR) system in an indoor environment is developed, which is within the scope the European Union's FP7 project OMEGA (www.ict-omega.eu). We focus on line of sight (LOS) data transmission using IR wavelengths. The physical layer analysis of integration and feasibility investigation of a Gbps IR system is presented. The system consists of a base station located at the ceiling and terminals that move around at the ground. Both transmitters and receivers are build

with seven elements in the demonstrator [MOF⁺10, OMF⁺10], where each element covers a relatively narrow field of view (FOV) and together a data link with a wide FOV is created.

In Chapter 7, the system model of the high speed IR transmission is introduced, where individual components suitable for Gbps IR system are analyzed and specified. In particular, we choose a non-return-to-zero (NRZ) on-off-keying (OOK) modulation scheme appropriate for the Gbps IR transmission due to its simplicity for the laser driver. Concerning the baseline wander effect that is induced by the AC-coupling inherent in the receiver's preamplifier, we propose a novel line coding named as concatenated flipped bit insertion (CFBI) code [LWH09]. Compared to the classic IBM code [WF83], the CFBI code offers a comparable susceptibility to the transient baseline wander effect while it is much easier to implement due to a very simple logic. Following that, the implementation of a 5th order Bessel low-pass filter is specified for noise rejection. Moreover, we discuss the selection of the first order RC high-pass filter for the Gbps IR system, which is applied to block the DC photocurrent generated by the received ambient light as well as to reduce the harmonics caused by the fluorescent lighting. After that the photodiode detectors for high speed IR transmission are discussed, including PIN photodiodes and the Avalanche photodiodes (APDs). Last but not least, it is important to analyze various noise sources generated in the IR system, including shot noise and thermal noise with constant power spectrum density (PSD), as well as the f^2 noise whose PSD increases with the square of the frequency.

Based on this analysis and the specification of the individual components, the receiver sensitivity with PIN and APD photodiodes and the link budget for the Gbps IR transmission with a narrow angle FOV are given in Chapter 8. Simulation results show that PIN photodiodes are mainly limited by the f^2 -noise for Gbps transmission while the receiver sensitivity of APDs are constrained by the white noise. Further, PIN photodiode does not outperform APDs and there exists approximately an 8 dB loss in the receiver sensitivity when comparing InGaAs PIN photodiodes to Si PIN photodiodes in order to obtain a 1 m Gbps IR link. Moreover, APDs offers further improvement while the Si APD gives the best performance. Therefore, the Si APD is strongly recommended for Gbps infrared system.

At last, the transmit and receive angle diversity are discussed in Chapter 9 in order to further extend the system FOV. We first discuss the configuration of the seven transmit or receive elements to ensure that the radiant intensity is always larger than half of the peak value even at the edge between any of two elements. Based on this configuration, the advantage of using the seven narrow angle elements configuration is addressed compared to a single transmit and receive element with a wide angle, in terms of the transmit and receive power gain, respectively. Following that, the link establishment process is illustrated. Finally, a preliminary analysis is given on the required radiant intensity per transmit element, which addresses a big challenge on the required average optical transmit power. To overcome this problem, either the data rate has to be reduced or the photodiode area needs to be increased.

As a continuous work, due the challenging system FOV requirement for Gbps infrared system, it is reasonable to build a low-cost high speed indoor infrared system balancing between the data rate and the FOV.

Acronyms

AF	amplify and forward
ANOMAX	algebraic norm maximization
APD	Avalanche photodiode
BC	broadcast channel
BD	block diagonalization
BER	bit error rate
BJT	bipolar junction transistor
BS	Base station
CDP	codeword disparity
CSI	channel state information
DF	decode and forward
DFT	Discrete Fourier Transform
FFR	fractional frequency reuse
FOV	field of view
Gbps	Gigabits per second
HPF	high-pass filter
IC	interference channel
InGaAs	Indium-Gallium-Arsenic
IR	infrared
IRC	interference relay channel
ISI	inter-symbol-interference
MAC	multiple access channel
MIMO	multiple-input multiple-output
MMSE	minimum mean square error
MRC	maximum ratio combining
NRZ	non-return-to-zero
OMEGA	hOME Gigabit Access

OOK	on-off-keying
PIN	positive-intrinsic-negative photodiode
PSD	power density spectrum
P2P	point-to-point
QoS	quality of service
RBD	regularized block diagonalization
RF	radio frequency
RSSI	received signal strength indicator
SAPHYRE	ShAring PHYSical REsources
Si	silicon
SINR	signal to interference plus noise ratio
SNR	signal to noise ratio
SVD	singular value decomposition
TDMA	time division multiple access
UT	user terminal
ZF	zero forcing
ZMCSCG	zero-mean cyclic symmetric complex Gaussian

Notation

\mathbf{a}	Vector
\mathbf{A}	Matrix
\mathbf{A}^T	Transpose of a matrix \mathbf{A}
\mathbf{A}^*	Complex conjugate of a matrix \mathbf{A}
\mathbf{A}^H	Hermitian transpose of a matrix \mathbf{A}
\mathbf{A}^{-1}	Inverse of a matrix \mathbf{A}
\mathbf{A}^+	Pseudo inverse of a matrix \mathbf{A}
$ a $	Absolute value of a scalar a
$\ \mathbf{a}\ _2$	Euclidean norm of a vector \mathbf{a}
$\ \mathbf{A}\ _F$	Frobenius norm of a matrix \mathbf{A}
$\text{tr}(\mathbf{A})$	Trace of a matrix
$\text{vec}(\mathbf{A})$	Vectorization of a matrix \mathbf{A}
$\text{rank}(\mathbf{A})$	Rank of a matrix \mathbf{A}
$\mathbf{I}_{M \times N}$	Identity matrix of size $M \times N$
$\mathbf{0}_{M \times N}$	M by N matrix with all entries equal to zero
$\mathbf{1}_{M \times N}$	M by N matrix with all entries equal to one
$\mathbf{A}_{i,j}$	The (i,j) -th entry of a matrix \mathbf{A}
$\mathbf{A} \otimes \mathbf{B}$	Kronecker product of matrices \mathbf{A} and \mathbf{B}
\mathbb{R}	Set of real numbers
\mathbb{C}	Set of complex numbers
$\mathcal{CN}(0, \sigma_n^2)$	Complex normal distribution with zero mean and variance σ_n^2
$\mathbb{E}(\cdot)$	Expectation of a random variable

Bibliography

Publications as First or Co-Author

- [GLWH09] L. Grobe, J. Li, M. Wolf, and M. Haardt, "Modulation and Coding Aspects for hOME Gigabit Access (OMEGA) using Wireless Infrared," in *Proc. 54th International Scientific Colloquium (IWK)*, Ilmenau, Germany, Sep. 2009.
- [KGH⁺11] E. Karipidis, D. Gesbert, M. Haardt, K. Ho, E. Jorswieck, E. G. Larsson, J. Li, J. Lindblom, C. Scheunert, M. Schubert, and N. Vucic, "Transmit Beamforming for Inter-Operator Spectrum Sharing," in *Proc. Future Network and Mobile Summit 2011 (FNMS 2011)*, Warsaw, Poland, Jun. 2011.
- [LH13] J. Li and M. Haardt, "Robust MIMO Relay Precoder Design for Multiple Operator One-Way Relaying with Imperfect Channel State Information," in *Proc. 10-th International Symposium on Wireless Communications Systems (ISWCS 2013)*, Ilmenau, Germany, Aug. 2013.
- [LKK⁺11] J. Luo, A. Kortke, W. Keusgen, J. Li, M. Haardt, P. Prochazka, and J. Sykora, "A Flexible Hardware-In-the-Loop Test Platform for Physical Resource Sharing Mechanisms in Wireless Networks," in *Proc. Future Network and Mobile Summit 2011 (FNMS 2011)*, Warsaw, Poland, Jun. 2011.
- [LLL⁺12] J. Luo, J. Lindblom, J. Li, R. Mochaourab, A. Kortke, E. Karipidis, M. Haardt, E. Jorswieck, and E. G. Larsson, "Transmit beamforming for inter-operator spectrum sharing: From theory to practice," in *Proc. 9-th International Symposium on Wireless Communications Systems (ISWCS 2012)*, Paris, France, Aug. 2012.
- [LRH11a] J. Li, F. Roemer, and M. Haardt, "Efficient Relay Sharing (EReSh) between Multiple Operators in Amplify-and-Forward Relaying Systems," in *Proc. IEEE 4th Int. Workshop on Computational Advances in Multi-Sensor Adaptive Processing (CAMSAP 2011)*, San Juan, Puerto Rico, Dec. 2011, pp. 249 – 252.
- [LRH11b] —, "Spectrum and Infrastructure Sharing in the MIMO Interference Relay Channels," in *Proc. 19-th European Signal Processing Conference (EUSIPCO 2011)*, Barcelona, Spain, Aug. 2011, pp. 181 – 185.
- [LSH11] J. Li, A. Sezgin, and M. Haardt, "Coordinated Beamforming for MIMO Interference Relay Channel with Multiple Stream Transmission," in *Proc. IEEE International ITG Workshop on Smart Antennas (WSA 2011)*, Aachen, Germany, Feb. 2011.
- [LWH09] J. Li, M. Wolf, and M. Haardt, "Investigation of the Baseline Wander Effect on Gbps Wireless Infrared System Employing 8B10B Coding," in *Proc. of IEEE International Conference on Telecommunications (ICT 2009)*, Marrakech, Morocco, May 2009, pp. 53–58.
- [LZR⁺11] J. Li, J. Zhang, F. Roemer, M. Haardt, C. Scheunert, E. Jorswieck, M. Hekrdla, and J. Sykora, "Relay-Assisted Spectrum and Infrastructure Sharing between Mul-
-

- multiple Operators,” in *Proc. Future Network and Mobile Summit 2011 (FNMS 2011)*, Warsaw, Poland, Jun. 2011.
- [MOF⁺10] H. Minh, D. O’Brien, G. Faulkner, O. Bouchet, M. Wolf, L. Grobe, and J. Li, “A 1.25-Gb/s Indoor Cellular Optical Wireless Communications Demonstrator,” *IEEE Photonics Technology Letters*, vol. 22, no. 21, pp. 1598–1600, Nov. 2010.
- [OMF⁺10] D. O’Brien, H. L. Minh, G. Faulkner, M. Wolf, L. Grobe, J. Li, and O. Bouchet, “High data-rate infra-red optical wireless communications: implementation challenges,” in *IEEE GLOBECOM Workshop on Optical Wireless Communications (OWC 2010)*, Miami, USA, Dec. 2010, pp. 1047–1051.
- [OTM⁺11] D. O’Brien, R. Turnbull, H. L. Minh, G. Faulkner, M. Wolf, L. Grobe, J. Li, O. Bouchet, and E. Gueutier, “A 280Mbit/s infrared optical wireless communications system,” *Proc. SPIE 8162*, Aug. 2011.
- [OTM⁺12] D. O’Brien, R. Turnbull, H. L. Minh, G. Faulkner, O. Bouchet, P. Porcon, M. E. Tabach, E. Gueutier, M. Wolf, L. Grobe, and J. Li, “High-speed optical wireless demonstrators: conclusions and future directions,” *Journal of Lightwave Technology*, vol. 30, no. 13, pp. 2181–2187, July 2012.
- [WGL09] M. Wolf, L. Grobe, and J. Li, “Choice of Modulation for Gbps Wireless Infrared Systems,” in *European workshop on photonic solutions for wireless, access, and in-house networks (IPHOBAC 2009)*, Duisburg, Germany, May 2009.
- [WLG⁺10] M. Wolf, J. Li, L. Grobe, D. O’Brien, H. L. Minh, and O. Bouchet, “Challenges in Gbps Wireless Optical Transmission,” in *2nd International Conference on Mobile Lightweight Wireless Systems (MOBILIGHT 2010)*, Barcelona, Spain, May 2010, pp. 484–495.

References by Other Authors

- [Agr05] G. P. Agrawal, *Lightwave Technology: Components and Devices*, 4th ed. McGraw-Hill, New York, 2005.
- [AHZ11] W. Ai, Y. Huang, and S. Zhang, “New results on Hermian matrix rank-one decomposition,” *Math. Program., Ser. A*, vol. 128, no. 1-2, pp. 253–283, Jun. 2011.
- [AK95] M. D. Audeh and J. M. Kahn, “Performance Evaluation of Baseband OOK for Indoor Infrared LAN’s Operating at 100 Mb/s,” *IEEE Transactions on Communications*, vol. 43, no. 6, pp. 2085–2094, June 1995.
- [BDHM01] R. Becher, M. Dillinger, M. Haardt, and W. Mohr, “Broadband wireless access and future communication networks,” *Proc. of the IEEE*, vol. 89, no. 1, pp. 58–75, Jan. 2001.
- [Bes] Bessel Filter Constants. [Online]. Available: <http://www.crbond.com/papers/bsf.pdf>
- [BKK⁺93] J. R. Barry, J. M. Kahn, W. J. Krause, E. A. Lee, and D. G. Messerschmitt, “Simulation of Multipath Impulse Response for Indoor Wireless Optical Channels,” *IEEE Journal on Selected Areas in Communications*, vol. 11, no. 3, pp. 367–379, Apr. 1993.
- [BL06] M. Bennis and J. Lilleberg, “Inter-Operator Resource Sharing for 3G Systems and Beyond,” in *Proc. IEEE Ninth International Symposium on Spread Spectrum Techniques and Applications (ISSSTA 2006)*, Manaus, Brazil, Aug. 2006, pp. 401–405.
-

- [Bou96] A. C. Boucouvalas, "Indoor ambient light noise and its effect on wireless optical links," *IEE Proc.-Optoelectronics*, vol. 143, no. 6, pp. 334–338, Dec. 1996.
- [BV04] S. Boyd and L. Vandenberghe, *Convex Optimization*. Cambridge University Press, 2004.
- [CA79] T. Cover and A. El. Gamal, "Capacity Theorems for the Relay Channel," *IEEE Trans. Inf. Theory*, vol. IT-27, no. 5, pp. 572–584, Sep. 1979.
- [Car78] A. Carleial, "Interference Channels," *IEEE Trans. Inf. Theory*, vol. 24, no. 1, pp. 60–70, Jan. 1978.
- [CHHT12] C. B. Chae, I. Hwang, R. W. Heath, and V. Tarokh, "Interference Aware-Coordinated Beamforming in a Multi-Cell System," *IEEE Trans. on Wireless Commun.*, vol. 11, no. 10, pp. 3692 – 3703, Oct. 2012.
- [CK00] J. B. Carruthers and J. M. Kahn, "Angle Diversity for Nondirected Wireless Infrared Communication," *IEEE Trans. Comm.*, vol. 48, no. 6, pp. 960–969, Jun. 2000.
- [Com11] Communication Systems/Line Codes, Dec. 2011. [Online]. Available: http://en.wikibooks.org/wiki/Communication_Systems/Line_Codes
- [CTHC08] C. Chae, T. Tang, R. W. Heath, and S. Cho, "MIMO Relaying with Linear Processing for Multiuser Transmission in Fixed Relay Networks," *IEEE Trans. Signal Processing*, vol. 56, no. 2, pp. 727–738, Feb. 2008.
- [CV09] B. K. Chalise and L. Vandendorpe, "MIMO Relay Design for Multipoint-to-Multipoint Communications With Imperfect Channel State Information," *IEEE Trans. Signal Processing*, vol. 57, no. 7, pp. 2785–2796, Jul. 2009.
- [CVL07] B. K. Chalise, L. Vandendorpe, and J. Louveaux, "MIMO Relaying for Multi-Point to Multi-Point Communication in Wireless Networks," in *Proc. IEEE 2nd Int. Workshop on Computational Advances in Multi-Sensor Adaptive Processing (CAMSAP 2007)*, St. Thomas, US Virgin Islands, Dec. 2007, pp. 217–220.
- [DI03] M. F. Demirkol and M. A. Ingram, "Stream Control in Networks with Interfering MIMO Links," in *Proc. IEEE Wireless Communications and Networking Conference (WCNC 2003)*, New Orleans, USA, Mar. 2003, pp. 343–348.
- [DK00] P. Djahani and J. M. Kahn, "Analysis of Infrared Wireless Links Employing Multi-Beam Transmitters and Imaging Diversity Receivers," *IEEE Trans. on Commun.*, vol. 48, no. 12, pp. 2077–2088, Dec. 2000.
- [DY10] H. Dahrouj and W. Yu, "Coordinated beamforming for the multicell multi-antenna wireless system," *IEEE Trans. Wireless Comm.*, vol. 9, no. 5, pp. 1748 – 1759, May 2010.
- [FLZS12] Z. Fang, F. Liang, S. Zhang, and J. Shi, "Protocol design and data detection for two-way relay networks with fractional asynchronous delays," *International Journal of Communication Systems*, Oct. 2012, doi: 10.1002/dac.2446.
- [GBY09] M. Grant, S. Boyd, and Y. Ye, "Matlab software for disciplined convex programming," Jan. 2009. [Online]. Available: www.stanford.edu/~boyd/papers/pdf/disc_cvx_prog.pdf
- [Gha08] Z. Ghassemlooy, "Investigation of the baseline wander effect on indoor optical wireless system employing digital pulse interval modulation," *IET Commun.*, vol. 2, no. 1, pp. 53–60, Jan. 2008.
-

- [GHH⁺10] D. Gesbert, S. Hanly, H. Huang, S. S. Shitz, O. Simeone, and W. Yu, "Multi-Cell MIMO Cooperative Networks: A New Look at Interference," *IEEE Journal Sel. Area Comm.*, vol. 28, no. 9, pp. 1380–1408, Dec. 2010.
- [GJHL08] R. J. Green, H. Joshi, M. D. Higgins, and M. S. Leeson, "Recent developments in indoor optical wireless systems," *IET Commun.*, vol. 2, no. 1, pp. 3–10, Jan. 2008.
- [GML08] R. Giuliano, C. Monti, and P. Loreti, "WiMAX fractional frequency reuse for rural environments," *IEEE Trans. Wireless Comm.*, vol. 15, no. 3, pp. 60–65, Jun. 2008.
- [Haa08] M. Haardt, rapporteur, "Future Mobile and Wireless Radio Systems: Challenges in European Research," Report on the FP 7 Consultation Meeting, European Commission, Information Society and Media, Brussels, Belgium, Feb. 2008.
- [Hay05] S. Haykin, "Cognitive radio: brain-empowered wireless communications," *IEEE Journal Sel. Area Comm.*, vol. 23, no. 2, pp. 201–220, Feb. 2005.
- [HJ85] R. A. Horn and C. R. Johnson, *Matrix Analysis*. Cambridge University Press, 1985.
- [HMZ05] A. Host-Madsen and J. Zhang, "Capacity Bounds and Power Allocation for Wireless Relay Channels," *IEEE Trans. Inf. Theory*, vol. 51, no. 6, pp. 2020–2040, Jun. 2005.
- [HP10] Y. Huang and D. P. Palomar, "Rank-Constrained Separable Semidefinite Programming with Applications to Optimal Beamforming," *IEEE Trans. Signal Processing*, vol. 58, no. 2, pp. 664 – 678, Feb. 2010.
- [HPI08] V. Heinonen, P. Pirinen, and J. Iinatti, "Capacity Gains through Inter-Operator Resource Sharing in a Cellular Network," Lapland, Finland, Sep. 2008.
- [IDM⁺11] R. Irmer, H. Droste, P. Marsch, M. Grieger, G. P. Fettweis, S. Brueck, H. Mayer, L. Thiele, and V. Jungnickel, "Coordinated multipoint: Concepts, performance, and field trial results," *IEEE Comm. Magazine*, Feb. 2011.
- [ITN10] M. Iwamura, H. Takahashi, and S. Nagata, "Relay Technology in LTE-Advanced," *NTT DOCOMO Technical Journal*, vol. 12, no. 2, pp. 29–36, Sep. 2010.
- [JBF⁺10] E. Jorswieck, L. Badia, T. Fahldieck, D. Gesbert, S. Gustafsson, M. Haardt, K.-M. Ho, E. Karipidis, A. Kortke, E. Larsson, H. Mark, M. Nawrocki, V. Palestini, R. Piesiewicz, P. Priotti, F. Roemer, M. Schubert, J. Sykora, P. Trossen, B. van den Ende, and M. Zorzi, "Resource Sharing in Wireless Networks: The SAPHYRE Approach," in *Proc. Future Network and Mobile Summit 2010*, Florence, Italy, June 2010.
- [JBF⁺11] E. Jorswieck, L. Badia, T. Fahldieck, M. Haardt, E. Karipidis, J. Luo, R. Pisz, and C. Scheunert, "Resource sharing improves the network efficiency for wireless operators," in *Wireless World Research Forum Meeting 27*, Duesseldorf, Germany, Oct. 2011.
- [JBF⁺12] E. Jorswieck, L. Badia, T. Fahldieck, M. Haardt, E. Karipidis, J. Luo, and R. Pisz, "Spectrum sharing improves the network efficiency for wireless operators," *submitted to IEEE Comm. Magazine*, Feb. 2012.
- [JBVS08] J. P. Javaudin, M. Bellec, D. Varoutas, and V. Suraci, "OMEGA ICT project: Towards convergent Gigabit home networks," in *Proc. Personal, Indoor and Mobile Radio Communications (PIMRC)*, Cannes, France, Sep. 2008, pp. 1–5.
- [JKHL09] J. Hwang, K.-J. Lee, H. Sung, and I. Lee, "Block Diagonalization Approach for Amplify-and-Forward Relay Systems in MIMO Multi-User Channels," in *Proc. Per-*
-

- sonal, *Indoor and Mobile Radio Communications (PIMRC)*, Tokyo, Japan, Sep. 2009, pp. 3149–3153.
- [JKJC01] H. Y. Jung, Y. J. Kim, B. M. Jin, and K. R. Cho, “Coding/Decoding System of Bit Insertion/Manipulation Line Code for High Speed Optical Transmission System,” *US Patent 6333704*, Dec. 2001.
- [KB97] J. M. Kahn and J. R. Barry, “Wireless infrared communications,” *Proc. IEEE*, vol. 85, pp. 265–298, Feb. 1997.
- [KGG05] G. Kramer, M. Gastpar, and P. Gupta, “Cooperative Strategies and Capacity Theorem for Relay Networks,” *IEEE Trans. Inf. Theory*, vol. 51, no. 9, pp. 3037–3063, Sep. 2005.
- [KJ03] M. Kavehrad and S. Jivcova, “Indoor broadband optical wireless communications: optical subsystems designs and their impact on channel characteristics,” *IEEE Trans. Wireless Comm.*, vol. 10, no. 2, pp. 30–35, Apr. 2003.
- [Krz89] W. A. Krzymien, “Transmission Pormance Analysis of a New Class of Line Codes for Optical Fibre Systems,” *IEEE Trans. on Commun.*, vol. 37, no. 4, pp. 402 – 404, Apr. 1989.
- [KSK08] Y.-W. Kim, B. Shin, and J.-K. Kang, “High Speed 8B/10B encoder design using a simplified coding table,” *IEICE Electronics Express*, vol. 5, no. 16, pp. 581 – 585, Aug. 2008.
- [LG07] K. D. Langer and J. Grubor, “Recent Developments in Optical Wireless Communications using Infrared and Visible Light,” in *Proc. ICTON*, Rome, Italy, July 2007, pp. 146–151.
- [LGB⁺08] K.-D. Langer, J. Grubor, O. Bouchet, M. Tabach, J. Walewski, S. Randel, M. Franke, S. Nerreter, D. O. G. Faulkner, I. Neokosmides, G. Ntogari, and M. Wolf, “Optical Wireless Communications for Broadband Access in home area networks,” in *International Conference on Transparent Optical Networks (ICTON 08)*, Athens, Greece, June 2008, pp. 149–154.
- [LMS⁺10] Z. Luo, W. Ma, A. M. So, Y. Ye, and S. Zhang, “Semidefinite Relaxation of Quadratic Optimization Problems,” *IEEE Signal Processing Magazine*, vol. 20, May 2010.
- [LP10] Y. Liu and A. Petropulu, “Cooperative Beamforming in Multi-Source Multi-Destination Relay Systems with SINR Constraints,” in *Proc. IEEE Internatinoal Conference on Acoustics, Speech, and Signal processing (ICASSP)*, Dallas, TX, Mar. 2010, pp. 2870–2873.
- [LVRWH05] C. K. Lo, S. Vishwanath, and J. R. W. Heath, “Rate Bounds for MIMO Relay Channels using Precoding,” in *Proc. Glob. telecom. Conf.*, St. Louis, MO, Nov. 2005, pp. 1172–1176.
- [LW00] J. N. Laneman and G. W. Wornell, “Exploiting Distributed Spatial Diversity in Wireless Networks,” in *Proc. Allerton Conf. Comm., Contro., Comp.*, Monticello, IL, Oct. 2000.
- [LWT01] J. N. Laneman, G. W. Wornell, and D. N. C. Tse, “An Efficient Protocol for Realizing Cooperative Diversity in Wireless Networks,” in *Proc. Int. Symp. Inf. Theory (ISIT 2001)*, Washington, DC, Jun. 2001, p. 294.
- [MF04] P. Marsch and G. P. Fettweis, *Coordinated Multi-Point in Mobile Communications*. Cambridge University Press, 2004.
-

- [MM99] J. Mitola and G. Q. Maguire, "Cognitive radio: making software radios more personal," *IEEE Personal Communications*, vol. 6, no. 4, pp. 13–18, Aug. 1999.
- [MMVA07] O. Muñoz-Medina, J. Vidal, and A. Agustin, "Linear Transceiver Design in Non-regenerative Relays With Channel State Information," *IEEE Trans. Signal Processing*, vol. 55, no. 6, pp. 2593–2604, Jun. 2007.
- [Muo84] T. V. Muoi, "Receiver Design for High-Speed Optical-Fiber Systems," *Journal of Lightwave Technology*, vol. LT-2, no. 3, pp. 243–267, June 1984.
- [NAK96] R. Narasimhan, M. D. Audeh, and J. M. Kahn, "Effect of electronic-ballast fluorescent lighting on wireless infrared links," *IEE Proc.-Optoelectronics*, vol. 143, no. 6, pp. 347–354, Dec. 1996.
- [NBK04] R. U. Nabar, H. Boelcskei, and F. W. Kneubuhler, "Fading Relay Channels: Performance Limits and Space-Time Signal Design," *IEEE J. Sel. Areas Commun.*, vol. 22, no. 6, pp. 1099–1109, Aug. 2004.
- [OFJ⁺03] D. C. O'Brien, G. E. Faulkner, K. Jim, E. B. Zyambo, D. J. Edwards, M. Whitehead, P. Stavrinou, G. Parry, J. Bellon, M. J. Sibley, V. A. Lalithambika, V. M. Joyner, R. J. Samsudin, D. M. Holburn, and R. J. Mears, "High-speed integrated transceivers for optical wireless," *IEEE Communications Magazine*, vol. 41, no. 3, pp. 58–62, Mar. 2003.
- [OKW⁺05] D. C. O'Brien, M. Katz, P. Wang, K. Kalliojarvi, S. Arnon, M. Matsumoto, R. J. Green, and S. Jivkova, "Shot -Range Optical Wireless Communications," in *Wireless World Reserch Forum 15*, Paris, France, Dec. 2005.
- [OME10] OMEGA Deliverable D4.2a, Mar. 2010. [Online]. Available: http://www.ict-omega.eu/fileadmin/documents/deliverables/Omega_D4.2a.pdf
- [PB95] H. Park and J. R. Barry, "Modulation Analysis for Wireless Infrared Communications," in *Proc. IEEE Int. Conf. on Commun. (ICC 95)*, Seattle, USA, June 1995, pp. 1182–1186.
- [Per77] S. D. Personick, "Receiver Design for Optical Fiber Systems," *Proc. of the IEEE*, vol. 65, no. 12, pp. 1670–1678, Dec. 1977.
- [PFOE01] F. Parand, G. E. Faulkner, D. C. O'Brien, and D. J. Edwards, "An optical wireless test-bed system using a multiple source transmitter and a segmented receiver to achieve signal tracking," in *Proc. International Society for Optical Engineering (SPIE), Optical Wireless Communications IV*, Denver CO, US, Aug. 2001, pp. 125–134.
- [PNG03] A. Paulraj, R. Nabar, and D. Gore, *Introduction to Space-Time Wireless Communications*. Cambridge University Press, 2003.
- [Pro00] J. Proakis, *Digital Communications*, 4th ed. McGraw-Hill, New York, 2000.
- [PSP10] J. Park, Y. Sung, and H. V. Poor, "On Beamformer Design for Multiuser MIMO Interference Channels," *submitted to IEEE Trans. Inf. Theory*, Nov. 2010.
- [Rec03] Recommendation ITU-R, M. 1645, "Framework and Overall Objectives of the Further Development of IMT-2000 and Systems Beyond IMT-2000," Jun. 2003.
- [Rec08] Recommendation ITU-R, M. 2134, "Requirements Related to Technical Performance for IMT-Advanced Radio Interface(s)," Nov. 2008.
- [RG98] G. Rechtsteiner and J. Ganske, "Using Natural and Artificial Light to Illustrate Quantum Mechanical Components," *The Chemical Educator*, vol. 3, no. 4, pp. 1–12, 1998.
-

- [RH09] F. Roemer and M. Haardt, "Algebraic Norm-Maximizing (ANOMAX) Transmit Strategy for Two-Way Relaying with MIMO Amplify and Forward Relays," *IEEE Signal Processing Letters*, vol. 16, no. 10, pp. 909–912, Oct. 2009.
- [RH10] —, "A Low-Complexity Relay Transmit Strategy for Two-Way Relaying with MIMO Amplify and Forward Relays," in *Proc. IEEE International Conference on Acoustics, Speech, and Signal processing (ICASSP)*, Dallas, TX, Mar. 2010, pp. 3254–3257.
- [RW04] B. Rankov and A. Wittneben, "On the Capacity of Relay Assisted Wireless MIMO Channels," in *Proc. IEEE Workshop on Signal Processing Advances in Wireless Comm.*, Lisbon, Portugal, Jul. 2004, pp. 323–327.
- [SCP11] X. Shang, B. Chen, and H. V. Poor, "Multiuser MISO interference channels with single-user detection: Optimality of beamforming and the achievable rate region," *IEEE Trans. Inf. Theory*, vol. 57, no. 7, pp. 4255–4273, July 2011.
- [SE07] O. Sahin and E. Erkip, "Achievable rates for the Gaussian interference relay channel," in *Proc. IEEE Global Telecommun. Conf.*, Wash., DC, Nov. 2007, pp. 1627–1631.
- [SEA03a] A. Sendonaris, E. Erkip, and B. Aazhang, "User Cooperation Diversity. part I. System Description," *IEEE Trans. Commun.*, vol. 51, no. 11, pp. 1927–1938, Nov. 2003.
- [SEA03b] —, "User Cooperation Diversity. part II. Implementation Aspects and Performance Analysis," *IEEE Trans. Commun.*, vol. 51, no. 11, pp. 1939–1948, Nov. 2003.
- [SES09] O. Sahin, E. Erkip, and O. Simeone, "Interference Channel with a Relay: Models, Relaying Strategies, Bounds," in *Proc. Inf. Theory and Application Workshop*, San Diego, CA, Feb. 2009, pp. 90–95.
- [SH08] V. Stankovic and M. Haardt, "Generalized Design of Multi-User MIMO Precoding Matrices," *IEEE Trans. on Wireless Commun.*, vol. 7, no. 3, pp. 953–961, Mar. 2008.
- [SKM⁺10] M. Sawahashi, Y. Kishiyama, A. Morimoto, D. Nishikawa, and M. Tanno, "Coordinated multipoint transmission/reception techniques for LTE-advanced [Coordinated and Distributed MIMO]," *IEEE Wireless Comm.*, vol. 17, no. 3, pp. 26–34, Jun. 2010.
- [SOSE98] K. Samaras, D. C. O'Brien, A. M. Street, and D. J. Edwards, "BER Performance of NRZ-OOK and Manchester Modulation in Indoor Wireless Infrared Links," *International Journal of Wireless Information Networks*, vol. 5, no. 3, pp. 219–233, 1998.
- [SRH10] B. Song, F. Roemer, and M. Haardt, "Flexible Coordinated Beamforming (Flex-CoBF) Algorithm for the Downlink of Multi-User MIMO Systems," in *Proc. ITG Workshop on Smart Antennas (WSA 2010)*, Bremen, Germany, Feb. 2010, pp. 414–420.
- [SRH13] —, "Flexible coordinated beamforming (FlexCoBF) for the downlink of multi-user mimo systems in single and clustered multiple cells," *Elsevier Signal Processing*, vol. 93, pp. 2462–2473, Sep. 2013.
- [SSE09] O. Sahin, O. Simeone, and E. Erkip, "Interference Channel Aided by an Infrastructure Relay," in *Proc. IEEE Int. Symp. Inf. Theory*, Seoul, Korea, Jun. 2009, pp. 2023–2027.
-

- [SSH04] Q. H. Spencer, A. L. Swindleherst, and M. Haardt, "Zero-Forcing Methods for Downlink Spatial Multiplexing in Multiuser MIMO Channels," *IEEE Trans. on Signal Processing*, vol. 52, no. 2, pp. 461–471, Feb. 2004.
- [SSOE97] A. M. Street, K. Samaras, D. O'Brien, and D. J. Edwards, "Closed form expressions for baseline wander effects in wireless IR applications," *IEE Electronics Letters*, vol. 33, no. 12, pp. 1060–1062, June 1997.
- [SY12] C. Sun and C. Yang, "Energy efficiency analysis of one-way and two-way relay systems," *EURASIP J. Wireless Communications and Networking*, vol. 2012, Feb. 2012.
- [Tel99] E. Telatar, "Capacity of Multi-Antenna Gaussian Channels," *Eur. Trans. Telecommun.*, vol. 10, no. 6, pp. 585–595, Nov. 1999.
- [TH07] X. Tang and Y. Hua, "Optimal Design of Non-Regenerative MIMO Wireless Relays," *IEEE Trans. on Wirelss Comm.*, vol. 6, pp. 1398–1407, Apr. 2007.
- [TW09] F.-S. Tseng and W.-R. Wu, "Joint Source/Relay for Precoders Design in Amplify-and-Forward Relay Systems: A Geometric Mean Decomposition Approach," in *Proc. IEEE Int. Conference on Acoustics, Speech, and Signal Processing (ICASSP 2009)*, Taipei, Taiwan, Apr. 2009, pp. 2641–2644.
- [TY09] Y. Tian and A. Yener, "The Gaussian Interference Relay Channel with a Potent Relay," in *Proc. IEEE Global Telecommun. Conf.(GLOBECOM 2009)*, Honolulu, US, Dec. 2009, pp. 1–6.
- [UC11] P. Ubaidulla and A. Chockalingam, "Relay Precoder Optimization in MIMO-Relay Networks With Imperfect CSI," *IEEE Trans. on Signal Processing*, vol. 59, no. 11, pp. 5473–5484, Nov. 2011.
- [UK08] T. Unger and A. Klein, "Duplex Schemes in Multiple Antenna Two-Hop Relaying," *EURASIP J. Adv. Signal Processing*, vol. 2008, no. 128592, Jan. 2008.
- [US 05] US patent 6968175, "Method and system for sharing transmission revenue between mobile operators and content providers," Nov. 2005.
- [US 07] US patent 7177645, "Spectrum sharing between wireless systems," Feb. 2007.
- [VH11] R. Vaze and R. W. Heath, "On the Capacity and Diversity-Multiplexing Tradeoff of the Two-Way Relay Channel," *IEEE Trans. Inf. Theory*, vol. 57, no. 7, pp. 4219–4234, July 2011.
- [WF83] A. X. Widmer and P. A. Franzaszek, "A DC-Balanced, Partitioned-block, 8B/10B Transmission Code," *IBM Journal of research and development*, vol. 27, no. 5, pp. 440 – 451, Sep. 1983.
- [Win02] S. Winder, *Analog and Digital Filter Design*, 2nd ed. Newens, 2002.
- [WK03] M. Wolf and D. Kress, "Short-Range Wireless Infrared Transmission: The Link Budget Compared to RF," *IEEE Wireless Communications Magazine*, vol. 10, no. 2, pp. 8–14, Apr. 2003.
- [WN97] D. Wisely and I. Neild, "A 100 Mb/s Tracked Optical Telepoint," in *Proc. Personal, Indoor and Mobile Radio Communications (PIMRC)*, Helsinki, Finland, Sep. 1997, pp. 964–968.
- [WZ03] B. Wang and J. Zhang, "MIMO Relay Channel and Its Application for Cooperative Communication in Ad Hoc Networks," in *Proc. 41st Allerton Conf. Commun., Control Comput.*, Monticello, IL, Oct. 2003, pp. 1556–1565.
-

-
- [WZHM05] B. Wang, J. Zhang, and A. Host-Madsen, "On the Capacity of MIMO Relay Channels," *IEEE Trans. Inf. Theory*, vol. 51, no. 1, pp. 29–43, Jan. 2005.
- [YL05] M. Yu and J. Li, "Is amplify-and-forward practically better than decode-and-forward or vice versa?" in *Proc. IEEE Int. Conference on Acoustics, Speech, and Signal Processing (ICASSP 2005)*, Philadelphia, PA, Mar. 2005, pp. 365–368.
- [ZCL09] R. Zhang, C. C. Chai, and Y.-C. Liang, "Joint Beamforming and Power Control for Multiantenna Relay Broadcasting Channel with QoS Constraints," *IEEE Trans. Signal Processing*, vol. 57, no. 2, pp. 726–737, Feb. 2009.
-

Erklärung

Ich versichere, dass ich die vorliegende Arbeit ohne unzulässige Hilfe Dritter und ohne Benutzung anderer als der angegebenen Hilfsmittel angefertigt habe. Die aus anderen Quellen direkt oder indirekt übernommenen Daten und Konzepte sind unter Angabe der Quelle gekennzeichnet.

Bei der Auswahl und Auswertung folgenden Materials haben mir die nachstehend aufgeführten Personen in der jeweils beschriebenen Weise entgeltlich/unentgeltlich geholfen:

1.
2.
3.

Weitere Personen waren an der inhaltlich-materiellen Erstellung der vorliegenden Arbeit nicht beteiligt. Insbesondere habe ich hierfür nicht die entgeltliche Hilfe von Vermittlungs- bzw. Beratungsdiensten (Promotionsberater oder anderer Personen) in Anspruch genommen. Niemand hat von mir unmittelbar oder mittelbar geldwerte Leistungen für Arbeiten erhalten, die im Zusammenhang mit dem Inhalte der vorgelegten Dissertation stehen.

Die Arbeit wurde bisher weder im In- noch im Ausland in gleicher oder ähnlicher Form einer Prüfungsbehörde vorgelegt.

Ich bin darauf hingewiesen worden, dass die Unrichtigkeit der vorstehenden Erklärung als Täuschungsversuch bewertet wird und gemäß § 7 Abs. 10 der Promotionsordnung den Abbruch des Promotionsverfahrens zur Folge hat.

(Ort, Datum)

(Unterschrift)
